Investigating the function of inhibition in the human primary motor cortex using multimodal approaches



Patrícia Čambálová

Exeter College

University of Oxford

A thesis submitted for the degree of

Doctor of Philosophy

Trinity Term 2025

Abstract

Studying the mechanisms that underpin motor control and the learning of new movements is necessary to understand the role of the primary motor cortex (M1) in planning, controlling, and executing voluntary movements. Novel techniques will allow us to study the acquisition of skills in healthy adults and may ultimately help us understand diseases that affect motor control in clinical populations. My thesis consists of several studies investigating metrics that reflect different aspects of inhibitory signalling in M1 using a variety of methods, and how this signalling changes throughout life.

Firstly, I aimed to determine the test-retest reliability of a novel transcranial magnetic stimulation (TMS) device, the controllable pulse TMS (cTMS). cTMS is the first device that enables modulation of pulse width. Pulses of different widths are believed to activate distinct populations of neurons, including the relatively small diameter inhibitory neurons. I delivered cTMS pulses of various intensities to acquire input-output curves at three pulse widths. The participants also completed two sensorimotor tasks that were associated with cTMS metrics. I found low test-retest reliability of cTMS input-output curve slopes, a common measure of corticospinal excitability, but I did not find evidence for selective recruitment of different neuronal populations.

In the second study, I investigated age-related changes in movement-related beta, slow- and mid-gamma band activity in a dataset from the Cambridge Centre for Ageing and Neuroscience (CamCAN). The magnetoencephalography (MEG) dataset included almost 620 participants ranging from 18 to 88 years of age. I observed age-related changes in beta and gamma band activity, including a reduction in the peak frequency of beta movement-related desynchronisation (ERD) and synchronisation (ERS), stronger ERD, and an increase in the peak frequency of slow-gamma ERS. I also observed changes associated with age in the localisation of activity of all bands except beta ERD.

In the third study, I assessed the influence of genetic polymorphisms on peak frequency and power of M1 mid-gamma band activity in the CamCAN dataset. I selected a single nucleotide polymorphism (SNP) in each of four genes that have been associated with inhibitory neurotransmission or gamma oscillations. I found evidence for a trend between two candidate SNPs in the *GAD1* and *BDNF* genes and mid-gamma peak frequency, but the associations were not significant when corrected for multiple comparisons.

Taken together, this work provides insight into the techniques which can be used to study M1, and mechanisms of motor control and provides the basis for further exploration.

This thesis contains approximately 35,000 words.

Acknowledgements

First and foremost, I would like to thank my supervisors, Professor Charlotte Stagg, Dr Catharina Zich, and Professor Martin Turner, for their inspiration, help, and support throughout my DPhil. In particular, thank you, Charlie and Catha, for your constant guidance, patience, and kindness. I believe that I would not have made it here without your support. It has been an honour to work with both of you and I have learnt so much from you. Both of you lead by example and have created a welcoming group full of brilliant scientists.

I also want to thank the organisations that helped fund my DPhil: Oxford Centre for Integrative Neuroimaging (OxCIN) for my main studentship and the University of Oxford, Funds for Women Graduates (FfWG), and the Goodger & Schorstein Research Scholarship for additional funding.

My DPhil would not have been possible without the wonderful Physiological Neuroimaging Group (PiNG), and especially without the help of my MSc student Katie along with Ioana, Oana, Yammi, and Loic, who helped me collect data. Valentina, thank you for working with me on the genetics project, co-writing the preregistration, and for all our adventures. Evan, for your supervision during my MSc and allowing me to gain experience with clinical populations during my DPhil. Ioana, for your kindness and for always being willing to help. Poly, for being an amazing person who is always positive, kind and supportive. Karen, an honorary member of PiNG, thank you for always being willing to discuss anything pulse width modulation-related. To the rest of PiNG, past and present, you have been an amazing group to work with and spend the last few years around. It has also been a pleasure to belong to the wider Neuroplastics group that provided the most friendly research environment that I could have hoped for.

I am very grateful for the friends I have made in Oxford, who have been with me on this journey and made Oxford feel like home: Murong, Verena, Tara, Matthias, Valentina, Jess, Ioana, Kengo, Eugenio, Atika, Kevin, Peter, and Rafa. My time on the Exeter College MCR committee has also provided me with an unforgettable experience.

Lastly, the biggest thank you goes to my family, especially my parents and brother, for their encouragement, unconditional love and support and for always believing in me.

Contents

Abstract **2**

Acknowledgements **3**

1 General Introduction **8**

1.1 Primary motor cortex (M1) . . . 8

1.1.1 Anatomy and structure of M1 . . . 8

1.1.2 Changes in excitability of M1 during movement due to inhibitory signalling . 10

1.2 Brain oscillations in the sensorimotor cortex . . . 11

1.2.1 Overview of M1 frequency band oscillations . . . 11

1.2.2 Inhibitory neurons drive M1 movement-related oscillatory activity . . . 14

1.3 Age-related changes in M1 . . . 17

1.3.1 Changes in motor function and M1 can be observed in advanced ageing . . . 17

1.3.2 Healthy ageing reduces inhibition . . . 19

1.3.3 Changes in oscillations throughout life and disease . . . 20

1.4 Aims . . . 22

2 Methods **23**

2.1 Transcranial magnetic stimulation (TMS) . . . 23

2.1.1 Single pulse TMS measures global excitability of the motor cortex and corticospinal pathways . . . 23

2.1.2 IO curves are a sensitive measure of changes in corticospinal excitability . . . 25

2.1.3 Approaches for the analysis of IO curves . . . 26

2.2 Sensorimotor tasks for evaluation of motor control and learning . . . 26

2.2.1 Action selection task . . . 27

2.2.2 Serial reaction time task . . . 27

2.3 Magnetoencephalography (MEG) . . . 28

2.3.1 MEG measures magnetic fields produced by the brain's electrical events . . . 28

2.3.2 MEG analysis approaches . . . 29

2.4 Single nucleotide polymorphisms (SNPs) . . . 32

2.4.1 Genetic sequencing . . . 33

3 Determining the test-retest reliability of cTMS metrics **34**

3.1 Introduction . . . 34

3.1.1 Novel cTMS device allows greater control of pulses delivered . . . 34

3.1.2 Strength-duration properties reveal neurophysiological properties of recruited neuronal populations . . . 34
3.1.3 Activation of inhibitory interneurons . . . 36
3.1.4 cTMS may enable selective recruitment of different neuronal types . . . 37
3.1.5 Aims . . . 38
3.2 Methods . . . 39
3.2.1 Participants . . . 39
3.2.2 Experimental design . . . 39
3.2.3 TMS data acquisition . . . 40
3.2.4 TMS data analysis . . . 41
3.2.5 Motor tasks . . . 42
3.2.6 Motor task data analysis . . . 43
3.2.7 Statistical analysis . . . 44
3.3 Results - %MSO method . . . 45
3.3.1 All but three of all 132 input-output (IO) curves were quantified . . . 45
3.3.2 Increasing pulse width increases input-output curve slope . . . 45
3.3.3 Correlation between slopes of IO curves acquired by pulses of different widths 45
3.3.4 Only longest pulse width IO curve slopes exhibit good test-retest reliability . 47
3.3.5 Test-retest reliability of other IO curve metrics . . . 49
3.3.6 Some motor task metrics show good test-retest reliability . . . 49
3.3.7 No significant correlations between task performance and IO curve slopes . . 53
3.4 Results - %rMT method . . . 53
3.4.1 Increasing pulse width does not have an effect on IO curve slope when curves are fitted to stimulation intensity relative to individual motor threshold . . . 53
3.4.2 Relationship between slopes of IO curves acquired by pulses of different widths 56
3.4.3 Correlation between %rMT and %MSO slopes . . . 56
3.4.4 IO curve slopes exhibit low test-retest reliability even when quantified using %rMT . . . 58
3.4.5 Test-retest reliability of other IO curve metrics . . . 58
3.4.6 No significant correlations between task performance and IO curve slopes . . 61
3.5 Discussion . . . 61
3.5.1 Increasing pulse width leads to steeper IO curve slopes only with one analysis method . . . 61
3.5.2 Does pulse width modulation enable the selective recruitment of neurons? . 64
3.5.3 Does the total amount of charge delivered matter? . . . 66
3.5.4 Future directions to understand the importance of pulse width . . . 68
3.5.5 Low test-retest reliability of TMS metrics . . . 68
3.5.6 Test-retest reliability of tasks . . . 72
3.5.7 Limitations . . . 73
3.5.8 Conclusion . . . 75

4 Investigating age-related changes in movement-related M1 beta and gamma band activity 76
4.1 Introduction . . . 76
4.1.1 Movement is associated with changes in beta and gamma band activity in the primary motor cortex . . . 76
4.1.2 Changes in oscillations throughout life . . . 77
4.1.3 Aims . . . 77
4.2 Methods . . . 78
4.2.1 Open-access CamCAN imaging dataset . . . 78
4.2.2 Participants . . . 78
4.2.3 Experimental design . . . 78
4.2.4 MEG and MRI data acquisition . . . 78
4.2.5 MEG data analysis . . . 79
4.2.6 Statistical analysis . . . 81
4.3 Results . . . 81
4.3.1 CamCAN dataset demographics . . . 81
4.3.2 Defining individual movement-related beta and gamma band activity . . . 81
4.3.3 Group movement-related time-frequency activity in beta and gamma bands 82
4.3.4 Relationship between age and movement-related activity metrics . . . 84
4.3.5 Relationship between age and the location of movement-related activity . . 84
4.4 Discussion . . . 91
4.4.1 Age-related changes in gamma band frequency . . . 91
4.4.2 Age-related changes in beta band frequency . . . 93
4.4.3 Age-related changes in movement-related activity localisation . . . 94
4.4.4 Limitations . . . 95
4.4.5 Conclusion . . . 96

5 Exploring the contribution of genetic polymorphisms to inter-individual variability in M1 gamma band activity 97
5.1 Introduction . . . 97
5.1.1 Inhibitory neurons drive gamma band activity . . . 97
5.1.2 Heritability of gamma band activity characteristics . . . 98
5.1.3 Genes of interest . . . 99
5.1.4 Aims . . . 102
5.2 Methods . . . 103
5.2.1 Open-access CamCAN imaging dataset . . . 103
5.2.2 Participants . . . 103
5.2.3 Analysis of sensorimotor task MEG data . . . 103
5.2.4 Statistical analysis . . . 104
5.2.5 Power calculation . . . 104

5.3 Results . . . 105
5.3.1 CamCAN dataset genotypes . . . 105
5.3.2 Study 1: GABAergic genes . . . 106
5.3.3 Study 2: Neuromodulatory genes . . . 108
5.4 Discussion . . . 109
5.4.1 No significant relationship between genotypes of selected GABAergic and neuromodulatory genes and MEG metrics of mid-gamma activity . . . 109
5.4.2 Trends in gamma peak frequency based on *GAD1* and *BDNF* genotype . . . 110
5.4.3 Limitations . . . 111
5.4.4 Conclusion . . . 113

6 General Discussion **114**
6.1 Thesis summary . . . 114
6.2 General limitations and future directions . . . 115
6.2.1 Test-retest reliability and reproducibility of TMS studies . . . 115
6.2.2 Can TMS specifically target inhibitory neurons? . . . 117
6.2.3 MEG-detected gamma band activity as a measure of inhibition . . . 118
6.2.4 Use of cTMS and MEG to study mechanisms of amyotrophic lateral sclerosis (ALS) . . . 119
6.3 Main conclusions . . . 121

List of Figures **122**

A Appendix **129**
A.1 Exclusion of input-output curves in Chapter 3 . . . 129

Bibliography **133**

Chapter 1

General Introduction

The motor system allows us to lead our daily lives, enabling actions and complex movements such as talking, writing, walking, or driving through voluntary control of our muscles. Understanding the mechanisms underpinning motor control and motor learning is necessary to enable us to facilitate the regaining of motor control or enhanced motor rehabilitation in clinical populations.

In order to understand the mechanisms within, and functions of the primary motor cortex (M1), the region responsible for executing voluntary movements, we need to develop new tools. Novel techniques will allow us to study the acquisition of skills in healthy adults, which may ultimately help us to understand diseases that affect motor control. In particular, inhibition mediated by the neurotransmitter GABA has been shown to contribute to motor learning[1]. My thesis consists of a number of studies investigating GABAergic signalling in M1 using a variety of methods and how this signalling changes throughout life. This work gives a unique insight into the mechanisms underpinning motor control in healthy adults and paves the way for the use of these tools to study healthy motor learning, and ultimately motor recovery in clinical populations.

1.1 Primary motor cortex (M1)

The cerebrum, the largest part of the brain, is composed of two hemispheres, each made up of four lobes: frontal, parietal, temporal, and occipital, in addition to several subcortical structures which are not lobar. Each lobe is responsible for different processes and functions. The cerebral neocortex refers to the thin layer of grey matter that covers the brain. Lobes are divided by, and contain, ridges and grooves known as gyri and sulci; these increase the surface area of the cerebral cortex and therefore enable more processing. M1 is found in the frontal lobe, anterior to the central sulcus.

1.1.1 Anatomy and structure of M1

Like the rest of the cerebral neocortex, M1 is composed of six layers of varying sizes (Figure 1.1). The most superficial one is layer I (L1), also known as the molecular layer, which

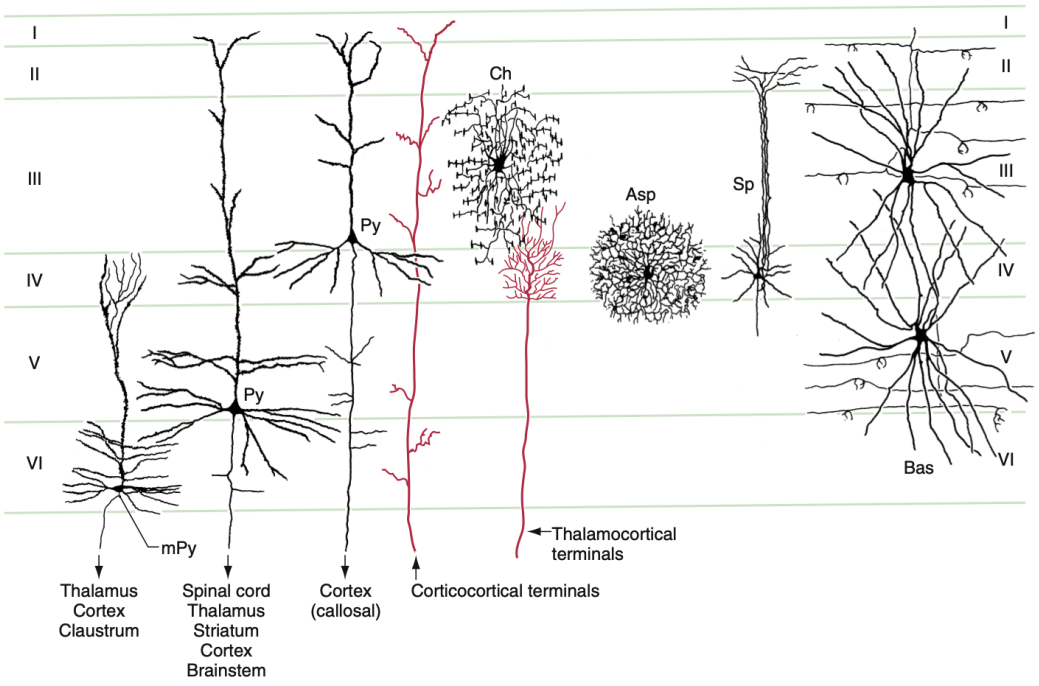


Figure 1.1: Representative cells in the six layers of M1. These include pyramidal (Py) and modified pyramidal (mPy), chandelier (Ch), aspiny (Asp) and spiny (Sp) stellate neurons, and basket (Bas) cells. Figure from Grow[6].

contains glial cells and very few neurons[2]. Layers II and III (L2/3) both contain densely packed pyramidal neurons that receive input from cortical and thalamic projections[2]. Layer IV (L4) in M1 is less distinct than in other parts of the cerebral cortex, but has been found to contain pyramidal neurons, have input from thalamus, outputs to L2/3 pyramidal neurons, and weaker long-range cortico-cortical inputs and outputs[3]. Layer V (L5) is the most prominent layer in M1, and contains the main output neurons, the Betz cells, which project to the spinal cord through the corticospinal tract[2]. Finally, the deepest layer VI (L6) contains heterogeneous groups of neurons and sends outputs to the thalamus[4]. Cortical neurons have extensive connections of inputs and outputs both between and within layers, forming circuits that are highly conserved across the cortex[5].

M1 contains both excitatory and inhibitory neurons

The most abundant class of neurons in the cerebral cortex are the excitatory neurons (up to 80% of all neurons), of which the majority are pyramidal neurons[2,5]. Pyramidal neurons release glutamate and enable the propagation of signals. Glutamate causes excitatory post-synaptic potentials (EPSPs), which increase the likelihood of postsynaptic action potentials. With the exception of L1, pyramidal neurons can be found in all layers, each with distinctive patterns of dendritic arbors and axonal projections[5].

The remaining approximately 20% of cortical neurons are inhibitory interneurons, the majority of which release the main inhibitory neurotransmitter in the mature brain, gamma-

aminobutyric acid (GABA)[2]. The binding of GABA to receptors causes inhibitory postsynaptic potentials (IPSPs), which reduce the likelihood of postsynaptic action potentials. Inhibitory interneurons are highly heterogeneous and can be divided into numerous groups depending on their morphological and electrophysiological properties[7,8]. Inhibitory neurons add complexity and computational power to seemingly simple networks of neurons by controlling excitation and regulating the timing of neuronal firing, synchronising circuits and generating oscillatory activity[7].

The balance of excitatory and inhibitory activity is tightly controlled for healthy brain function. Dysfunction in excitation-inhibition balance through changes in motor cortical circuits is believed to underlie many disorders, including Parkinson's and Alzheimer's diseases[2].

1.1.2 Changes in excitability of M1 during movement due to inhibitory signalling

There is substantial evidence suggesting that modulation of M1 excitability is a major mechanism underlying not only the preparation of movements[9] , but also motor learning in both humans[10] and rodents[11]. Modulation of M1 excitability appears to be largely driven by local inhibitory changes, which are almost entirely GABAergic[10].

When human M1 is probed during the preparation of a movement, an initial decrease in excitability early in movement preparation can be observed[12–14], followed by an increase in excitability immediately before the movement[15] (Figure 1.2). This later increase in excitability occurs because of reduced GABAergic signalling[16,17]. Corticospinal excitability is again reduced approximately 0.5-1s after movement termination[18]. Fluctuations in inhibitory interneuron signalling are important for changes in M1 excitability which enable the preparation and execution of movements.

Moreover, motor learning-induced plasticity can result in a long-lasting increase in M1 excitability[20]. In rodent M1, somatostatin-expressing inhibitory neurons exhibit a reduction in the number of synaptic boutons after motor learning, reflecting reduced inhibition of excitatory neurons[21]. Administering a GABA agonist to rats blocks long-term potentiation (LTP), the main mechanism for brain plasticity and learning[22]. In humans, measuring GABA concentration using magnetic resonance spectroscopy (MRS) reveals that GABA decreases while learning a motor task[1,23] and GABA levels early in motor learning predict subsequent performance[1]. Therefore, modulation of M1 excitability via changes in inhibitory signalling appears to be crucial for motor control and learning.

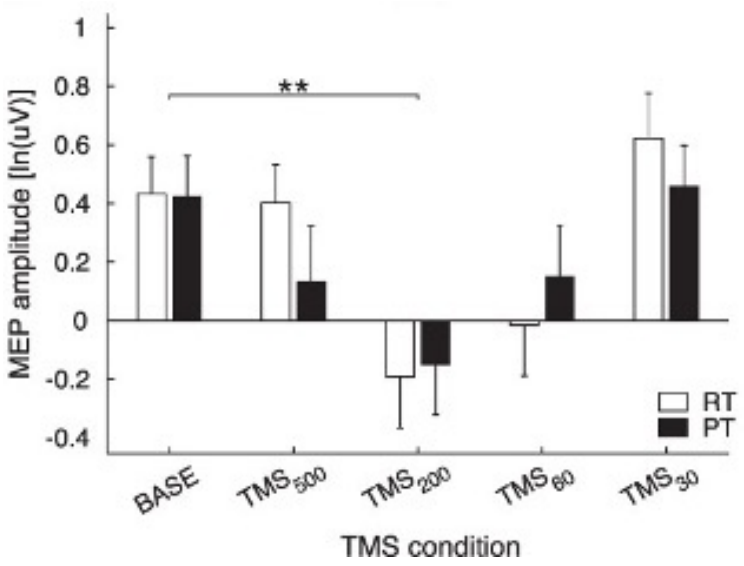


Figure 1.2: Dynamics of corticospinal excitability during movement preparation. Movement-evoked potentials (MEPs) are a measure of corticospinal excitability. Excitability was probed at various time points before expected movement onset (30 to 500 ms). MEPs of higher amplitudes represent higher excitability. PT and RT refer to task used in the original study. Corticospinal excitability first decreased in comparison to baseline (TMS_{200}), then increased (TMS_{30}). Figure from Ibáñez et al.[19].

1.2 Brain oscillations in the sensorimotor cortex

The brain is always active, with almost all neurons demonstrating spontaneous action potentials, independent of sensory input. These spontaneous action potentials form the majority of brain activity, and are tightly controlled[24]. It is thought that all processing in the brain occurs through changes in the rate, rhythm and connectivity of this ongoing neuronal activity. The synchronous electrical activity of neuronal populations is often referred to as neuronal oscillations. EPSP- and IPSP-driven dendritic currents from all neurons contribute to the oscillatory activity that can be measured non-invasively in humans, although at least 10,000 synchronised neurons are required for the signal to be detectable[25]. Oscillations in the brain, emerging from coherent synchronous patterns of neurons, coordinate activity between different areas[24].

External inputs, such as sensory stimuli, disturb the brain's spontaneous default activity patterns. Brain oscillations appear to have roles in processing these sensory stimuli and perception, and also in key processes like producing movements, motor control, and cognition[26–28]. In humans, the most common techniques to measure oscillations are electroencephalography (EEG) and magnetoencephalography (MEG).

1.2.1 Overview of M1 frequency band oscillations

Brain oscillations can be observed at various frequencies in the brain. In this section, I will provide an overview of the frequency bands of oscillatory activity in the primary motor cortex

that are key to its functions, from slowest to fastest, starting from the theta band. I omitted the delta band (0.5-4 Hz), which does not have a clear link to motor control or learning and is instead associated with integrating sensory information and coordination with sensory areas[29].

Theta (4-8 Hz)

Rhythms in the theta band have been most extensively studied in the hippocampus, where theta activity has been linked to memory and learning[30]. The most likely mechanism through which theta contributes to these processes is by cross-frequency modulation[26], where activity in one frequency band can modulate the activity in a different band. In humans, theta rhythms are coupled with gamma activity in a phase-amplitude coupled manner: the maximum gamma power occurs at the peak of theta rhythms[31]. Increasing theta power strengthened theta-gamma coupling[31] and driving theta-gamma coupling through transcranial alternating current stimulation (tACS), a type of non-invasive brain stimulation, improved motor skill acquisition[32].

Mu (8-13 Hz)

Mu rhythms (occurring at alpha frequencies, 8-13 Hz) are specific to the sensorimotor cortex. At rest, mu power is at its maximum. During movement, power in the mu band decreases[33]. The movement-related decrease in power is commonly known as event-related desynchronisation (ERD). Mu band ERD also occurs when observing movements[34] via mirror neurons, a class of neurons in the premotor cortex that activate during the observation of movements performed by others[35]. Stronger mu ERD has been associated with better learning[36].

Beta (13-30 Hz)

Beta band activity, along with gamma, is one of the two most commonly studied rhythms in M1. The role of beta has been extensively studied in the motor system and has been reported in multiple brain areas that control motor function such as the sensorimotor cortex and basal ganglia[37–39]. One possible model for spontaneous generation of beta activity is that it emerges in the cortex, but is controlled by synaptic drive from the basal ganglia or the thalamus[40]. In the cortex, it is considered to arise in the deeper layers[41], but it is not yet clear what cells or circuits underlie beta activity.

In preparation for movement, beta band activity decreases in power followed by an even larger reduction during the movement (event-related desynchronisation, ERD). Beta band activity power then exceeds pre-movement levels after movement cessation (event-related synchronisation, ERS) before returning to pre-movement baseline levels[42,43] (Figure 1.3). ERD also occurs during observed, imagined, or passive movements[44].

There are multiple lines of evidence showing that beta activity is more than an epiphe-

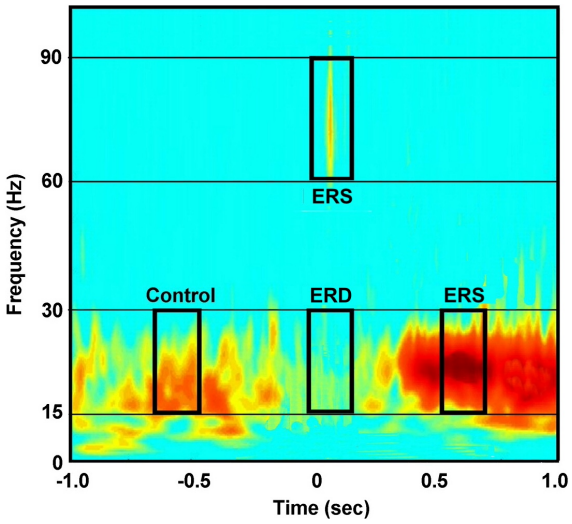


Figure 1.3: Movement-related changes in M1 oscillations. Time 0 s denotes a button press. In the beta frequency band (15-30 Hz in this figure), a decrease in oscillatory activity can be observed (beta ERD) compared to baseline (Control) followed by an increase after movement terminates (beta ERS). Activity in the gamma band (30-100 Hz, especially around 75 Hz) increases (gamma ERS) as movement is executed. Figure adapted from Hall et al.[45].

nomenon for motor control. Beta ERS has a somatotopic organisation, with stronger ERS following a larger hand movement compared to a finger movement[43]. Beta activity may play a role in motor learning, as beta ERD amplitude has a negative linear relationship with the speed of movement[46] and both beta ERS[47,48] and ERD[48] become stronger with motor learning. Moreover, power of beta activity in the basal ganglia is enhanced in patients with Parkinson's disease[49,50]. Suppressing beta activity through medication or deep-brain stimulation improves motor symptoms of patients[51], providing clear evidence for the role of beta activity in movement control and execution.

There is also substantial evidence for an anti-kinetic role of beta activity, since applying beta tACS slows movements[52]. Engel and Fries propose that beta activity acts to maintain status quo of the system[27], but the role of beta activity is still not fully clear. It is possible that beta band consists of distinct lower and higher beta bands, each playing a separate role in producing movements, or that beta ERS and ERD are separate processes and functional roles[39]. Beta ERD has been implicated in a relative shift from inhibition to excitation in imagined movements[44]. On the other hand, beta ERS is modulated by both force output and rate of force development in muscle flexion[53], has been associated with prediction of movement error[47,54] and may represent processing of the movement outcome[39,55]. Although beta band activity is not fully understood, these studies together suggest that the functional roles of ERS and ERD can be varied.

Gamma (>30 Hz)

Gamma band activity (often defined as 30-120 Hz) was discovered much later than slower rhythms[56,57], as it is typically recorded at much lower amplitudes through the skull, likely both because it arises from smaller neural circuits and it is attenuated by the bone. Gamma is thought to be more spatially and temporally specific compared to slower rhythms and to reflect the contribution of smaller ensembles of neurons[57]. It tends to be more prominent in more superficial cortical layers[58]. Gamma has been found to be involved in cognitive processes in a number of brain regions[58] and in M1, gamma is generally considered pro-kinetic[28].

In contrast to beta, activity in the gamma band increases during movement, especially around 75 Hz, resulting in an ERS that is temporally linked to movement onset[43,56,59–63] (Figure 1.3). In addition, gamma band activity has also been implicated in learning. Gamma ERS amplitude decreases with practice[64] and driving gamma activity by applying 75 Hz tACS improved performance in a motor learning task[65]. A positive relationship between movement speed and gamma power has also been found[66].

There is evidence for the division of gamma band into various sub-bands which might all be coupled to different phases of theta cycles[58,67]. Specifically, slow-gamma (30-60 Hz) and mid-gamma (60-90 Hz) have been shown to represent different functional states[68], although most of the work has been performed in the rodent hippocampus. Most human M1 work has explored the mid-gamma band, but there is limited evidence to suggest the existence of the slow-gamma band in the human M1[43,56,69]. In a recent study from my group, M1 movement-related slow-gamma peak frequency, the frequency that shows the strongest slow-gamma ERS, was found to be associated with a TMS measure of inhibition, while mid-gamma power was associated with motor leaning[70]. However, the division of gamma sub-bands and their roles are not yet fully clear.

1.2.2 Inhibitory neurons drive M1 movement-related oscillatory activity

Normal operation of the brain is widely understood to be dependent on a tightly controlled balance between excitation and inhibition. In this section, I will provide a summary of evidence to support the hypothesis that oscillatory activity, especially in the beta and gamma bands, also relies on a balance of excitatory and inhibitory networks.

Beta and inhibition

Activity in the beta band is thought to be generated by local connections between excitatory and inhibitory neurons in the M1, with excitatory input from other brain regions[40,71,72]. In the visual system, modelling showed that stimulus-evoked peak frequency of beta activity depends on the time constant of deep pyramidal neurons and the excitatory drive of deep pyramidal neurons onto inhibitory neurons[41], while beta power was most strongly dependent

on the strength of inhibitory interneuron drive onto deep pyramidal neurons[41]. In particular, somatostatin (SOM)-expressing interneurons have been linked to the generation of V1 beta oscillations[73].

The decrease in activity in the beta band during beta ERD has been thought to represent asynchronous activity of neurons[74] and may be related to the release of inhibition and the subsequent activation of neurons. Beta ERS may represent the subsequent inhibition of the motor cortex following movement termination[61,75], since the maximum of beta ERS coincides with reduced excitability of motor cortical neurons[43]. Recent evidence suggests that beta activity is composed of many transient high-amplitude bursting events lasting up to 150 ms at the level of a single trial, even though it appears to be a slowly modulated signal when averaged over multiple trials[40,76,77]. Therefore, ERD may represent a decline in the probability and amplitude of beta bursts while during ERS, an increase in the probability and amplitude of bursts has been observed[78].

Pharmacological interventions can provide direct evidence for the involvement of specific inhibitory processes in generating beta activity. Zolpidem, a positive allosteric modulator of the $GABA_A$ receptor which increases the effects of GABA, enhanced beta power measured using in vitro cortical recordings from rat brain slices and MEG recordings of a movement task performed by human participants[79]. Diazepam, another positive allosteric modulator of the $GABA_A$ receptor, increased movement-evoked beta ERD power but had no effect on beta ERS[45]. Administration of tiagabine, a blocker of the GABA transporter 1 (GAT-1), which transports GABA from the synaptic cleft into the glia, increased baseline beta power, enhanced beta ERD and reduced beta ERS[80]. All three drugs that enhance GABA effects caused a change in beta, showing the importance of inhibitory processes in generating beta activity. Further pharmacological in vitro studies suggest that beta power is also dependent on glutamatergic excitation[81].

Endogenous levels of GABA can be measured by magnetic resonance spectroscopy (MRS). Due to the low temporal specificity of MRS, it is unlikely that levels of GABA are linked to synaptic activity. It is thought that MRS-measured GABA represents extrasynaptic (tonic) inhibition[82,83]. Studies measuring GABA using MRS alongside MEG or EEG recordings support the involvement of inhibition in generating beta activity. A positive relationship between resting beta peak frequency and MRS GABA has been reported[84]. Following a movement, beta ERS power also had a positive relationship with MRS GABA[85,86]. Although there are no reports about an association between MRS GABA and beta ERD, the resting and ERS data provide insight into the link between inhibition and beta activity.

Gamma and inhibition

The neurophysiological processes underlying gamma band activity are also thought to reflect activity of inhibitory neurons. Two models for generation of gamma oscillations have emerged: the interneuron gamma (ING), and the pyramidal-interneuron gamma (PING)

mechanisms that likely work together to produce gamma rhythms[57,58,87]. The ING model relies only on inhibitory interneurons mutually connected to each other, while PING is based on a reciprocal connection between interneurons and excitatory pyramidal neurons[58].

Several lines of evidence point to the contribution of inhibitory neurons in generating gamma band activity. Inhibitory postsynaptic potentials have been found to be more effective at phase-locking and modulating the synchronisation of cortical pyramidal cells than excitatory postsynaptic potentials[88]. Since $GABA_B$ receptors tend to be slow-conducting, $GABA_A$ synapses were thought to be involved in mediating phase-locking[88]. Moreover, gamma band oscillations have been reported in regions of the brain that contain many inhibitory synapses, specifically those containing $GABA_A$ receptors[58]. Utilising in vitro pharmacological blockade of $GABA_A$ receptors reduces gamma power[89]. Moreover, modelling has shown that inhibitory interneuron time constant predicts gamma peak frequency[41]. These results suggest that inhibitory synapses, and especially $GABA_A$ receptors, are important for gamma band activity.

Of the numerous types of inhibitory neurons found in the brain, parvalbumin-expressing (PV) interneurons are implicated in generating gamma[58]. The specific class of PV interneurons that contribute to gamma band activity is believed to be fast-spiking basket cells[58] which target the soma and proximal dendrites of pyramidal neurons and other interneurons[8]. Activating cortical fast-spiking PV interneurons at various frequencies via optogenetics can amplify gamma band activity, while pyramidal cell activation only amplifies oscillations at frequencies lower than gamma[90]. On the other hand, optogenetic inhibition of cortical PV interneurons suppresses gamma oscillations[91]. These studies highlight the involvement of PV interneurons in the generation of gamma band activity.

Modulating of gamma band activity may occur through another inhibitory mechanism: tonic inhibition. This process is mediated by $GABA_A$ receptors located at extrasynaptic sites activated by a low resting level of extracellular GABA and synaptic spillover[92]. In the cortex and hippocampus, a major class of receptors found extrasynaptically are $\alpha 5$ subunit-containing $GABA_A$ receptors. In hippocampal slices from mice lacking the $\alpha 5$ subunit, gamma band activity is higher in amplitude compared to wild type mice[93]. Moreover, gamma peak frequency has been shown to be related to the $GABA_A$ time constant[94]. Therefore, $\alpha 5$ subunit-containing $GABA_A$ receptors in particular may be involved in modulating gamma band activity.

More evidence supporting the crucial role of inhibition in gamma activity comes from human research utilising non-invasive brain stimulation, neuroimaging, and pharmacological interventions. For example, driving gamma band activity in M1 by applying transcranial alternating current stimulation (tACS) at 75 Hz induced an increase in a $GABA_A$-sensitive TMS measure[65].

Neuroimaging, especially MRS, suggests an association between inhibition and gamma activity. MRS-measured levels of GABA predict gamma band power in the superior temporal

sulcus[95]. However, in the auditory cortex, no metrics of gamma band activity showed a relationship with MRS GABA[96]. The peak frequency of movement-evoked M1[85] and stimulus-induced visual cortex[97] gamma band activity detected by magnetoencephalography (MEG) was predicted by MRS-measured GABA, although the visual cortex findings were not replicated in two more studies with similar paradigms[98,99].

Visual stimulus-induced gamma oscillations have been explored using another imaging modality, positron emission tomography (PET), in combination with MEG. PET scans were acquired after participants were administered a radiotracer [11C]flumazenil, which selectively binds to $GABA_A$ receptors as a ligand at the benzodiazepine site. This method can be used to study $GABA_A$ receptor density, which was found to have a positive relationship with gamma peak frequency and a negative relationship with power[100]. Gamma peak frequency also has a negative relationship with functional magnetic resonance (fMRI) blood oxygen level-dependent (BOLD) response in the visual cortex[97]. Although neuroimaging evidence is mixed, it supports the association of cortical excitation and inhibition balance with gamma band activity.

Pharmacological interventions allow us to specifically manipulate inhibitory networks in the brain. Administration of diazepam, a positive $GABA_A$ receptor modulator, had no effect on movement-related gamma band activity measured by MEG[45]. Tiagabine, a drug that blocks a GABA uptake transporter and therefore increases levels of GABA, also had no effect on movement-related gamma band activity metrics[80]. However, tiagabine did affect resting slow- and mid-gamma power[101]. In a later study, the administration of tiagabine was combined with the acquisition of PET with [11C]flumazenil, the selective $GABA_A$ receptor radiotracer. Gamma band power measured during a cognitive task was positively associated with the tiagabine-associated change in [11C]flumazenil binding[102]. Based on these studies, it is not possible to conclude the exact GABAergic receptors underpinning gamma band activity.

1.3 Age-related changes in M1

As humans age, the brain undergoes many structural, functional, and biochemical changes that can significantly affect general brain function and motor abilities. The importance of studying these changes has become increasingly apparent with ageing populations worldwide.

1.3.1 Changes in motor function and M1 can be observed in advanced ageing

Reductions in brain volume with age have been observed for the past several decades. Post-mortem morphometry revealed that reduction in brain volume is not due to a lower number of neurons, but because of smaller cell bodies of cortical neurons[103]. Moreover, these changes are region-specific. The region encompassing premotor and supplementary motor areas had a

43% reduction in cell body size in brains from people over 65 years compared to those under 45 years of age[103].

Age-related brain changes can also be observed in rodent models. Hippocampal slices from aged rats showed reduced glutamate receptor function, as well as impaired long term potentiation (LTP), a primary mechanism for brain plasticity and learning[104]. M1 neurons from aged mice imaged in vivo show reduced numbers of dendritic spines and higher turnover with reduced long-term survival of spines in comparison to younger mice[105].

Human imaging studies also provide evidence for age-related changes in M1. A recent study aggregated over 123,000 structural MRI scans from more than 100 primary studies to determine structural changes in the brain throughout the human life span from gestation to 100 years old. Reductions in all brain volume metrics with age were observed[106]. Similarly to post-mortem findings, MRI scans show region-specific effect of ageing on cortical thickness, with significant atrophy in M1 in particular[107,108].

Older adults have also been found to have less segregated motor networks[109]. In younger people, between-network connections are relatively sparse while within-network connections are relatively dense, but this changes with age. Less segregated sensorimotor networks in older adults were also associated with worse performance on a sensorimotor task[109]. Moreover, resting functional connectivity in motor networks increases with age and worse performance is linked to greater connectivity[110]. Therefore, there are changes associated with ageing both in the structure of the brain and in brain activity at rest.

Age-related changes can be observed when fMRI scans are acquired as participants execute movements. In general, older participants exhibit worse performance on motor tasks[111,112]. More ipsilateral M1 BOLD activation is present in older adults during a simple finger movement task[111,113], suggesting that older adults have less selective recruitment of brain regions.

Older adults seem to have broader activation in both motor and non-motor areas. For example, greater BOLD activation in supplementary motor area[114,115], primary sensory cortex and the lateral premotor area[115] with age has been observed. PET scans collected during movement reveal an association of ageing to bilaterally increased movement-related activation in premotor cortex[116]. There is also more activation in non-motor areas, e.g. visual areas[111], suggesting older adults may need to use more mental imagery strategies to perform tasks. Indeed, their performance on a reaching and grasping task was reduced when their hand and the target were concealed compared to younger participants[112]. More dependence on cognition has been observed in older adults who perform bimanual tasks compared to younger adults[117]. Overall, more brain areas, including non-motor regions, are involved in executing a movement in older people compared to younger people.

Motor function also changes due to age. Control of motor output i.e., the ability to maintain a constant submaximal contraction of a finger represented by an increased variability in exerted force, was reduced in older adults, suggesting reorganisation of motor units (the muscle fibres

one motor neuron innervates)[118]. fMRI BOLD activity during a hand gripping task showed less modulation in older adults, suggesting reduced ability to control motor output[119]. The above findings suggest that the ability to perform movements reduces with age, reducing the mobility of elderly people.

1.3.2 Healthy ageing reduces inhibition

Over the course of a lifespan, decreasing levels of GABA have been reported[85,120], although these findings are not consistent across studies. In humans, for example, no difference has been found in M1 proteins related to GABAergic signalling, such as GABA receptor subunits, transporters and synthesising enzymes, with increased age in a post-mortem analysis of human cortical tissue[121].

Animal data do reveal changes in inhibitory mechanisms in the brain. For example, age-related reductions in proteins involved in GABA metabolism, such as GABA-synthesising enzyme glutamic acid decarboxylase (GAD)[122], GABA receptors[123], as well as altered $GABA_A$ receptor subunit[124] composition have been observed in the rat auditory cortex. Loss of somatostatin-expressing interneurons in the rat hippocampus has also been reported[125]. Aged cats show loss of inhibitory neurons in the visual cortex[126]. Finally, MRS measurements in primate posterior cingulate cortex detected an age-related decrease of GABA[127]. These animal studies support an age-related decline in inhibition.

MRS provides direct in vivo measurements of GABA levels and therefore can provide valuable insight into the effect of ageing on inhibition in humans. A negative relationship between MRS-measured GABA in the human neocortex and age has been observed, but was only studied up to middle age[85,120]. Another study reported that MRS-measured changes in GABA with age may be due to bulk tissue changes rather than a true decrease in GABA, although this may be region specific[128]. Later, Cassady et al. found a relationship between age and GABA even after accounting for tissue differences in grey matter, white matter, and cerebrospinal fluid[109]. MRS-measured GABA in older adults was also linked to poorer performance on a sensorimotor task, as well as less segregated sensorimotor networks (i.e. weaker functional connectivity within the network but stronger connectivity with other networks)[109]. These results suggest that GABA reduction with age may underlie changes in functional connectivity and worsened motor performance. Several other studies, however, did not find an association between age and GABA in non-motor areas[129,130]. MRS studies thus provide mixed evidence into the relationship between age and GABA; conclusions are made even more difficult due to changes in tissue composition with age.

A recent study performed longitudinal MRS measurements of GABA four years apart in healthy participants. They found no cross-sectional effect of age on GABA, but longitudinally, there was a within-participant reduction in GABA with age[131]. However, the age range of the participants was relatively narrow (65-81 years) so if the decline in GABA started earlier

in some participants, it could explain the lack of significant cross-sectional findings. In addition, they observed that the longitudinal findings were regional, with the sensorimotor cortex showing a significant decrease in GABA[131].

Non-invasive brain stimulation protocols probing M1 inhibition offer conflicting results as to changes in GABA with age. Older adults were found to exhibit stronger inhibition[132], although it can be dependent on orientation of the transcranial magnetic stimulation (TMS) coil[133]. A meta-analysis exploring the effects of ageing on M1 neurophysiology using TMS found an overall reduction in cortical excitability, with mixed findings on inhibition protocols[134]. Associating TMS with MRS GABA measurements did not determine an association between sensorimotor GABA levels and any TMS measure of excitability[135]. They did not see a difference between MRS GABA in older and young adults but found reduced inhibition measured by TMS in older adults[135]. Although TMS findings are mixed, MRS and animal experiment data point to a decline in GABA as an inhibitory neurotransmitter with age. Moreover, age-related declines in cortical inhibition and worsened motor performance can be associated to reduced mobility, increased frailty and overall reduction in well-being[136]. Balance learning in older adults improved balance and increased a TMS measure of intracortical inhibition, and those with largest changes in inhibition also showed greatest improvements in balance[136]. Therefore, age-related neurophysiological changes are closely related to clinically meaningful outcomes.

1.3.3 Changes in oscillations throughout life and disease

Spontaneous oscillations are thought to shift from lower (e.g. theta) to higher (beta) frequencies with age[137–139]. Moreover, the two main bands of oscillatory activity in M1, beta and gamma, both rely on inhibitory networks. Since there is a likely age-related reduction in M1 inhibition, oscillatory activity in both bands should change with age.

Beta

At rest, power of beta activity increases with age[140–142], while peak frequency decreases[142]. This age-related beta frequency decrease is associated with a decline in cortical thickness, which is known to decrease with age[141]. These findings are consistent with an increase in inhibition with age[142], which would be in opposition to my hypothesis of an overall age-related decline in inhibition. One possible explanation for this is that inhibition only represents one aspect of resting beta activity and other processes that change with age may mediate the increase in resting power. Conversely, it could be a compensatory mechanism. Older participants show higher beta activity during postural tests compared to younger adults, suggesting that the observed changes in resting beta may reflect an increased demand in neural activation required to maintain balance and stability at rest, even though cortical resources may be more limited in older adults[143]. These findings also provide a link between age-related changes in beta band activity and functional impairments, such as a decline

postural control, that may contribute to an increased risk of falls in older adults.

As discussed above, when preparing a movement, activity in the beta band decreases (event-related desynchronisation, ERD). After movement termination, beta activity then increases, surpassing baseline levels (event-related synchronisation, ERS) before returning to baseline. ERS power[144–147] and peak frequency[145] both show age-related reductions. In a more complex motor task that requires either switching from bimanual to unimanual movements, older participants exhibited worse performance and larger beta ERS compared to younger participants, which was believed by the authors to be an adaptation mechanism to successfully stop the non-moving hand[147]. Therefore, age-related changes to beta ERS could be task-specific depending on complexity.

In contrast, an age-related increase in ERD power has been consistently shown[140,142,145,146,148,149]. Although older adults exhibit stronger beta ERD relative to baseline compared to younger adults, in terms of absolute power, beta power is still stronger in older adults[140,149]. ERD power has a negative relationship with resting beta power[140], suggesting that ERD is linked to resting beta activity.

Lower beta ERD peak frequency, the frequency that shows the strongest ERD, in the ipsilateral hemisphere of older adults has been observed[142]. Older participants also exhibit more symmetric ERD, while younger participants have a more asymmetric pattern of desynchronisation[150]. These findings point to clear age-related changes in beta during movement.

Exploring age-related changes in beta burst rate revealed increased pre-movement baseline and normalised peak power with higher age[151], which is also consistent with previously mentioned findings of increased resting beta. During movement, there was no significant association between age and burst rate, however, the increased baseline in older participants resulted in stronger ERD as the magnitude of change in pre-movement and movement burst rates was higher compared to younger participants[151], suggesting that age-related changes in ERD may be due to alterations in pre-movement baseline rather than the process of ERD. A decrease in post-movement burst rate comparable to reduced ERS was present[151]. This pattern of age-related changes in beta bursts during movement is in line with conclusions from studies mentioned above that averaged beta ERD over many trials. Post-movement beta bursts were more focal to sensorimotor cortex in younger compared to older participants, and the overall estimated source of beta bursts shifted anteriorly with age[152]. Taking all the evidence together, age-related declines in ERS power and ERD peak frequency and stronger beta ERD seem to occur. Moreover, there may be a change in the localisation of beta activity.

Gamma

The relationship between age and gamma activity has been explored less compared to beta, but there is some evidence for age-related changes in gamma. At rest, a quadratic effect of age on global gamma power has been demonstrated[141]. Moreover, resting gamma power in

sensorimotor networks was negatively predicted by cortical thickness, which decreases with age[141].

Substantial evidence showing age-related changes in gamma activity comes from research on the visual system. Visual gamma peak frequency has been found to reduce with age in participants aged up to 45 years old[99,153–155]. A study encompassing young adults and the elderly also found reduced visual gamma peak frequency, along with a decline in peak power in bands that the authors defined as slow (20-34 Hz) and fast (36-66 Hz) gamma bands[156]. Unlike at rest, lower cortical thickness was associated with age and lower visual gamma peak frequency[155]. In general, visual gamma peak frequency and power seem to decrease with age.

Movement-related gamma peak frequency[66,85] and power[66,145] in the 60-90/60-95 Hz band has also been found to reduce with age. Based on these findings, I would expect an age-related decline in M1 peak frequency and power in both the mid-gamma (60-90 Hz) and slow-gamma (30-60 Hz) bands during movement.

1.4 Aims

In this thesis, I aim to study inhibitory neurotransmission in M1 using a variety of techniques.

First, I provide a summary of the techniques used to acquire data in this thesis in the Methods chapter (Chapter 2): TMS, MEG, and sequencing of genetic polymorphisms.

In the first experimental chapter (Chapter 3), I use the controllable pulse parameter TMS (cTMS), which is the first TMS device to enable changes in pulse shape. I utilise the ability to modulate pulse width to assess whether it is possible to selectively activate inhibitory neurons in M1 by comparing cTMS measures and the performance of participants on motor tasks. I also determine the test-retest reliability of the cTMS measures and the tasks.

In Chapter 4, I investigate age-related changes in movement-related M1 activity in the beta and gamma bands using a big MEG open-access dataset from the Cambridge Centre for Ageing and Neuroscience (CamCAN) repository.

In Chapter 5, I assess the contribution of genetic polymorphisms to the CamCAN MEG data metrics I extracted in Chapter 4.

Lastly, in the General Discussion (Chapter 6), I summarise the results from the three experimental chapters and provide general limitations and future directions based on my findings.

Chapter 2

Methods

In this chapter, I will describe the techniques and methods that I use throughout the thesis.

2.1 Transcranial magnetic stimulation (TMS)

Transcranial magnetic stimulation (TMS) is a form of non-invasive brain stimulation that enables us to indirectly investigate M1 neurophysiology and corticospinal excitability. In this thesis, I determined the test-retest reliability of a TMS measure of corticospinal excitability, the input-output curve slope.

When using TMS, an electromagnetic coil that produces a rapidly changing magnetic field is held on the scalp[157]. If placed over the primary motor cortex (M1), TMS pulses of sufficient strength induce electric currents in the underlying brain tissue, which lead to activation of corticospinal neurons that connect to muscles. TMS pulses can therefore induce activity in the targeted muscles called motor evoked potentials (MEPs), which can be measured using electromyography (EMG) (Figure 2.1A). In my TMS study, I specifically targeted the first dorsal interosseous muscle (FDI) of the left hand by stimulating the right M1 of young, healthy participants.

2.1.1 Single pulse TMS measures global excitability of the motor cortex and corticospinal pathways

One core TMS-related measure of corticospinal excitability is the resting motor threshold (rMT), which is defined as the intensity threshold for TMS at which MEPs can be elicited in the resting muscle in 50 percent of trials. rMT is commonly considered to reflect overall membrane excitability[159,160]. Higher rMTs indicate lower excitability. However, thresholds vary substantially between individuals for a variety of factors other than membrane excitability. Factors such as coil-to-cortex distance[161,162] and age[161] can both considerably affect the rMT. Therefore, rMT alone may not be the best measure to assess changes in brain physiology due to, for example, disease.

Applying different intensities of single TMS pulses enables the acquisition of input-output (IO) curves (Figure 2.1B) that are thought to reflect overall corticospinal excitability[163].

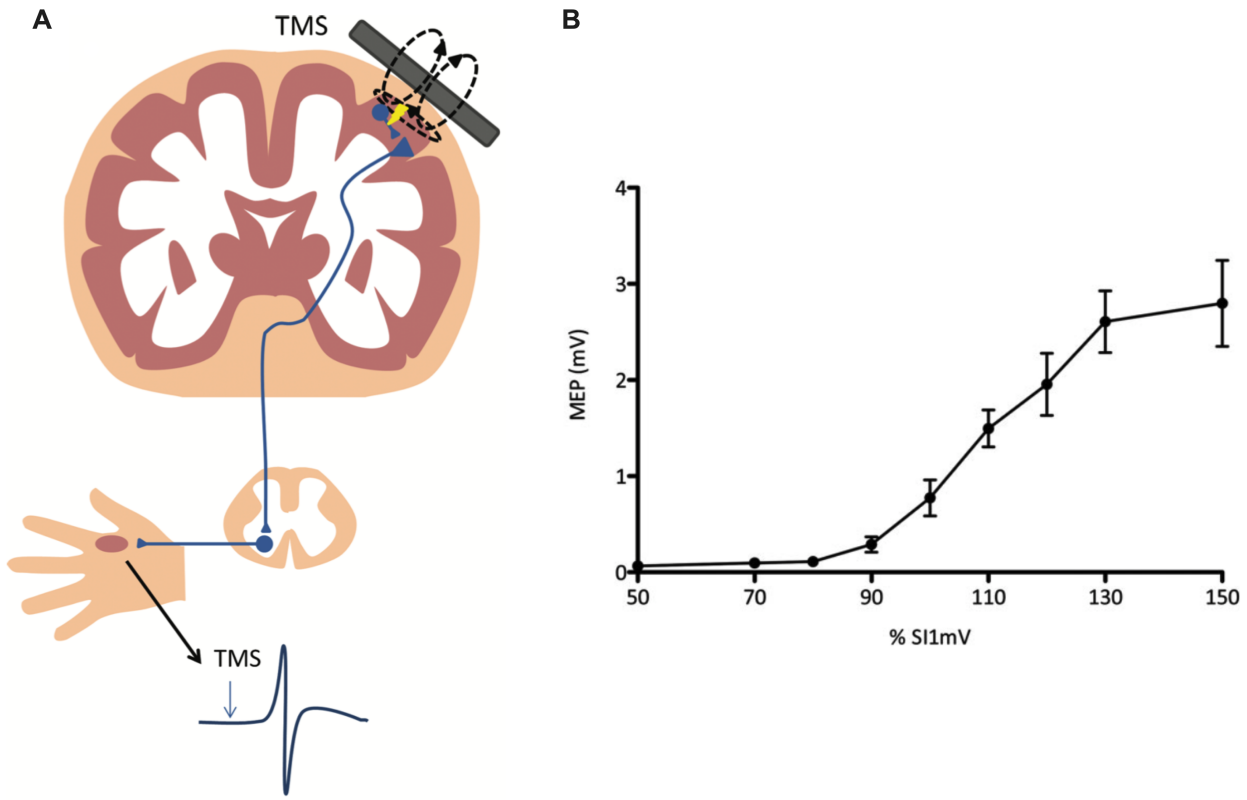


Figure 2.1: Transcranial magnetic stimulation (TMS) and an input-output (IO) curve. A: TMS involves the use of a changing magnetic field to induce electrical currents in cortical neurons. When a magnetic pulse is applied through a coil held over the primary motor cortex, it causes activation of muscles through corticospinal projections. The muscle responses, motor-evoked potentials (MEPs), can be measured by surface electromyography (EMG). The location of muscle activation depends on the region of the motor cortex stimulated. Amplitude of the MEP depends on corticospinal excitability and other factors.[158] B: IO curve is generated by acquiring MEPs at a range of stimulation intensities. The graph shows the relationship between the stimulation intensity relative to the stimulation intensity required to elicit a 1 mV MEP (%SI1mV) and the resulting MEP amplitude.[82]

Since IO curves are acquired at multiple intensities, the trial-to-trial variability common to TMS[164] may be less prominent in IO curves than rMT recordings, which are based on a single stimulus intensity.

MEP amplitude increases with pulse intensity in a sigmoid relationship. The initial segment of the IO curve is flat and increases approximately at the threshold stimulus intensity. The second part, usually corresponding to intensities between 120% and 140% of the rMT, is the steepest and represents an approximately linear relationship between stimulus intensity and MEP[164]. Finally, at intensities greater than approximately 140% relative to the threshold, the IO curves plateau.

The steepness of the slope of an IO curve is commonly used as a marker of corticospinal excitability, with steeper slopes representing increased excitability[163,164] and has been linked to underlying physiological mechanisms. Slopes were shown to reflect magnetic resonance

spectroscopy (MRS)-measured concentration of the excitatory neurotransmitter glutamate in M1[82] and MEP amplitudes at IO curve plateaus to have a negative relationship with glutamate[165]. A linear combination of glutamate and GABA predicted the mean MEP at rMT[165], showing that both neurotransmitters impact the measures of corticospinal excitability. IO curves were found to be influenced by drugs that target GABAergic and monoaminergic systems, as well as sodium and calcium channel function[166]. These studies provide a link between TMS metrics of corticospinal excitability and levels of neurotransmitters that maintain the brain's excitation-inhibition balance.

2.1.2 IO curves are a sensitive measure of changes in corticospinal excitability

IO curves have been used to probe how various processes and diseases affect corticospinal excitability. For instance, IO curve slopes differ in different muscles at rest and can be used to study synergy between muscles[167]. Further, the steepness of IO curve slopes increases when the targeted muscle is undergoing a voluntary contraction during pulse delivery compared to when the muscle is at rest[163,168]. The slope of the IO curve is also steeper when M1 is probed as participants perform a coordinated precision grip compared to a simple abduction task[169], indicating an increase in excitability while performing a more complex movement. Plasticity-induced changes, for instance, due to learning or repetitive TMS (rTMS), can also be measured using IO curve paradigms. After training of a rapid wrist extension task, the slope steepness of an agonist muscle increases, while it decreases in an antagonist muscle[170]. Similarly, the slope steepness increased after both low- and high-frequency plasticity-inducing rTMS[171].

IO curves have been found to change as a result of disease. For example, patients with chronic stroke exhibit lower IO curve plateaus and higher rMT, although there is no difference in the slope between patients and healthy controls[172]. The reduced plateau was associated with worse motor function of the affected hand post-stroke[172]. Higher integrity of corticospinal tracts (i.e., white matter motor pathway) was associated with steeper IO curve slopes in stroke patients[173], indicating that higher corticospinal excitability could be used to predict functional outcomes in stroke survivors. In a different pathology, amyotrophic lateral sclerosis (ALS), patients have steeper IO curves compared to healthy controls[174], suggesting that cortical hyperexcitability may be involved in the disease pathology. Pre-symptomatic carriers of a genetic mutation in SOD-1, a gene implicated in ALS, also have steeper IO curve slopes[174]. Since cortical hyperexcitability precedes symptom development, IO curves could be used as markers of disease progression.

In my TMS study, I used the controllable pulse parameter TMS (cTMS), which is the first TMS device to allow modulation of pulse shape. Specifically, pulse width has a well-documented inverse relationship with threshold for activation, where decreasing the pulse

width increases threshold in both peripheral[175] and central nervous systems[176]. I compared the slopes of IO curves acquired with pulses of different widths to determine whether excitability of neurons changes when modulating the width of TMS pulses.

2.1.3 Approaches for the analysis of IO curves

Two methods are commonly used to acquire IO curves. Pulses of different intensities can be applied in a certain range as a percentage of the absolute maximum stimulator output (%MSO), usually in increments of several percentages of MSO points, either until reaching a plateau of MEP amplitude, 100%MSO, or until participants cannot tolerate the stimulation intensity anymore. However, since the rMT differs between participants, a more efficient method to acquire the whole IO curve in all participants is to derive stimulus intensities from the rMT[164]. A sigmoid line of best fit is then estimated from the resulting MEP amplitudes at varying intensities. Comparing different IO curve acquisition methods in a small population of stroke survivors, but analysing them by converting to %MSO, demonstrated no significant effect of the acquisition method[177].

Further, independent of the acquisition method, there are different ways to fit IO curves, e.g. with either the stimulation intensity on the x axis represented relative to each participant's rMT (%rMT), or the absolute intensity set by the TMS device (%MSO). The previously mentioned Massie and Malcolm study[177] did not investigate the effect of the fitting method, since both data acquisition methods were converted to %MSO . Using %rMT to quantify IO curves may reduce between-subject variability in IO curves, which are influenced by the rMT and therefore by factors that do not necessarily depend on neuronal excitability, such as coil-to-cortex distance[161,162]. However, using %MSO may be more objective, since it is less dependent on acquiring the correct rMT. I am not aware of any comparisons between the curve quantification methods for analysis. Here, I use one acquisition method based on %rMT, but use two analysis approaches to either fit IO curves to stimulation intensities represented by %rMT, or converted to %MSO.

Previous cTMS work has used %MSO to fit IO curves and found differences between the slopes based on pulse width[176,178]. However, they did not report whether they also used %rMT to quantify IO curves or whether the effect of pulse width was present using this method. In my study, I used both IO curve analysis methods to determine whether differences between the two approaches when modulating the pulse width.

2.2 Sensorimotor tasks for evaluation of motor control and learning

Alongside neurophysiological measures, it is important to investigate behaviour and determine how they relate to each other. To probe motor control and motor learning, I employed

two behavioural tasks: an action selection task, and a serial reaction time task.

2.2.1 Action selection task

The action selection task consists of two different types of trials (execute and select blocks) that differentiate execution and the selection of a motor task[179].

In execute blocks, participants respond to the appearance of a visual cue, regardless of the size or shape of the cue, with the press of either their index or middle finger, depending on the instruction at the beginning of the trial. The response time to press the button is used as a measure of motor execution. For select blocks, participants learn a complex rule, based on which they respond to the appearance of a visual cue on a screen and consider the size and shape of the cue to determine whether to use their index or middle finger to press the button. The response time to press the correct button is measured. To determine the time needed for the selection of the correct action, execute block reaction times are subtracted from select block response times. The action selection time represents a purer measure of the time needed for the selection of actions, since the select response time also includes the motor execution time.

Each block type is associated with activity in specific regions of the brain. Motor execution is linked to broad activity in the primary motor, premotor, and parietal cortices[180]. Action selection relies on the premotor-parietal network with more spatially specific activation[180]; the left dorsal premotor cortex (PMd) especially plays a key role in selection of actions[179–183]. In my study using the novel cTMS device, the relationship between TMS and action selection task metrics was assessed to determine whether pulse width modulation may selectively activate neurons in areas linked to performance on the task.

2.2.2 Serial reaction time task

The serial reaction time task (SRTT) is commonly used to measure motor sequence learning.

Participants are instructed to perform a simple movement by pressing a button in a specific sequence, similar to learning a simple piano piece. The sequence of movements is shown through a sequence of visual stimuli, where each stimulus corresponds to a different movement, i.e. instructs a specific finger to press a specific button[1,184,185]. The response times to press the buttons are measured. As participants learn the sequence throughout the task, response times decrease. The task also includes control trials, where participants are shown the visual stimuli in a random order.

Performance on the SRTT relies on different motor areas, such as the supplementary motor area (SMA) and M1[186], although it may also involve perceptual learning due to the visual nature of cues[185]. Moreover, it is hypothesised that changes in inhibition and the levels of GABA could underlie motor learning[1,187]. In my cTMS study, I used the SRTT to determine

if there is an association between motor learning and TMS metrics.

2.3 Magnetoencephalography (MEG)

Although transcranial magnetic stimulation (TMS) and sensorimotor tasks provide valuable information about the neurophysiology of M1 and behaviour, the measures have low temporal resolution - usually, there is only one data point per several seconds. In order to understand neuronal dynamics at a millisecond scale, techniques with higher temporal resolution must be used. One such method is magnetoencephalography (MEG). In this thesis, I used MEG to measure movement-related activity in the beta (13-30 Hz) and gamma (30+ Hz) bands.

2.3.1 MEG measures magnetic fields produced by the brain's electrical events

Neurons in the brain are constantly active; most of the activity is spontaneous and is tightly controlled[24]. Connected populations of neurons are able to synchronise and form complex and dynamic patterns of activity known as neuronal oscillations. MEG works by measuring magnetic fields produced within and between populations of neurons. All individual neurons contribute to the signal detected by MEG, and based on computational models, a minimum of approximately 10,000 to 50,000 neurons are required for MEG to detect the signal[25].

The magnetic fields generated by brain activity detectable by MEG are on the scale of fT (10^{-15} T), which is approximately 10-100 million times smaller than the magnetic field of the Earth[188]. Consequently, MEG sensors need to be highly sensitive, but they also require shielding from the Earth's magnetic field, and so MEG recordings take place in magnetically shielded rooms. Unlike electroencephalography (EEG), the MEG signal is not significantly distorted by the skull, skin, and other tissues, improving spatial resolution[188].

Postsynaptic potentials are considered to be the main contributor to MEG signal, but all currents, including action potentials, generate magnetic fields[189]. The elongated morphology of pyramidal neuron axons[25], and their orientation relative to the cortical surface[190], enables the generation of stronger magnetic fields. Therefore, the large output pyramidal neurons in layer 5 of M1 may contribute more to MEG signal than neurons with more symmetrical morphologies. A study that performed parallel MEG and in vitro recordings revealed MEG signal is consistent with a mixture of outputs from cortical layers 3 and 5, and that the same cortical area can give rise to activity at multiple frequencies[79]. MEG signal corresponding to desynchronisation in the beta band (15-25 Hz) and synchronisation in the gamma band (55-70 Hz) has been found to be spatio-temporally aligned with the functional magnetic resonance imaging (fMRI) marker of neuronal activity, the blood-oxygen-level-dependent (BOLD) response[191,192].

The first recording of magnetic fields produced by the brain was performed by David Cohen in the 1960s using a single magnetic detector[193]. Since then, the technology of MEG detectors has rapidly advanced through the development of sensors named superconducting interference devices (SQUIDs). SQUIDs are extremely sensitive devices which detect and amplify tiny magnetic fields and convert them to recordable electric signals[188]. SQUIDs are cooled with liquid helium to almost -270°C to maintain their superconductivity.

The SQUID MEG system used in the studies described in this thesis was made by Elekta (now MEGIN). Their system consists of 102 sensor elements, each containing three simultaneously sampling separate channels: one magnetometer and two planar gradiometers, resulting in 306 independent channels over the whole head. Magnetometers are more sensitive sensors than planar gradiometers and are able to detect magnetic fields from deeper regions of the brain, however, their increased sensitivity also makes them more susceptible to detecting noise[194]. Magnetometers are most sensitive to perpendicular magnetic fields[194], so they mostly measure activity from cortical gyri[189] (Figure 2.2). Planar gradiometers are most sensitive to signals closer to the surface and are more robust to noise[194], therefore improving signal quality[188]. Since SQUID sensors are contained within a helmet and are not attached to the scalp, the distance from the sensors to the neural sources in the brain can affect the measured MEG signal. Therefore, the position of the head is usually monitored with head position indicator (HPI) coils[188].

A recent innovation in MEG technology is the development of optically pumped magnetometers (OPMs). These sensors work on the basis of detecting changes in properties of alkali metal vapours when exposed to magnetic fields[196]. Because OPM sensors do not require helium cooling, they are attached to a wearable and portable helmet. This could lead to many novel insights into changes in the brain during natural and more complex movement compared to what is possible in a conventional MEG scanner, where even small head movements can affect data quality and signal-to-noise ratio. Moreover, it may enable the participation of children or patients who find the position in a conventional MEG scanner uncomfortable, who struggle staying still, or experience claustrophobia.

2.3.2 MEG analysis approaches

The typical output signal of MEG is a continuous variation of the magnetic fields in the brain, measured by the 306 sensors. There are several ways to analyse these signals, one approach being to use the data directly measured by the sensors. Sensor space analysis is relatively fast, straight-forward, and provides a direct representation of the measured magnetic fields[197,198]. However, since head size and head position differ between every participant and the measured MEG signal depends on distance from the sensor, it may not be possible to make definite between-subject comparisons. It may also be difficult to interpret sensor space data because data from each sensor contains overlapping signals from the brain areas[199]. Sensor level measurements are therefore not independent from each other.

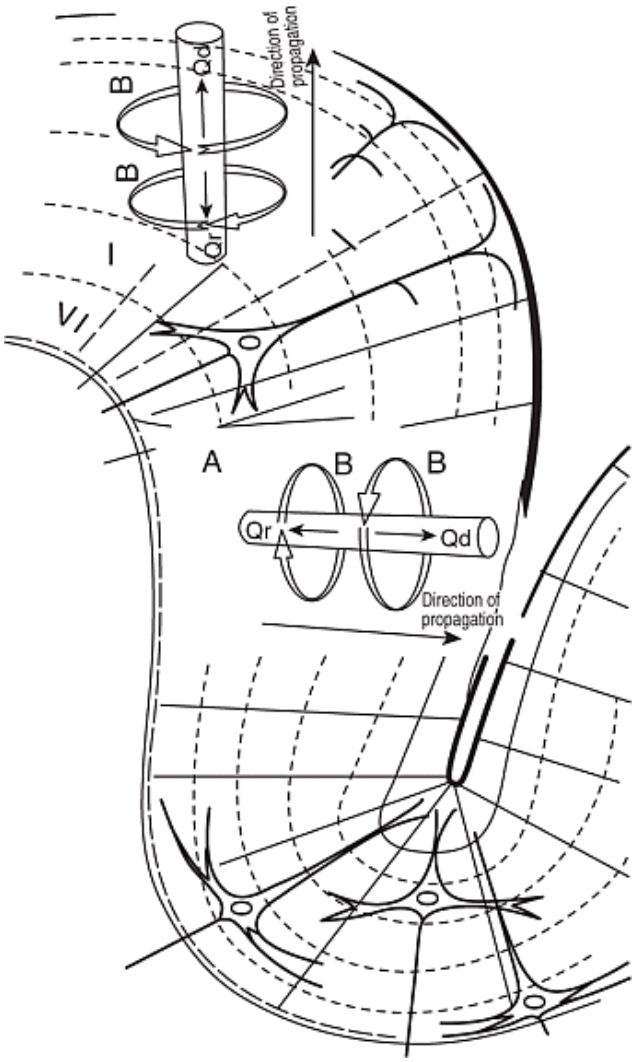


Figure 2.2: Magnetic fields generated in the cortex. Neuronal activity within cortical columns in sulcal walls generate tangential magnetic fields detectable by MEG. In contrast, activity at the top of gyral crowns induces radial magnetic fields, which can not be detected by MEG. Therefore, most activity detected by MEG is activity from neurons orientated perpendicularly to the skull. Figure from Henson et al. [195].

Source level analysis

Active sites in the brain need to be determined from externally recorded magnetic fields. The inverse problem refers to the theoretically infinite number of sources in the brain, making the accurate identification of source challenging [189,200]. Source reconstruction is used to estimate the neural sources of the signal. In addition to overlapping measurements at various sensors, source reconstruction also needs to consider that multiple neural sources could generate the same magnetic fields recorded by MEG based on their configuration [197]. In addition, some neurons can not produce signals measurable by MEG due to their location or orientation. Various approaches have been developed to optimise constrained estimates of neural sources of signals although there is no universal approach, as each is limited by a different set of assumptions, which can also introduce biases [197,199,201]. For more precise and accurate source

reconstruction, individual structural MRI scans are recommended to create a model of the head so that MEG data can be aligned to each participant's anatomical brain structure, further increasing the cost of MEG experiments. MNI152 standard-space T1-weighted average structural template images can be used if MRI scans are not possible to obtain. Although source level analysis is more computationally demanding compared to sensor level, it also provides a higher signal-to-noise ratio, enables the mapping of activity onto brain structures and creates a standardized space, making between-subject comparisons easier.

There are two widely used categories of source localisation methods: minimum norm estimation (MNE), and linearly constrained minimum variance (LCMV) beamformers. MNE fits source distribution that best describes the measured data, while minimising the overall power. It assumes a Gaussian distribution for noise[202]. LCMV beamformer uses spatial filters to estimate source activity at a specific location while suppressing activity from other locations; it assumes that sources at different locations are uncorrelated and that noise is not correlated with the sources[202]. In the MEG study in this thesis, I only look at movement-related activity in the primary motor cortex, so I utilised the LCMV beamformer[203] because it is effective at reducing activity from other brain regions. LCMV beamformers are also more stable with varying levels of signal-to-noise ratio[202,204], which was important with a large dataset and a separate analysis for each of the frequency bands of interest.

Time-frequency analysis of epoched MEG data

Following source reconstruction, the MEG signal is still continuous and covers the entire duration of the recording. However, many MEG paradigms, including the study in this thesis, consist of performing tasks. In these cases, most experimenters are interested in the times before, during, and after each trial (epoch). There are multiple approaches to analysing task MEG data. Because averaging trials can cancel out between-trial variability, techniques such as the continuous wavelet transform can be used to evaluate signals that may not be fully time-locked to the task[205]. However, averaging trials increases the signal-to-noise ratio[205], so it can be advantageous for weaker signals. Event-related fields (ERFs) are one method of analysing averaged epoched data, typically resulting in a waveform showing a change in magnetic fields over a specific time frame, although they do not provide any information in the frequency domain.

The conventional method to study frequency spectra is to perform a time-frequency analysis, which examines both the time and frequency domains. Time-frequency analysis detects changes in power in response to an event in a pre-defined frequency spectrum and time window, and decomposes the signal into its constituent frequencies over time. It is most useful to visualise event-related power changes such as synchronisation (ERS) and desynchronisation (ERD). There are multiple approaches to calculate power changes in the time-frequency domain[206]. In this thesis, , since I analysed each band separately, I used a discrete prolate spheroidal sequences (DPSS)-based multitaper[207], which is very effective in reducing leakage

between different frequency bands. I used this approach to investigate age-related changes in primary motor cortex activity in the beta and gamma frequency bands that occur relative to button presses.

2.4 Single nucleotide polymorphisms (SNPs)

Genes are the basic units of genetic inheritance that are passed on from parents to their offspring. They represent long sections of deoxyribonucleic acid (DNA). Each gene can be transcribed and translated into proteins.

DNA is made up of four basic building blocks called nucleotides which contain nitrogenous bases: adenine (A), cytosine (C), guanine (G), and thymine (T). DNA consists of two strands that are held together by bonds formed by pairs of bases in a combination of A and T, or C and G (Figure 2.3). Genes can range from 100 to several million base pairs in length[208]. Proteins consist of up to twenty unique amino acids, and each amino acid is encoded by a different combination of three nitrogenous bases.

Proteins have many different functions, so variations (mutations) in the gene encoding them can affect the function of the protein. Some common variations in base pairs of genes include large-scale changes in DNA such as insertions, deletions, and duplications, but the most common type are single nucleotide polymorphisms (SNPs)[209]. SNPs are genomic variations that involve a substitution in only one base pair. The two possible bases at a certain SNP are called alleles. To be classified as a SNP, the variant must be present in more than 1% of the population. The more frequent allele is referred to as major, and the less common is the minor allele.

Over 80 million SNPs have been identified in the human genome[210]. Although some SNPs are

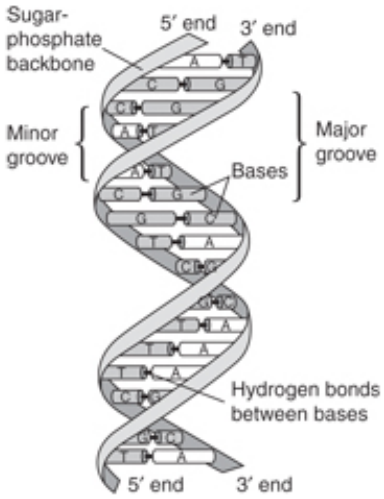


Figure 2.3: DNA double helix. Figure from Fletcher and Hickey[208].

found within the coding regions of genes and can influence the amino acid composition of the resulting protein, most SNPs are located outside genes, in non-coding DNA, and are known as silent SNPs[209,211]. The silent SNPs can alter the expression of the gene by influencing promoter affinity, or the stability and localisation of transcribed messenger ribonucleic acid (mRNA) or translated proteins. These variations can carry a protective effect from a certain trait or disorder, but they can also be associated with a risk of developing a trait or a disease.

SNPs can associated with the risk of developing disorders like glioma[212], breast cancer[213], Alzheimer's disease[214], and various psychiatric disorders including major depressive disorder, schizophrenia and bipolar disorder[215]. However, SNPs may also influence phenotypes such as height and hair texture[211]. In this thesis, I will study the contribution of SNPs to metrics of MEG-measured movement-related gamma band activity. Gamma band activity is a highly heritable trait; the heritability of visually-induced gamma-band peak frequency has been shown to be approximately 91% in twins[216], but the genes that contribute to the variation in gamma oscillations have not been determined yet.

2.4.1 Genetic sequencing

Over the past decades, sequencing technology has rapidly advanced and now enables efficient, automated, relatively low-cost, and large-scale sequencing of whole genomes. The genetic dataset I analysed in this thesis was sequenced using a bead-based microarray. These arrays have very small silica microbeads coated with oligonucleotides specific to various locations in the genome[217]. After a DNA sample is added to the microarray probe, it binds to the oligonucleotides that are designed to stop one base before the SNP site of interest[218]. Fluorescently labelled single nucleotides are then washed over the microarray, allowing the determination of the allele[218]. The specific microarray used for sequencing in this thesis is the Illumina Infinium OmniExpressExome chip, which covers almost one million markers throughout the genome[219]. This allowed me to select SNPs of interest from a large variety of candidate genes available. The influence of the genotype of the selected SNPs on movement-related MEG metrics was then assessed.

Chapter 3

Determining the test-retest reliability of cTMS metrics

3.1 Introduction

3.1.1 Novel cTMS device allows greater control of pulses delivered

Transcranial magnetic stimulation (TMS) is a non-invasive brain stimulation method that can be used to probe brain and corticospinal activity using magnetic pulses. Conventional TMS devices produce pulses to which large-diameter myelinated axons of pyramidal cells are thought to be more susceptible compared to smaller, non-myelinated axons of interneurons[220]. In the peripheral nervous system, modulation of pulse width has been used to study strength-duration properties of different populations of nerves for decades[221–223]. Thus, modulating TMS pulse width to selectively activate different primary motor cortical (M1) neuronal populations could bring novel insights into the links between TMS metrics and M1 neurophysiology. However, only a recent advance in TMS technology, the **controllable pulse parameter TMS (cTMS) device**, enables the adjustment of various pulse parameters, including the pulse width[224–226].

3.1.2 Strength-duration properties reveal neurophysiological properties of recruited neuronal populations

Whether a TMS pulse is able to induce an action potential in a given neuronal axon depends on various stimulus parameters. The excitability properties of neurons can be described by their strength-duration relationship by measuring the minimum stimulus strength (intensity) at various durations (widths) of a pulse necessary to activate a neuron (Figure 3.1A). Two measures can be derived from the strength-duration curve for a given neuron: rheobase and chronaxie. Rheobase is defined as the minimum pulse intensity that leads to the generation of an action potential. Chronaxie (strength-duration time constant) is the pulse width required for neuronal activation with the strength of a pulse set at double that of the rheobase.

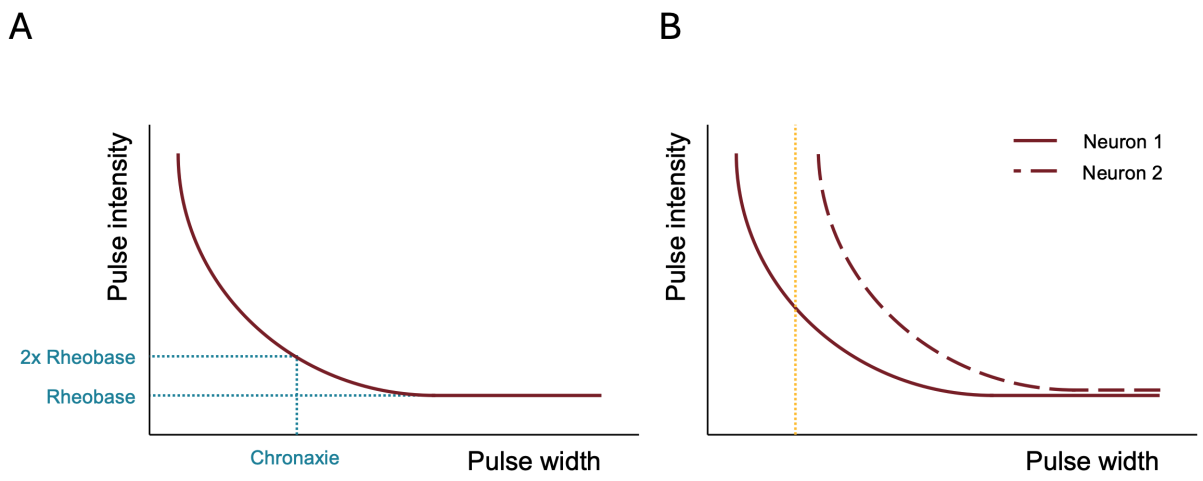


Figure 3.1: Strength-duration relationship. A: Rheobase and chronaxie can be derived from the strength-duration curve. Rheobase is the minimum pulse strength required for neuronal activation. Chronaxie (strength-duration time constant) is the pulse width required to produce a response at double the strength of the rheobase. B: Strength-duration properties of neuron 1 (solid line) and neuron 2 (dashed line) allow their selective activation. If pulse width is shorter than the yellow dotted line, supra-threshold stimuli would result only in activation of neuron 1, but not neuron 2.

For neurons that have similar rheobases, the chronaxie provides a relative measure of their excitability, with more excitable neurons exhibiting lower chronaxie[227]. These properties may enable selective recruitment of different neuronal populations (Figure 3.1B).

Various factors determine strength-duration measures. The dependence of recruitment of peripheral nerves on axon diameter was one of the first properties explored. Thinner axons exhibit higher activation thresholds, i.e. higher intensities are required to activate thinner axons,[221,228–230]. The threshold stimulus strength is inversely proportional to the square of the axon diameter[221,230]. Strength-duration curves shift downward with increasing axon diameter[221], but also depending on the axon length for axons of the same diameter. Shorter axons exhibit higher excitability in models of central neurons, especially when applying short magnetic pulses[230]. Therefore, both the length and diameter of axons may play a role in determining their strength-duration properties.

Electrical stimulation of peripheral nerves in human participant can be utilised to compare the strength-duration properties of known peripheral nerve fibre types such as sensory and motor nerves. Larger sensory fibres were preferentially activated over smaller motor fibres except at short stimuli, where the relationship was reversed[228]. Although fibre diameter underlies differences in thresholds, it does not explain the diverging recruitment of the two nerve types at short pulse widths, which was hypothesised to be due to different chronaxies of the nerve fibres[228]. A higher rheobase and shorter chronaxie of motor fibres over sensory fibres were also confirmed by a later study[231].

The chronaxie is thought to be a measure of membrane excitability at the nodes of Ranvier[222],

the gaps in myelin along axons that propagate action potentials. The chronaxie likely reflects both the passive membrane time constant, which is determined by the resistance and capacitance properties of membrane, and the contribution of a non-classical voltage-dependent sodium channel that is active at rest[232,233]. Therefore, differences in chronaxies between peripheral nerve fibre types may reflect differential ion channel expression[222,231,232]. Indeed, sensory fibres are likely to have a higher representation of persistent sodium channels compared to motor fibres[234]. These persistent sodium channels are also widely present in the nodes of Ranvier of neurons in the central nervous system[235], not just in the peripheral nerves, and therefore may determine chronaxies of neurons in the brain.

Different parameters may influence the chronaxie. In the monkey primary visual cortex, chronaxie is lower in deeper cortical layers than in those closer to the surface[236]. Along the same peripheral nerve fibre, the chronaxie is constant at different sites[222], but can change with disease. For example, chronaxie increases with demyelination[231]. Compared to healthy controls, patients with the neurodegenerative disorder amyotrophic lateral sclerosis (ALS) exhibit a longer peripheral motor fibre chronaxie and a lower rheobase relative to the rheobase of sensory fibres[234]. This is likely because motor axons of ALS patients have more persistent sodium conductance compared to healthy controls[234], which has been further supported by animal studies. In a mouse model of ALS, an age-dependent change in cell body expression of persistent sodium channels leads to hyperexcitability of layer 5 pyramidal neurons in the motor cortex, but not other cortical areas[237]. In summary, the chronaxie is a measure of neuronal excitability sensitive enough to detect changes in channel expression determining neuronal membrane excitability on a scale of whole neurons and nerves.

3.1.3 Activation of inhibitory interneurons

A recent study modelling peripheral activation by magnetic stimulation concluded that selective neuronal stimulation based on axon diameter is not influenced by pulse shape or width[229], contrary to previous studies listed above. Thinner axons only showed a slight dependence on pulse width when stimulated by shorter electromagnetic stimuli. However, they found that the threshold for activation of an axon with a diameter of 5.7 μm was six times higher compared to an axon with a diameter of 16 μm[229]. The authors hypothesised it was unlikely that the smaller axons could be activated by transcranial magnetic stimulation, as the intensities required to activate them would probably be beyond the maximum output of TMS devices[229]. However, TMS likely activates a mixture of different cell types[238,239] and many factors other than axon diameter, such as the axonal arbour (branching at the ends of axons) size, myelination and sodium channel expression may influence excitability of neurons and their activation based on chosen pulse parameters.

Even though inhibitory neurons are generally smaller than excitatory neurons[239–241], a study that used realistic morphology of neurons to model TMS-evoked activation of neurons found the threshold and chronaxie of interneurons in layer 4 to be similar to those of excitatory layer

5 pyramidal neurons[242]. However, sub-threshold stimuli are conventionally used to selectively activate inhibitory interneurons when paired with a supra-threshold pulse in the short-interval intracortical inhibition (SICI) protocol[243], which should not be possible with such similar strength-duration properties of inhibitory and excitatory neurons. Therefore, the model may not accurately reflect the entirety of interneuronal strength-duration properties and may have overestimated the chronaxie of inhibitory interneurons. Considering the hypothesized sub-threshold activation of interneurons, it is plausible to believe their thresholds and chronaxie would be lower than those of pyramidal neurons.

The neurophysiological properties of interneurons (e.g. high myelination) make them a likely candidate for TMS-based activation. In animal neocortical[244,245] and hippocampal regions[245], a large fraction of myelin ensheathes axons of parvalbumin-positive (PV) inhibitory neurons. Increased myelination has been linked to reduced activation thresholds, particularly for shorter pulses[238]. Moreover, inhibitory interneurons have extensive axonal arbours[246] and modelling has shown that axonal arbour diameter and threshold are negatively related[238]. Axonal terminals, which are found at the ends of the axonal arbours, are considered to be the main site of activation by TMS pulses[239].Therefore, the extensive axonal arbours of interneurons may make them particularly susceptible to activation by TMS.

There are many subtypes of cortical interneurons with different physiological properties[247] that may affect their response to TMS. We lack experimental measurements of strength-duration properties of cortical interneurons[239] that could provide more insight into the optimal pulse parameters to specifically activate interneurons by TMS rather than other neuronal types. However, I hypothesise that the properties of interneurons listed here may allow them to be selectively recruited by modulating TMS pulse width.

3.1.4 cTMS may enable selective recruitment of different neuronal types

The cTMS device provides the first opportunity to modulate the pulse width (Figure 3.2A), enabling characterisation of the central strength-duration relationship in humans non-invasively for the first time. Similar to peripheral studies[175,222,248], decreasing cTMS pulse width also leads to an increased motor threshold (MT)[176,178,224,249,250]. In addition, input-output (IO) curve slopes, which are widely used as a marker of corticospinal excitability, increase as a function of pulse width[176,178] (Figure 3.2B). These results indicate that the excitability of neurons recruited by changing pulse widths differs. cTMS IO curve slopes are inversely proportional to MT both within and across pulse widths[176]. In the peripheral nervous system, increasing pulse width also increases the slope of recruitment curves, suggesting that short pulses increase the threshold difference between different diameter nerve fibres[175].

I hypothesise that shorter pulses may activate inhibitory interneurons more selectively. This is because shorter width pulses are spatially more selective[248,251,252], and may more prefer-

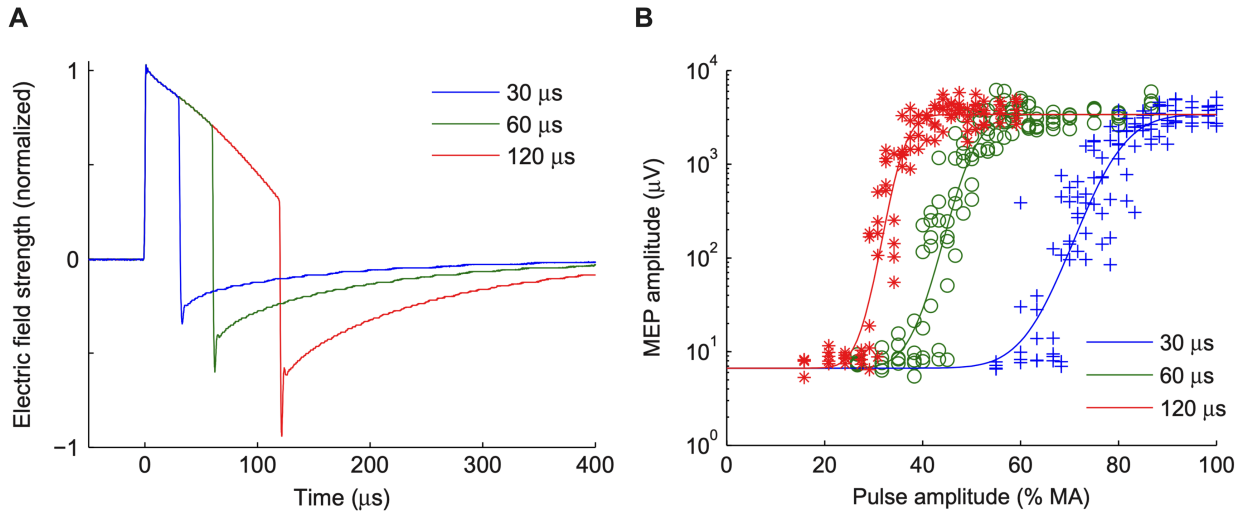


Figure 3.2: cTMS pulses and IO curves. A: Waveforms for pulses of three different pulse widths: 30, 60, and 120 μs.[176] B: IO curves generated by pulses of the same widths. Each marker represents individual MEP.[176]

ably recruit smaller diameter neurons[229]. Further, inhibitory interneurons have properties resulting in reduced activation thresholds especially for shorter pulses[238,239] (e.g. strong and frequent inputs[253], large axonal arbours and extensive myelination).

cTMS is the first device that is able to generate pulses as short as 30 μs. Some common conventional TMS devices are Magstim Bistim^2 and Deymed DuoMag MP for which the widths of the first positive phase of the pulse are 82[254], and 100 μs[255], respectively. The use of cTMS to enable selective recruitment of neurons is clinically relevant, since interneurons are hypothesised to be among the first neuronal populations to be lost in the neurodegenerative disorder amyotrophic lateral sclerosis (ALS)[256,257]. Therefore, shorter pulses generated by cTMS may facilitate novel insights into M1 neurophysiology in health and disease.

3.1.5 Aims

cTMS is a novel device, and only several are used worldwide, which is why its test-retest reliability is unknown. However, measures of test-retest reliability are very important to validate TMS outcomes, which are generally known to have high variability[258]. To close this gap, my first aim was to conduct a study to determine test-retest reliability of IO curves over two sessions. In addition, I investigated cTMS in relation to motor learning. Since motor learning depends on changes in inhibition in M1 (described in more detail in chapter 1) and I hypothesised that inhibitory neurons may be selectively recruited by shorter pulses, motor performance and learning was measured. I hypothesised a relationship between metrics from IO curves and motor task performance would depend on pulse widths. Finally, I compared two approaches to analyse IO curves (described in more detail in chapter 2) to evaluate whether the effect of pulse width on IO curve slope previously described is true with both

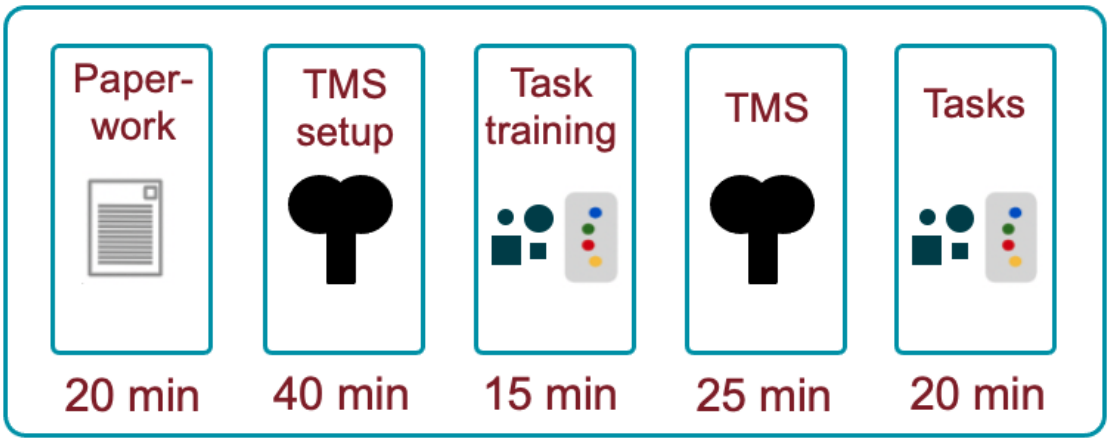


Figure 3.3: Study design. The study session started with initial paperwork consisting of the consent, brain stimulation safety screening, and handedness forms. Then, TMS was configured as described in section 3.2.3, including finding hotspot and motor thresholds. The participants were then familiarised with two motor tasks. TMS IO curve data was then acquired, followed by completing the two tasks.

approaches.

3.2 Methods

3.2.1 Participants

All participants gave informed consent to every experimental procedure, as approved by the Central University Research Ethics Committee (reference: R74764/RE004). 27 healthy right-handed (determined by the Edinburgh Handedness Inventory[259]) volunteers aged 18-35 took part in the study. However, we were not able to elicit reliable muscle responses with the cTMS in one participant, who was therefore excluded. Another participant had a very high resting motor threshold. Three participants were unable to complete the second session in time. Data from these five participants was excluded from all analysis described here. Data from the remaining 22 participants (mean age 24.18 ± standard deviation (SD) 3.83, 13 females) was used for further analysis.

3.2.2 Experimental design

This study had a within-subject design with experiments performed on two separate sessions to investigate the test-retest reliability of the controllable pulse parameter TMS (cTMS) device metrics. Participants attended two sessions at least one week, but not more than two months, apart. The protocol for both sessions was identical, taking approximately 2 hours in total (Figure 3.3) and starting at the same time of day. Sessions were on on average 11.5 days apart (mean ± SD 6.3).

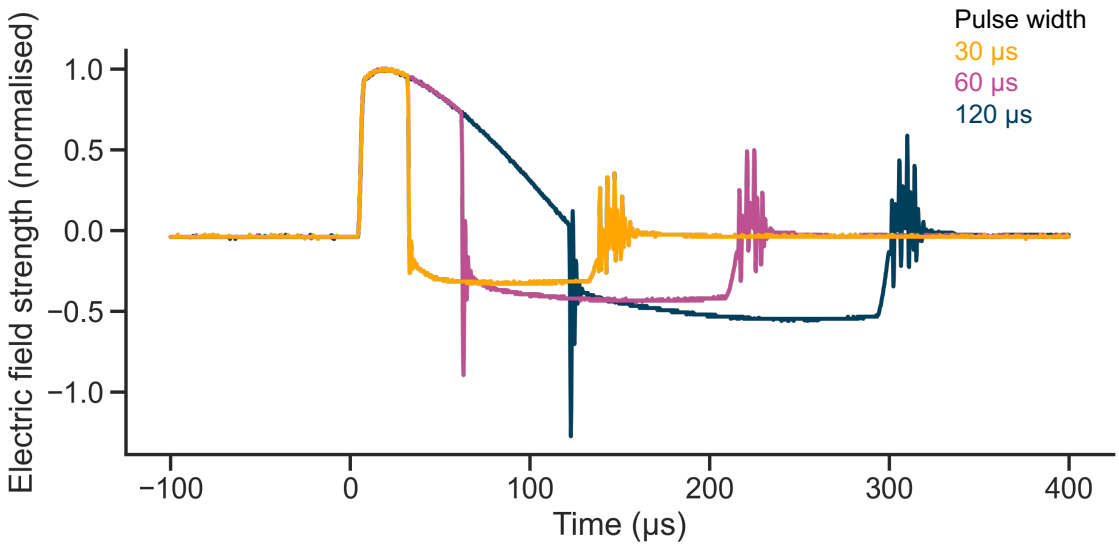


Figure 3.4: Electric field waveforms of cTMS pulses recorded with a search coil. Ripple at the end of the negative phase of pulses is a recording artefact.

3.2.3 TMS data acquisition

Neurophysiological assessment was performed using cTMS (also known as ElevateTMS; Rogue Research Inc). The cTMS allows independent control of pulse width[225]. Three pulse widths were used: 30, 60, and 120 μs[176,178] (Figure 3.4). The pulse width refers to the width of the positive phase of the pulse. M-ratio of 0.2 was used to create monophasic pulses[249].

Surface electromyography (EMG) was recorded using 30 mm disposable adhesive gel disc electrodes (Cardinal Health Inc) placed in a muscle belly-tendon montage over the left first dorsal interosseous (FDI) muscle with the ground electrode placed over the ulnar styloid process. Signals were sampled at 5000 Hz, amplified, and filtered (5-1000 Hz) using a D440-4 amplifier (Digitimer Ltd). Power line noise at 50 Hz was reduced using a Mains Noise Eliminator (Digitimer Ltd). The EMG signal was converted using a Micro1401-4 analogue-to-digital converter (Cambridge Electronic Design Ltd) and recorded using Signal 7.06 software (Cambridge Electronic Design Ltd).

The participants were seated on a comfortable chair. The right primary motor cortex (M1) hotspot for the FDI was targeted, comprising the position where the highest motor evoked potentials (MEPs) could be elicited alongside localised twitches in the left FDI muscle at the lowest stimulation intensity using 120 μs pulses. The TMS coil was held at 45° to the midsagittal line with the handle pointing posteriorly. The Brainsight Neuronavigation System (Rogue Research Inc) was used during the session to track coil position and maintain precise targeting of the hotspot.

The resting motor threshold (rMT) was defined as the lowest stimulation intensity that

evoked MEPs 50 μV or larger in at least 5 out of 10 trials[164]. rMT was determined at the hotspot for the three pulse widths in a randomised order, which was reversed for the second session.

Input-output (IO) curves were obtained for each pulse width by delivering stimulation at pulse intensities ranging from 80% to 150% relative to the rMT in 10% increments. For each combination of pulse intensity and width, ten pulses were delivered. IO curves for the different pulse widths were acquired sequentially, using a randomised order. For each pulse width, the order of pulse intensities applied was randomised, and pulses at each intensity were delivered in groups of 10 with an inter-stimulus interval of 5 seconds. If any intensity relative to a participant's threshold exceeded the maximum stimulator output (%MSO), that intensity was omitted only for that pulse width. Orders of pulse intensities and widths were reversed for the second session.

3.2.4 TMS data analysis

EMG analysis was performed using Python 3.7.11.

Every frame was automatically checked for contraction in muscle preceding the TMS pulse. Frames in which root mean square (RMS) of the EMG amplitude exceeded 0.01 mV in 80 ms preceding the pulse (overall mean 1.59 frames per IO curve) were excluded from further analysis. Peak-to-peak amplitudes of all MEPs were measured and log-transformed to normalise the MEP distribution[176]. For each combination of pulse intensity and width, outliers were excluded by detecting frames with MEPs that were outside 2 standard deviations of the mean MEP amplitude[184] (mean 3.46 frames per IO curve were excluded). The mean MEP amplitude was calculated from the remaining MEPs.

Quantifying IO curves

A sigmoid curve of best fit to the mean MEP amplitudes as a function of maximum stimulator output was determined by the Python SciPy library[260] using the Boltzmann function[163]:

$$\text{y (s)} = \text{Bottom} + \frac{\text{Top - Bottom}}{1 + e^{\frac{\text{S50 - s}}{\text{k}}}}$$

I used two methods of fitting the curves, where s either represented the stimulation intensity in terms of the absolute percentage of maximum stimulator output (%MSO), or the relative value of the rMT individualised to every participant (%rMT). s was limited to the minimum intensity acquired - 10% of rMT, and to the maximum intensity acquired + 10% rMT. *Bottom* and Top refer to the bottom and top plateaus of the sigmoid curve, respectively, and $S50$ is the stimulation intensity (s) that produces an MEP halfway between the bottom and top plateaus. The inverse of the sigmoid curve k ($1/k$) representing the steepness of the rising phase of the curve[163] was used in further analysis as slope. Higher values represent steeper

slopes.

If excluding frames due to either pre-contraction or outlier detection resulted in less than 6 frames per condition, this condition was excluded since at least 5-6 MEPs per condition should be recorded according to TMS guidelines for clinical use[261]. If this criterion resulted in 4 or fewer intensities per IO curve, that IO curve was excluded. In total, data from 4 curves were removed because 4 or fewer intensities remained. If 5 intensities remained, the IO curves were manually inspected. There were 8 curves with 5 intensities each. If the 5 intensities represented a good spread of intensities sampling the IO curve, where a plateau was visible, those IO curves were kept, which happened in 6 out of 8 instances. The remaining two IO curves did not have a good spread of intensities and they were excluded. Data were also excluded for an IO curve if a sigmoid line of best fit could not be quantified (3 cases). All of these scenarios are shown in the Appendix.

3.2.5 Motor tasks

Action selection task

The action selection (AS) task was adapted from a previous study[179] and was run in PsychoPy v1.85.6. The AS task measures participants' response times when executing and selecting movements. Participants were instructed to use their left middle and index fingers to press buttons 1 ("o" button on the keyboard) and 2 ("p") respectively on a laptop keyboard (Dell Latitude E5540).

The task consisted of execute (EB) and select (SB) blocks. In EB, participants were instructed to respond to a cue by either pressing button 1 or 2, for any cue shape or size. In SB, participants were instructed to press button 1 if a small square or a big circle appeared, and button 2 if a small circle or big square appeared (Figure 3.5A). The task had 4 blocks (2 EB, 2 SB) in a random order. Each block consisted of 34 trials. Participants were familiarised with a shorter version of the task prior to completing the full task (5 trials/block x 4 blocks) (Figure 3.3). Participants were asked to respond as quickly and accurately as possible.

Serial reaction time task

An explicit serial reaction time task (SRTT) was based on a previous study[184] as a measure of motor learning. Participants were instructed to use their left little, ring, middle, and index fingers to press buttons on a button box (Current Designs Inc) in response to a cue.

SRTT was run on Matlab 2019a using Psychtoolbox version 3.0.13. The task started with a presentation of four dashes on the screen, one of which was replaced with a circle that instructed participants to press the corresponding button. The speed was self-paced. There were two types of blocks: random and sequence. Random blocks had 48 trials during which the order of visual cues was random, so that the participants could not anticipate the position

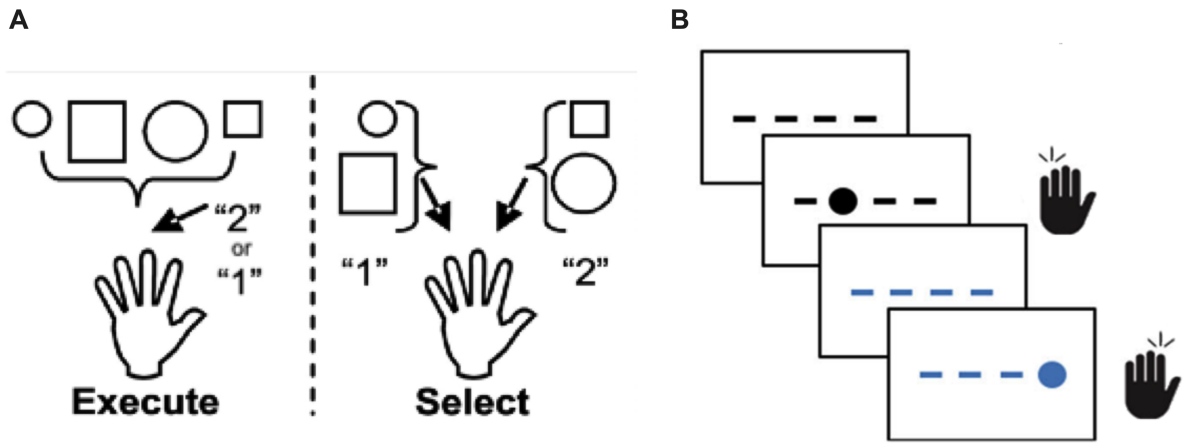


Figure 3.5: Motor tasks. A: Action selection task.[179] B: Serial reaction time task.[184]

of the next button press. Sequence blocks consisted of 4 repeats of a 12-button sequence which stayed the same throughout the session. There were two random blocks, one at the beginning and one at the end with 10 sequence blocks in between. Information about the type of block appeared on the screen prior to the start of each block. The blocks were also colour-coded, random cues were black, while sequence blocks had blue cues (Figure 3.5B). Participants were asked to respond as quickly and accurately as possible and to press the button only after a cue appeared on the screen.

Two sequences were used with a different sequence in each session (sequence 1: 342131241324, sequence 2: 231434124213). The order of sequences (sequence 1, sequence 2) was randomised for every participant. Participants were familiarised with a shorter version of the task containing one random block prior to the full task (Figure 3.3).

3.2.6 Motor task data analysis

Motor task analysis was performed in Matlab 2021a.

Action selection

Response times (RTs) were calculated from Execute (EB) and Select (SB) trials with the correct response as the time between stimulus onset and button press. RTs that were outside 2.7 standard deviations from the mean RT for each type of trial were excluded from further analysis. The median RT for each trial type was then calculated. The metrics used in statistical analysis were median Execute RTs and Action selection times, which were calculated by subtracting the median Execute RT from the median Select RT as a measure of pure action selection time.

Serial reaction time task

RTs were calculated from random and sequence trials with the correct response as the time between stimulus onset and button press. RTs that were outside 2.7 standard deviations from the mean RT for each type of trial were excluded from further analysis. The median RTs for each block were calculated. Linear lines of best fit were fitted to the median RTs of sequence blocks as a metric of learning.

3.2.7 Statistical analysis

A multiple comparisons mixed-effects analysis was used to compare slopes of IO curves acquired with different pulse widths over the two sessions. Spearman's correlations were conducted to test relationships between slopes of IO curves acquired using different pulse widths and performance in motor tasks in session 1. Both tests were performed in GraphPad Prism 9.

Test-retest reliability

Analysis was performed using the Python Pingouin 0.2.1 package[262].

Test-retest reliability was measured through multiple metrics, all providing different information about reliability. The first metric was the two-way random effects, single-score absolute agreement, intraclass correlation coefficient (ICC2,1) with its 95% confidence intervals, which measure the proportion of variance attributable to different measurements and inform us of how well we can distinguish between individuals based on those measurements[263]. High ICC values (> 0.75) indicate good reliability[264].

The second metric was the standard error of measurement (SEM), which assesses agreement between repeated measurements[265,266]. Low SEM values indicate good agreement. SEM was calculated using the following equation[265]:

$$\text{SEM} = \frac{\text{standard deviation of difference between sessions}}{\sqrt{2}}$$

However, SEM is a property of the measure and is relative to it; therefore, there is no universal threshold for high reliability. The relative SEM (SEM%) informs of the relative noisiness of a given measure and is normalised to the measurement mean[266,267]. Therefore, it has a cutoff value for which measures to be considered highly reliable: $<10\%$[266]. SEM% was calculated using this equation[267]:

$$\text{SEM\%} = \frac{\text{SEM}}{\text{mean of data from both session}} \cdot 100$$

Finally, I calculated the smallest detectable change (SDC), which represents the value an observation would need to exceed to overcome measurement noise and to be considered a

genuine change[266,268] in an individual (SDC_{ind}) or a group (SDC_{group}) given sample size n. Lower SDC indicate better agreement between sessions. Since SDC is derived from SEM, there is also no universal cutoff value for high reliability. SDC_{ind} represents 95% confidence interval of SEM, while SDC_{group} is normalised to the number of participants. SDC was calculated as[266]:

$$SDC_{ind} = SEM \cdot \sqrt{2} \cdot 1.96$$
$$SDC_{group} = \frac{SDC_{ind}}{\sqrt{n}}$$

3.3 Results - %MSO method

3.3.1 All but three of all 132 input-output (IO) curves were quantified

Input-output (IO) curve data were acquired at three pulse widths (30, 60, 120 μs) using the controllable pulse parameter TMS (cTMS) over two sessions. To acquire IO curves, TMS pulses of varying intensities were delivered to the hand area of the primary motor cortex (M1) and resulting muscle responses were recorded. The IO curves were fitted using a sigmoid curve of best fit (Figure 3.6). I was able to quantify 129 out of 132 curves, so data for the three remaining individual IO curves were excluded (see Figures A.4 in the Appendix for more detail). After applying the exclusion criteria described in section 3.2.4, I quantified 15, 20, and 22 IO curves for 30, 60, and 120 μs cTMS pulses, respectively, in each session.

3.3.2 Increasing pulse width increases input-output curve slope

A repeated measures mixed-effects model analysis with fixed effects of pulse width and session was performed to compare slopes of IO curves collected over two sessions using pulses of different widths. I found a statistically significant effect of width on IO curve slope ($F(2, 63) = 10.89, p = 0.0001$, Figure 3.7), but no significant effect of session ($F(1, 54) = 3.70, p = 0.06$) or interaction of width and session ($F(2, 54) = 0.82, p = 0.45$). A *post-hoc* Šidák's multiple comparisons test revealed a statistically significant difference between slopes acquired using 30 and 120 μs pulses ($t(63) = 4.54, p < 0.0001$), 60 and 120 ($t(63) = 3.15, p = 0.008$) μs pulses, but not between 30 and 60 μs pulses ($t(63) = 1.44, p = 0.39$).

3.3.3 Correlation between slopes of IO curves acquired by pulses of different widths

Aiming to determine whether pulses of different widths activate separate neuronal circuits, I then tested the relationship between slopes of IO curves acquired by different pulses widths

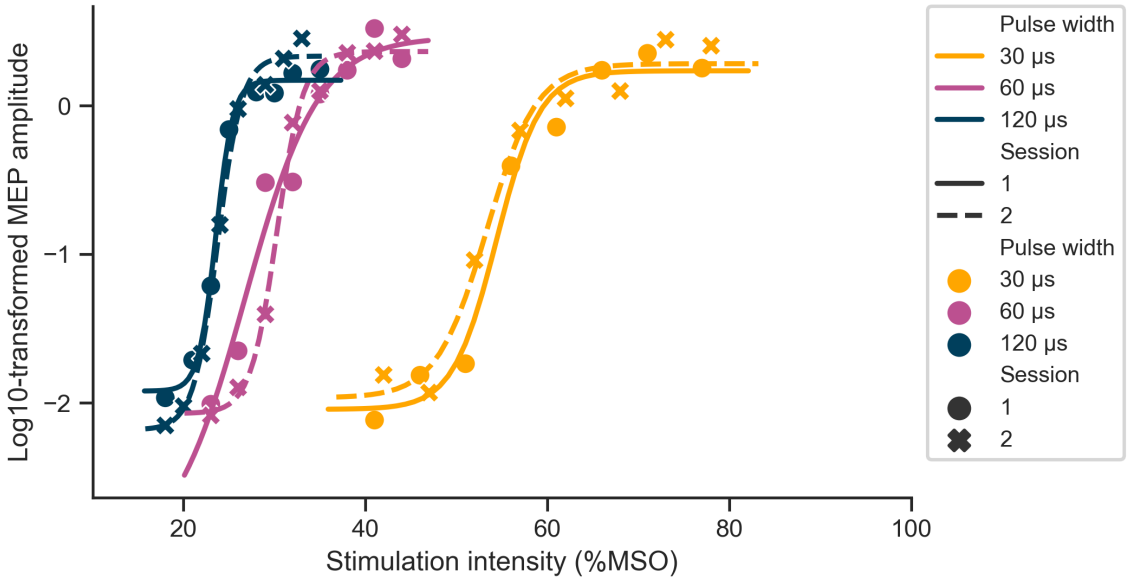


Figure 3.6: Example input-output (IO) curves of one participant for pulse widths 30 (orange), 60 (pink) and 120 (blue) μs acquired in session 1 (solid line/circle marker) and 2 (dashed line/cross marker). The markers represent mean log-transformed amplitude of motor evoked potentials (MEPs) elicited by TMS pulses of various intensities represented as percentage of maximum stimulator output (% MSO). At every combination of TMS pulse intensity and width, 10 trials were recorded. Mean MEP amplitude was calculated from remaining trials after exclusion criteria were applied during data pre-processing. Lines show sigmoid curves of best fit to the mean MEPs.

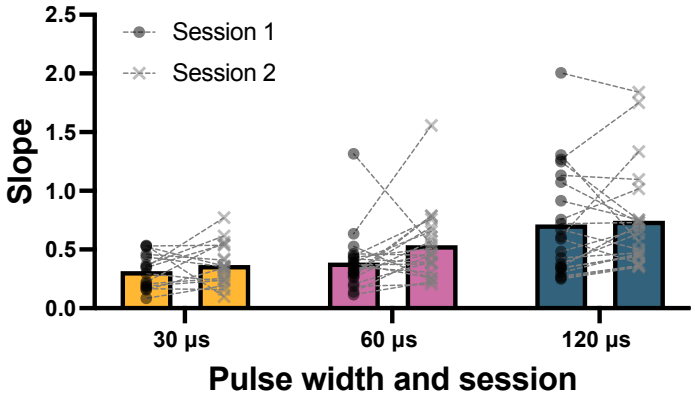


Figure 3.7: Comparison of input-output (IO) curve slopes acquired using all pulse widths in both sessions. Each marker represents an individual participant ($n = 15$ for 30, $n = 20$ for 60, and $n = 22$ for 120 μs pulses), lines connecting the markers show a change between sessions for individual participants.

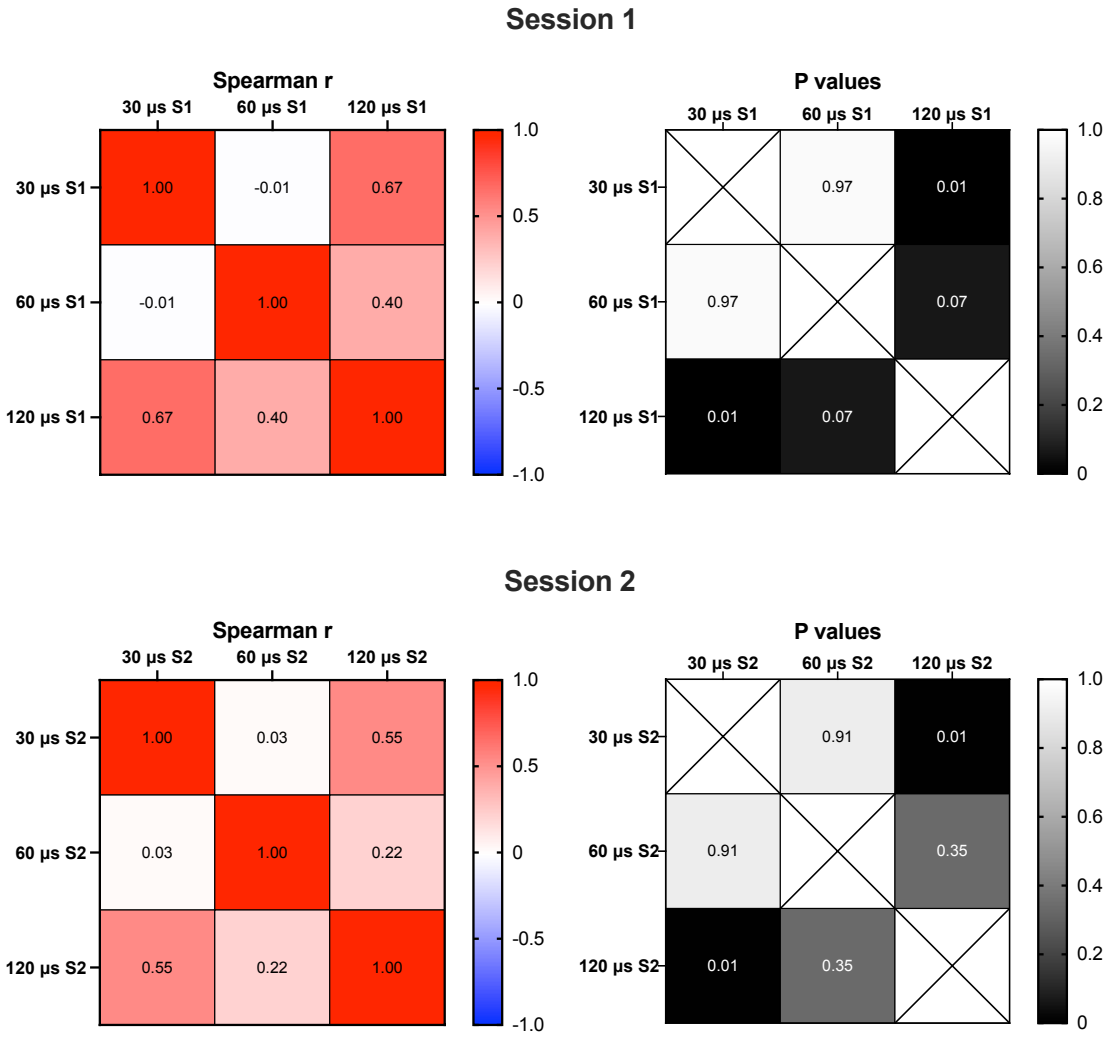


Figure 3.8: Correlations between IO curve slopes acquired using different pulse widths in sessions 1 (top, 30: n = 15, 60: n = 20, and 120: n = 22) and 2 (bottom, 30: n = 21, 60: n = 21, and 120: n = 22).

(Figure 3.8). Spearman's correlation revealed a significant relationship between 30 and 120 μs pulse slopes in both session 1 ($r(14) = 0.67, p = 0.006$) and session 2 ($r(19) = 0.56, p = 0.01$). No significant correlation was found between 30 and 60 μs pulse slopes in session 1 ($r(13) = -0.01, p = 0.97$) or 2 ($r(18) = 0.03, p = 0.91$), or between 60 and 120 μs pulse slopes in either session 1 ($r(19) = 0.40, p = 0.07$) or 2 ($r(19) = 0.22, p = 0.35$).

3.3.4 Only longest pulse width IO curve slopes exhibit good test-retest reliability

Determining test-retest reliability is important for understanding the utility of the cTMS device, whether it can be used to detect changes over time, between participants, or between different group populations. Therefore, I then performed various analyses to determine the test-retest reliability of IO curves acquired by pulse of different widths, summarised in Table 3.1.

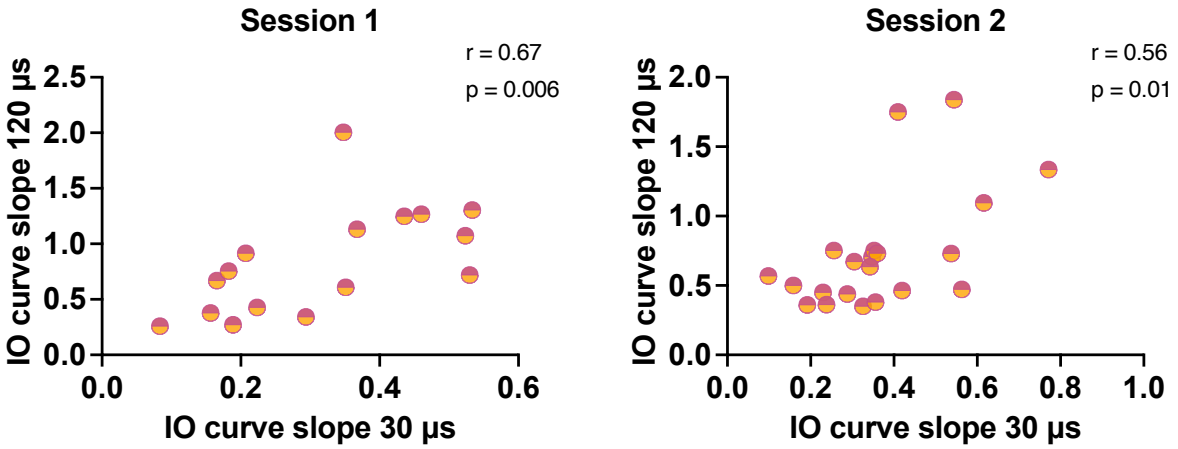


Figure 3.9: Correlations between IO curve slopes acquired using by 30 and 120 μs pulses in sessions 1 (left, n = 16) and 2 (right, n = 21).

Every test-retest reliability metric describes a different aspect of reliability, so they all need to be interpreted separately. Firstly, the intraclass correlation coefficient (ICC) quantifies the ability of the metric to distinguish between participants in a sample. >0.75 is considered high reliability, moderate if 0.5-0.75 and poor if ICC <0.5[264].

The standard error of measurement (SEM) assesses agreement between repeated measurements and is a property of the measure, so there is no cut-off range for SEM. Relative SEM (SEM%) provides a measure of the relative noisiness of the metrics with an arbitrary threshold of 10%[266,267], under which measurements can be considered reliable and stable. Smallest detectable change represents the value necessary to exceed the measurement noise in an individual (SDC_{ind}) or a group of a certain sample size (SDC_{group})[266]. SDC_{group} reduces with increasing sample sizes, thus allowing group comparisons even if measurement error is too great to be able to compare individuals[266].

IO curve slopes in general did not show good reliability. Only based on the ICC do the 120 μs slopes exhibit good reliability, with the 60 μs and 30 μs slopes showing poor reliability. All slopes had high SDC_{ind} values relative to the mean slopes, indicating that on an individual level, changes in slopes within participants could not be detected. SEM% values for all slopes were above the cut-off of 10, with 120 μs slopes having the lowest value indicating the best reliability among all pulse widths.

Bland-Altman plots can also be used to assess agreement, bias, and variability of measurements between sessions. Figure 3.10 plots the mean IO curve slope in both sessions against the test-retest difference in slope between the two sessions for each participant. IO curves acquired by 120 μs pulses showed the least amount of bias calculated as average of the test-retest differences for all participants (30 μs: 0.05, 60 μs: 0.14, 120 μs: 0.03).

Table 3.1: Test-retest reliability measures for IO curve slope data acquired using three pulse widths. n = 15 for 30, n = 20 for 60, and n = 22 for 120 μs pulses). Metrics are highlighted in bold if they reach high reliability for ICC or SEM%, since these measures have threshold values for reliability.

Metric	Session 1 mean± SD	Session 2 mean ± SD	ICC (95% CI)	SEM	SEM%	SDC_{ind}	SDC_{group}
Slope 30 μs	0.32 ± 0.15	0.38 ± 0.19	0.24 (-0.28, 0.66)	0.13	42.69	0.42	0.03
Slope 60 μs	0.39 ± 0.25	0.53 ± 0.30	0.22 (-0.18, 0.58)	0.24	52.67	0.67	0.03
Slope 120 μs	0.71 ± 0.46	0.74 ± 0.42	**0.75** (0.48, 0.89)	0.23	31.01	0.63	0.03

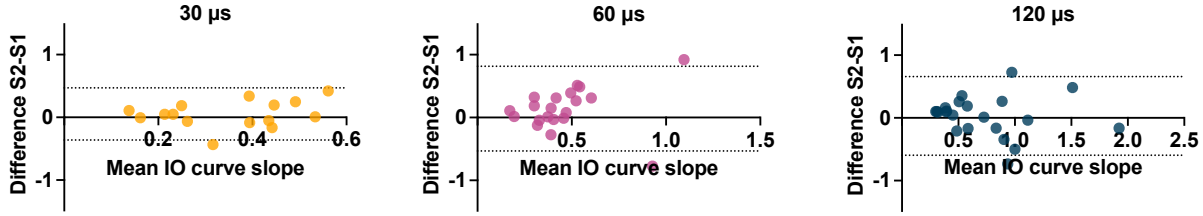


Figure 3.10: Bland-Altman plots showing agreement between IO curve slopes acquired in session 1 (S1) and session 2 (S2). Mean slope is plotted against the test-retest difference calculated as the difference between slopes acquired in both sessions for every participant and pulse width. Each point represents an individual participant. The dashed lines represent the 95% limits of agreement.

3.3.5 Test-retest reliability of other IO curve metrics

I then performed a test-retest analysis on the resting motor threshold (rMT) acquired during the session, as well as other parameters that can be extracted from IO curve fitting: the top and bottom plateaus of the IO curve, and S50, which represents the stimulation intensity that produces an MEP half of the value of the difference between top and bottom plateaus (Table 3.2). rMTs at all pulse widths exhibit high reliability, with all ICCs above 0.75 and all SEM% values below 10. Top plateau ICCs reveal poor to moderate test-retest reliability, but all SEM% values are above 10. Bottom plateau values have poor test-retest reliability, although the 120 μs pulse IO curve bottom pleateau SEM% value is 14.13, closest to reaching the threshold of 10 for good reliability. S50 values show moderate (30 μs pulses) and high reliability (60 and 120 μs pulses) based on ICC, and all SEM% values are below 10, indicating good test-retest reliability.

3.3.6 Some motor task metrics show good test-retest reliability

Participants also completed two motor tasks (action selection [AS] and serial reaction time task [SRTT]) during both sessions, which enabled me to determine the test-retest reliability of task metrics. I was interested in two measures in the AS task. The first measure are execute response times, which represent simple response times as the median response time (RT) of execute blocks. The second AS task measure are action selection times (AST), which represent time for pure action selection accounting for individual differences in simple

Table 3.2: Test-retest reliability measures for other characteristics of IO curves acquired using three pulse widths. n = 15 for 30, n = 20 for 60, and n = 22 for 120 μs pulses. Metrics are highlighted in bold if they reach high reliability for ICC or SEM%, since these measures have threshold values for reliability.

Metric	Session 1 mean ± SD	Session 2 mean ± SD	ICC (95% CI)	SEM	SEM%	SDC_{ind}	SDC_{group}
rMT 30 μs	59.47 ± 7.94	60.20 ± 8.24	**0.92** (0.77, 0.97)	2.37	**3.96**	6.56	0.43
rMT 60 μs	37.35 ± 7.39	36.85 ± 6.20	**0.82** (0.61, 0.93)	2.90	**7.81**	8.03	0.40
rMT 120 μs	28.09 ± 5.37	27.91 ± 4.86	**0.88** (0.74, 0.95)	1.78	**6.36**	4.94	0.22
Top plateau 30 μs	0.52 ± 0.21	0.46 ± 0.28	0.63 (0.21, 0.86)	0.15	30.97	0.42	0.03
Top plateau 60 μs	0.53 ± 0.20	0.47 ± 0.19	0.48 (0.08, 0.75)	0.14	28.00	0.39	0.02
Top plateau 120 μs	0.47 ± 0.24	0.41 ± 0.29	0.62 (0.29, 0.82)	0.16	37.16	0.45	0.02
Bottom plateau 30 μs	-2.23 ± 0.54	-2.39 ± 1.26	-0.28 (-0.74, 0.28)	1.09	47.03	3.01	0.2
Bottom plateau 60 μs	-2.37 ± 0.51	-2.18 ± 0.41	-0.04 (-0.45, 0.39)	0.48	21.00	1.32	0.07
Bottom plateau 120 μs	-2.19 ± 0.46	-2.10 ± 0.37	0.46 (0.07, 0.73)	0.30	14.13	0.84	0.04
S50 30 μs	60.75 ± 9.36	60.39 ± 9.73	0.62 (0.15, 0.85)	6.04	**9.98**	16.76	1.12
S50 60 μs	38.10 ± 8.89	37.39 ± 5.46	**0.76** (0.49, 0.90)	3.65	**9.68**	10.13	0.51
S50 120 μs	29.12 ± 5.75	28.96 ± 4.88	**0.84** (0.65, 0.93)	2.18	**7.49**	6.03	0.27

Table 3.3: Test-retest reliability measures for task performance data. n = 22.

Metric	Session 1 mean ± SD	Session 2 mean ± SD	ICC (95% CI)	SEM	SEM%	SDC_{ind}	SDC_{group}
Execute response time (s)	0.28 ± 0.02	0.28 ± 0.02	**0.80** (0.59, 0.91)	0.01	**3.53**	0.03	0.001
Action selection time (s)	0.37 ± 0.09	0.37 ± 0.08	0.37 (-0.07, 0.68)	0.07	18.88	0.20	0.009
SRTT learning gradient	-0.01 ± 0.01	-0.01 ± 0.01	0.50 (0.11, 0.76)	0.005	78.54	0.01	0.0006

response time, calculated as the difference between median select and execute block RTs (Figure 3.11).

In SRTT, motor learning was measured by recording RTs of participants responding to positions of a sequence of cues by pressing a button of a button box. The measure of interest for the SRTT was the gradient of a linear line fitted to median RTs of sequence blocks (Figure 3.12).

Table 3.3 summarises the test-retest reliability of task performance. Execute RTs had a high ICC value (0.80) and a SEM% of 3.13, as well as low SDC_{ind}, indicating high test-retest reliability for this metric. ASTs had poor reliability based on both ICC and SEM%. SRTT learning gradients showed a moderate ICC value, however, also a very high SEM%, indicating low test-retest reliability.

Figure 3.13 shows the Bland-Altman plots for execute RTs and ASTs. Both measures show some bias in larger differences between sessions 1 and 2 for participants with longer average execute RTs and ASTs. This bias is not present for SRTT learning gradients (Figure 3.14).

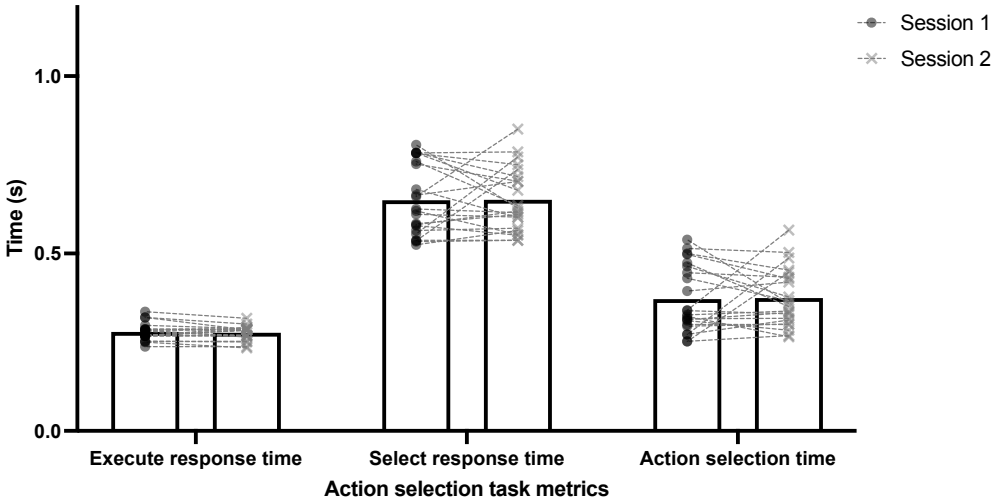


Figure 3.11: Action selection (AS) task performance in both sessions. Execute and select categories of the figure represent the median response time for execute and select blocks of the AS task. Action selection times were calculated as the difference between median response times in select and execute blocks. Each marker represents an individual participant ($n = 22$), lines connecting the markers show a change between sessions for every participant.

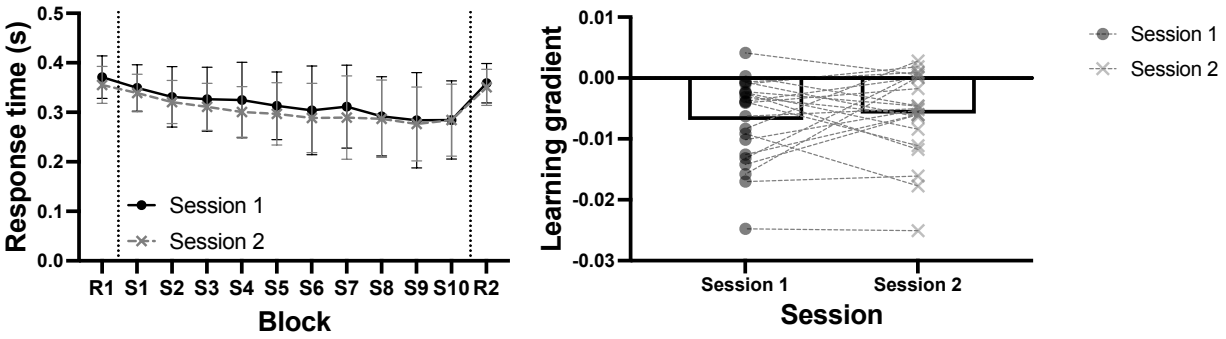


Figure 3.12: Serial reaction time task (SRTT) performance in both sessions. Left: Response time for every SRTT block, which had a random (R) order of cues or a sequence (S) of cues. Each marker represents a median value from all participants ($n = 22$). Error bars represent standard deviations. Right: The gradient of a linear line fitted to the response times of sequence blocks for every participant was used as a metric of learning. Each marker represents an individual participant, lines connecting the markers show a change between sessions for every participant.

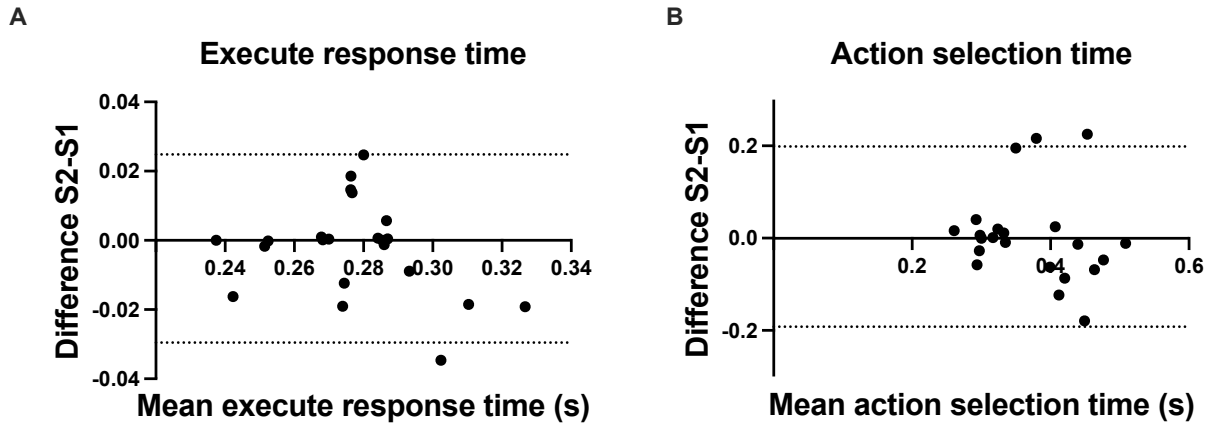


Figure 3.13: Bland-Altman plots showing agreement between execute response times (left) and action selection times (right) acquired over two sessions. Mean times are plotted against the test-retest difference calculated as the difference between times acquired in both sessions for every participant. Each point represents an individual participant. The dashed lines represent the 95 % limits of agreement.

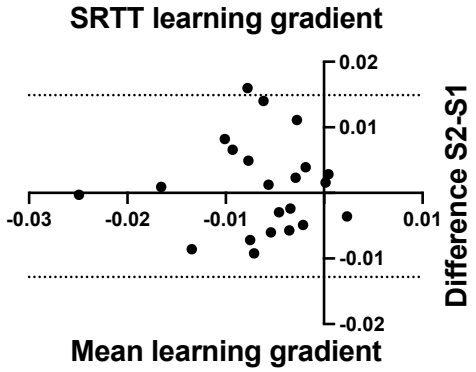


Figure 3.14: Bland-Altman plots showing agreement between SRTT linear gradients acquired over two sessions. Mean gradients are plotted against the test-retest difference calculated as the difference between the gradients acquired in both sessions for every participant. Each point represents an individual participant. The dashed lines represent the 95 % limits of agreement.

3.3.7 No significant correlations between task performance and IO curve slopes

Since motor task performance has been linked to levels of GABA in the motor cortex[1], I correlated IO curves slopes acquired by different pulse widths to task performance in both sessions, to establish whether it is possible to elucidate circuits recruited by TMS pulses of different widths.

No significant correlations were found between execute RTs and slopes of IO curve acquired using pulses of either width (Figure 3.15) in session 1 (30 μs pulses: $r(14) = 0.07, p = 0.77$; 60 μs: $r(19) = -0.24, p = 0.29$; 120 μs: $r(20) = -0.34, p = 0.56$)) or session 2 (30 μs pulses: $r(19) = -0.09, p = 0.71$; 60 μs: $r(19) = 0.02, p = 0.94$; 120 μs: $r(20) = -0.31, p = 0.17$). There were also no significant correlations between ASTs and slopes of IO curve acquired using either width in session 1 (30 μs pulses: $r(14) = 0.06, p = 0.84$; 60 μs: $r(19) = -0.06, p = 0.81$; 120 μs: $r(20) = 0.23, p = 0.30$) or session 2 (30 μs pulses: $r(19) = -0.34, p = 0.13$; 60 μs:$r(19) = -0.16, p = 0.49$; 120 μs: $r(20) = -0.04, p = 0.86$).

No significant correlations were found between SRTT learning gradients and slopes of IO curves at either pulse width in session 1 (30 μs pulses: $r(14) = -0.09, p = 0.73$; 60 μs: $r(19) = -0.05, p = 0.83$; 120 μs: $r(20) = -0.25, p = 0.26$), Figure 3.15) or session 2 (30 μs pulses: $r(19) = 0.05, p = 0.85$; 60 μs: $r(19) = 0.04, p = 0.86$; 120 μs: $r(20) = -0.31, p = 0.16$), Figure 3.15).

3.4 Results - %rMT method

3.4.1 Increasing pulse width does not have an effect on IO curve slope when curves are fitted to stimulation intensity relative to individual motor threshold

Previous research conducted using cTMS that studied the effect of pulse width modulation on IO curve slopes all acquired, fitted and analysed the curves the same way: data were acquired by ramping up the stimulus intensity as percentage of the maximum stimulator output (%MSO), and curves were then also fitted to %MSO on the x axis[176,178]. I was interested to see if I could replicate results from section 3.3 by fitting curves to %rMT on the x axis, another common method of quantifying IO curves (see section 2.1.3). To my knowledge, no one has compared the impact of the curve fitting method, only comparing acquisition between %rMT and %MSO and then fitting both using using %MSO[177].

Figure 3.16 shows the IO curves quantified with the %rMT method for the same participant shown in Figure 3.6, where the %MSO method was used.

A repeated measures mixed-effects model analysis with fixed effects of pulse width and session

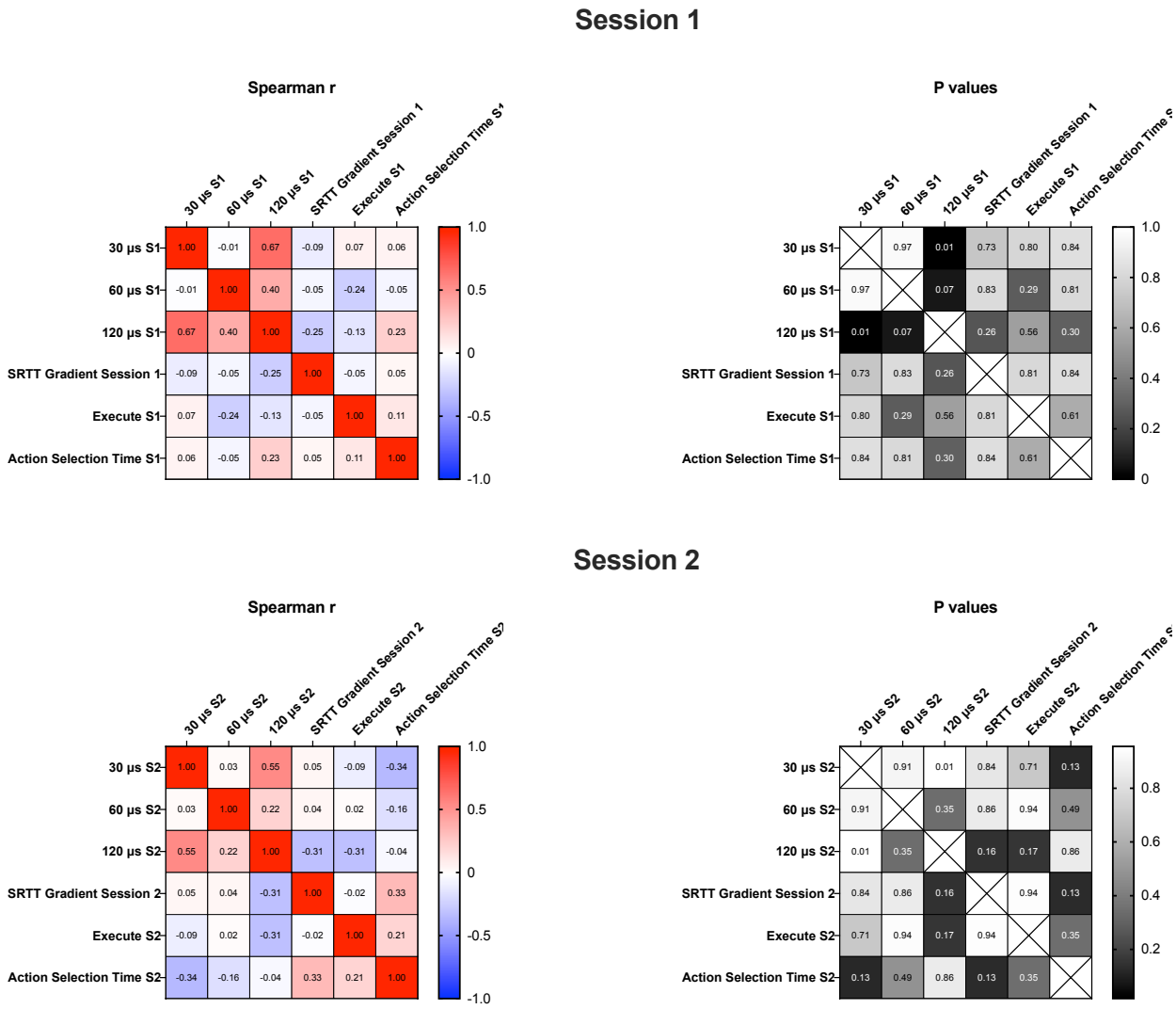


Figure 3.15: Correlations between task (action selection and SRTT) performance metrics and IO curve slopes dependent on pulse width in sessions 1 (top) and 2 (bottom). Execute response times (RT) represent simple response times of button press after visual stimulus. Action selection times are calculated by subtracting execute RTs from select block RTs, where participants select which finger to press based on visual cue size and shape and represent the pure time for action selection. Learning gradients are the linear lines of best fit to median response times in sequence blocks of the SRTT. The task measures were correlated with IO curve slopes acquired using different pulse widths in session 1 (30: n = 15, 60: n = 20, and 120: n = 22) and session 2 : (30: n = 21, 60: n = 21, and 120: n = 22).

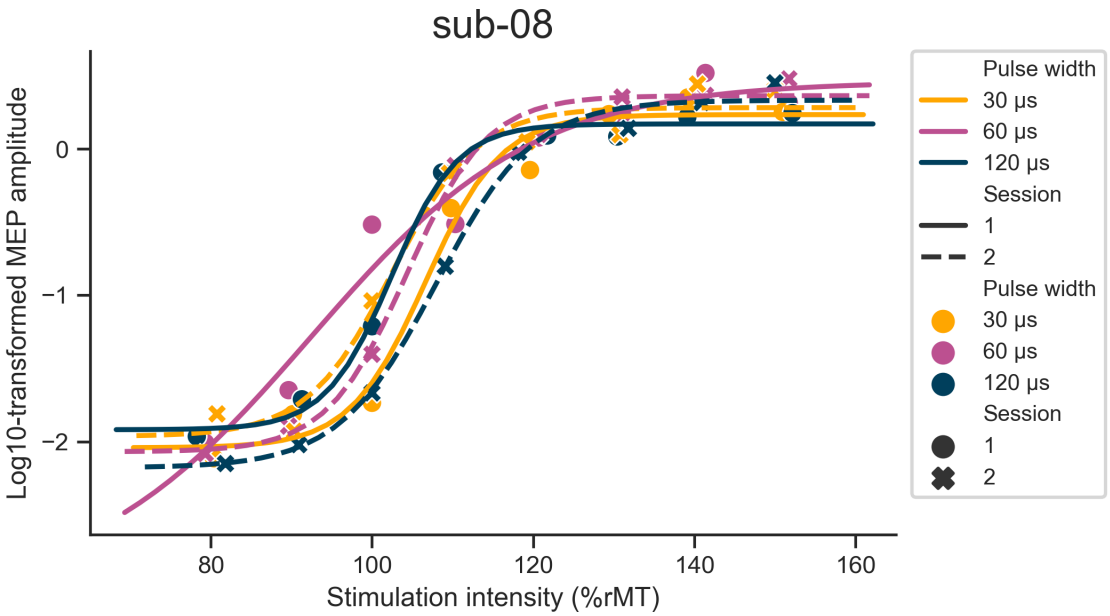


Figure 3.16: Example input-output (IO) curves fitted using the %rMT method of same participant as in Figure 3.6 for pulse widths 30 (orange), 60 (pink) and 120 (blue) μs acquired in session 1 (solid line/circle marker) and 2 (dashed line/cross marker). The markers represent mean log-transformed amplitude of motor evoked potentials (MEPs) elicited by TMS pulses of various intensities represented as percentage of the participant's resting motor threshold (%rMT). At every combination of TMS pulse intensity and width, 10 trials were recorded. Mean MEP amplitude was calculated from remaining trials after exclusion criteria were applied during data pre-processing. Lines show sigmoid curves of best fit to the mean MEPs.

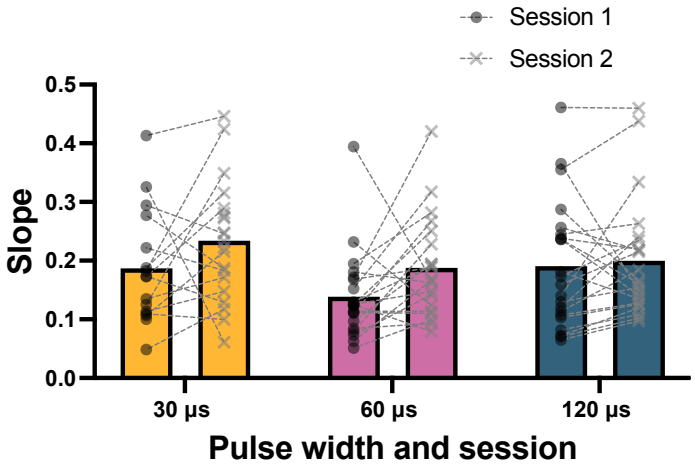


Figure 3.17: Comparison of input-output (IO) curve slopes acquired using all pulse widths in both sessions. Each marker represents an individual participant ($n = 15$ for 30, $n = 20$ for 60, and $n = 22$ for 120 μs pulses), lines connecting the markers show a change between sessions for individual participants.

was performed to compare slopes of IO curves collected over two sessions using pulses of different widths, now quantified by fitting curves to %rMT on the x axis. There was no longer a statistically significant effect of width on IO curve slope ($F(2, 63) = 2.02, p = 0.14$, Figure 3.17), but there was a significant effect of session ($F(1, 54) = 6.13, p = 0.02$). The effect of interaction of pulse width and session on slope was not significant ($F(2, 54) = 0.92, p = 0.40$). A *post-hoc* Šidák's multiple comparisons test revealed no statistically significant difference between slopes acquired using 30 and 60 ($t(63) = 1.96, p = 0.15$), 30 and 120 ($t(63) = 0.65, p = 0.89$), or 60 and 120 μs pulses ($t(63) = 1.35, p = 0.45$).

3.4.2 Relationship between slopes of IO curves acquired by pulses of different widths

I then tested the relationship between slopes of IO curves acquired by pulses different widths, but quantified with the %rMT method (Figure 3.18). Spearman's correlation revealed a significant relationship 30 and 120 μs pulse slopes in session 1 ($r(14) = 0.70, p = 0.004$) and session 2 ($r(19) = 0.52, p = 0.02$). No significant correlation was found between 30 and 60 μs pulse slopes in session 1 ($r(13) = 0.05, p = 0.85$) or 2 ($r(18) = -0.02, p = 0.94$), or between 60 and 120 μs pulse slopes in session 1 ($r(19) = 0.37, p = 0.09$) or 2 ($r(19) = 0.05, p = 0.82$).

3.4.3 Correlation between %rMT and %MSO slopes

I then looked at the relationship between slopes quantified by the two fitting methods. IO curve slopes acquired using the same pulse width, but fitted using either the %rMT or %MSO method, showed a statistically significant correlation for all three pulse widths (Figures 3.19 and 3.20) in both session 1 (30 μs: $r(14) = 0.96, p = 3.15 \times 10^{-8}$; 60 μs: $r(19) = 0.88, p = 1.04 \times 10^{-7}$; 120 μs: $r(20) = 0.93, p = 1.88 \times 10^{-12}$) and 2 (30 μs: $r(19) = 0.90, p = 4.43 \times 10^{-8}$;

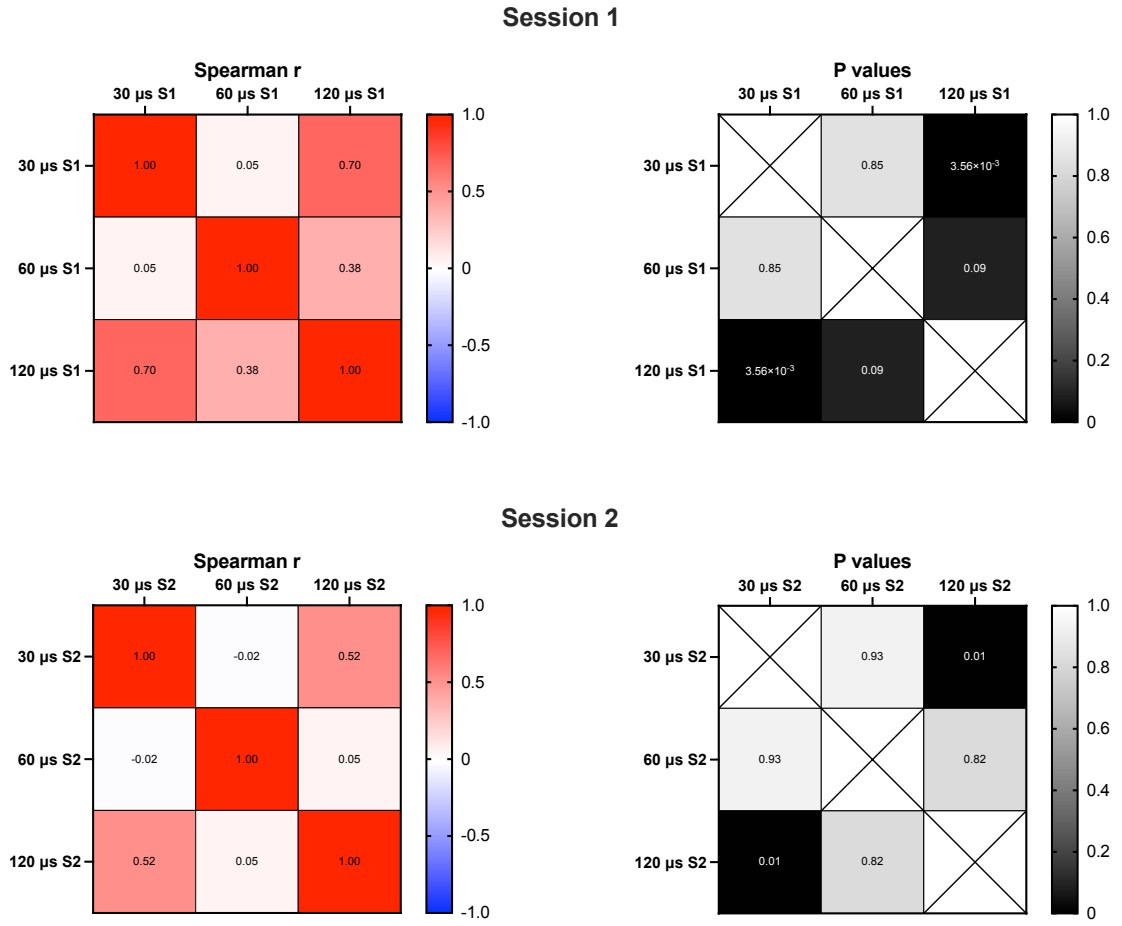


Figure 3.18: Correlations between IO curve slopes acquired using different pulse widths in sessions 1 (top, 30: n = 15, 60: n = 20, and 120: n = 22) and 2 (bottom, 30: n = 21, 60: n = 21, and 120: n = 22).

Table 3.4: Test-retest reliability measures for IO curve slope data acquired using three pulse widths. n = 15 for 30, n = 20 for 60, and n = 22 for 120 μs pulses). Metrics are highlighted in bold if they reach high reliability for ICC or SEM%, since these measures have threshold values for reliability.

Metric	Session 1 mean± SD	Session 2 mean ± SD	ICC (95% CI)	SEM	SEM%	SDC_{ind}	SDC_{group}
Slope 30 μs	0.19 ± 0.10	0.23 ± 0.12	0.31 (-0.21, 0.70)	0.09	43.01	0.25	0.02
Slope 60 μs	0.14 ± 0.08	0.19 ± 0.09	0.14 (-0.24, 0.52)	0.07	45.65	0.21	0.01
Slope 120 μs	0.19 ± 0.11	0.20 ± 0.10	0.66 (0.34, 0.85)	0.06	31.25	0.17	0.01

60 μs: $r(19) = 0.96, p = 1.12 \times 10^{-11}$; 120 μs: $r(20) = 0.90, p = 1.25 \times 10^{-8}$).

3.4.4 IO curve slopes exhibit low test-retest reliability even when quantified using %rMT

I repeated the test-retest reliability analysis of IO curves acquired by pulses of different widths but quantified by the %rMT method, summarised in Table 3.4.

IO curve slopes in general did not show good reliability. Only 120 μs slopes exhibited moderate reliability, while 60 μs and 30 μs slopes had poor reliability based on ICC. All slopes had high SDC_{ind} values relative to the mean slopes, indicating that at an individual level, changes in slopes within participants could not be be detected. SEM% values for all slopes were above the cutoff of 10, with 120 μs slopes having the lowest value indicating highest reliability among all pulse widths. Therefore, using the %rMT method for analysis of IO curves did not seem to improve the overall test-retest reliability of slopes.

Bland-Altman plots were used again to assess agreement, bias, and variability of measurements between sessions. Figure 3.21 plots the mean IO curve slope in both sessions against the test-retest difference for each participant. IO curves acquired by 120 μs pulses showed the least amount of bias calculated as the mean of the test-retest differences for all participants (30 μs: 0.05, 60 μs: 0.03, 120 μs: 0.008).

3.4.5 Test-retest reliability of other IO curve metrics

Next, I performed test-retest analysis of other IO curve parameters for the %rMT method (Table 3.5).

Top plateau ICCs revealed moderate test-retest reliability, but all SEM% values were above 10. Bottom plateaus had poor test-retest reliability. S50 values showed poor reliability based on ICC, but all SEM% values were below 10. Therefore, it is not possible to conclude whether S50 values show good reliability for the %rMT method compared to the %MSO method.

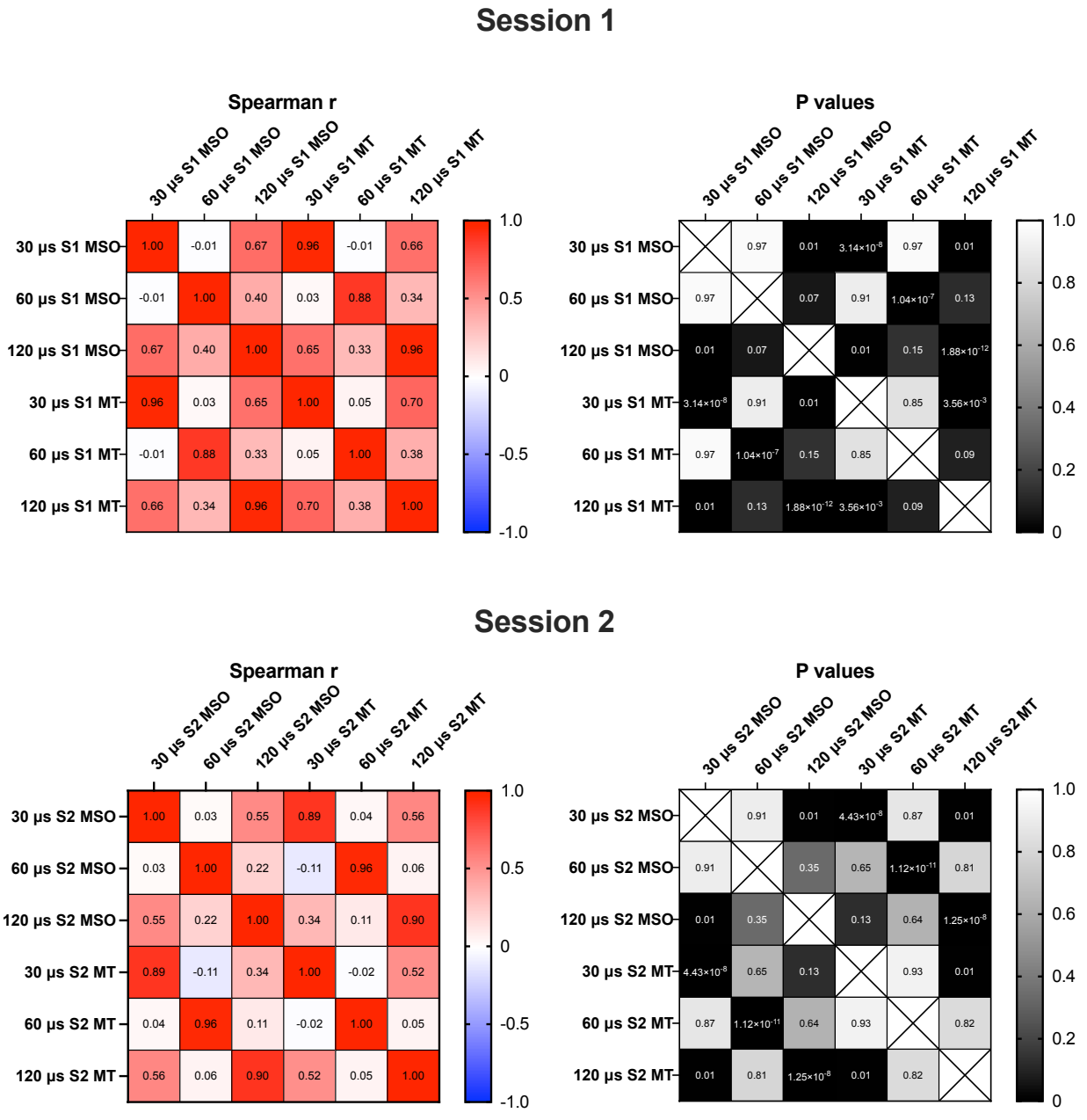


Figure 3.19: Correlations between IO curve slopes analysed using different methods acquired using different pulse widths in sessions 1 (top) and 2 (bottom).

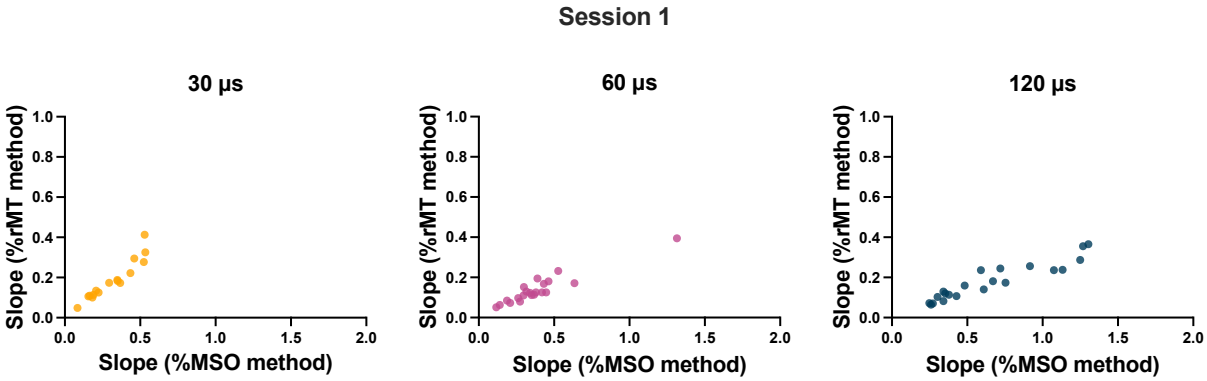


Figure 3.20: Scatterplot of relationships between IO curve slopes analysed using different methods acquired using different pulse widths in session 1.

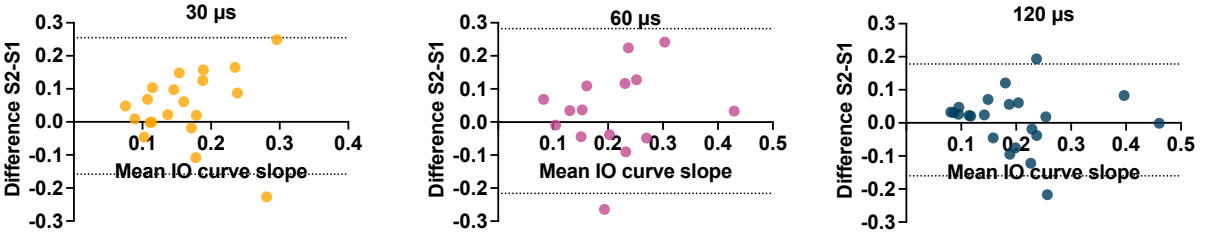


Figure 3.21: Bland-Altman plots showing agreement between IO curve slopes acquired over two sessions. Mean slope is plotted against the test-retest difference calculated as the difference between slopes acquired in both sessions for every participant and pulse width. Each point represents an individual participant. The dashed lines represent the 95 % limits of agreement.

Table 3.5: Test-retest reliability measures for other characteristics of IO curves acquired using three pulse widths. n = 15 for 30, n = 20 for 60, and n = 22 for 120 μs pulses. Metrics are highlighted in bold if they reach high reliability for ICC or SEM%, since these measures have threshold values for reliability.

Metric	Session 1 mean ± SD	Session 2 mean ± SD	ICC (95% CI)	SEM	SEM%	SDC_{ind}	SDC_{group}
Top plateau 30 μs	0.52 ± 0.21	0.46 ± 0.28	0.63 (0.21, 0.86)	0.15	30.97	0.42	0.03
Top plateau 60 μs	0.53 ± 0.20	0.47 ± 0.19	0.48 (0.08, 0.75)	0.14	28.00	0.39	0.02
Top plateau 120 μs	0.47 ± 0.24	0.41 ± 0.29	0.62 (0.29, 0.82)	0.16	37.16	0.45	0.02
Bottom plateau 30 μs	-2.23 ± 0.54	-2.39 ± 1.26	-0.28 (-0.74, 0.28)	1.09	47.03	3.01	0.20
Bottom plateau 60 μs	-2.37 ± 0.51	-2.18 ± 0.41	-0.04 (-0.45, 0.39)	0.48	21.00	1.32	0.07
Bottom plateau 120 μs	-2.19 ± 0.46	-2.10 ± 0.37	0.46 (0.07, 0.73)	0.30	14.13	0.84	0.04
S50 30 μs	102.14 ± 7.27	100.42 ± 9.63	-0.11 (-0.62, 0.43)	8.95	**8.84**	24.80	1.65
S50 60 μs	101.63 ± 8.29	101.94 ± 6.41	-0.31 (-0.70, 0.17)	8.42	**8.42**	23.34	1.17
S50 120 μs	103.78 ± 7.96	103.95 ± 4.85	0.48 (0.07, 0.75)	4.81	**4.63**	13.32	0.61

3.4.6 No significant correlations between task performance and IO curve slopes

I then looked at the relationship between the IO curves acquired by different pulse widths for the %rMT fitting method, and the task metrics (Figure 3.22). No significant correlations were found between execute response times and slopes of IO curve acquired using pulses of either width in session 1 (30 μs pulses: $r(14) = 0.02, p = 0.96$; 60 μs: $r(19) = -0.01, p = 0.965$; 120 μs: $r(20) = -0.01, p = 0.96$) or session 2 (30 μs pulses: $r(19) = 0.005, p = 0.98$; 60 μs: $r(19) = 0.10, p = 0.68$; 120 μs: $r(20) = -0.20, p = 0.36$). There were also no significant correlations between action selection times and slopes of IO curve acquired using either width in session 1 (30 μs pulses: $r(14) = -0.03, p = 0.93$; 60 μs: $r(19) = -0.12, p = 0.60$; 120 μs: $r(20) = 0.19, p = 0.41$) or session 2 (30 μs pulses: $r(19) = -0.24, p = 0.30$; 60 μs: $r(19) = -0.12, p = 0.60$; 120 μs: $r(20) = 0.05, p = 0.81$).

No significant correlations were found between SRTT learning gradients and slopes of IO curves (Figure 3.22) at either pulse width in session 1 (30 μs pulses: $r(14) = -0.16, p = 0.56$; 60 μs: $r(19) = -0.006, p = 0.98$; 120 μs: $r(20) = -0.27, p = 0.22$) or session 2 (30 μs pulses: $r(19) = 0.19, p = 0.40$; 60 μs: $r(19) = 0.20, p = 0.39$; 120 μs: $r(20) = -0.16, p = 0.48$).

3.5 Discussion

In this study, I used the controllable pulse parameter TMS (cTMS) device to characterise the within-subject test-retest reliability of different metrics of corticospinal excitability. These metrics were extracted from input-output (IO) curves, acquired by modulating pulse width and intensity over two testing sessions. During the sessions, participants also completed two sensorimotor tasks. I assessed the relationship between IO curves acquired at different pulse widths and motor performance and learning.

The effect of pulse width on the IO curve slope was dependent on the analysis method. I did not find a statistically significant relationship between slopes of IO curves acquired with different pulse widths and task performance on either the action selection or serial reaction time task. Although the lack of a significant result may be due to the small sample size, it may also suggest that slopes of IO curve are not a sensitive enough measure for detecting differential neuronal activation.

3.5.1 Increasing pulse width leads to steeper IO curve slopes only with one analysis method

IO curves are commonly used as a measure of corticospinal excitability, the slopes of IO curves reflect the gain in MEP amplitude as stimulus intensity increases[164]. I acquired IO curves with the cTMS using three pulse widths: 30, 60, and 120 μs. I found that the steepness of

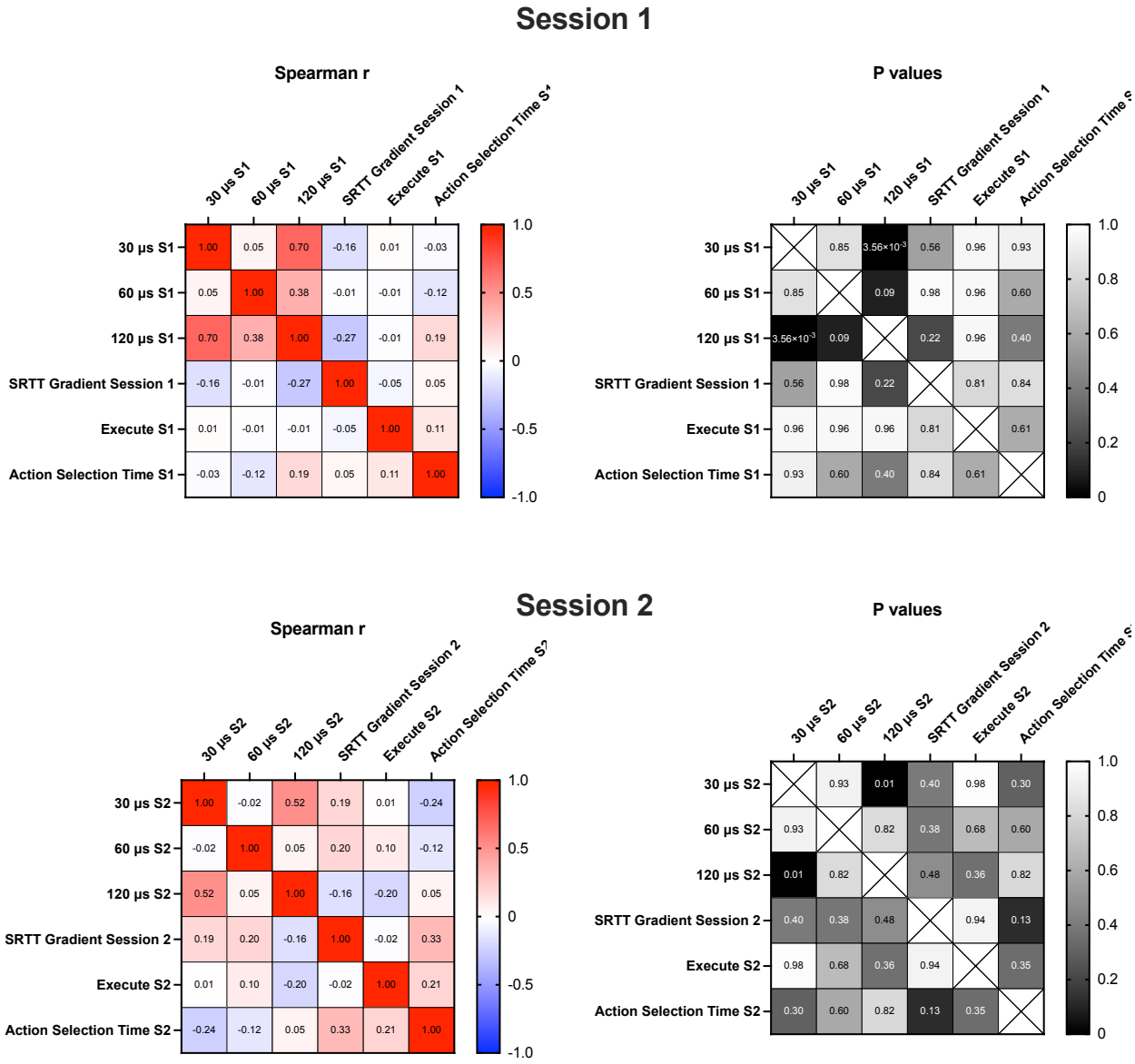


Figure 3.22: Correlations between task (action selection and SRTT) performance metrics and IO curve slopes dependent on pulse width (quantified by %rMT method) in sessions 1 (top) and 2 (bottom). Execute response times (RT) represent simple response times of button press after visual stimulus. Action selection times are calculated by subtracting execute RTs from select block RTs, where participants select which finger to press based on visual cue size and shape and represent the pure time for action selection. Learning gradients are the linear lines of best fit to median response times in sequence blocks of the SRTT. The task measures were correlated with IO curve slopes acquired using different pulse widths in session 1 (30: n = 15, 60: n = 20, and 120: n = 22) and session 2 : (30: n = 21, 60: n = 21, and 120: n = 22).

IO curve slopes increased with longer pulse widths, which is consistent with previous cTMS work on which I modelled my analysis steps[176,178]. *Post-hoc* analysis revealed a significant difference between slopes of IO curves acquired with 30 and 120, and 60 and 120 μs pulses. This suggests that the excitability of neuronal circuits activated by pulses of different widths differs. My procedure for sampling the IO curve (intensities of pulses were calculated based on individual participants' motor thresholds which reduced the time of the session, more detail on the procedure in section 3.2.3) differed from the two other studies (increasing pulse intensity in small increments with the maximum pulse intensity limited by the output allowed by the device or participants' discomfort[176,178]). Therefore, using a different sampling method did not have an effect on the dependence of IO curve slope on pulse width.

I also used a different method of quantifying IO curves from previous studies, where the curve was fitted to the x variable (intensity) that was relative to the resting motor threshold of each individual participant (%rMT), instead of the absolute percentage of maximum stimulator output (%MSO). This method of IO curve quantification is commonly used in other studies acquiring IO curves[82,170,269,270], and I wanted to test whether a similar effect of pulse width on IO curve slope remained with this method. The slopes of the IO curve acquired by pulses of the same width and quantified by the two methods showed a statistically significant correlation. However, I no longer found a significant effect of pulse width on IO curve slope quantified with %rMT.

Only one previous study investigated the effect of changing pulse width on IO curves using the %rMT method[254]. They did not find an effect of width on the area under the IO curve, and did not determine the slopes. However, due to the limitations of the devices they used, only two pulse widths relatively close together (82 and 114 μs) were applied[254]. Therefore, it is not possible to determine whether the lack of significant effect of the pulse width was due to the range of intensities used, or because pulse width modulation did not allow differential neuronal activation. In another study, IO curve slope, which was quantified using %MSO and then normalised by multiplying the slope with the rMT, was found to be independent of pulse width[176]. This may suggest that modulating pulse widths with an IO curve protocol may not result in differential neural recruitment.

A study exploring the relationship of different metrics describing IO curves, for example, IO curve slope, top plateau of the curve and area under the curve, used principal component analysis to demonstrate that most IO curve metrics acquired using a conventional TMS device capture the same characteristics[270]. Comparing how measures of IO curves acquired using different pulse widths and quantified with the two analysis methods relate to each other using principal component analysis could bring insights into how they describe corticospinal excitability, whether they all capture the same characteristics, and whether pulse width modulation results in activation of different populations of neurons.

3.5.2 Does pulse width modulation enable the selective recruitment of neurons?

Taken together, my results suggest that the IO curve slope may not be a measure sufficiently sensitive to capture any potential differences in selective recruitment of neurons by modulating the pulse width, or that there may be no effect of pulse width.

Previous research that utilised the cTMS device provides evidence that pulse width modulation does have an effect on neuronal activation and may also provide some understanding of the types of neurons activated by pulses of different widths. Although there is ample evidence to suggest pulse width modulation affects MEP amplitude, the exact relationship has not been elucidated yet. Strength-duration curves acquired by recording the motor threshold intensity at different cTMS pulse widths enable the estimation of the strength-duration parameter chronaxie, which describes the dependence of stimulation threshold on the pulse intensity and width. It represents the shortest pulse width at double the minimum intensity of any width that results in supra-threshold activation (more detail in section 3.1.2). The chronaxie was estimated to be 196 [181-210] μs at rest using the cTMS[176]. In another study, strength-duration curve parameters were established using different coil orientations and muscle states. It is well established that posterior-anterior (PA) and anterior-posterior (AP) coil orientations activate different neuronal circuits[239] likely due to a spatial shift of activation[242], however, AP and PA chronaxies were different when the targeted muscle was active, but not at rest[178]. In the PA configuration at rest, replicating the calculation of chronaxie used by the study above[176], a different value for chronaxie was determined at 243 μs[178]. Since the chronaxie is longer than the longest cTMS pulse (120 μs), it limits the accuracy of strength-duration curve parameter estimation. However, both of the estimated chronaxies are similar to modelled chronaxies of various primary motor cortical (M1) pyramidal cells[238].

Local motor cortical changes in activity evoked by TMS pulses measured by electroencephalography (EEG) also vary based on pulse width. Longer 80 μs monophasic PA pulses induce higher early local mean field power in electrodes positioned over M1 after TMS pulse delivery compared to shorter 30 μs pulses[250]. Early TMS-evoked responses are thought to be modulated by GABAergic activity, suggesting that shorter pulses had greater effects on inhibitory interneurons than longer pulses[271]. No effect of pulse width on global brain TMS-evoked activity was found[250], suggesting that different pulse widths activate different local motor cortical circuits in the absence of overall differences in cortical excitability.

More evidence supporting selective activation of different neuronal circuits using pulse width modulation comes from TMS experiments with an AP coil configuration. The latency of MEPs evoked by AP (but not PA) TMS pulses varies with pulse width, with shortest pulses producing MEPs with the longest latency[178,272], suggesting the recruitment of different neuronal pools across pulse widths. Repetitive TMS (rTMS) delivered with AP pulses of different widths at 1 Hz frequency also resulted in diverging effects. Shorter pulse widths induced de-

creases in cortical excitability, while longer pulses induced excitatory after-effects[249].

Effects of pulse width on neurotransmitter and neuromodulator systems

In addition to the above studies examining the effects of pulse width on cortical excitability, a number of studies have been performed that aimed to investigate the effects of pulse widths on various neurotransmitter systems using different TMS protocols.

Short-latency afferent inhibition (SAI) combines a TMS test pulse with a peripheral median nerve conditioning stimulus to elicit inhibition of the evoked MEP and is thought to be primarily a measure of cholinergic activity involving the primary somatosensory cortex[272]. Short test pulses delivered in an AP configuration were associated with greater SAI than shorter PA or longer AP or PA pulses when a muscle was contracting[272]. No differences were found at rest. These results indicate that short AP pulses activate neuronal circuits that exhibit different functional properties than those activated by other pulse types. However, it is thought that AP pulses may recruit neurons in the premotor cortex in addition to M1[273], so the contributions of the premotor and primary motor cortical areas could not be disentangled. Moreover, AP pulses typically have higher thresholds than PA pulses[178,274]. In my study, where I used PA pulses, several participants had to be excluded because I could not acquire full IO curves before I reached the cTMS device output limit. If I had used the AP configuration, the number of excluded participants would have likely been even higher. However, it will be important for future studies to consider both the current direction (AP versus PA), and the activity within the targeted muscle to fully understand the physiological effects of differing pulse widths.

In a short-interval intracortical inhibition (SICI) protocol, a first sub-threshold stimulus is paired with a second supra-threshold one at various inter-stimulus intervals (ISIs) several milliseconds apart, to assess aspects of GABAergic signalling. The application of such sub-threshold pulses suppresses MEP amplitudes, and depending on the inter-stimulus interval is sensitive to different aspects of GABAergic signalling. One study has used the cTMS in a SICI protocol. When shorter 30 μs and longer 120 μs AP pulses were delivered for the conditioning stimulus during a sustained muscle contraction, shorter conditioning stimuli elicited less pronounced inhibition than longer ones at an ISI of 2 ms, commonly thought to reflect GABA-A synaptic activity[274].

In a study that utilised more pulse widths adapted to every individual participant's rMTs, the effect of pulse width on SICI was found to be similar to that of changing the conditioning intensity with a conventional TMS device. Modulation of pulse width resulted in a U-shaped curve, with the shortest and longest pulses eliciting the most inhibition[275]. For intracortical facilitation (ICF), a paired-pulse TMS protocol that reflects both glutamatergic and GABAergic activity, longer pulses evoked more excitation[275].

There is evidence to show that modulating pulse width with cTMS can elicit differential neu-

ronal recruitment, as summarised above. However, based on the studies that find differences between pulse widths, whether it is in EEG-measured TMS response, SICI, or delivering pulses during a muscle contraction, the differences in selective neural recruitment may be at sub-threshold levels. Therefore, further study of protocols that use sub-threshold pulses such as ICF and SICI, or protocols where pulses are delivered during a muscle contraction like the cortical silent period (CSP) may allow us to explore this relationship better, as well as the use of AP coil configurations. Currently, there is no consensus on the exact mechanisms explaining differential neuronal recruitment.

3.5.3 Does the total amount of charge delivered matter?

In order to elucidate the mechanisms of how pulse width modulation could lead to selective activation of neurons, it is important to understand how changing the pulse width affects the amount of energy that is delivered to the M1.

Based on the results of their SICI and ICF study, Shirota et al. suggest that the major determinant for neural activation is not the absolute intensity delivered, but the total amount of charge, which could be thought of as the product of intensity and pulse width[275]. They altered the total amount of charge by changing the pulse width, which is normally done by changing the intensity of a conventional TMS device. Based on their findings, it is not possible to conclude whether modulation of these parameters results in selective neural recruitment, since only a small range for pulse width modulation of 12 μs was used. If the product of pulse width and intensity matters, it may explain why Hannah et al., found less inhibition with shorter pulses[274]. The 30 μs pulse thresholds were not four times greater than those for 120 μs, therefore less total charge might have been delivered.

It is difficult to know from my results whether this explanation is valid, since the cTMS pulse shape is not perfectly rectangular (Figure 3.4), and calculating charge is imprecise. Additionally, because the shape of cTMS pulses varies with width, longer pulses are less rectangular[176].

In the peripheral nervous system, the charge-duration relationship has been investigated and found to be linear with a positive association[222,231,234,276]. Therefore, it is expected that shorter pulses should deliver less charge.

In order to determine the amount of charge delivered with each cTMS pulse, I used my electric field recordings (Figure 3.23A, also shown in Figure 3.4). 30, 60, and 120 μs pulses were recorded at the same intensity (40%MSO). I calculated the integral of the normalised electric field to get the current (Figure 3.23B) to minimise the effect of pulse shape varying with width. To calculate the charge, the current was integrated again. The charge for each pulse width was then multiplied by the rMT of every participant. This was repeated for only the positive phase of the pulse since cTMS pulse widths are defined by the positive phase.

I found that increasing the pulse width in general increased the charge, similar to peripheral

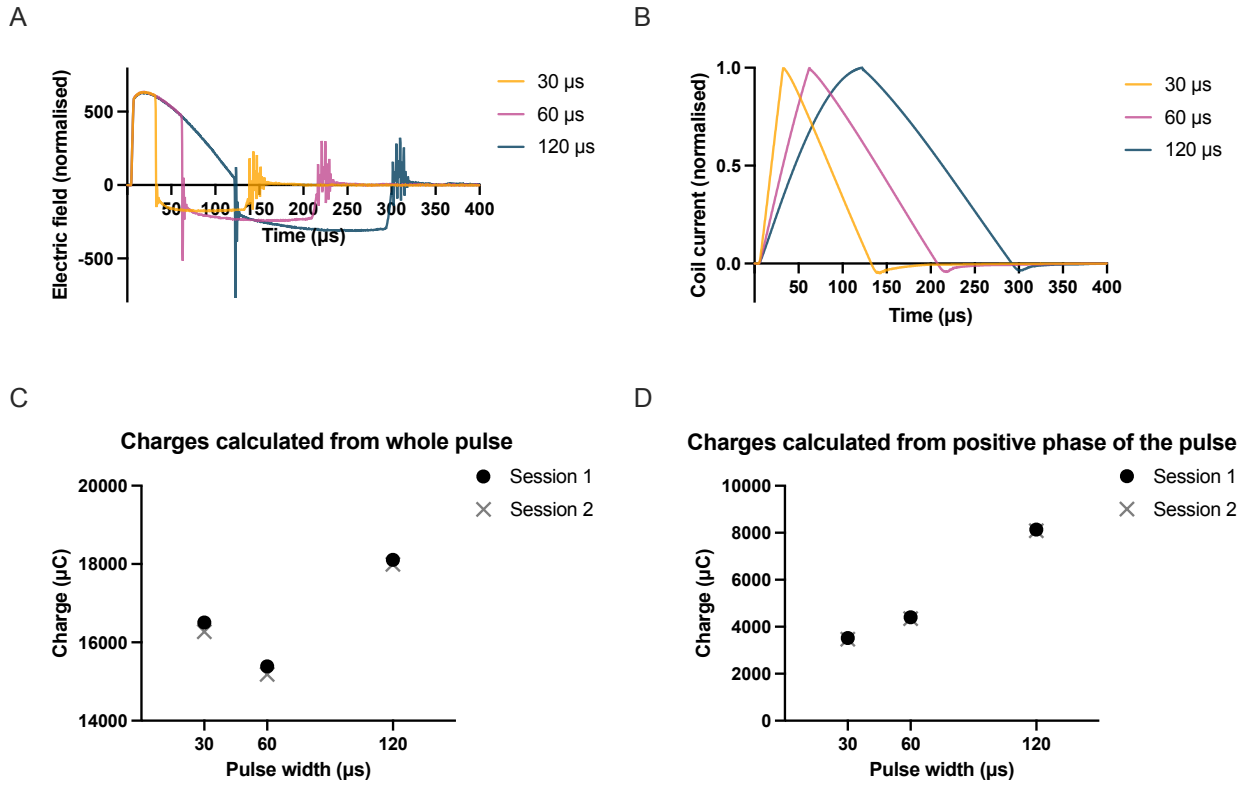


Figure 3.23: Calculation of charges delivered by the cTMS device. A: Electric field waveforms of cTMS pulses recorded with a search coil. B: Coil current calculated by integrating the electric field. C: Mean charge calculated for all participants for all three pulse widths from the whole pulse. D: Mean charge calculated for all participants for all three pulse widths, but only considering the positive phase of the pulse.

charge-duration data. For full pulses including the negative and the positive phase, the relationship was not linear, since threshold charges for 60 μs pulses were lower compared to 30 μs pulses (Figure 3.23C). On the other hand, when only the positive phase of the pulse was considered, the charge-duration relationship was more linear (Figure 3.23D) and resembled peripheral charge-duration associations more closely (for example from Mogyoros et al.[231]).

It is not clear whether using both phases of the pulse to calculate the charge, or only the positive phase, is more valid. Firstly, literature has no consistent definition of pulse width. cTMS pulses are defined by the positive phase[176], some monophasic TMS devices cite the negative and positive phases separately[255], while biphasic pulses are usually defined by the full pulse[277]. Moreover, the determination of the central charge-duration relationship has not been possible to explore until the recent advancements in pulse width modulation technology in TMS devices. The positive phase matches peripheral nervous system studies that use square or rectangular pulses with no negative phase[222]. However, the negative phase of the TMS is delivered, so it is difficult to determine if only using the positive phase is valid. The contribution of each phase to the activation of M1 neurons and resulting MEPs is not explicitly defined. Comparing biphasic stimuli with equal positive and negative phases, or monophasic stimuli with opposing current orientations shows that they are all able to acti-

vate neurons, however, it is hypothesised that distinct populations are activated by different phases[273]. From the data collected in this study, it is not possible to disentangle the effects of the two pulse phases. More experiments would be needed to determine how each phase contributes to M1 activation, how it interacts with charge delivered, and finally, how varying charge affects neural activation.

3.5.4 Future directions to understand the importance of pulse width

In order to understand the neuronal circuits activated by pulses of different widths, TMS measures should be combined with other modalities such as magnetic resonance spectroscopy (MRS), which allows measurements of different chemicals in the brain including neurotransmitters[278]. Different parameters that describe IO curves have been shown to relate to MRS measures of GABA or glutamate[82,165]. Combining MRS and TMS data with task performance showed that participants with faster response times have larger MEPs, but larger MEPs are also associated with GABA[279]. Investigating the relationship of TMS measures acquired using different pulse widths and comparing them to MRS measures may enable us to better understand the physiological mechanisms underlying neuronal activation by TMS and pulse width modulation.

3.5.5 Low test-retest reliability of TMS metrics

One of the main aims of this study was to determine the test-retest reliability of IO curves using the cTMS.

I found mixed test-retest reliability results for IO curves acquired by pulses of different widths. In general, longest pulses showed better reliability. Intraclass correlation coefficients (ICCs) were high for 120 μs slopes, revealing good reliability. Resting motor thresholds and S50 values, representing the TMS pulse intensity at which we can elicit half-maximal MEPs, both had good reliability for all pulse widths. Bottom plateaus did not show good reliability and top plateaus only exhibited moderate reliability.

Although it is commonly used to evaluate test-retest reliability[258], ICC represents the ability of a measure to distinguish between participants and relates more to the samples rather than to the measurement[265,266]. Since our participants were young, healthy adults, and a relatively homogeneous sample, large inter-individual differences were not expected, meaning low ICC for 30 and 60 μs pulse slopes may not signify low test-retest reliability.

Standard error of measurement (SEM) may be a better indicator of how stable measurements were over the two sessions. SEM is more directly related to the measurement rather than the sample[265,266]. However, SEM values calculated here ignore systematic differences between sessions due to the formula used[265], meaning I could be overestimating the values. Variance

decomposition is necessary to calculate SEM values that also consider systemic differences[266]. Smallest detectable change (SDC), derived from SEM, represents the difference necessary to surpass measurement error and be interpreted as real change[266,268]. Although they provide important information for the design of further studies and power calculations, SEM and SDC are harder to interpret because there are no universal thresholds. However, relative SEM (SEM%), which is derived from SEM, has been used with an arbitrary cutoff of <10%[267].

Neither SEM% value for IO curve slopes, top, or bottom plateaus was lower than 10%, indicating low reliability. SEM% for all rMTs and S50 measures were all below 10%, confirming the high reliability indicated by ICC. These results suggest that changes in the threshold for activation do not underlie the poorer reliability of the IO curve metrics compared to rMTs. Moreover, S50 has been suggested to be a good measure for assessing individual changes in cortical excitability since it produces half-maximal MEPs, which may be an ideal pulse intensity upon which measures of inhibition (SICI) and excitation (ICF) can be based[168]. This study found S50 to be a reliable measure for all pulse widths and analysis methods.

Multiple previous test-retest reliability studies show IO curve slopes to be reliable[280–282] but it is dependent on the targeted muscle[283] and how many pulses are used for every condition[168]. However, there are also some instances of low test-retest reliability for IO curve slopes[266,269,284]. These studies are summarised in Tables 3.6 and 3.7. Most studies calculated ICC to determine test-retest reliability. In the four unique studies that found ICC higher than 0.75 indicating good reliability, there are no characteristics that could distinguish them from those studies that did not find good reliability. For example, four experiments from two unique studies used a circular coil[282,285] rather than a figure-of-eight coil. One of the studies with good reliability had a higher mean age of 44.8, while participants' mean age in the other studies was younger, between 26 and 28 years of age. The time between sessions also varied between 24 hours and 4 weeks. Three unique studies that found good reliability applied stimuli that were expected to be determine the slope of the IO curve in 5% increments of intensity[280,282,283], but one study achieved good reliability even with 10% increments[281]. However, the studies that did not find good reliability used both increments of 5 and 10%. Three studies acquired the IO curves in ascending order of intensities[281–283], while one delivered pulses in random order[280]. Inter-trial intervals ranged between 3.33 and 8 seconds and both dominant and non-dominant hemispheres were targeted. All studies reported here, whether they found good reliability or not, used Magstim TMS devices. Overall, based on these studies, it is not possible to conclude whether there is a protocol that would increase test-retest reliability and explain the low reliability of my findings. In general, a systematic review has found a small amount of research into the test-retest reliability of TMS metrics[258]. They also observed that these metrics were likely affected by differences in protocols, such as time between the test and retest sessions, or number of stimuli that were delivered[258]. Standardised protocols may be needed to improve test-retest reliability of TMS metrics.

I found good test-retest reliability of rMTs and S50 values. These results are consistent with

Table 3.6: Studies determining test-retest reliability of IO curves. In study populations, healthy stands for participants with no neurological or psychiatric disorders, and no upper limb injury that could affect TMS metrics.

Study	Age range	Mean age	Number of participants	Number of sessions	Time between sessions	Hemispheres	Muscle	TMS coil orientation	Recruitment curve acquisition	Number of pulses per intensity	Order of intensities	Inter-trial interval (s)
[282]	22-74	44.8	50	2	4 weeks	Left or right (dominant)	TA	AP	30-100%MSO in 5% steps	3	Ascending[o]	3.33-5
[280]	22-36	-	8	3	More than 24 hours	Left[h]	FDI	PA	95, 100, 105, 110, 115, 120, 130%rMT	10	Random in blocks of 3-4 (grouped by intensity)	6-8
[269]	-	70	26	2	1 week	Left (dominant)	FDI	PA	90, 110, 120, 130, 150%rMT	10	Random order of blocks of 10 (grouped by intensity)	5-10
[281] *	-	27.4	14	2	1 week	Non-dominant (for healthy)	FDI	PA	100-150%rMT in 10% steps	10	Ascending, in blocks of 5 then repeated	5
[283]	21-36	26.9	20	2	2 weeks	Left (dominant)	FDI	PA	30-100%MSO in 5% steps	5	Ascending[o]	3.33-5
[283]	21-36	26.9	20	2	2 weeks	Left (dominant)	APB	PA	30-100%MSO in 5% steps	5	Ascending[o]	3.33-5
[283]	21-36	26.9	20	2	2 weeks	Left (dominant)	EDC	PA	30-100%MSO in 5% steps	5	Ascending[o]	3.33-5
[283]	21-36	26.9	20	2	2 weeks	Left (dominant)	FCR	PA	30-100%MSO in 5% steps	5	Ascending[o]	3.33-5
[266] *	-	64.7	21	4	Twice daily on two consecutive days	Right (non-dominant)	FDI	PA	100, 110, 130, 150, 170% rMT	10	Ascending	7
[266] *	-	64.7	21	4	Twice daily on two consecutive days	Left (dominant)	FDI	PA	100, 110, 130, 150, 170% rMT	10	Ascending	7
[284]	44-75	54	9	3	1-2 weeks	Right (non-dominant)	EDC	PA	90%MSO-plateau in 10% steps	5	Ascending	5
[284]	44-75	54	9	3	1-2 weeks	Left (dominant)	EDC	PA	90%MSO-plateau in 10% steps	5	Ascending	5

* notes studies which also include patient populations, but only results for the healthy control groups are included in this table

[h] Hemisphere was not explicitly stated, however figure shows right hand

TA: Tibialis anterior

FDI: First dorsal interosseous

APB: Abductor pollicis brevis

EDC: Extensor digitorum communis

FCR: Flexor carpi radialis

AP: TMS coil with handle pointing anteriorly, resulting in a anterior-to-posterior current direction

PA: TMS coil with handle pointing posteriorly, resulting in a posterior-to-anterior current direction

%MSO: Percentage of maximum stimulator output

%rMT: Percentage of resting motor threshold

[o] Order was not explicitly stated, assumed to be ascending from the stated range of intensities

Table 3.7: Studies determining test-retest reliability of IO curves. In study populations, healthy stands for participants with no neurological or psychiatric disorders, and no upper limb injury that could affect TMS metrics.

Study	TMS device	Coil type	Pulse width[w]	ICC type	ICC	SEM	%SEM	SDC_{ind}	Coefficient of variance	Note
[282]	Magstim 200	Circular coil	-	ICC(A,k0)	0.78	1.78	-	4.93	-	Coil parallel to midline, 0.5-1cm lateral to vertex
[280]	Magstim 200	Figure-of-eight 80 mm	-	ICC (A,3)	0.75	-	-	-	-	
[269]	Magstim 200	Figure-of-eight 70 mm	82	ICC(2,k)	0.346	5.53	69.11	15.34	-	
[281] *	Magstim - type not reported	Figure-of-eight 70 mm	?	ICC(3)	0.75	0.08	-	0.22	-	
[283]	Magstim 200	Circular coil	-	ICC(A,k)	0.82	-	-	-	-	
[283]	Magstim 200	Circular coil	-	ICC(A,k)	0.78	-	-	-	-	
[283]	Magstim 200	Circular coil	-	ICC(A,k)	0.83	-	-	-	-	
[283]	Magstim 200	Circular coil	-	ICC(A,k)	0.6	-	-	-	-	
[266] *	Magstim BiStim2	Figure-of-eight 70 mm	82	ICC(2,k)	0.07	0.76	-	2.1	-	Natural log of slope, therefore calculation of %SEM not possible
[266] *	Magstim BiStim2	Figure-of-eight 70 mm	82	ICC(2,k)	0.03	0.66	-	1.83	-	Natural log of slope, therefore calculation of %SEM not possible
[284]	Magstim 200	Figure-of-eight 90 mm	-	-	-	-	-	-	74.70%	Four investigators, but each participant was tested by same investigator
[284]	Magstim 200	Figure-of-eight 90 mm	-	-	-	-	-	-	68.10%	Four investigators, but each participant was tested by same investigator

* notes studies which also include patient populations, but only results for the healthy control groups are included in this table

[w] Pulse width for most Magstim devices is reported for 70 mm coil [254], however different coils will change the pulse width

ICC: Intraclass correlation coefficient

SEM: Standard error of measurement

%SEM: Relative standard error of measurement

SDC_{ind}: Individual smallest detectable change

previous conventional TMS test-retest reliability studies[168,266,266,280–283].

3.5.6 Test-retest reliability of tasks

I also calculated the test-retest reliability of the two sensorimotor tasks, since participants completed them in both sessions.

The sensorimotor tasks also had mixed test-retest reliability. For the action selection task, execute response times had a high reliability according to both ICC and SEM%. Action selection times had low ICC, but SEM% was approximately 18, while the threshold value for good reliability is under 10%. SRTT learning gradients had a moderate reliability based on ICC, but a large SEM% value.

I did not find any previous studies that determined test-retest reliability of the action selection task. However, there are tasks similar to the individual action selection block types. Simple reaction time tasks are essentially identical to the execute blocks since participants respond to a stimulus by pressing a key on a keyboard, or a button on a computer mouse. Test-retest reliability measured by ICC was found to be good (0.83) in healthy young participants who completed two sessions 24 hours apart in such a task[286]. In a different study with a week between the test-retest session, the ICC was found to be 0.73[287], just below the threshold for good reliability. These results are consistent with good test-retest reliability of execute blocks in my study.

A two-choice reaction time task is simpler than the select block of the action selection task because it involves only two different stimuli which dictate the response, rather than 4. Test-retest reliability of a two-choice reaction time task measured after 24 hours expressed by ICC was 0.75, therefore showing good reliability[286]. In a population of patients with Lewy body dementia, the ICC was high for the inverse of the mean choice reaction time after 5 days following the first session, but also at 4- and 12-week follow-ups[288]. In my study, I found a low ICC for the action selection times, which could be because the task was more complex with four stimuli that determine the correct response.

Test-retest reliability of the SRTT has often been measured using correlations, with mixed reliability found by a meta-analysis[289]. However, correlations are not a good measure of test-retest reliability, since they reveal an association between measures, but not necessarily agreement[266]. For example, if in a second session, a metric is measured to be twice the value of the first session, the correlation would be 1, but there would not be an agreement between the two sessions[266]. Therefore, it is difficult to compare these findings with my SRTT test-retest reliability results.

3.5.7 Limitations

There are aspects of the project that were outside the scope of this study but should be acknowledged, as well as some possible limitations that may explain my findings.

In this study, I did not model strength-duration curves. However, since they are derived from rMT values, I would expect them to be reliable over time. Moreover, studies that have estimated the strength-duration chronaxie from cTMS data have determined it to be in the range of 190-250 μs[176,178], which is longer than the longest cTMS pulse we can generate. This may then affect the accuracy of the chronaxie estimation. cTMS pulses, especially the longer ones, are not perfectly rectangular[176] (Figure 3.4), which may impact the strength-duration relationship in neuronal activation.

Central strength-duration relationship is more difficult to understand compared to peripheral because of the complexity of the central nervous system. There are multiple synapses between the activated neurons and the output we measure from the muscle. Various factors such as complex neuronal morphology, cortical folding, and cortical layers may all affect which neuronal populations and areas are activated by TMS pulses, unlike in the peripheral system, where strength-duration parameters are considered a purer reflection of the excitability properties of the nerves themselves. There are no experimentally measured chronaxies of different neuronal subtypes in the motor cortex[239] that would allow us to understand their contributions to the strength-duration parameters. However, strength-duration curves may deviate in the case of patients with neurodegenerative diseases where a specific subtype of neurons is affected. For example, in amyotrophic lateral sclerosis (ALS), inhibitory neurons are thought to be affected first[256,257]. Utilising pulse width modulation TMS in ALS patient populations might help us understand how these neurons contribute to the strength-duration parameters.

I found that, in general, IO curve slopes were not a reliable metric with the experimental protocol that I used. When acquiring IO curves, randomisation of stimulation intensity order is often used to reduce the effect of hysteresis on MEPs[290]. Hysteresis is a well-known phenomenon in TMS, where a preceding TMS pulse can affect the amplitude of the succeeding MEP by a short-term change in corticospinal excitability[290]. For example, a strong TMS pulse preceding a weaker pulse would likely result in a larger MEP than if another weak pulse preceded it. At the time my study started, it was not yet possible to programmatically control the cTMS. Therefore, pulses were applied in groups of 10 of the same intensity. The order of intensities was randomised to reduce the effects of hysteresis, but the order was reversed for the second session. If hysteresis affected my data, the effects would have been opposite in the second session, lowering test-retest reliability. Additionally, more pulses could be used in the region of interest of the curve around the slope[168], which could be optimised using the sequential parameter estimation (SPE) method[291].

The slopes of IO curves acquired with 120 μs pulses, which are most comparable to conven-

tional TMS pulses, were the most reliable, however, they were also the curves with the most data (n = 22). The other two pulse widths had less data from both sessions (n = 15 for 30 μs, n = 21 for 60 μs pulses). I expected the best reliability for 60 μs pulse IO curves since this pulse width allows for saturation of the IO curve most frequently[176]. The top plateau reliability, although not high, was the best for 60 μs pulses of all pulse widths. I selected the pulse widths in order to replicate previous cTMS research that used IO curves, which means that I did not sample the pulse widths of conventional TMS devices such as Magstim Bistim^2 (82 μs) or Deymed DuoMag MP (100 μs). Comparison of these pulses would be valuable to determine whether modulating the pulse width itself impacts test-retest reliability.

In TMS, large trial-to-trial MEP variability is a well-known phenomenon. One factor contributing to this could be naturally fluctuating oscillatory activity of neurons. MEP amplitude has been shown to depend on phase and power of motor cortical oscillations[292,293]. Since shorter pulses are thought to be more spatially selective[248,252], they may be more influenced by fluctuations in neuronal oscillations. Shorter pulses are also more temporally specific, so they may be more selective to the phase of oscillations compared to the longer pulses, which may cover more phases. More MEPs may need to be recorded for each condition when using short pulses to counteract the larger variability.

The use of the neuronavigation system helped to maintain the stimulation target consistent throughout the session. Since I did not have participants' MRI scans, between-session targets were different because the position of neuronavigation trackers could not be replicated exactly. Although I aimed to elicit a twitch in the same muscle, I did not mark electrode placement on skin, which is recommended for better test-retest reliability[258,266,282,294]. Hand muscles have high cortical representation and given the high number of motor units innervating them, small changes in between-session electrode positioning could affect TMS outcomes[285,295].

Cortical excitability changes throughout the menstrual cycle[296]. Over half of my participants were female, potentially affecting the reliability of IO curve slopes between sessions. The time between the test and retest sessions was not consistent for all participants and ranged from 1 up to 8 weeks. Moreover, there may be an effect of sleep and circadian rhythm on TMS excitability. The relationship between these metrics is controversial with some studies reporting an effect[297–299], while others do not observe an effect of sleep[300]. Although I started both sessions at the same time of day, in my analysis, I did not control for the amount of sleep participants had the night before taking part in the session.

There may be various reasons explaining why I did not find good test-retest reliability of cTMS IO curves, such as the experimental protocol for the acquisition of IO curves. More calculations and studies could be conducted to determine the effect of pulse width modulation on neural recruitment.

3.5.8 Conclusion

I replicated the findings of previous studies, where increasing cTMS pulse width increases the slope of IO curves, markers of corticospinal excitability. This effect, however, depended on the analysis method. With a commonly used individually threshold-adapted method, this effect was no longer present. This contrast between the analysis methods suggest that IO curves are not a measure sensitive enough to detect selective activation of different populations of neurons by pulse width modulation. Different protocols may be more suitable to elucidate whether pulse width modulation enables selective recruitment of different neuronal populations. The test-retest reliability of IO curve metrics was mixed. I did not find evidence for the neuronal circuits activated by different pulse widths, since IO curves did not have a relationship with sensorimotor task metrics. Multimodal studies with imaging will be more appropriate to detect the neuronal populations recruited by different pulse widths.

Chapter 4

Investigating age-related changes in movement-related M1 beta and gamma band activity

4.1 Introduction

4.1.1 Movement is associated with changes in beta and gamma band activity in the primary motor cortex

Oscillatory activity in the brain is the result of coherent rhythmic patterns of neurons[24]. Changes in various bands of oscillatory activity have been linked to function of the primary motor cortex (M1) for decades, notably in the beta frequency range (13-30 Hz)[301–304]. Specifically, a reduction in beta power is seen prior to and during voluntary movements (event-related desynchronisation (ERD))[305], but an increase is seen upon the termination of movement (event-related synchronisation (ERS))[42,43,45].

In recent years, increasing evidence supports the functional pro-kinetic role of higher frequency activity in the gamma band (30-100 Hz) in movement[65]. In contrast to beta, an increase in gamma band activity in M1 occurs during movement execution (gamma ERS), centred at approximately 75 Hz[43,56,59–63]. Driving gamma band activity in M1 by applying transcranial alternating current stimulation (tACS) at 75 Hz induced an increase in motor learning and modulated TMS-measured $GABA_A$ activity[65]. Gamma ERS has been found to be stronger with larger movements and for the first movement of a sequence[62]. Conversely, gamma ERS is absent in passive movement and during isometric contractions[62]. Taking these results together, it seems likely that gamma activity is actively involved in motor control, rather than just being a simple indication of muscle contraction. In addition, recent evidence supports the existence of gamma-band activity at approximately 45 Hz, which is thought to be controlled by a separate mechanism to 75 Hz gamma[68,70], although its role in M1 is not yet fully clear.

Movement-related gamma band activity depends on inhibition in the cortex and is considered

to arise from the reciprocal connection of parvalbumin-expressing inhibitory interneurons (PVI) and excitatory pyramidal cells[58,90,91]. In humans, magnetic resonance spectroscopy (MRS)-measured GABA concentration has been related to gamma ERS peak frequency in both M1[85] and the visual cortex[97], although this relationship has not been seen consistently[98]. Movement-related beta activity also depends on the activity of inhibitory neurons[40,71], particularly somatostatin-expressing interneurons[73].

Beta and gamma activity in the M1 appear to arise from different neuronal circuits, with beta arising from the deeper cortical layers and gamma seemingly generated closer to the surface[306]. However, even though beta and gamma are generated by separate networks, they are kept in balance and exhibit a reciprocal relationship: in action planning, gamma power increases as beta power is attenuated[307]. Beta and gamma band activity are both important in movement control and execution, and have been shown to depend on inhibitory drive. Therefore, changes in the balance between excitation and inhibition in the brain would likely affect M1 oscillatory activity and motor function.

4.1.2 Changes in oscillations throughout life

Ageing is associated with a large number of structural, functional, and biochemical changes in the brain, summarised in section 1.3 of the General Introduction.

Oscillatory activity has also been shown to change with age. In the beta band, ERS power[144–147] and peak frequency[145] have exhibited an age-related reduction, while ERD power has been shown to increase with age[140,142,145,146,148,149]. Movement-related gamma ERS peak frequency[66,85] and power[66,145] both reduced with age. However, most of these studies contain smaller samples of participants, some with a limited range of ages, meaning that it is not clear how replicable the findings are.

In this chapter, I was able to access and analyse magnetoencephalography (MEG) recordings from the Cambridge Centre for Ageing and Neuroscience (CamCAN) repository. CamCAN contains data from up to 100 participants in every decade between 18 and 88 years of age as they perform a simple finger movement task[308,309]. Therefore, these data may provide closer insight into changes in oscillatory activity throughout a lifespan.

4.1.3 Aims

Higher frequency oscillations are generally observed at lower amplitudes in the human brain than those at lower frequencies, making them more difficult to detect. Even in animal models, gamma activity can be harder to detect in comparison to slower rhythms[57]. In a previous study from my group, movement-related M1 gamma band activity could not be reliably detected in all individuals using time-frequency analysis[65]. In this study, I utilised a method developed in my group[70], that considers all three domains of MEG data (temporal, spectral and spatial) to reliably detect gamma band activity. I aimed to further investigate age-related

spectral and spatial changes in movement-related M1 beta and gamma band activity by using MEG data from the CamCAN repository.

4.2 Methods

4.2.1 Open-access CamCAN imaging dataset

Data used in the preparation of this work were obtained from the CamCAN repository[308,309] (available at `http://www.mrc-cbu.cam.ac.uk/datasets/camcan/`). Data collection and data sharing for this project were provided by the Cambridge Centre for Ageing and Neuroscience (CamCAN). CamCAN funding was provided by the UK Biotechnology and Biological Sciences Research Council (grant number BB/H008217/1), together with support from the UK Medical Research Council and University of Cambridge, UK.

4.2.2 Participants

700 participants aged 18-88 were recruited into the brain imaging Stage 2 of the CamCAN project[309], and 643 of those participants had task magnetoencephalography (MEG) data acquired. Of the 643, 617 participants also had structural magnetic resonance imaging (MRI) scans acquired. Data from these 617 participants were used for this study.

4.2.3 Experimental design

MEG data were acquired while participants were completing a sensorimotor task consisting of a right index finger button press cued by unimodal or simultaneous bimodal auditory, visual, or audio-visual stimuli[309]. The auditory stimuli were 300 ms binaural tones at one of three frequencies (300, 600, or 1200 Hz). The visual stimuli were two checkerboards that appeared for 34 ms to the left and right of the central fixation cross. Upon the appearance of one or both of the stimuli, the participants were instructed to respond by pressing a button. Inter-stimulus intervals ranged from 2 to 26 seconds.

4.2.4 MEG and MRI data acquisition

MEG data were acquired by CamCAN as previously described[309]. In brief, a whole-head 306-channel system consisting of 204 gradiometers and 102 magnetometers (Elekta Neuromag, Helsinki) was used. Data were sampled at 1 kHz with a band-pass filter of 0.03-330 Hz. Head position was continuously estimated using four head-position indicator (HPI) coils. Vertical and horizontal electrooculogram (EOG) electrodes were used to record blinks and eye movements, and electrocardiogram (ECG) electrodes were used to record ECG activity.

MRI data were collected using a 3T Siemens scanner. T1-weighted structural images used

for co-registration with MEG data were acquired as described by CamCAN[308]: using an MPRAGE sequence, a GRAPPA parallel imaging technique with an acceleration factors of 2, a repetition time (TR) of 2250 ms, echo time (TE) of 2.99 ms, inversion time (TI) of 900 ms, flip angle of 9°, voxel size 1 mm^3, and field of view of 256 x 240 x 192 mm. The images were de-faced by CamCAN to protect the anonymity of participants.

4.2.5 MEG data analysis

Maxfiltered data from CamCAN with external noise removed using spatio-temporal signal-space separation and head movement compensation based on head position indicator (HPI) coil data was used for data analysis. Further MEG analysis was performed using the OHBA Software Library (OSL: `https://ohba-analysis.github.io/osl-docs/`) in Matlab 2021a (version 9.10.0.1710957).

Preprocessing of sensor level data

Co-registration Registration between structural MRI images and MEG data using fiducial landmarks was carried out using the RHINO (Registration of Headshapes Including Nose in OSL) toolbox. Even though MRI images were de-faced, I was still able to use the nasion fiducial landmark along with left (LPA) and right pre-auricular (RPA) points.

Downsampling and filtering Continuous MEG data were downsampled to 250 Hz to reduce computing demands. A band-pass filter (1-100 Hz) was used to remove very slow trends and high frequencies, and two notch filters (49-51 Hz, and 99-101 Hz for harmonic noise) to remove line noise were then applied.

Bad segment detection MEG data can contain non-physiological artefacts. An automatic bad segment detection algorithm was used to exclude time windows identified as outliers from further analysis. Bad segments were identified by calculating the standard deviation of the signal across all sensors in 1 second non-overlapping windows using the generalized extreme studentized deviate test[310]. A significance level for outlier detection was set to 0.05. A mean of 0.9% of the dataset per participant were excluded for magnetometer sensors and mean of 0.7% were excluded for planar gradiometer sensors.

Independent component analysis MEG recordings also contain physiological noise. To correct for physiological artefacts, automatic independent component analysis (ICA) was performed using OSL AFRICA which utilises the FastICA algorithm[311]. ICA separates a signal into a set of independent components that are statistically independent from each other[203]. The independent components were correlated with EOG and ECG to identify components likely to be physiological noise. Any correlations greater than $r = 0.3$ were

excluded. A mean of 2.6 components per participants were excluded from further analysis. Because each independent component has the duration of the whole MEG recording, exclusion of a short-lived artefact can impact the whole dataset. However, since I removed less than 3 components as expected (one for each physiological channel, 2 EOG and 1 ECG), this likely did not impact my data.

Sensor normalisation The Elekta MEG system contains two sensor types: magnetometers and planar gradiometers, each with a different sensitivity and therefore different variances. The two sensor types were normalised so that they both contribute equally by computing an eigenvalue decomposition across each sensor type, which was then divided by the smallest eigenvalue within each one[312].

Division of frequency bands In general, amplitude of brain signals decreases with higher frequencies. Activity in the beta and gamma bands is therefore on different orders of magnitude. To maximise the signal-to-noise ratio, data were filtered to three frequency bands (beta: 13-30 Hz, slow-gamma: 30-60 Hz, mid-gamma: 60-85 Hz). The following steps were performed separately for each band.

Epoching Epochs were then defined as time windows -2 and +2 seconds relative to the button press. Trials with a response time of 1 second or longer were excluded from further analysis, because this indicates poor task performance and can impact the data by introducing noise into neural processes in the pre-movement period.

Source level analysis

Source reconstruction and parcellation In order to extract the source of signals, a linearly constrained minimum variance (LCMV) vector beamformer was applied to the epoched data[203,312,313]. The LCMV beamformer projected continuous sensor data onto an 8 mm grid within the skull of the MRI T1 scan. This was only applied to the M1 parcel defined by the Desikan-Killiany atlas, resulting in 92 voxels. A covariance matrix was calculated across the whole time course and regularised to 55 dimensions using principal component analysis (PCA) rank reduction[203]. Maxfilter reduces the dimensionality of MEG data to 64, which is further reduced by removal of 2-3 ICA components during preprocessing, excluding further smaller components, which removes their influence and thus preserves the contribution of the larger components[203].

Time-frequency analysis In order to extract the temporal, spectral, and spatial domains, time-frequency analysis was applied to single epochs on all 92 voxels within the M1 parcel using discrete prolate spheroidal sequences (DPSS)-based multitaper (steps = 50 ms) with a frequency resolution of 1 Hz. All epochs were baseline corrected using the mean baseline (-1 to

-0.5 s relative to button press). This resulted in trial-by-trial baseline corrected power across time (-2 to +2 seconds relative to the button press), frequency (beta: 13-30 Hz, slow-gamma: 30-60 Hz, mid-gamma: 60-85 Hz), and space (all 92 voxels in the M1 parcel).

Identifying movement-related characteristics Movement-related power was obtained by averaging across time from -0.2 to 0.2 s relative to button press for the mid- and slow-gamma bands[145], 0.5 to 1 s for beta ERS and -0.1 to 0.4 s for beta ERD. Movement-related power was then averaged across all epochs, resulting in a two-dimensional matrix containing the baseline-corrected power across epochs at each frequency at each voxel in the M1 parcel. The maximum (minimum for ERD) of the matrix was defined as the individual's power, which defined the individual's peak frequency and the individual's peak location (voxel in M1).

4.2.6 Statistical analysis

Linear regression was used to investigate the relationship between age and MEG metrics: peak frequency, peak power ($\log_{10}$-transformed to normalise distribution and reduce the variance between participants), and peak voxel coordinates. The analysis was performed separately for each frequency range of interest (mid-gamma ERS, slow-gamma ERS, beta ERS, and beta ERD), and each MEG metric. Linear regressions were fitted using the Statistics and Machine Learning Toolbox in Matlab 2021a (version 9.10.0.1602886).

4.3 Results

4.3.1 CamCAN dataset demographics

Of the 617 participants in the CamCAN dataset that had both a magnetoencephalography (MEG) and magnetic resonance imaging (MRI) scan, two were excluded from further analysis because of an unsuccessful co-registration. Further two datasets were excluded because after trials with long response times were omitted, less than 59 trials[145] remained. Therefore, statistical analysis was performed on 613 datasets. Figure 4.1 plots the distribution of the ages of the 613 participants by sex. The mean age of the 613 participants was 55.1 years (standard deviation ±18.2, range 18.5-88.9, 317 females).

4.3.2 Defining individual movement-related beta and gamma band activity

I obtained an individual peak voxel, frequency, and power for every participant, which enabled me to consider all three signal domains of MEG data: temporal, spectral, and spatial. Subject-specific power, peak frequency and peak voxel were identified for beta (13-30 Hz)

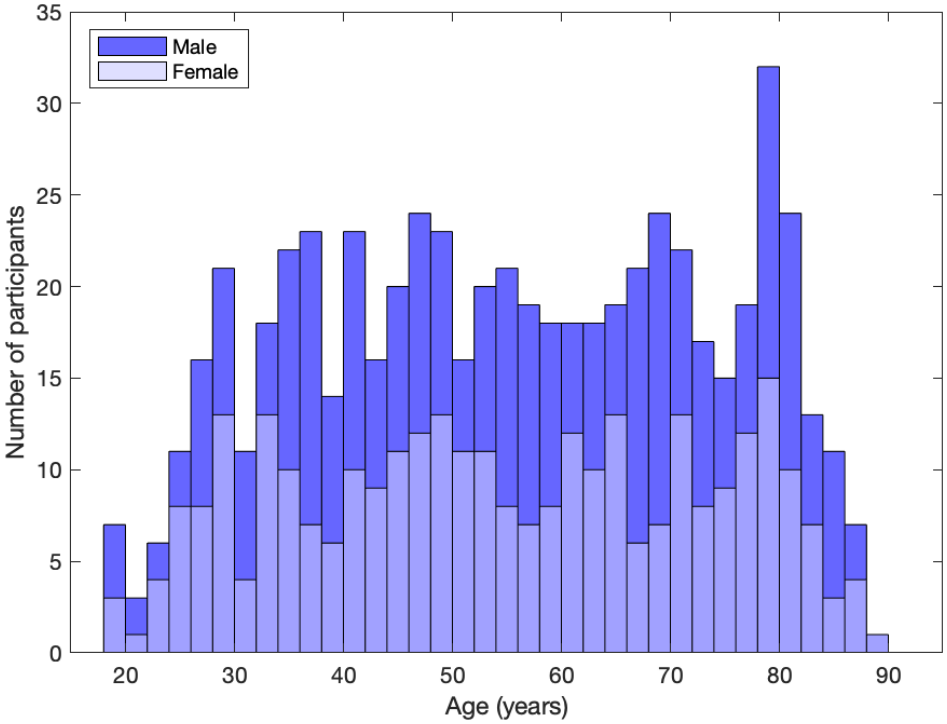


Figure 4.1: Histogram of participant ages split by sex.

event-related desynchronisation (ERD), beta event-related synchronisation (ERS) and ERS at two gamma frequency bands: slow- (30-60 Hz) and mid-gamma (60-85 Hz). Figure 4.2 shows an example of one participant's mid-gamma ERS and identification of their peak power, frequency, and voxel.

4.3.3 Group movement-related time-frequency activity in beta and gamma bands

Figure 4.3 shows the grand average plots of movement-related responses relative to a button press of each frequency band at peak voxel, with both ERS and ERD shown for the beta band.

In mid-gamma, I observed a clear movement-related ERS based on the pre-defined time windows for peak power detection (-0.2 to 0.2 seconds relative to button press for gamma band ERS, more detail in section 4.2.5 of this chapter). The strongest activity across subjects was found at 67 Hz and 0.024 seconds after the button press. For slow-gamma, the strongest activity across subjects was found at 54 Hz and 0.024 seconds before the button press. However, there was also a clear movement-related decrease in activity around the time of the movement followed by an increase in activity at frequencies between 30 and 50 Hz (Figure 4.3).

In the beta band, the expected ERD and ERS responses were observed. There was a clear decrease in beta activity around the time of the movement, followed by a clear rebound. The

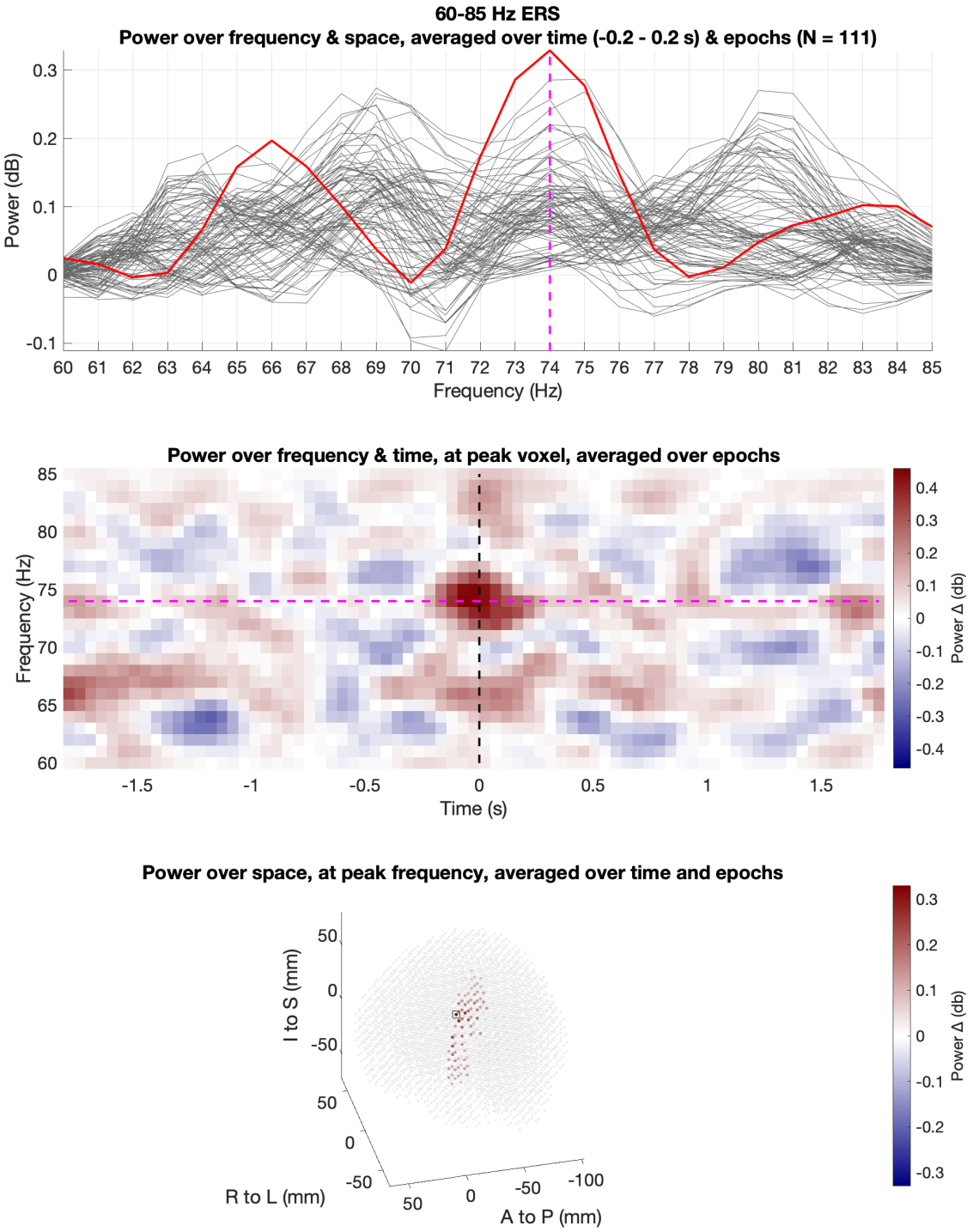


Figure 4.2: Mid-gamma (60-85 Hz) movement-induced event-related synchronisation (ERS). Top panel: power as a function of space (each line represents data from one voxel) and frequency (x-axis) averaged over time (-0.2 to 0.2 s) and all epochs. The red line illustrates data from the peak voxel. The vertical magenta line illustrates the peak frequency (74 Hz). Middle panel: power as a function of time and frequency at the peak voxel, averaged over all epochs. The horizontal magenta dashed line identifies the peak frequency, black dashed line indicates the button press. Bottom panel: power as a function of space. Peak voxel was determined by the peak frequency (74 Hz) averaged over all epochs over time between -0.2 to 0.2 s relative to button press. Location of the peak voxel defined by coordinates on the right-left (R to L), anterior-posterior (A to P), and inferior-superior (I to S) axes is highlighted by a black square.

Table 4.1: Relationship between age and power and peak frequencies of movement-related activity described by linear regression models.

Response	Metric	Intercept	Slope	*p-value*	R^2
Mid-gamma ERS	Peak frequency	71.46	-0.016	0.20	0.0027
Mid-gamma ERS	log_{10} of peak power	-0.53	-0.003	0.075	0.0052
Slow-gamma ERS	**Peak frequency**	**43.08**	**0.057**	**0.002**	**0.016**
Slow-gamma ERS	log_{10} of peak power	-0.61	-0.00056	0.70	0.00025
Beta ERS	**Peak frequency**	**20.13**	**-0.023**	**0.0017**	**0.016**
Beta ERS	log_{10} of peak power	0.41	-0.00070	0.59	0.00047
Beta ERD	**Peak frequency**	**20.53**	**-0.018**	**0.010**	**0.011**
Beta ERD	**log_{10} of peak power**	**0.12**	**0.0071**	**2.3e^{-8}**	**0.050**

strongest ERD activity across subjects was at 18 Hz and 0.12 seconds after the button press. The strongest ERS activity across subjects was at 17 Hz and 0.70 seconds after the button press.

Figure 4.4 shows the group mean location of mid-gamma ERS, slow-gamma ERS, beta ERS, and beta ERD respectively.

4.3.4 Relationship between age and movement-related activity metrics

The individually identified peak frequencies and power values were next assessed in relation to the participants' ages. Figure 4.5 shows each response characteristic for each band as a function of age. The plots include a linear regression line with 95% confidence intervals. The results of all linear regressions are summarised in Table 4.1.

There is evidence for an age-related increase in slow-gamma ERS peak frequency ($p = 0.0020, R^2 = 0.016$), and an increase in beta ERD peak power reflecting stronger ERD ($p = 2.3e^{-8}, R^2 = 0.050$). Participants' ages also predicted a decrease in peak frequencies of beta ERS ($p = 0.0017, R^2 = 0.016$) and beta ERD ($p = 0.010, R^2 = 0.011$). There was no significant association between age and either mid-gamma ERS peak frequency or power, slow-gamma ERS peak power, or beta ERS peak power.

4.3.5 Relationship between age and the location of movement-related activity

Next, I explored the relationship between age and coordinates of the individual peak voxel coordinates (Figure 4.6). Table 4.2 summarises the changes in X (left-right axis), Y (anterior-posterior), and Z (superior-inferior) coordinates of the peak voxels as a function of age mod-

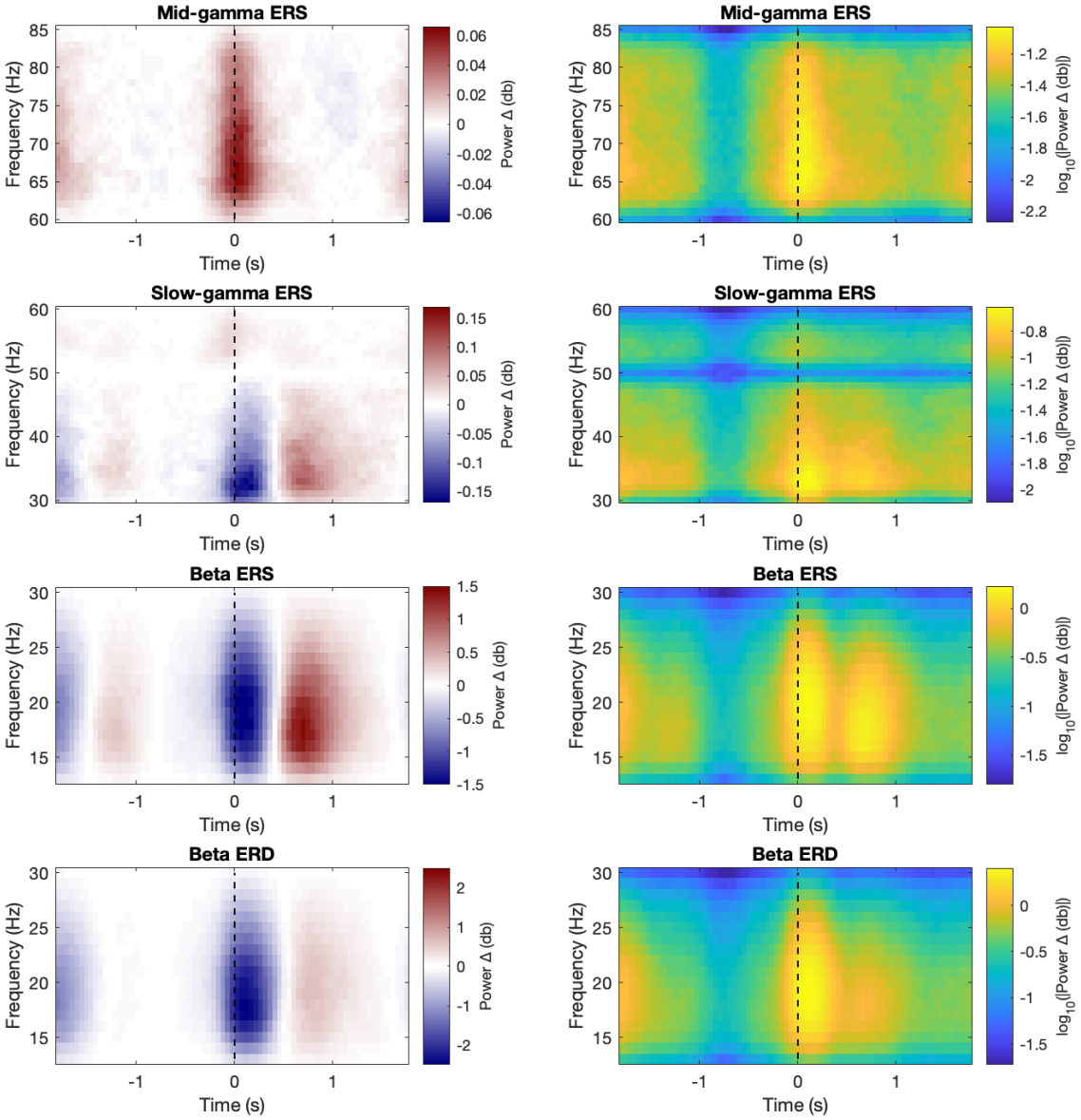


Figure 4.3: Grand average plots showing the temporal and spectral characteristics of movement-related responses from each participant's peak voxel. The left column represents median changes in power relative to baseline (-1 to -0.5 s before button press, which happens at time 0) for the following frequency bands and movement-related responses, from top to bottom: mid-gamma ERS, slow-gamma ERS, beta ERS, and beta ERD. Plots in the right column visualise the mean log_{10}-transformed absolute power change relative to the same baseline for the same frequency bands.

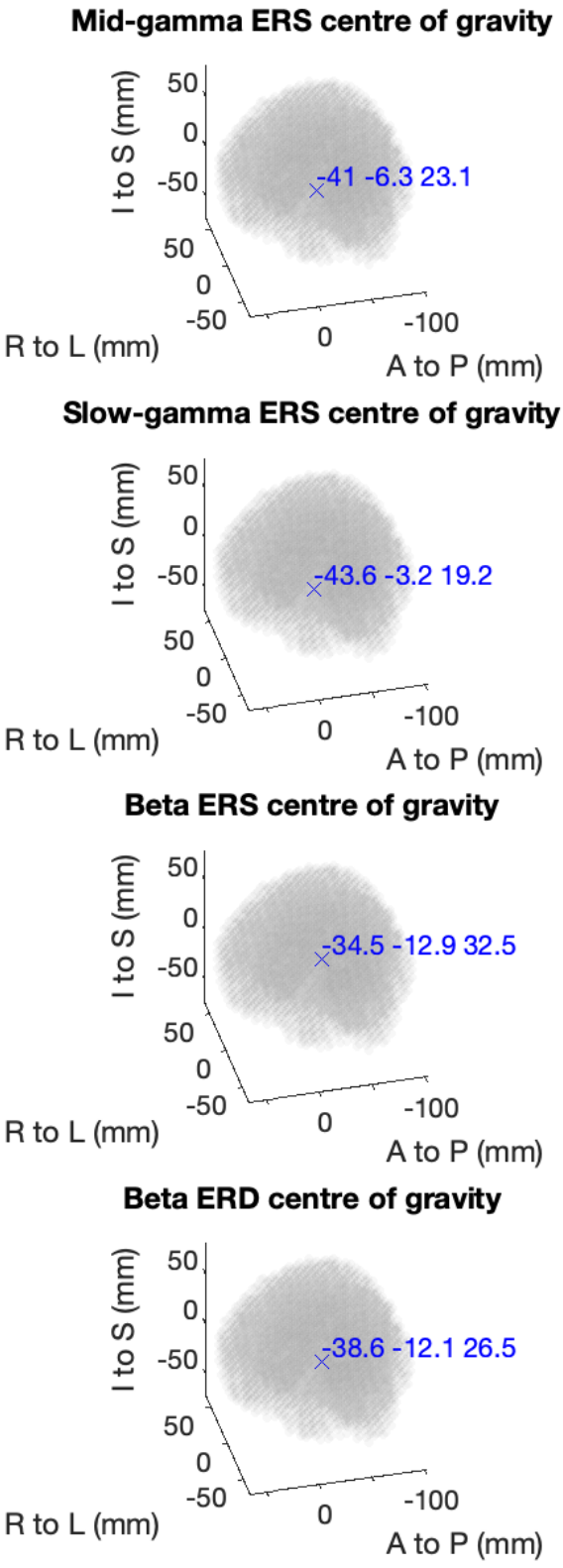


Figure 4.4: Group average of the centre of gravity of movement-related activity. The centre of gravity was calculated by taking the means of peak voxel x (left-right axis), y (anterior-posterior axis), and z (superior-inferior axis) coordinates respectively from all participants.

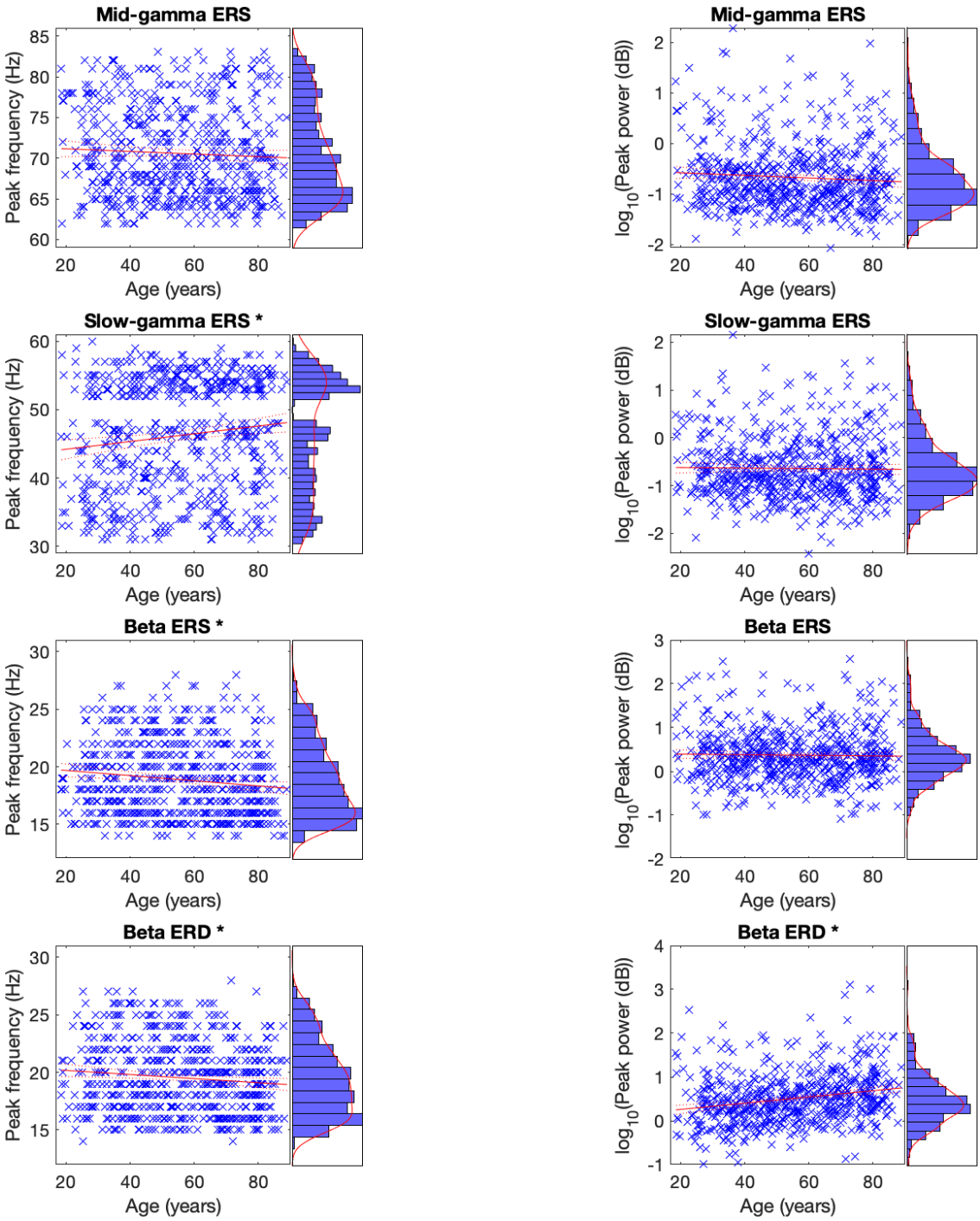


Figure 4.5: Relationship between age and peak frequency (left) and power (right) for mid- and slow-gamma ERS, beta ERS and ERD. In the scatterplots, each point represents an individual participant's data, the red solid line represents the linear regression fit and the dotted red lines the 95% confidence bounds. In the histogram, the red line is the probability density estimate. An asterisk (*) next to response metric indicates p-value below 0.05.

Table 4.2: Relationship between age and peak voxel coordinates of movement-related activity described by linear regression models.

Response	Peak voxel coordinate	Intercept	Slope	*p-value*	R^2
Mid-gamma ERS	**X**	**-35.93**	**-0.093**	**0.0012**	**0.017**
Mid-gamma ERS	**Y**	**-9.00**	**0.049**	**0.046**	**0.0065**
Mid-gamma ERS	Z	26.50	-0.061	0.094	0.0046
Slow-gamma ERS	**X**	**-39.49**	**-0.074**	**0.0039**	**0.014**
Slow-gamma ERS	Y	-4.56	0.026	0.27	0.002
Slow-gamma ERS	Z	20.98	-0.032	0.40	0.0012
Beta ERS	**X**	**-30.75**	**-0.069**	**0.00023**	**0.022**
Beta ERS	**Y**	**-20.14**	**0.13**	**$2.8e^{-8}$**	**0.049**
Beta ERS	**Z**	**41.68**	**-0.17**	**$1.8e^{-7}$**	**0.044**
Beta ERD	X	-37.59	-0.019	0.22	0.0024
Beta ERD	Y	-12.94	0.015	0.49	0.00077
Beta ERD	Z	28.21	-0.031	0.30	0.0018

elled by linear regressions.

Participant's ages predicted a shift to the left for mid-gamma ERS ($p = 0.0012, R^2 = 0.017$), slow-gamma ERS ($p = 0.0039, R^2 = 0.014$), and beta ERS ($p = 0.00023, R^2 = 0.022$), but not beta ERD. There is evidence for an age-related anterior shift for mid-gamma ERS ($p = 0.046, R^2 = 0.0065$) and beta ERS ($p = 2.8e^{-8}, R^2 = 0.049$), but not slow-gamma ERS or beta ERD. Finally, the only statistically significant association between age and the Z coordinate of peak voxels was an inferior shift in beta ERS ($p = 1.8e^{-7}, R^2 = 0.0044$).

To better visualise the age-related changes in peak voxel coordinates, centres of gravity of the youngest 150 (aged 18-40) and oldest 150 (aged 71-89) participants for each movement-related response are shown in Figure 4.7. The centre of gravity for mid-gamma ERS was positioned anteriorly and to the left in the oldest participants (*x: -38.4*, *y: -7.7*, z: 25.0 in the youngest 150 participants and *x: -42.6*, *y: -5.5*, z: 21.9 in the oldest 150 participants). Slow-gamma centre of gravity was comparable between the youngest and oldest participants, except for a shift to the left in the oldest group (*x: -41.7*, y: -3.9, z: 21.0 in the youngest 150 participants and *x: -45.1*, y: -1.9, z: 18.4 in the oldest 150 participants). The beta ERS centre of gravity was shifted left, anteriorly and inferiorly in the oldest participants (*x: -36.5, y: -9.4, z: 28.6*) compared to the youngest ones (*x: -32.6, y: -16.0, z: 37.3*). For beta ERD, the centre of gravity was comparable between the youngest 150 (x: -38.1, y: -12.2, z: 27.6) and oldest participants (x: -39.1, y: -12.3, z: 26.4).

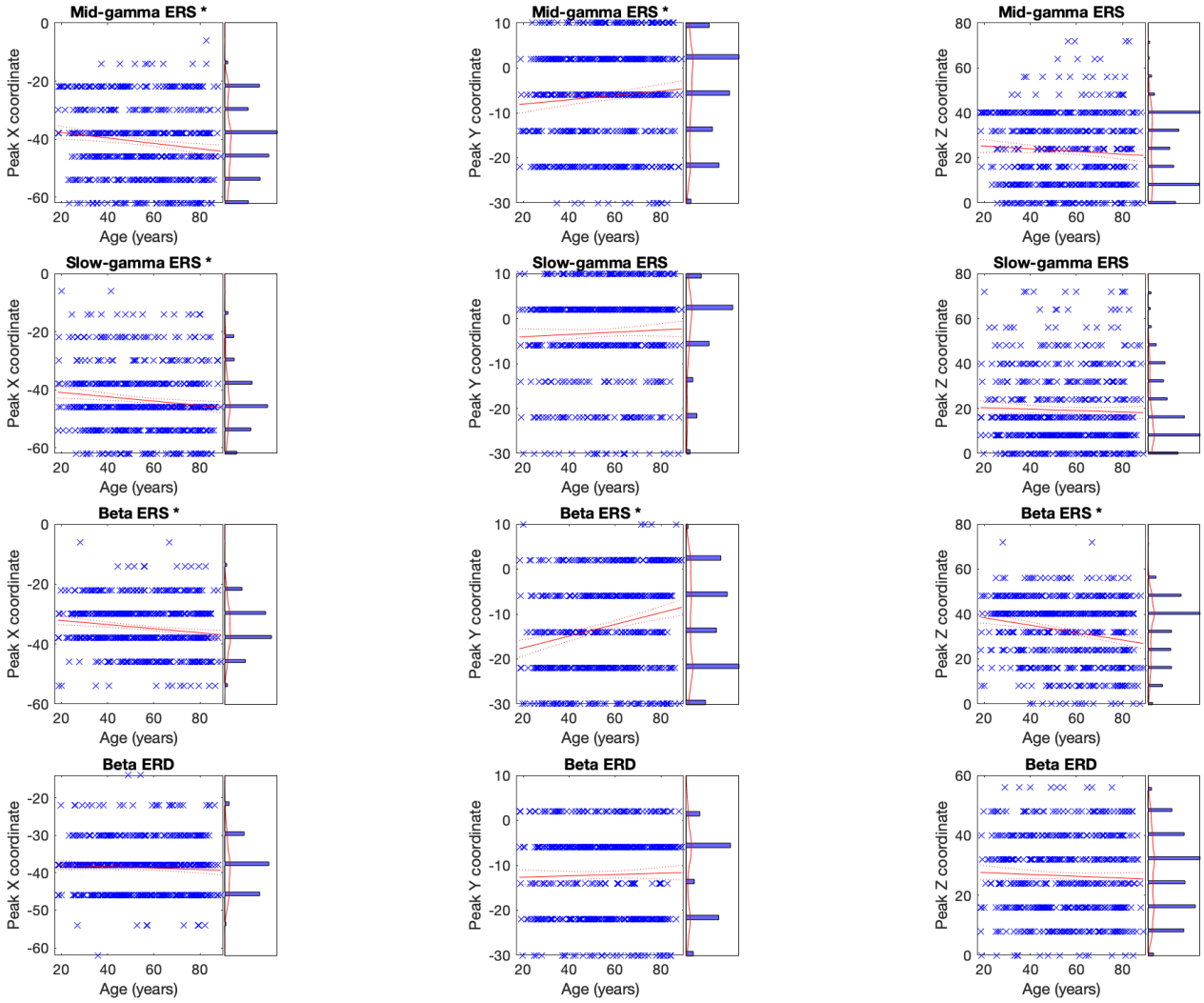


Figure 4.6: Relationship between age and peak voxel coordinates x (left column, left-right axis), y (middle, anterior-posterior axis), and z (right, superior-inferior axis) for mid- and slow-gamma ERS, beta ERS and ERD. In the scatterplots, each point represents an individual participant's data, the red solid line represents the linear regression fit and the dotted red lines the 95% confidence bounds. In the histogram, the red line is the probability density estimate. An asterisk (*) next to response metric indicates p-value below 0.05.

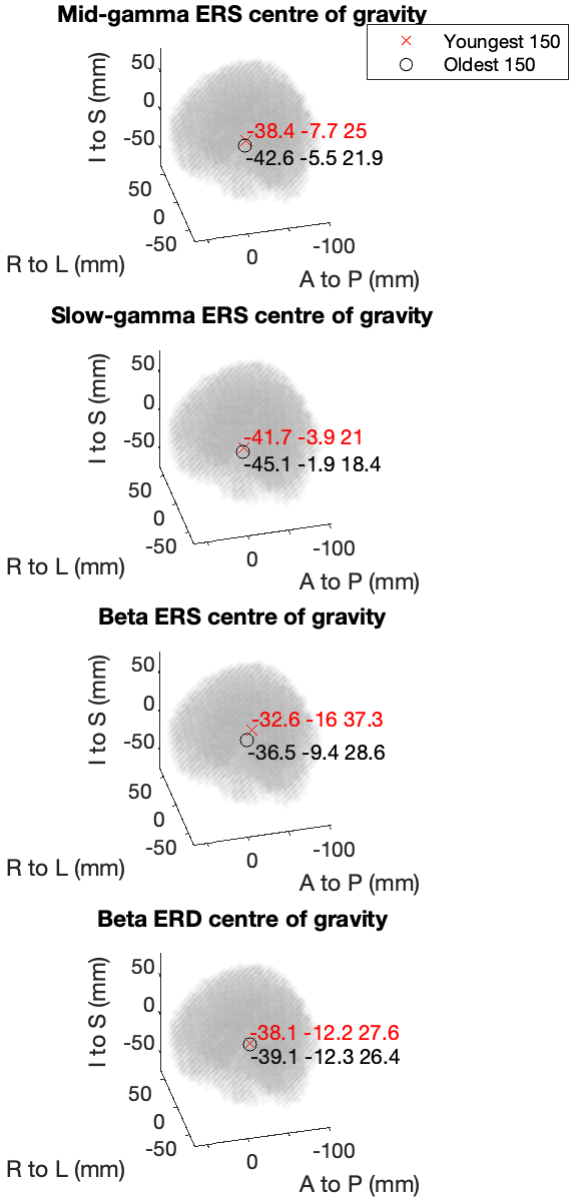


Figure 4.7: Comparison of the movement-related activity centre of gravity between the youngest and oldest participants. The centre of gravity was calculated by taking the means of peak voxel x (left-right axis), y (anterior-posterior axis), and z (superior-inferior axis) coordinates respectively from the youngest 150 (age range 18-40) and the oldest 150 (age range 71-89) participants.

4.4 Discussion

This study investigated age-related changes in button press-related primary motor cortex (M1) activation in healthy adults. I aimed to replicate peak power and frequency results from a previous study[145] using the same dataset with an analysis method where I obtained an individual peak voxel, frequency and power for each participant and each frequency band separately. I used the Cambridge Centre for Ageing and Neuroscience (CamCAN) dataset, which enabled me to look at a larger participant pool compared to most previous studies while also encompassing a wide range of ages (18-88 years). I found age-related changes in amplitude, power of movement-related activity, as well as a shift in localisation of activation for some of the frequency bands and responses.

4.4.1 Age-related changes in gamma band frequency

Movement-related activity in the gamma frequency band is less explored compared to other frequency bands. This is partly because the amplitude of oscillations is reduced with increased frequency and therefore harder to detect. For example, in a previous study from my group, movement-related M1 gamma band activity could not be reliably detected in more than half of participants[65]. Here, I split the gamma band into two separate bands: slow-gamma (30-60 Hz) and mid-gamma (60-85 Hz) based on previous literature that indicates they represent different functional states[68,314]. Analysing each frequency band separately, especially from beta, aided in more reliable detection of gamma band activity.

Expected age-related changes in mid-gamma peak frequency and power were not observed

In the mid-gamma band, I observed the expected strong movement-related ERS response that reached its peak around the time of movement, consistent with previous literature[28,62]. I did not find evidence for an age-related change in mid-gamma peak frequency or power as hypothesised. This is inconsistent with the previous CamCAN study[145], which found a decrease in mid-gamma power associated with increased age, although there was no significant association between age and peak frequency. However, I believe their mid-gamma ERS detection method did not work perfectly. Based on their data distribution, many mid-gamma peak frequencies were at the ceiling or floor of the band that they defined as 60-95 Hz. Therefore, this may also have affected the power data.

The relationship between age and mid-gamma band responses has not been consistently observed in past research. An age-related movement-related gamma peak frequency decrease was noted by one study[85] but was not observed in another that found a negative relationship between age and mid-gamma power[61]. Significantly lower movement-related peak frequency and power in the mid-gamma band have been found in older compared to younger adults[66].

Moreover, in the auditory system, there is evidence of a decrease in gamma peak frequency in older participants[315], while no significant relationship was seen for somatosensory gamma peak frequency[316]. In the visual cortex, there are numerous studies showing reduced gamma peak frequency with age[99,153–156].

Mid-gamma band activity in M1 is often considered pro-kinetic[28], the mid-gamma peak power has been linked to movement speed[66] and motor learning[70]. Therefore, it may be useful to relate the participants' mid-gamma power to button press response times in this study. Conversely, studies characterising movement-related gamma activity found that gamma power is stronger in initial trials and during larger movements[62] and decreases with practice[64]. One potential reason for not finding a relationship between age and mid-gamma activity could be that the button press may be too simple as a task. A more complex task may be needed to find age-related changes in mid-gamma activity.

Slow-gamma peak frequency increases with age

Activity in the slow-gamma band is less well understood compared to mid-gamma. Most evidence for the existence of this band comes from the rodent hippocampus[68,314], where the slow-gamma band is thought to be mediated by separate subsets of interneurons compared to faster gamma rhythms[317]. Slow- and mid-gamma activity is thought to encode different types of information in the hippocampus[314]. In a recent study from my group, M1 movement-related slow-gamma peak frequency was found to be associated with a non-invasive brain stimulation measure of inhibition[70]. In contrast, mid-gamma peak power was related to motor learning. However, in the same study, slow-gamma ERS occurred around movement offset, while in the present study, the group peak of slow-gamma ERS was before the button press. An older study found that maximum movement-related 40 Hz activity occurred shortly before movement onset[43], which would be more consistent with my findings. The study from my group observed a clear slow-gamma ERS with a mean peak of 43 Hz. In the present study, at 40-43 Hz, slow-gamma band exhibits a strong decrease in activity followed by an increase. These changes in activity temporally resemble the dynamics of beta ERD and ERS and may be caused by spillover from the beta band. The analysis methods were very similar between the two studies, except for one major difference, in that the other study recorded muscle activity while participants performed a button press. Their analysis aligned MEG signal to movement onset, while in this study, it was relative to the button press. Movement onset-locked data based on EMG provides improved temporal precision, better alignment to neural processes and higher sensitivity to more subtle changes in neural activity compared to locking to the button press, and may explain why I could not reliably measure slow-gamma ERS.

In the previous CamCAN study by Bardouille, grand average plots also reveal a pattern of ERD followed by ERS up to approximately 50 Hz[145] consistent with my results. The same is true for another study investigating movement-related gamma[85]. However, neither study

looked at the relationship between age and slow-gamma band activity, only mid-gamma. Although I found that slow-gamma peak frequency increases with age, it is not clear whether it is a true association, or due to the spillover from beta.

4.4.2 Age-related changes in beta band frequency

Activity in the beta band (13-30 Hz) has been repeatedly described in the last decades. At the time of movement, beta band activity decreases in power (event-related desynchronisation, ERD), exceeds pre-movement levels after movement cessation (ERS) before returning to pre-movement baseline levels[42]. I observed movement-related beta ERD and ERS responses consistent with previous research.

Beta synchronisation peak frequency decreases with age

I observed an age-related decrease in the peak frequency of movement-related beta ERS, with no significant relationship between age and peak power. In contrast, the CamCAN study found both a reduced peak frequency and amplitude of beta ERS with age[145]. One difference that could explain why I did not find a significant relationship between age and peak power of beta ERS, while Bardouille et al. did, is that they excluded trials where button presses occurred within 3 seconds of each other[145]. I did not set a threshold for excluding trials that were close together. Beta ERS is specific to movement termination[140] and can occur 0.5-1.25 seconds following movement. Therefore, it is possible that in my analysis, beta ERS may have been cancelled out by the subsequent trial.

Previous studies have also identified age-related reductions in beta ERS peak power in tasks with complexity similar to that used in the CamCAN study[144,146]. However, neither of these studies reported age-related changes in peak frequencies.

Beta desynchronisation becomes stronger with age

I found an age-related decrease in beta ERD peak frequency and an increase in peak power. Although the other CamCAN study did not find a relationship between age and beta ERD peak frequency, they also observed stronger ERD with increasing age[145].

Both my peak frequency[142] and peak power[61,146,148,149,318] findings are consistent with previous literature and my hypotheses. However, they are in contrast to the expected reduction in GABA and inhibition with age[85,109,120]. Diazepam, a positive allosteric modulator of the $GABA_A$ receptors, reduces beta ERD peak frequency and increases power[45]. Tiagabine, a GABA transporter blocker, also increases resting beta ERD peak power[80]. Increasing inhibition using pharmacological approaches leads to stronger beta ERD, although increased beta ERD is also found in older adults whose brains are believed to have lower levels of GABA. Therefore, the observed age-related changes in beta ERD activity are likely due to different mechanisms rather than pure GABAergic influence.

Increased ERD in older adults has been suggested to reflect over-activation[319]. This is supported by evidence showing that absolute beta power during ERD is higher in older adults compared to younger adults, even if the relative decrease is larger in older participants[140,149]. Older adults also have higher resting beta power, which in turn has a positive relationship with relative beta ERD power[140]. Stronger resting beta power could mean that its suppression necessary for a movement to occur would also be greater, which may require more time[140]. For example, in Parkinson's disease, patients show higher beta activity in the basal ganglia, and treatment that reduces beta correlates with functional improvement[320], showing that increased resting beta power may present a hurdle in reaching a threshold for movement execution. Relating the measures of beta ERD activity to participants' response times would help determine whether this may be the case. Moreover, the relationship between beta ERD and endogenous levels of GABA measured by magnetic resonance spectroscopy (MRS) has not yet been reported, but would aid in explaining the mechanisms of beta ERD.

4.4.3 Age-related changes in movement-related activity localisation

The spatial changes in patterns of activation of sensorimotor task-related MEG signals due to age are not well understood, especially for distinct frequency bands. Older participants generally have broader activation in motor and non-motor areas[114,115]. Previously, Bardouille et al. showed that gamma ERS occurs mainly in the contralateral hemisphere, while beta band activity is more bilateral with a contralateral dominance[145]. However, they did not look at changes in activation with age.

In my study, I looked at the individual coordinates of peak voxels in relation to participants' ages. I observed that activation in the mid-gamma frequency band shifted anteriorly and left (lateral for left hemisphere) with increased age. Slow-gamma frequency band activation became more lateral with age. When performing a simple finger movement, older participants exhibit greater fMRI activity in the lateral premotor area[115] compared to younger adults, which is consistent with my findings of an anterior and lateral shift in activation. However, a different study found greater fMRI activation in the premotor cortex in younger participants[114]. Although the localisation of fMRI and MEG source signals have been found to be similar[321], the comparison between different frequency bands and fMRI signal is not clear.

I found a significant age-related anterior, lateral and inferior shift for beta ERS. In a different CamCAN study, post-movement transient beta bursts shifted anteriorly with age[152], although they did not find an association with coordinates in lateral-medial or inferior-superior dimensions. In contrast to beta ERS, I found no age-related change in location with age for peak beta ERD activity. Previously, Pfurtscheller and Lopes da Silva suggested that stronger ERD could represent the involvement of a larger neural network[43]. Since beta ERD was stronger in older participants, activity may have been more widespread spatially, but centred on the

same area as beta ERD of younger participants.

In summary, I found some age-related changes in the localisation of movement-related activity. Previous literature, particularly on changes in specific frequency bands, is limited; therefore, it is difficult to draw definite conclusions on this association.

4.4.4 Limitations

In this study, I investigated age-related changes in movement-related M1 activation in healthy adults. However, there are some limitations of the methods and my findings that should be considered.

Even though some relationships between age and MEG metrics were statistically significant, the observed R^2 values were very small in some of these instances. Higher R^2 values indicate better fit of the model to data and, therefore, age did not explain a large proportion of the variance in the dependent variables in the models. Having a large sample size means that even small effects can be detected. However, there are likely other factors than just age that contributed to the metrics of interest.

In the pre-processing stage, I had to utilise several filters to remove noise and artefacts that impact signal in the gamma band frequency ranges. I used a 50 Hz notch filter to reduce power line noise. This likely affected slow-gamma (30-60 Hz) quantification, since the grand average peak frequency for all participants was 54 Hz. Furthermore, the low-pass filter used for the upper threshold of the frequency band also attenuated the signal just below 60 Hz (Figure 4.3), which could have further impacted peak power and frequency determination. Finally, I had to set the upper limit for the mid-gamma band to 85 Hz rather than the standard 90 Hz[65,80,85] due to an artefact at 88 Hz present in some channels in datasets from most participants.

I only investigated linear relationships between age and MEG metrics. The CamCAN dataset includes participants ranging from 18 to 88. However, the brain develops into the 20s[322], thus associations may not be linear. Indeed, Power and Bardouille, who also analysed the CamCAN dataset, observed that the localisation pattern of beta burst source estimations in the 18-32 age group was least similar to older participants[152]. Exploring non-linear relationships may provide further insight into studying age-related brain changes.

MEG power in the beta and gamma frequency bands has a positive relationship with cortical thickness, which, in turn, decreases with age[141]. I did not account for cortical thickness in my analysis, but cortical thinning could contribute to changes in the localisation of movement-related activity. Primary motor and sensory cortices have been shown to experience significant thinning in older adults compared to younger adults[107,108]. If M1 thins more or earlier than premotor areas, it could contribute to shifts in activity as power would be increased in areas with higher cortical thickness.

I also did not account for participants' levels of physical activity; staying physically active may counteract some of the effects of ageing. Younger adults and active older adults have less fMRI-measured activation in ipsilateral M1 during a simple finger movement task compared to sedentary older adults, representing reduced interhemispheric inhibition[323]. Physical fitness may therefore reduce or delay some effects of ageing which I didn't account for.

In my analysis, I averaged over trials to find movement-related MEG metrics of interest. However, recent evidence has increasingly supported the hypothesis that at the level of a single trial, beta activity consists of transient intermittent burst-like events that only appear as a sustained and slowly modulated signal when averaged over many trials[76,77,324–326]. Averaging these bursts results in a loss of temporal dynamics[327], which could be an important factor in the mechanisms of ageing. Beta bursts have also been found to be spatially more specific compared to averaged beta ERS activity[77], which could reveal changes in activation localisation due to age in more detail. Age-related changes in beta bursts have already been explored in the CamCAN dataset[151,152], but the paradigm was not sensitive to gamma bursts. Developing an analysis method for detecting transient gamma burst activity could help determine movement-related changes due to age in the gamma frequency band.

Data used in this study are cross-sectional rather than longitudinal. Age-related changes in MRS-measured levels of GABA have been seen longitudinally with no cross-sectional effect of age on GABA[131]. Since I hypothesised that some MEG movement-related metrics are linked to GABA and inhibition in M1, some effects of age on MEG metrics may also be only seen longitudinally. CamCAN are working on extending their dataset with longitudinal data[308], which will allow better investigation of age-related changes in MEG metrics of interest.

4.4.5 Conclusion

I investigated age-related changes in brain activity detected by MEG during a sensorimotor task. I found the following age-related changes in MEG response: increased slow-gamma peak frequency, reduced beta ERS and ERD peak frequency, and increased beta ERD power with age. I did not find a change in mid-gamma peak frequency or power as expected. Therefore, I was only able to replicate some previously published results using the same dataset. I also explored age-related changes in the localisation of movement-related responses. Mid-gamma ERS shifted anteriorly and laterally with increased age, slow-gamma ERS shifted anteriorly, and beta ERS shifted anteriorly, laterally and inferiorly.

Chapter 5

Exploring the contribution of genetic polymorphisms to inter-individual variability in M1 gamma band activity

5.1 Introduction

Neural oscillations are ubiquitous in the human brain and are a fundamental mechanism for coordination of neuronal activity. Oscillations in the gamma band frequency (30-100 Hz) are strongly associated with active brain processing, including sensory stimulation in the auditory, visual and somatosensory domains[328–330], active movement[331], working memory[332] and long-term memory[333].

There is high inter-individual variability in the amplitude and peak frequency of gamma band activity in the human visual cortex[154]. Task parameters, such as stimulus contrast, speed, and size have been shown to affect gamma peak frequency and power[334–336]. It has been further suggested that some neurophysiological parameters, such as recurrent connections between inhibitory interneurons and superficial pyramidal cells might account for gamma band power, and self-modulatory connections of pyramidal neurons might account for peak frequency[41]. Here, I explore the contribution of specific physiological factors to gamma band power and frequency, via studying the effects of specific single nucleotide polymorphisms in a large human dataset.

5.1.1 Inhibitory neurons drive gamma band activity

Several studies have investigated the neurophysiological underpinnings of gamma band activity. Gamma band oscillations have been related to the activity of fast-spiking parvalbumin interneurons (PVI)[8,58,90,337,338], which control spike timing in excitatory neurons[90,339,340]. Optogenetic manipulation of neuronal circuits has shown that depolarization of PVI leads to an increase in gamma band power, while hyperpolarisation leads to a decrease in gamma band power[91]. Although optogenetic stimulation is not physiological and may not fully represent processes in the brain, these findings provide additional evidence to the involvement

of PVI in gamma band generation. PVI undergo profound maturational changes during the transition from adolescence to adulthood[341,342], including epigenetic modifications[343,344], and fluctuations in the glutamatergic drive onto PVI through N-methyl-d-aspartate receptors (NMDARs)[345,346]. Therefore, it is likely that both GABAergic and glutamatergic neurons are critical for establishing gamma frequency oscillations.

Another inhibitory mechanism modulating gamma band activity is thought to be tonic inhibition. This process is mediated by $GABA_A$ receptors located at extrasynaptic sites through a low resting level of extracellular GABA and synaptic spillover[92]. In the cortex and hippocampus, a major class of receptors found extrasynaptically are $\alpha 5$ subunit-containing $GABA_A$ receptors. In hippocampal slices from mice lacking the $\alpha 5$ subunit, gamma band activity is higher in amplitude compared to wild type mice with no change in frequency[93]. Mice lacking δ subunit-containing $GABA_A$ receptors exhibited an increase in gamma frequency in the hippocampus[92]. $GABA_A$ receptors are therefore highly implicated in the modulation of gamma band activity.

Cortical dopamine modulates the intrinsic excitability of GABAergic and glutamatergic cortical neurons[347–349]. The modulatory effects of dopamine are mediated by different classes of dopaminergic receptors, which can enhance or decrease NMDA conductance of both pyramidal neurons and PVI responsible for the generation of gamma band oscillations[350,351]. Thus, GABAergic, glutamatergic and dopaminergic neuromodulation all appear to be important in the elicitation of gamma band oscillations.

5.1.2 Heritability of gamma band activity characteristics

Gamma band activity is a highly heritable trait, with the heritability of visually-induced gamma band peak frequency being around 91% in twins[216]. The deletion of some genes implicated in neural transmission also seems to affect the integrity of gamma band oscillations[352]. However, it is not clear which genes are associated with gamma band activity and the potential clinical implications of these genetic variants.

So far, some studies have analysed several candidate genes such as *COMT* and *BDNF* in relation to gamma band activity by using different sensory and cognitive EEG and MEG paradigms. However, no study has yet investigated the relationship between motor-related gamma band activity and genetic polymorphisms. I hypothesize that there may be a relationship between gamma band activity change and movement, since changes in gamma band activity have been observed in movement disorders such as Parkinson's disease[353–356] and parkinsonian dyskinesia[357,358], isolated dystonia[359,360] and amyotrophic lateral sclerosis (ALS)[361].

Here, I will discuss single nucleotide polymorphisms (SNPs) of some candidate genes that may be associated with inter-individual variability in MEG-measured motor gamma band activity. First, I will focus on two genes associated with GABAergic neural transmission,

given the strong association of inhibitory interneurons with gamma band activity. Then, I will discuss two genes involved in neuromodulation that have previously been associated with gamma band oscillations in previous M/EEG human studies.

5.1.3 Genes of interest

GABRA5: SNP rs12916303(G:T)

$GABA_A$ receptors are the major inhibitory receptors in the brain[362]. They are pentameric, made up of at least three different subunits and act as chloride channels when activated by GABA[362]. The *GABRA5* gene encodes the $\alpha 5$ subunit of $GABA_A$ receptors[362]. $\alpha 5$ subunit-containing $GABA_A$ receptors are often found at extrasynaptic sites on neurons in the neocortex and hippocampus and are thought to mediate tonic inhibition through a low resting level of extracellular GABA and synaptic spillover[363]. In hippocampal slices from mice lacking the $\alpha 5$ subunit, gamma band activity is higher in amplitude compared to wild type mice[93]. Similarly, administration of diazepam, which activates $\alpha 5$ subunit-containing neurons, leads to higher power of spontaneous gamma band activity in the sensorimotor cortices of healthy participants[72].

Although there is not yet an identified *GABRA5* SNP that alters GABAergic neurotransmission directly, there is evidence linking impaired GABAergic transmission to gamma band activity in patients with schizophrenia. The distribution volume of a positron emission tomography (PET) radiotracer, [11C]flumazenil, which selectively binds to $GABA_A$ receptors as a ligand at the benzodiazepine site, was lower in schizophrenia patients after the administration of tiagabine, a drug that increases extracellular GABA[102]. The affinity of the benzodiazepine site for [11C]flumazenil is generally thought to increase with higher levels of GABA[102]. The drug-associated change in [11C]flumazenil binding was positively associated with gamma band activity measured during a cognitive EEG task in healthy participants, but not in the schizophrenia group[102]. Moreover, the expression of $\alpha 5$ subunit mRNA was reduced in layer 4 of the dorsolateral prefrontal cortex (DLPFC) in postmortem brains of patients with schizophrenia compared to healthy controls[364]. Overall, these results suggest that there may be an impairment in both GABAergic neurotransmission and gamma band activity mediated by extrasynpatic $GABA_A$ receptors in schizophrenia.

To find a suitable *GABRA5* SNP that affects whole gene expression and therefore could plausibly be associated with changes in GABAergic transmission, we looked at RNA sequencing analysis of postmortem human brain from the BrainSeq consortium[365,366]. The SNP rs12916303 fits these criteria. Although the effect of the polymorphism on protein expression cannot be predicted from the data, the minor allele is linked to lower expression of the $\alpha 5$ subunit mRNA in the DLPFC.

GAD1: SNP rs3749034(G:A)

Glutamic acid decarboxylase (GAD) is a key enzyme in the synthesis of cortical GABA by catalysing glutamate to GABA. There are two isoforms in the brain, a 67 kDa isoform (GAD67) encoded by the gene *GAD1*, and a 65 kDa isoform (GAD65) encoded by *GAD2*[367]. The rs3749034 SNP is located in the first exon of *GAD1* at the 5' untranslated region, which is hypothesised to be a promoter region[368], and may be therefore linked to changes in expression. For example, *GAD1* expression has been found to be reduced in prefrontal cortex of patients with schizophrenia[369]. Moreover, a recent meta-analysis found reduced parvalbumin cell density and parvalbumin mRNA levels in post-mortem brains of schizophrenia patients compared to healthy controls[370]. Knockdown of *GAD1* in parvalbumin interneurons leads to a decrease in GABA release probability[371]. Changes in *GAD1* function or expression may therefore have further effect on gamma band activity.

There is no direct evidence regarding the involvement of *GAD1* in gamma band activity from human research. However, changes in function, changes in expression and genetic polymorphisms in *GAD1* are linked to disorders that are associated with altered gamma band activity. In panic disorder, four single-nucleotide polymorphisms (SNPs), including rs3749034, were associated with a significant genotype x gender interaction[372]. Polymorphisms in *GAD1* SNP rs3749034 are associated with childhood-onset schizophrenia[373], with reduced GAD67 mRNA expression in the dorsolateral prefrontal cortex (DLPFC)[368] and an increased likelihood of a diagnosis of treatment-resistant schizophrenia compared to healthy controls[374]. In ADHD, the presence of the major allele in rs3749034 is associated with more severe symptoms in the hyperactive/impulsive symptoms domain[375].

Despite the evidence of a link between *GAD1* genotype and several psychiatric disorders characterized by impaired gamma band oscillations, to the best of our knowledge, no studies have ever directly investigated the association between *GAD1* polymorphism and gamma band oscillations in human data. In mice lacking *GAD1* in PVI, high gamma and ripple (60–200 Hz) powers are decreased in the neocortical upper layers[376]. Given these results from mice, the causal relationship between function of parvalbumin interneurons and gamma band oscillations[90], and some evidence in M/EEG studies showing a correlation between the peak frequency and power of gamma band oscillation and GABA levels measured by magnetic resonance spectroscopy (MRS)[95,97], I hypothesize that *GAD1* genotype may partially account for the individual variability in gamma band power and peak frequency observed in healthy adults.

BDNF: SNP rs6265(C:T)

The brain-derived neurotrophic factor (BDNF) is implicated in the maintenance, survival, growth of neurons, and in activity-dependent synaptic plasticity[377,378]. The SNP rs6265 resulting in a Val66Met mutation is the most investigated of the *BDNF* gene, leading to

lower BDNF secretion[379]. The Val66Met polymorphism has been associated with a wide array of disorders, including neurodegenerative diseases such as Alzheimer's and Parkinson's diseases[380] and psychiatric disorders including schizophrenia[381], depression and anxiety[382].

BDNF genotype has been shown to influence GABAergic transmission. *BDNF* heterozygous mice present with impaired presynaptic GABA release and a general shift toward reduced inhibition in the brain[383]. A decreased number of PVI was found in mice with severely reduced activity-dependent BDNF expression, as well as impaired GABAergic transmission[384]. Met/Met genotype mice showed reduced PVI dendritic volume, branching, and spine density[385]. On the other hand, in young adults, BDNF serum levels were found to have a negative association with MRS-measured GABA levels[386].

Moreover, there is growing evidence linking *BDNF* to synaptic plasticity and hippocampal[379,387] and motor learning[388]. A study in mice has shown that cortico-striatal depletion of BDNF can affect motor learning[389]. In humans, the *BDNF* genotype contributes to inter-individual variability in learning speed[390,391] and has been suggested to mediate the effects of transcranial direct current stimulation (tDCS) on motor learning when applied to the primary motor cortex (M1)[392]. The Val66Met *BDNF* polymorphism has been shown to affect motor rehabilitation in stroke survivors[393,394].

BDNF has also been linked to gamma band activity. In vitro depletion of BDNF from the hippocampal subfield CA3 reduced the power of gamma band oscillations in CA1[395], and Val/Met genotype mice exhibited reduced gamma band response to auditory stimuli compared to wild-type mice[396]. MEG resting-state studies in humans have revealed reduced gamma band functional connectivity in participants with a Met/Met genotype[397,398], and a correlation between BDNF serum levels and gamma band activity power[399]. However, it is not clear if there is also an association between gamma band oscillations elicited by motor activity and *BDNF* genotype. Preliminary evidence from TMS studies indicates that the excitability of M1 and the balance between excitatory and inhibitory neural transmission may be associated with the *BDNF* genotype, with carriers of the Met allele exhibiting less TMS-induced plasticity[400]. Given the role of BDNF in motor learning and the influence on excitation-inhibition balance, I hypothesize that there may be a correlation between *BDNF* genotype and movement-related gamma band oscillations.

COMT: SNP rs4680(G:A)

The Catechol-O-methyl transferase (*COMT*) gene encodes a catabolic enzyme involved in the degradation of catecholamines such as dopamine. In humans, there is a functional polymorphism (Val158Met) in which the Val allele renders the COMT enzymes more active than the Met allele, thus inactivating extracellular dopamine more slowly, leading to higher levels of dopamine in individuals with the Met allele[401]. Dopamine is believed to increase the excitability of PVI through D1 dopamine receptors[402]. Val/Val allele carriers are therefore believed to have lower prefrontal dopamine levels. People with the Val/Val allele indeed

show reduced performance in working memory and executive function tasks[403] compared to heterozygotes and Met/Met homozygotes.

The *COMT* Val158Met polymorphism has been proposed to be associated with the cognitive phenotype of several neuropsychiatric disorders, including schizophrenia and Alzheimer's disease[404–407]. Furthermore, deletion of the chromosome fragment containing the COMT gene results in a complex syndrome, psychiatric manifestations of which include schizophrenia and other psychotic disorders[408,409]. In this population, *COMT* expression can also modulate the response to GABAergic medications[410], supporting the idea that dopaminergic modulation of interneurons may be implicated in the behavioural manifestations of the syndrome.

In the general population, MEG studies found Val allele carriers to have a reduced gamma band response during a working memory task[411] and Met/Met carriers to have higher resting functional connectivity in the gamma band[398]. Moreover, there is preliminary evidence to indicate a relationship between the Val158Met polymorphism and gamma band oscillations elicited by other types of stimuli, such as auditory stimulation during an attentional task[412]. Similarly, the presence of the Val allele has been associated with the upregulation of GABAergic genes[413]. Overall, these studies suggest the *COMT* genotype may contribute to the inter-individual variability in gamma band response.

Control SNP: rs11062102(T:C) in *SLC6A13*

I also performed a negative control analysis between genetic polymorphisms and gamma band activity by using a SNP from a gene that encodes a protein closely related to the GABA genes discussed above, but not widely expressed in the brain. I selected the gene *SLC6A13*, which encodes GABA transporter 2 (GAT2).

5.1.4 Aims

I split this project into two separate studies based on the function of genes. In both, the impact of genetic polymorphisms on MEG metrics of gamma band activity will be assessed. First, the impact of genes that are directly involved in GABAergic transmission will be tested. In the second study, the genes tested were those involved in neuromodulation, which therefore affect inhibitory neurotransmission indirectly. I tested the following hypotheses, which were pre-registered[414]:

Study 1: GABAergic genes

1. *GABRA5*: Alleles associated with lower expression of the extrasynaptic $\alpha 5$ subunit-containing $GABA_A$ receptor (SNP rs12916303, minor allele T) will be associated with higher gamma peak frequency and power.

2. *GAD1*: Alleles associated with lower mRNA expression of the GABA synthesising

enzyme GAD67 (SNP rs3749034, major allele G) will be associated with lower gamma peak frequency and power.

3. *SLC6A13* (control analysis): I expect no significant association between the expression of GABA transporter GAT2 (SNP rs11062102) and gamma peak frequency and power.

Study 2: Neuromodulatory genes

1. *BDNF*: Alleles associated with lower BDNF secretion (SNP rs6265, minor allele T) will be associated with lower gamma peak frequency and power.

2. *COMT*: Alleles associated with higher activity of the COMT enzyme (SNP rs4680, major allele G) will be associated with lower gamma peak frequency and power.

3. *SLC6A13* (control analysis): I expect no significant association between the expression of GABA transporter GAT2 (SNP rs11062102) and gamma peak frequency and power.

5.2 Methods

5.2.1 Open-access CamCAN imaging dataset

For this study, I used participant data from the Cambridge Centre for Ageing and Neuroscience (CamCAN) dataset[308,309] (available at `http://www.mrc-cbu.cam.ac.uk/datasets/camcan/`). Data collection and sharing for this project was performed by CamCAN. CamCAN funding was provided by the UK Biotechnology and Biological Sciences Research Council (grant number BB/H008217/1), together with support from the UK Medical Research Council and the University of Cambridge, UK.

Participants taking part in CamCAN's study also had the option of providing a saliva sample. The genetic sequencing of these samples was performed by CamCAN as described by Henson et al.[415] using the Illumina Infinium OmniExpressExome chip, which covers more than 960,000 single nucleotide polymorphisms (SNPs) throughout the genome.

5.2.2 Participants

All CamCAN participants were healthy and did not have dementia, any cognitive impairment, or a serious psychiatric disorder at the time of recruitment (Shafto et al., 2014). In this study, data from the same 613 participants were used as in the study described in Chapter 4. Of these, 537 participants had their genetic data sequenced.

5.2.3 Analysis of sensorimotor task MEG data

The full details of the MEG data analysis is described in section 4.2.5 of Chapter 4. Briefly, after registration between structural MRI images and maxfiltered MEG data, continuous

MEG data were down-sampled to 250 Hz. A band-pass filter and two notch filters were then applied to remove slow trends, high frequencies, and power line noise with its harmonics. Bad segment detection was used to exclude outlier time windows and automatic independent component analysis (ICA) was performed to identify and exclude components associated with physiological noise. The two Elekta system sensor types (magnetometers and gradiometers) were normalised. Data were then filtered to the mid-gamma frequency band (60-85 Hz). A linearly constrained minimum variance (LCMV) vector beamformer was applied on epoched data to extract the source of signals. Parcellation was performed using the primary motor cortex (M1) parcel in the Desikan-Killiany atlas to only include movement-evoked M1 data.

In order to extract the temporal, spectral, and spatial domains, time-frequency analysis was applied to single epochs in all 92 virtual sensors within the M1 parcel. Time-frequency analysis resulted in trial-by-trial time-frequency decomposition for all virtual sensors. From this data, the individual peak power, the individual peak frequency, and the M1 sensor were defined for each participant.

5.2.4 Statistical analysis

All statistical analyses were performed in R (version 4.5.0). Analysis was conducted separately for each study (GABAergic and neuromodulatory genes). I used an analysis of covariance (ANCOVA) model with two covariates: age (due to changes in GABA with healthy ageing[85]) and sex (e.g. gamma peak frequency is affected by sex[155]) to determine the association between each SNP (*GABRA5*, *GAD1*, *SLCA613* in study 1 and *BNDF*, *COMT*, *SLCA613* in study 2) and each MEG outcome measure (peak frequency and power) with an additive genetic model. The additive genetic model assumes a linear and uniform increase in the effect of a gene on a phenotype with increasing number of copies of the given allele. The model was implemented by assigning a numeric value to each genotype: 0 for major homozygous, 1 for heterozygous, and 2 for minor homozygous.

For each of these analyses, the sample was divided based on genotype into the following groups: minor allele homozygotes, heterozygotes and major allele homozygotes. Post-hoc comparisons between groups were performed using t-tests.

In each study, a Bonferroni-corrected alpha value of $0.05/18 = 0.0028$ was used (given two outcome variables, three genotypes and three genes). The alpha value for post-hoc t-tests was 0.05.

5.2.5 Power calculation

I was not able to find any past research comparable to the proposed studies (i.e. the effect of either of our selected genetic polymorphisms on task-evoked gamma band activity). The only study that fulfilled these criteria did not report their F-values (Altamura et al., 2016b). Therefore, I was not able to calculate the effect sizes.

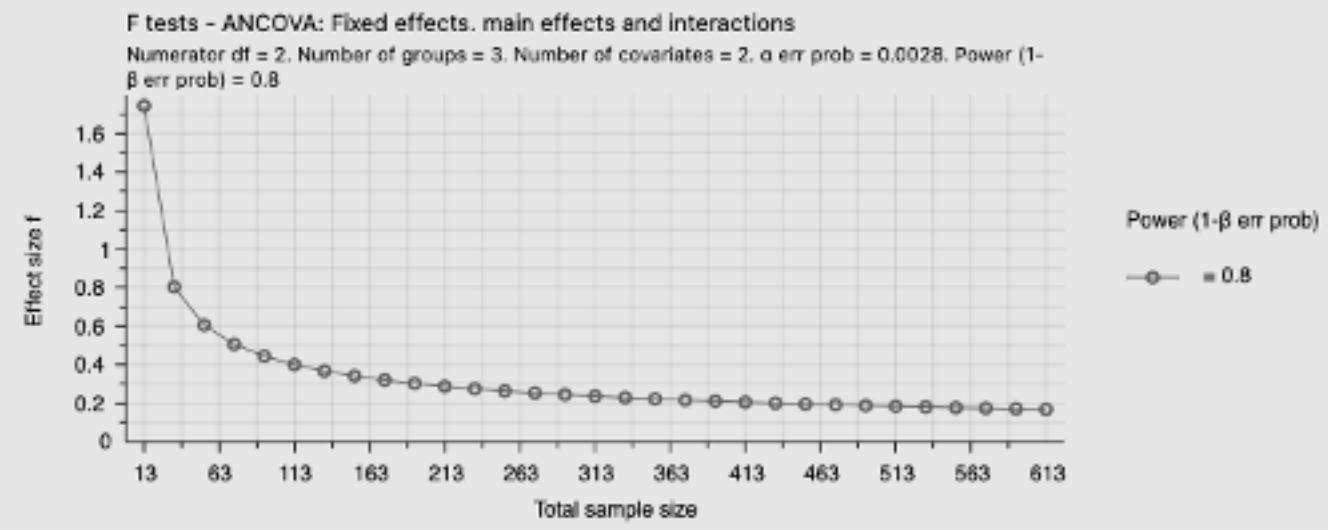


Figure 5.1: Sensitivity curves for a sample size up to 613 participants for the ANCOVA analysis.

Consequently, I performed a sensitivity power analysis for the main ANCOVA statistical analysis to determine the smallest effect sizes that could be detected with our sample size of 613 participants (alpha = 0.0028, power = 0.8, degrees of freedom = 2). With a total sample size of 613, I would be able to detect effect sizes f larger than 0.15 (i.e. small to medium effects[416], Figure 5.1).

5.3 Results

5.3.1 CamCAN dataset genotypes

Of the 613 participants in the CamCAN dataset whose data were analysed in Chapter 4, 537 provided a genetic sample that was sequenced. Table 5.1 contains the number of participants with the genotype for each single nucleotide polymorphism (SNP) in the following genes: *GABRA5* (SNP rs12916303), *GAD1* (SNP rs3749034), *BDNF* (SNP rs6265), *COMT* (SNP rs4680), and *SLC6A13* (SNP rs11062102).

For the analyses in this chapter, I split the dataset into two studies based on the function of the gene. The first set of genes controls GABAergic transmission (*GABRA5* and *GAD1*), while the second set contains genes that are involved in neuromodulation (*BDNF* and *COMT*). In both studies, the impact of genetic polymorphisms on magnetoencephalography (MEG)-measured movement-related mid-gamma (60-85 Hz) band activity metrics, peak frequency and peak power, was tested. Both sets of analyses included a control gene that is not widely expressed in the brain (*SLC6A13*).

Table 5.1: Number of participants with each genotype for the following single nucleotide polymorphisms (SNPs): *GABRA5*: rs12916303(G:T), *GAD1*: rs3749034(G:A), *BDNF*: rs6265(C:T), *COMT*: rs4680(G:A), *SLC6A13*: rs11062102(T:C).

Genotype	*GABRA5*	*GAD1*	*BDNF*	*COMT*	*SLC6A13*
Major homozygous	325	338	343	129	66
Heterozygous	186	173	169	276	220
Minor homozygous	26	26	25	132	251

5.3.2 Study 1: GABAergic genes

I first wanted to determine whether there were any additive relationships between our SNPs coding for GABAergic activity and MEG metrics. An analysis of covariance (ANCOVA) was performed to determine the association between each participant's SNP genotype and mid-gamma event-related synchronisation (ERS) peak frequency and peak power using an additive genetic model. The results of the ANCOVA are summarised in Table 5.2. After correcting for multiple comparisons, no relationship between SNPs and MEG metrics of mid-gamma band activity remained significant using Bonferroni-corrected alpha values. However, I found a negative trend between the *GAD1* SNP and mid-gamma peak frequency, suggesting that gamma peak frequency was higher in people with more copies of the major allele.

I further explored the trend between the *GAD1* SNP rs3749034 and peak frequency. Figure 5.2A shows the peak gamma ERS frequency of every participant, grouped by genotype. Major homozygous participants exhibited the highest mid-gamma peak frequency (mean ± SD: 71.14 ± 5.63, n = 338), followed by the minor homozygous group (mean ± SD: 70.50 ± 6.06, n = 26). Participants with a heterozygous phenotype had the lowest peak frequency (mean ± SD: 69.61 ± 5.33, n = 173). Post-hoc t-tests showed a significant difference between the major homozygous and heterozygous genotypes ($t(363.50) = 3.01, p = 0.0028$), but not between major and minor homozygous ($t(28.43) = 0.52, p = 0.61$), or heterozygous and minor homozygous ($t(31.12) = -0.71, p = 0.49$) genotypes.

I then visualised the relationship between age and peak frequency depending on the *GAD1* SNP rs3749034 (Figure 5.2B), because I was interested in age-related changes in MEG metrics in Chapter 4. Although the confidence intervals were wide, indicating a high degree of uncertainty in the estimate, the peak frequency in participants with a minor homozygous genotype increased with age. In the heterozygous group, peak frequency decreased with age. The peak frequency appeared relatively constant with age in the major homozygous group. To determine whether any of these relationships were significant, I performed a post-hoc ANCOVA looking only at the effect of the interaction between the *GAD1* SNP rs3749034 genotype and age on peak frequency. The interaction was not significant ($tvalue = -0.108, p = 0.91$), suggesting that the effects of age on peak frequency did not significantly differ based on *GAD1* genotype.

Table 5.2: Effect of genotypes of polymorphisms in GABAergic genes *GABRA5* and *GAD1* on movement-related mid-gamma metrics peak frequency and peak power modelled by an analysis of covariance (ANCOVA) using an additive genetic model. *SLC6A13* gene is used as a control. Age and sex were added as covariates.

Predictor	MEG metric	Estimate	Standard error	t value	p
Intercept	Peak frequency	71.65	0.94	75.86	2E-16
	Peak power	-0.66	0.11	-6.00	3.7E-09
GABRA5 rs12916303	Peak frequency	-0.027	0.41	-0.066	0.95
	Peak power	0.047	0.048	0.98	0.33
GAD1 rs3749034	Peak frequency	-1.01	0.42	-2.43	0.016
	Peak power	0.059	0.049	1.21	0.23
SLC6A13 rs11062102	Peak frequency	-0.28	0.35	-0.80	0.43
	Peak power	0.012	0.041	0.29	0.77
Age	Peak frequency	-0.0061	0.013	-0.46	0.65
	Peak power	-0.00042	0.0016	-0.27	0.79
Sex (male)	Peak frequency	0.24	0.48	0.51	0.61
	Peak power	-0.11	0.057	-1.87	0.062

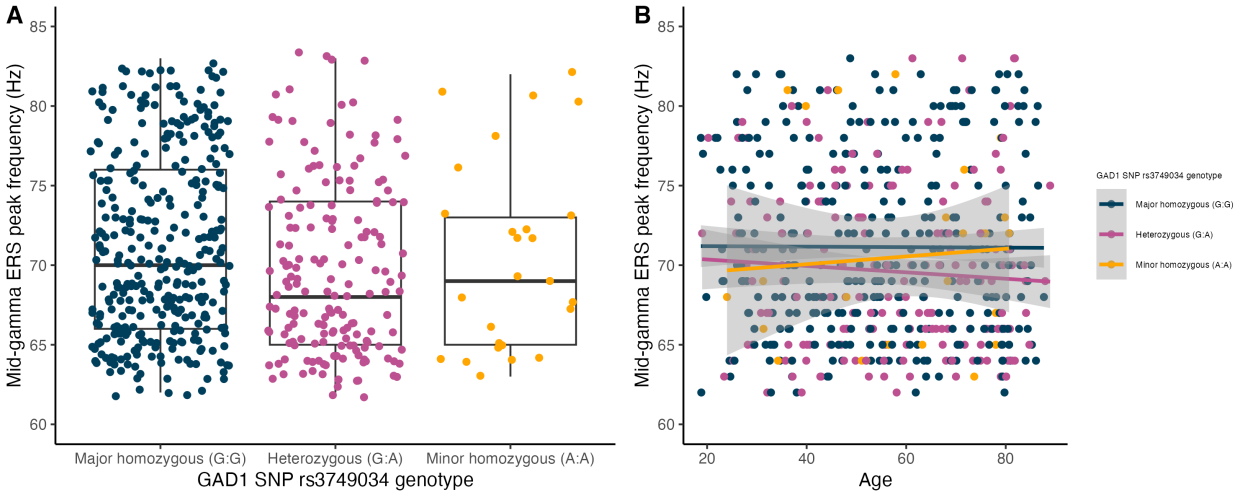


Figure 5.2: Effect of GAD1 SNP rs3749034 genotype on mid-gamma event-related synchronisation (ERS) peak frequency A: Individual participants' peak frequencies grouped by genotype. B: Relationship between age and movement-evoked mid-gamma peak frequency by GAD1 SNP rs3749034 genotype. Plot shows individual data points and lines representing linear regression fits.

Table 5.3: Effect of genotypes of neuromodulatory genes *BDNF* and *COMT* on movement-related mid-gamma metrics peak frequency and peak power modelled by an analysis of covariance (ANCOVA) using an additive genetic model. *SLC6A13* gene is used as a control. Age and sex were added as covariates.

Predictor	MEG metric	Estimate	Standard error	t value	p
Intercept	Peak frequency	71.62	1.01	71.00	2E-16
	Peak power	-0.61	0.12	-5.15	3.7E-07
BDNF rs6265	Peak frequency	-0.84	0.42	-1.99	0.047
	Peak power	-0.046	0.049	-0.94	0.35
COMT rs4680	Peak frequency	0.18	0.35	0.53	0.60
	Peak power	0.017	0.041	0.42	0.68
SLC6A13 rs11062102	Peak frequency	-0.20	0.35	-0.58	0.56
	Peak power	0.0084	0.041	0.20	0.84
Age	Peak frequency	-0.012	0.013	-0.89	0.37
	Peak power	-0.00049	0.0016	-0.31	0.76
Sex (male)	Peak frequency	0.19	0.48	0.39	0.70
	Peak power	-0.10	0.057	-1.84	0.066

5.3.3 Study 2: Neuromodulatory genes

In order to determine the effects of neuromodulation on gamma frequency, I performed the same analysis for SNPs in the two neuromodulatory genes, *BDNF* and *COMT* (Table 5.3). Again, no relationship between SNPs and peak frequency or peak power remained significant after correcting for multiple comparisons. However, a negative trend was present between a *BDNF* SNP and mid-gamma peak frequency.

I then investigated the trend between the *BDNF* SNP rs6265 and mid-gamma peak frequency. Figure 5.3A visualises peak frequency based on genotype. Similarly to *GAD1*, major homozygous participants exhibited the highest mid-gamma peak frequency (mean ± SD: 70.99 ± 5.68, n = 343), followed by the minor homozygous (mean ± SD: 70.12 ± 5.17, n = 25) and heterozygous (mean ± SD: 69.94 ± 5.43, n = 169) genotypes. Post-hoc t-tests showed a significant difference between the major homozygous and heterozygous genotypes ($t(348.15) = 2.038, p = 0.042$), but not between major and minor homozygous ($t(28.40) = 0.81, p = 0.43$), or heterozygous and minor homozygous ($t(32.37) = -0.17, p = 0.87$) genotypes.

Similarly to the *GAD1* findings, the effect of the *BDNF* SNP rs6265 genotype on mid-gamma peak frequency showed trends depending on age based on visual inspection (Figure 5.3B). I performed a post-hoc ANCOVA test to determine the effect of the interaction between the *BDNF* SNP rs6265 genotype and age on peak frequency. The interaction was not statistically

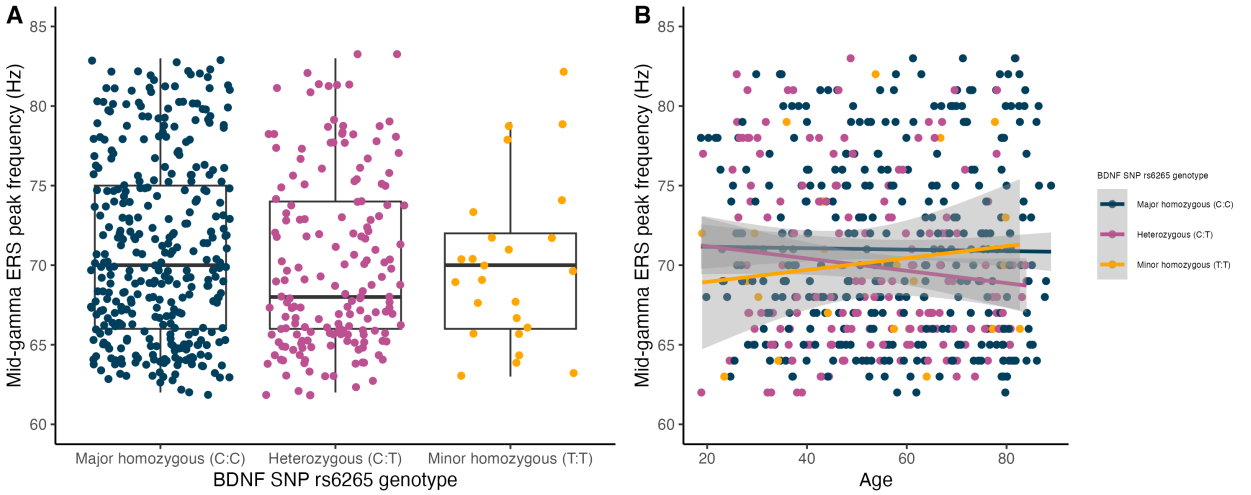


Figure 5.3: Effect of BDNF SNP rs6265 genotype on mid-gamma event-related synchronisation (ERS) peak frequency A: Individual participants' peak frequencies grouped by genotype. B: Relationship between age and movement-evoked mid-gamma peak frequency by BDNF SNP rs6265 genotype. Plot shows individual data points and lines representing linear regression fits.

significant ($tvalue = -0.35, p = 0.73$); the BDNF genotype had no significant effect on age-related changes in peak frequency.

5.4 Discussion

5.4.1 No significant relationship between genotypes of selected GABAergic and neuromodulatory genes and MEG metrics of mid-gamma activity

Here, I used genetic sequencing in conjunction with magnetoencephalography (MEG) in an exploratory study to assess the influence of genetic variation on movement-related gamma band activity. I selected one single nucleotide polymorphism (SNP) in each of four candidate genes that I hypothesised to have a role in generating or modulating gamma band activity. The four genes were the following:

1. *GABRA5* encoding the $\alpha 5$ subunit of $GABA_A$ receptors.
2. *GAD1* encoding the GABA-synthesising enzyme glutamate decarboxylase (GAD67).
3. *BDNF* encoding brain-derived neurotrophic factor (BDNF). BDNF is implicated in the maintenance and growth of neurons and synaptic plasticity.
4. *COMT*, which encodes an enzyme that degrades neuromodulators such as dopamine.

SNPs in genes were analysed in two separate analyses based on their function. I first investigated GABAergic inhibition (*GABRA5* and *GAD1*), and then I separately investigated

the potential effects of neuromodulation (*BDNF* and *COMT*) on gamma band activity. The two pairs of SNPs were analysed in separate analysis of covariance (ANCOVA) models, along with a control SNP in a gene that is not expressed in the brain (*SLC6A13*), to assess their influence on movement-related mid-gamma band (60-85 Hz) activity metrics of peak frequency and peak power. Sex and age were added as covariates to the model.

I did not find an association between any SNP and MEG metric that remained statistically significant after the Bonferroni correction for multiple comparisons. However, there were two associations with p values below the standard alpha value of 0.05: *GAD1* SNP rs3749034 and peak frequency, and *BDNF* SNP rs6265 and peak frequency. Even though these relationships were not significant when corrected for multiple comparisons, I further explored the trends for any potential mechanisms of generation and modulation of gamma band activity.

5.4.2 Trends in gamma peak frequency based on *GAD1* and *BDNF* genotype

GAD1

I hypothesised that the major allele of *GAD1* SNP rs3749034 would be associated with lower movement-related mid-gamma peak frequency and power. The minor allele (A) is believed to create a predicted transcription factor binding site, enabling higher expression of the GAD67 enzyme, while the major allele has been linked to lower expression of GAD67[372,373], resulting in decreased production of GABA. In mice, knockdown of *GAD1* in parvalbumin interneurons (PVI) leads to a decline in probability of GABA release[371] and a reduction in the power of gamma band activity[376]. In a unpublished PhD thesis that explored the effect of SNPs in GABAergic genes on inhibition, the genotype of the SNP rs3749034 in *GAD1* was related to GABA levels measured by magnetic resonance spectroscopy (MRS) in a recessive model, where minor homozygous participants had the highest levels of GABA[417]. MRS GABA exhibits a positive relationship with movement-related[85] and visual[97,418] gamma band peak frequency. The density of $GABA_A$ receptors also had a positive relationship with visual gamma peak frequency[100], indicating that higher levels of inhibition may lead to an increased peak frequency. Moreover, modelling a break-down of the excitation-inhibition balance resulted in a lower gamma frequency[419]. In this study, I predicted that lower levels of GABA in individuals with the major allele of the *GAD1* SNP rs3749034 would disrupt the pacing of inhibitory neuron firing and therefore would be linked to a decrease in the peak frequency of movement-related mid-gamma band activity. However, I observed the opposite trend in my results. Major homozygous participants exhibited higher peak frequencies than heterozygous or minor homozygous ones.

There is evidence that supports an increase in peak frequency with a disrupted excitation-inhibition balance through reduced inhibition or increased excitation, based on both animal and human studies. Ablation of δ subunit-containing $GABA_A$ receptors[420] and activation of

excitatory NMDA receptors[92] in hippocampal regions of mice resulted in increased frequency of gamma band activity. In an optogenetic experiment, photoinhibition of somatostatin (SST)-containing hippocampal neurons in mice also increased the peak frequency of gamma band activity[421]. The authors of the study explain this increase through the dependence of gamma oscillations on inhibitory postsynaptic potentials in pyramidal neurons[421]. Smaller overall inhibitory synaptic currents as a result of photoinhibition of SST neurons could result in shorter-lasting inhibition, allowing pyramidal neurons to fire faster, increasing the frequency. However, sustained excitation of PVI (leading to greater net inhibition) also increased the peak frequency of carbachol-induced gamma band oscillations[421]. Although manipulation of SST neurons modulated activity in the gamma band more robustly than PVI manipulation[421], it resulted in opposite effects on peak frequency.

Increasing inhibition by administering two positive modulators of $GABA_A$ receptors that enhance inhibition, alcohol[422] and lorazepam[423], resulted in a decreased gamma frequency in humans. These findings are consistent with the direction of the GABA-peak frequency trend I observed. On the other hand, lorazepam did not affect sensorimotor gamma frequency[423]. These studies show that the relationship between inhibition-excitation balance and peak frequency is complex and the influence of SNP genotype may depend on the brain regions and neuronal subtypes in which the genes of interest are expressed.

BDNF

The major allele (C) of the *BDNF* SNP rs6265 has been linked to increased secretion of the brain-derived neurotrophic factor (BDNF) compared to the minor allele (T). BDNF plays an important role in neuronal growth, survival, maintenance, and synaptic plasticity. Furthermore, impairments in the GABAergic system have been observed in mice with reduced production of BDNF[383,384]. Therefore, I hypothesised that the major allele of the rs6265 SNP would be associated with an increased peak frequency due to higher secretion of BDNF. I observed a non-significant trend in this direction in my data; participants with a major homozygous genotype had the highest peak frequency.

5.4.3 Limitations

Overall, this study has some limitations in methodology that could explain the lack of significant results. One such major limitation is the single candidate SNP approach. In order to minimise the impact of adjusting for multiple comparisons, I selected two candidate SNPs per study with one control SNP. These four genes and SNPs had strong evidence for a potential role in the generation or modulation of gamma band activity. However, the systems involved in oscillatory activity are very complex and involve countless proteins that could affect the resulting frequency and power. For example, approximately 20 SNPs in *GABRA2*, the gene encoding the $\alpha 2$ subunit of $GABA_A$ receptors, have been linked to power of beta band activity and alcohol dependence[424]. Variations in other genes encoding proteins that

could influence GABAergic transmission include GABA transporter 1 (GAT-1) that removes GABA from the synaptic cleft, vesicular GABA transporter (VGAT) that moves GABA into synaptic vesicles, $GABA_B$ receptors, or different subunits of $GABA_A$ receptors. Because gamma band activity depends on the reciprocal connections between inhibitory and excitatory neurons, there are also numerous glutamatergic proteins that could influence peak frequency and power. Furthermore, each gene includes many potential SNPs that could affect the gene's transcription, translation, and expression. Many SNPs in these genes have not been explored in depth, and the evidence is lacking. The SNPs that I chose have all been linked to changes in inhibitory transmission, gamma band activity, or psychiatric disorders, but there may be other SNPs with stronger influence that have not been discovered yet.

Moreover, a single SNP may not be sufficient to influence a specific phenotype. The interaction between multiple SNPs may be what affects gamma band metrics more strongly. According to the principle of linkage disequilibrium (LD), there is a non-random association between alleles of genetic loci that lie in proximity to each other. These alleles can be inherited together more frequently than expected by chance. For example, several *GAD1* SNPs in the anterior cingulate cortex have strong associations between each other[425]. Therefore, the effects of some SNPs could be compounded but would not be detected by my approach. I am also not able to account for potential compensation for the decreased expression of the selected gene, or reduced activity of the resulting protein, by other proteins with related functions. Glutamate decarboxylase 2 (GAD2) is the other enzyme that can produce GABA in the brain, although it contributes much less to the production than GAD1. However, it has been hypothesised that GAD2 may compensate for the lower expression of GAD1 caused by SNPs such as rs3749034 by increasing GABA synthesis[425]. There may be underlying mechanisms behind the lack of significant findings in my study that cannot be disentangled using the approach available here.

Another potential limitation is the sample size. The CamCAN study had 537 participants who took part in all three of the MEG, magnetic resonance imaging (MRI) and genetic sequencing components. This number of participants is much higher relative to comparable studies that looked at the influence of single SNPs on MEG metrics (range of 22-116 participants[411,417,425], but this dataset still contained only 25-26 participants with minor homozygous genotypes. Genome-wide studies that focus on associations between alleles and disorders, such as the the Psychiatric Genomics Consortium, recruit participants on the order of tens to hundreds of thousands[426]. The UK Biobank dataset includes MRI scans and sequenced genomes from approximately 85000 participants, although their neuroimaging focus is MRI rather than MEG, and is performed at multiple sites. Therefore, the CamCAN dataset is large for a single-site neuroimaging study, since neuroimaging is more costly and time-consuming compared to purely genetic studies.

Lastly, I analysed the dataset using an additive model, which assumes a linear increase in the effect of a gene or a SNP on a trait based on the number of copies of each allele. In my

model, each copy of a minor allele was hypothesised to cause a linear increase or decrease in phenotype. The additive model is the most commonly used model in genetic studies as it is straightforward to implement and interpret[427], and its use was a condition of the data release from CamCAN for this project. However, the additive model has been found to not perform well in the case of recessive traits where minor allele frequency is below 50%[428]. A thesis that has not been peer-reviewed showed evidence of a trend between the *GAD1* SNP rs3749034 and MRS-GABA when testing the relationship with a recessive model, but not using an additive model. Therefore, if the relationship between the genotypes and MEG metrics is not linear and additive, I may not have been able to detect it.

5.4.4 Conclusion

I investigated the contribution of common single-nucleotide polymorphisms (SNPs) on inter-individual variation in magnetoencephalography (MEG) metrics, movement-related peak frequency and power, in the mid-gamma frequency band (60-85 Hz). I selected a SNP in four genes that have been shown to relate to inhibitory neurotransmission or directly to gamma oscillations. I found evidence for a trend between two candidate SNPs in the *GAD1* and *BDNF* genes and gamma peak frequency, although the associations were not significant when correcting for multiple comparisons. This study was exploratory and provides potential candidates for genes that may influence the generation and modulation of gamma band activity in the motor cortex.

Chapter 6

General Discussion

My thesis aimed to assess methods of studying inhibition in the brain and to investigate the function of inhibitory neurons in the primary motor cortex (M1) using multimodal approaches. I utilised a novel type of non-invasive brain stimulation called controllable pulse parameter transcranial magnetic stimulation (cTMS) to determine its test-retest reliability in measuring corticospinal excitability. I also investigated inhibition-dependent M1 activity in the beta and gamma frequency bands in magnetoencephalography (MEG) data recorded during movement, and how they change with age. Lastly, I explored the contribution of genetic polymorphisms to the variability of gamma band activity during the same movement task.

6.1 Thesis summary

In the first chapter of this thesis, I reviewed the basic anatomy and structure of M1, and the two main functional groupings of neurons in the brain: excitatory and inhibitory. The balance of excitation and inhibition in the brain is tightly controlled and is modulated when preparing and executing movements. I summarised oscillatory activity found in M1 in various frequency bands with a particular focus on two bands: beta and gamma. The generation of both bands depends on the function of inhibitory neurons. Finally, I discussed how the brain, inhibitory neurotransmission, and oscillatory activity in the beta and gamma bands change due to age throughout adulthood.

In the second chapter, I introduced the techniques used in this thesis. Specifically, I discussed how TMS probes corticospinal excitability through input-output curves and the two main approaches for analysis of input-output curves. I also described two sensorimotor tasks that evaluated motor control and motor learning. I outlined the neurophysiological basis of MEG signals, how their sources can be determined, and the primary method of studying movement-related M1 activity. Finally, I provided a brief overview of single nucleotide polymorphisms and genetic sequencing.

In chapter 3, the first experimental chapter, I determined the test-retest reliability of the cTMS device. First, I described the difference between conventional TMS devices and the cTMS, which enables the adjustment of various pulse parameters including the pulse width.

Pulses of different widths are believed to activate different populations of neurons, such as inhibitory neurons. I performed a between-session, within-participant study where I delivered cTMS pulses of various intensities at three different widths in order to acquire input-output curves. The participants also completed two sensorimotor tasks. I found low test-retest reliability of cTMS input-output curve slopes, the main measure of corticospinal excitability with mixed reliability of other metrics. I did not find evidence for selective recruitment of different populations as input-output curve slopes did not have an association with performance on sensorimotor tasks.

In chapter 4, I investigated age-related changes in beta, slow- and mid-gamma band activity during the execution of simple movements. I used a large MEG dataset from the Cambridge Centre for Ageing and Neuroscience (CamCAN) repository that includes almost 650 participants ranging from 18 to 88 years of age. I found some age-related changes in beta and gamma band activity, including a reduction in the peak frequency of beta movement-related desynchronisation (ERD) and synchronisation (ERS), and stronger ERD. I also observed an age-related increase in the peak frequency of movement-related ERS in the slow-gamma band, but found no relationship between age and frequency or power of mid-gamma. Finally, I found changes associated with age in the localisation of activity of all bands except beta ERD.

In chapter 5, I performed an exploratory analysis assessing the influence of genetic polymorphisms on MEG metrics of M1 gamma band activity, peak frequency and power in the CamCAN dataset. I selected a single-nucleotide polymorphism (SNP) in each of four genes that have been associated with inhibitory neurotransmission or gamma oscillations. I found evidence for a trend between two candidate SNPs in the *GAD1* and *BDNF* genes and gamma peak frequency, but the associations were not significant after correcting for multiple comparisons. However, my findings point to potential genes and proteins that may be involved in the generation and modulation of movement-related gamma band activity.

6.2 General limitations and future directions

6.2.1 Test-retest reliability and reproducibility of TMS studies

The number of TMS studies investigating the neurophysiology of M1 has been increasing over the past several decades, but very little attention has been paid to the quality of the measurements[258,266]. For example, only in 2012, after more than 20 years of extensive TMS use, was the first set of recommendations for reporting TMS studies published[429]. In repetitive TMS research, approximately only 50% of studies are able to reproduce previously published TMS results[430].

TMS as a technique is inherently noisy. The outcome measure, the motor evoked potential

(MEP), is influenced by the state of M1 at the time of TMS pulse delivery[239] and large trial-to-trial MEP variability is a well-known phenomenon. An important factor contributing to this variability is believed to be the naturally fluctuating oscillatory activity of neurons. MEP amplitude has been shown to depend on the phase and power of M1 alpha[293,431] and beta[292,293,432] activity. Trial-to-trial variability of MEPs would affect the sensitivity and test-retest reliability of TMS.

There is also a lack of consistency in TMS methodology. In Tables 3.6 and 3.7 in Chapter 3, I summarised other input-output curve studies determining test-retest reliability. There is variability in the number of trials per condition, the number of tested intensities, the order they were applied, as well as the number of trials for each condition and inter-trial interval. In TMS research, there is very little cohesion in the protocols and study design, further reducing the measured reliability metrics.

A systematic review of 34 TMS test-retest reliability studies found that the mean sample size was 17 participants, meaning that TMS studies are often small and possibly underpowered[258]. Authors of those studies also did not provide rationales for the sample sizes, or power calculations, which I also did not do. However, the data I acquired will be useful for calculating expected effect sizes for power calculations of experiments using the cTMS. TMS studies generally have small sample sizes[258,429], however, power can be increased by increasing the number of trials[266]. Indeed, acquiring 20 MEPs per condition has been shown to be ideal for good test-retest reliability, although 10, like in my cTMS study, can be adequate[433]. Based on the table 3.6 in Chapter 3, only four out of seven studies determining the test-retest reliability of input-output curves acquired 10 or more trials for each condition, with the others measuring three or five. Therefore, most of these studies are likely underpowered.

Individual differences in anatomy can also contribute to a lower reproducibility of TMS findings. Because the magnetic field induced by TMS pulses attenuates exponentially with distance from the TMS coil[261], the individual distance between the scalp and the targeted M1 cortical surface can impact the response to TMS pulses. For example, in my study, I administered TMS pulses to the hand region of the non-dominant hemisphere. In one participant, I was not able to achieve stable MEPs in the non-dominant hemisphere, while TMS to the dominant hemisphere produced very stable MEPs with supra-threshold pulses. Therefore, even within the same participant, TMS response can vary based on their anatomy. The impact of individual anatomy is even more important for repetitive TMS studies that set the dose of pulses based on responses in a different brain region, as the variability of cortical depth across the brain is high[434]. In these cases, having structural magnetic resonance imaging (MRI) scans could help adjust the intensity of TMS pulses based on individual anatomy.

6.2.2 Can TMS specifically target inhibitory neurons?

It is well documented that TMS targets axons of both excitatory and inhibitory neurons, mainly at the top of the gyral crowns[239]. However, the specific cell types preferentially activated by TMS are still not completely understood. The strongest evidence for selective activation of inhibitory neurons using conventional TMS is the short-interval intracortical inhibition (SICI) protocol, in which pulses are administered in a pairs with a specific interval between the paired pulses[243]. In this thesis, I explored selective activation of inhibitory neurons by utilising the pulse width modulation properties of the cTMS device.

In the Introduction to Chapter 3, I summarised the evidence for selective recruitment of inhibitory neurons and hypothesised that shorter pulses may activate inhibitory interneurons more selectively. However, most of the evidence for the mechanism by which pulses of different widths could selectively activate neurons based on their properties comes from electrical stimulation of peripheral nerves. The peripheral nervous system has less diverse neurons and more direct connections to the output muscles. In contrast, the central nervous system has numerous different neuronal subtypes, and its activation by TMS pulses passes through multiple synapses before reaching the output muscle. Moreover, there are no experimentally measured strength-duration parameters of different neuronal subtypes in M1 that describe the dependence of activation based on pulse width[239]. However, in vitro evidence from mouse brain slices suggests inhibitory neurons all exhibit distinct neurophysiological properties[247].

The cTMS is the first commercially available TMS device that allows the modulation of pulse width in the central nervous system. Previous studies using the cTMS have shown that pulse width modulation enables the recruitment of different neuronal populations with the SICI protocol[274] as well as depending on the orientation of the TMS coil[178,272]. In this thesis, I acquired input-output curves to determine if they also enable recruitment of different types of neurons, but I was not able to conclude whether or not this was the case. However, since writing the chapter, a study acquiring input-output curves from a variety of muscles utilised a new method of analysing the input-output curves[435] that could help determine whether I was able to activate different neuronal populations. More TMS protocols, especially those that use sub-threshold stimuli such as SICI or the cortical silent period, should be tested in conjunction with pulse width modulation to provide an insight into differential activation of neuronal populations. In addition, experimentally measured properties of M1 neurons would be necessary to definitively determine activated populations of neurons. The TMS outcomes should also be confirmed by other measures of inhibition, such as GABA levels measured by magnetic resonance spectroscopy (MRS).

6.2.3 MEG-detected gamma band activity as a measure of inhibition

In section 1.2.2 of the General Introduction, I summarised the evidence for the dependence of oscillatory activity in the beta and gamma bands on inhibition. In this thesis, I focused more on gamma band activity, as recent findings from my group have supported its importance in motor learning[32,70].

Gamma band activity is generated by reciprocal connections between excitatory and inhibitory neurons, but also by inhibitory neurons mutually connected to each other. The specific class of inhibitory neurons implicated in gamma band activity are parvalbumin-expressing interneurons (PVI). Therefore, gamma band activity is not a direct measure of inhibition, but can act as a proxy because it is so closely associated with inhibitory neurotransmission.

MEG is one of the most commonly used methods for detecting gamma band activity. However, MEG has relatively low spatial sensitivity due to the distances between sensors and the brain, which can be more than 2 cm[436]. Furthermore, the signal-to-noise ratio of gamma band signals is lower compared to lower amplitude signals such as beta, which may be due to the signal originating from smaller cortical areas and groups of neurons[436]. Therefore, the detection of gamma band activity is inherently limited, although I maximised the signal-to-noise ratio by analysing each band (beta, slow-gamma, and mid-gamma) separately after comprehensive filtering and reduction of noise in the data.

In my studies in Chapters 4 and 5, I extracted two metrics to describe gamma band activity: peak frequency and peak power. However, the link between these metrics and inhibition is less straightforward. M1 gamma peak frequency has been shown to be linked to a TMS measure of inhibition[70] and to have a positive relationship with MRS-measured GABA levels[85], but a relationship with GABA has not been confirmed in the auditory cortex[96]. Visual cortex gamma band activity has also been found to be predicted by MRS-measured GABA in one study[97], but not in two others[98,99]. MRS-measured levels of GABA predicted the peak power of gamma band activity in the superior temporal sulcus[95] but not in the auditory[96] or visual cortex[98]. Movement-related peak power also did not show any relationship to a TMS measure of inhibition[70]. Moreover, pharmacological modulation of $GABA_A$ receptors[45] and reuptake of GABA from the synaptic cleft[80] had no effect on the frequency[80] or power[45,80] of movement-related gamma band ERS. Therefore, the evidence for the relationships of peak frequency and peak power to inhibition is mixed and the physiological processes underlying the MEG metrics are not clear. One potential method by which to overcome this limitation is to perform a multimodal study with, for example, a MEG scan performed in the same session as TMS. The pulse width modulation ability of the cTMS device could be utilised with a protocol such as SICI to explore the link between inhibition and the conventional metrics of movement-related MEG analysis, peak frequency, and power.

MEG data could also be analysed with a different approach that I introduced in the discussion of Chapter 4: by exploring individual burst dynamics. The shape of brain oscillation waveforms has been shown to contain valuable information that is lost in traditional spectral analysis that averages over many trials[324,325]. Activity in both beta[77,326,437] and gamma[326,437] bands may consist of transient intermittent burst-like events that only appear as a sustained signal when averaged over trials, resulting in a loss of specificity in temporal dynamics[327]. Two publications have explored age-related changes in beta bursts in the CamCAN dataset[151,152], but their approach was less sensitive to gamma bursts[152]. Developing an analysis method for detecting transient gamma burst activity could provide a more detailed representation of the physiological mechanisms that underpin brain oscillations. Analysis of gamma bursts could therefore provide more sensitivity to detecting age-related changes in oscillatory activity compared to conventional averaging methods, and also more power in detecting the effects of genetic polymorphisms on oscillatory activity.

Another approach to analyse the MEG data could have been to perform a phase-amplitude coupling analysis. Gamma band activity has been shown to be coupled with activity in the theta band (4-8 Hz) in a phase-amplitude manner in human M1, where the maximum gamma power occurs at the peak of theta rhythms[31]. The strength of gamma band power is predicted by the power of theta band activity[438]. Theta-gamma coupling is also thought to represent a balance of excitation and inhibition, as cholecystokinin-expressing inhibitory basket neurons may initiate the coupled rhythm in the hippocampus[439]. A study from my group has shown that driving theta-gamma coupling in M1 through transcranial alternating current stimulation (tACS) improved the acquisition of motor skills[32]. Therefore, to extract the most information out of theta-gamma phase-amplitude coupling, a motor learning task may be more appropriate than the simple button press task performed by participants in the CamCAN study.

6.2.4 Use of cTMS and MEG to study mechanisms of amyotrophic lateral sclerosis (ALS)

Initially, this thesis aimed to use the cTMS device in patients with amyotrophic lateral sclerosis (ALS). I hoped to complete the cTMS test-retest reliability study in Chapter 3, then follow up with a multimodal study correlating cTMS with MRI measures, and finally use the cTMS to measure the activity of interneurons in ALS patients. However, due to pandemic restrictions at the beginning of my DPhil when in-person experimental sessions were not allowed, I started working on the CamCAN MEG analysis project in Chapter 4, which I then expanded by requesting the genetic dataset in Chapter 5. Although I was unable to complete the planned projects, since this thesis started with an interest in ALS, I would like to include a short section discussing future directions of the ALS projects in light of my findings.

ALS is a devastating neurodegenerative disease with a very short life expectancy. Due to a lack of objective and reliable markers of the disease, there are no definitive tests for ALS, and diagnosis is based on expert clinical opinions. Patients can wait up to a year for a formal diagnosis. In the original proposal, my aim was to develop neurophysiological markers of the early stages of the disorder.

ALS is marked by a progressive and selective loss of central motor neurons in the brain and spinal cord[440]. One major hypothesis for the mechanism underpinning the pathology of ALS is through glutamate excitotoxicity caused by cortical hyperexcitability[174,441,442] alongside an early loss of inhibitory neurons[440]. For example, the expression of $GABA_A$ receptors is reduced in M1 of ALS patients[443,444], suggesting further breakdown of the excitation-inhibition balance. Riluzole, the only currently approved treatment for ALS, works by blocking glutamate transmission[445], although it only extends the lifespan of patients by a few months[446]. Therefore, the early loss of inhibitory neurons may be a useful marker of early disease and could be studied using various modalities like TMS and MEG.

Several TMS studies have explored the early loss of inhibition in ALS. SICI paradigms show lesser attenuation of motor-evoked potential (MEP) responses in ALS patients compared to healthy controls[174,447–451]. The reduction in SICI worsens as the disease progresses[452,453], although riluzole therapy was partially able to reverse the SICI deficiency in patients with ALS[454,455]. This evidence points to impairments in inhibitory neurotransmission in M1 of ALS patients. Moreover, axonal excitability measures of strength-duration characteristics of peripheral neurons show longer chronaxies (strength-duration time constants)[456]. Therefore, exploring the strength-duration characteristics of central neurons in ALS using the cTMS could provide novel insight into the pathology of the disease.

MEG and EEG studies have also determined changes in brain oscillatory activity in ALS patients. At rest, the power of sensorimotor beta band activity was reduced, while sensorimotor gamma band power was increased in ALS compared to healthy controls[457]. When performing a motor task, post-movement ERS in the beta band was reduced[458] and delayed[459] in ALS patients. No changes to ERD were detected in ALS patients[458], although asymptomatic carriers of genes implicated in ALS showed stronger ERD[459]. In the literature I reviewed, there were no studies examining movement-related gamma band activity in ALS patients. Because ALS is characterised by the loss of inhibitory neurons in ALS and gamma band activity is dependent on inhibitory neurotransmission, changes in movement-related gamma band activity in ALS patients would be expected. Furthermore, a motor task MEG study focusing on gamma band activity could also be performed in asymptomatic carriers of genes implicated in ALS to study the early changes in M1 excitation-inhibition balance.

6.3 Main conclusions

In this thesis, I explored methods of studying inhibition in the brain and investigated the function of inhibitory neurons in the primary motor cortex (M1) using various approaches. The major conclusions from my thesis are as follows.

1. With the protocol I used, cTMS measures of corticospinal excitability did not have good test-retest reliability.
2. I did not find evidence for differential activation of neuronal circuits by different pulse widths
3. There were some age-related changes in movement-related beta and gamma band frequency activity and localisation.
4. I found evidence for a trend between single nucleotide polymorphisms in the *GAD1* and *BDNF* genes and MEG gamma peak frequency.

List of Figures

1.1 **Representative cells in the six layers of M1**. These include pyramidal (Py) and modified pyramidal (mPy), chandelier (Ch), aspiny (Asp) and spiny (Sp) stellate neurons, and basket (Bas) cells. Figure from Grow[6]. 9

1.2 **Dynamics of corticospinal excitability during movement preparation**. Movement-evoked potentials (MEPs) are a measure of corticospinal excitability. Excitability was probed at various time points before expected movement onset (30 to 500 ms). MEPs of higher amplitudes represent higher excitability. PT and RT refer to task used in the original study. Corticospinal excitability first decreased in comparison to baseline (TMS_{200}), then increased (TMS_{30}). Figure from Ibáñez et al.[19]. 11

1.3 **Movement-related changes in M1 oscillations.** Time 0 s denotes a button press. In the beta frequency band (15-30 Hz in this figure), a decrease in oscillatory activity can be observed (beta ERD) compared to baseline (Control) followed by an increase after movement terminates (beta ERS). Activity in the gamma band (30-100 Hz, especially around 75 Hz) increases (gamma ERS) as movement is executed. Figure adapted from Hall et al.[45]. 13

2.1 **Transcranial magnetic stimulation (TMS) and an input-output (IO) curve**. A: TMS involves the use of a changing magnetic field to induce electrical currents in cortical neurons. When a magnetic pulse is applied through a coil held over the primary motor cortex, it causes activation of muscles through corticospinal projections. The muscle responses, motor-evoked potentials (MEPs), can be measured by surface electromyography (EMG). The location of muscle activation depends on the region of the motor cortex stimulated. Amplitude of the MEP depends on corticospinal excitability and other factors.[158] B: IO curve is generated by acquiring MEPs at a range of stimulation intensities. The graph shows the relationship between the stimulation intensity relative to the stimulation intensity required to elicit a 1 mV MEP (%SI1mV) and the resulting MEP amplitude.[82] 24

2.2 **Magnetic fields generated in the cortex.** Neuronal activity within cortical columns in sulcal walls generate tangential magnetic fields detectable by MEG. In contrast, activity at the top of gyral crowns induces radial magnetic fields, which can not be detected by MEG. Therefore, most activity detected by MEG is activity from neurons orientated perpendicularly to the skull. Figure from Henson et al.[195]. 30

2.3 **DNA double helix.** Figure from Fletcher and Hickey[208]. 32

3.1 **Strength-duration relationship**. A: Rheobase and chronaxie can be derived from the strength-duration curve. Rheobase is the minimum pulse strength required for neuronal activation. Chronaxie (strength-duration time constant) is the pulse width required to produce a response at double the strength of the rheobase. B: Strength-duration properties of neuron 1 (solid line) and neuron 2 (dashed line) allow their selective activation. If pulse width is shorter than the yellow dotted line, supra-threshold stimuli would result only in activation of neuron 1, but not neuron 2. 35

3.2 **cTMS pulses and IO curves**. A: Waveforms for pulses of three different pulse widths: 30, 60, and 120 μs.[176] B: IO curves generated by pulses of the same widths. Each marker represents individual MEP.[176] 38

3.3 **Study design**. The study session started with initial paperwork consisting of the consent, brain stimulation safety screening, and handedness forms. Then, TMS was configured as described in section 3.2.3, including finding hotspot and motor thresholds. The participants were then familiarised with two motor tasks. TMS IO curve data was then acquired, followed by completing the two tasks. 39

3.4 **Electric field waveforms of cTMS pulses** recorded with a search coil. Ripple at the end of the negative phase of pulses is a recording artefact. 40

3.5 **Motor tasks**. A: Action selection task.[179] B: Serial reaction time task.[184] . . 43

3.6 **Example input-output (IO) curves** of one participant for pulse widths 30 (orange), 60 (pink) and 120 (blue) μs acquired in session 1 (solid line/circle marker) and 2 (dashed line/cross marker). The markers represent mean log-transformed amplitude of motor evoked potentials (MEPs) elicited by TMS pulses of various intensities represented as percentage of maximum stimulator output (% MSO). At every combination of TMS pulse intensity and width, 10 trials were recorded. Mean MEP amplitude was calculated from remaining trials after exclusion criteria were applied during data pre-processing. Lines show sigmoid curves of best fit to the mean MEPs. 46

3.7 **Comparison of input-output (IO) curve slopes acquired using all pulse widths in both sessions.** Each marker represents an individual participant (n = 15 for 30, n = 20 for 60, and n = 22 for 120 μs pulses), lines connecting the markers show a change between sessions for individual participants. 46

3.8 **Correlations between IO curve slopes acquired using different pulse widths** in sessions 1 (top, 30: n = 15, 60: n = 20, and 120: n = 22) and 2 (bottom, 30: n = 21, 60: n = 21, and 120: n = 22). 47

3.9 **Correlations between IO curve slopes acquired using by 30 and 120 μs pulses** in sessions 1 (left, n = 16) and 2 (right, n = 21). 48
3.10 **Bland-Altman plots** showing agreement between IO curve slopes acquired in session 1 (S1) and session 2 (S2). Mean slope is plotted against the test-retest difference calculated as the difference between slopes acquired in both sessions for every participant and pulse width. Each point represents an individual participant. The dashed lines represent the 95% limits of agreement. 49
3.11 **Action selection (AS) task performance** in both sessions. Execute and select categories of the figure represent the median response time for execute and select blocks of the AS task. Action selection times were calculated as the difference between median response times in select and execute blocks. Each marker represents an individual participant ($n = 22$), lines connecting the markers show a change between sessions for every participant. 51
3.12 **Serial reaction time task (SRTT) performance** in both sessions. Left: Response time for every SRTT block, which had a random (R) order of cues or a sequence (S) of cues. Each marker represents a median value from all participants ($n = 22$). Error bars represent standard deviations. Right: The gradient of a linear line fitted to the response times of sequence blocks for every participant was used as a metric of learning. Each marker represents an individual participant, lines connecting the markers show a change between sessions for every participant. 51
3.13 **Bland-Altman plots** showing agreement between execute response times (left) and action selection times (right) acquired over two sessions. Mean times are plotted against the test-retest difference calculated as the difference between times acquired in both sessions for every participant. Each point represents an individual participant. The dashed lines represent the 95 % limits of agreement. 52
3.14 **Bland-Altman plots** showing agreement between SRTT linear gradients acquired over two sessions. Mean gradients are plotted against the test-retest difference calculated as the difference between the gradients acquired in both sessions for every participant. Each point represents an individual participant. The dashed lines represent the 95 % limits of agreement. 52

3.15 **Correlations between task (action selection and SRTT) performance metrics and IO curve slopes dependent on pulse width** in sessions 1 (top) and 2 (bottom). Execute response times (RT) represent simple response times of button press after visual stimulus. Action selection times are calculated by subtracting execute RTs from select block RTs, where participants select which finger to press based on visual cue size and shape and represent the pure time for action selection. Learning gradients are the linear lines of best fit to median response times in sequence blocks of the SRTT. The task measures were correlated with IO curve slopes acquired using different pulse widths in session 1 (30: n = 15, 60: n = 20, and 120: n = 22) and session 2 : (30: n = 21, 60: n = 21, and 120: n = 22). 54

3.16 **Example input-output (IO) curves fitted using the %rMT method** of same participant as in Figure 3.6 for pulse widths 30 (orange), 60 (pink) and 120 (blue) μs acquired in session 1 (solid line/circle marker) and 2 (dashed line/cross marker). The markers represent mean log-transformed amplitude of motor evoked potentials (MEPs) elicited by TMS pulses of various intensities represented as percentage of the participant's resting motor threshold (%rMT). At every combination of TMS pulse intensity and width, 10 trials were recorded. Mean MEP amplitude was calculated from remaining trials after exclusion criteria were applied during data pre-processing. Lines show sigmoid curves of best fit to the mean MEPs. 55

3.17 **Comparison of input-output (IO) curve slopes acquired using all pulse widths in both sessions.** Each marker represents an individual participant (n = 15 for 30, n = 20 for 60, and n = 22 for 120 μs pulses), lines connecting the markers show a change between sessions for individual participants. 56

3.18 **Correlations between IO curve slopes acquired using different pulse widths** in sessions 1 (top, 30: n = 15, 60: n = 20, and 120: n = 22) and 2 (bottom, 30: n = 21, 60: n = 21, and 120: n = 22). 57

3.19 **Correlations between IO curve slopes analysed using different methods** acquired using different pulse widths in sessions 1 (top) and 2 (bottom). . 59

3.20 **Scatterplot of relationships between IO curve slopes analysed using different methods** acquired using different pulse widths in session 1. 60

3.21 **Bland-Altman plots** showing agreement between IO curve slopes acquired over two sessions. Mean slope is plotted against the test-retest difference calculated as the difference between slopes acquired in both sessions for every participant and pulse width. Each point represents an individual participant. The dashed lines represent the 95 % limits of agreement. 60

3.22 **Correlations between task (action selection and SRTT) performance metrics and IO curve slopes dependent on pulse width (quantified by %rMT method)** in sessions 1 (top) and 2 (bottom). Execute response times (RT) represent simple response times of button press after visual stimulus. Action selection times are calculated by subtracting execute RTs from select block RTs, where participants select which finger to press based on visual cue size and shape and represent the pure time for action selection. Learning gradients are the linear lines of best fit to median response times in sequence blocks of the SRTT. The task measures were correlated with IO curve slopes acquired using different pulse widths in session 1 (30: n = 15, 60: n = 20, and 120: n = 22) and session 2 : (30: n = 21, 60: n = 21, and 120: n = 22). 62

3.23 **Calculation of charges delivered by the cTMS device.** A: Electric field waveforms of cTMS pulses recorded with a search coil. B: Coil current calculated by integrating the electric field. C: Mean charge calculated for all participants for all three pulse widths from the whole pulse. D: Mean charge calculated for all participants for all three pulse widths, but only considering the positive phase of the pulse. 67

4.1 **Histogram of participant ages** split by sex. 82

4.2 **Mid-gamma (60-85 Hz) movement-induced event-related synchronisation (ERS)**. Top panel: power as a function of space (each line represents data from one voxel) and frequency (x-axis) averaged over time (-0.2 to 0.2 s) and all epochs. The red line illustrates data from the peak voxel. The vertical magenta line illustrates the peak frequency (74 Hz). Middle panel: power as a function of time and frequency at the peak voxel, averaged over all epochs. The horizontal magenta dashed line identifies the peak frequency, black dashed line indicates the button press. Bottom panel: power as a function of space. Peak voxel was determined by the peak frequency (74 Hz) averaged over all epochs over time between -0.2 to 0.2 s relative to button press. Location of the peak voxel defined by coordinates on the right-left (R to L), anterior-posterior (A to P), and inferior-superior (I to S) axes is highlighted by a black square. . 83

4.3 **Grand average plots showing the temporal and spectral characteristics of movement-related responses** from each participant's peak voxel. The left column represents median changes in power relative to baseline (-1 to -0.5 s before button press, which happens at time 0) for the following frequency bands and movement-related responses, from top to bottom: mid-gamma ERS, slow-gamma ERS, beta ERS, and beta ERD. Plots in the right column visualise the mean log_{10}-transformed absolute power change relative to the same baseline for the same frequency bands. 85

4.4 **Group average of the centre of gravity of movement-related activity.** The centre of gravity was calculated by taking the means of peak voxel x (left-right axis), y (anterior-posterior axis), and z (superior-inferior axis) coordinates respectively from all participants. 86
4.5 **Relationship between age and peak frequency (left) and power (right)** for mid- and slow-gamma ERS, beta ERS and ERD. In the scatterplots, each point represents an individual participant's data, the red solid line represents the linear regression fit and the dotted red lines the 95% confidence bounds. In the histogram, the red line is the probability density estimate. An asterisk (*) next to response metric indicates p-value below 0.05. 87
4.6 **Relationship between age and peak voxel coordinates** x (left column, left-right axis), y (middle, anterior-posterior axis), and z (right, superior-inferior axis) for mid- and slow-gamma ERS, beta ERS and ERD. In the scatterplots, each point represents an individual participant's data, the red solid line represents the linear regression fit and the dotted red lines the 95% confidence bounds. In the histogram, the red line is the probability density estimate. An asterisk (*) next to response metric indicates p-value below 0.05. 89
4.7 **Comparison of the movement-related activity centre of gravity between the youngest and oldest participants**. The centre of gravity was calculated by taking the means of peak voxel x (left-right axis), y (anterior-posterior axis), and z (superior-inferior axis) coordinates respectively from the youngest 150 (age range 18-40) and the oldest 150 (age range 71-89) participants. 90

5.1 **Sensitivity curves** for a sample size up to 613 participants for the ANCOVA analysis. 105
5.2 **Effect of GAD1 SNP rs3749034 genotype on mid-gamma event-related synchronisation (ERS) peak frequency** A: Individual participants' peak frequencies grouped by genotype. B: Relationship between age and movement-evoked mid-gamma peak frequency by GAD1 SNP rs3749034 genotype. Plot shows individual data points and lines representing linear regression fits. 107
5.3 **Effect of BDNF SNP rs6265 genotype on mid-gamma event-related synchronisation (ERS) peak frequency** A: Individual participants' peak frequencies grouped by genotype. B: Relationship between age and movement-evoked mid-gamma peak frequency by BDNF SNP rs6265 genotype. Plot shows individual data points and lines representing linear regression fits. . . . 109

A.1 **Exclusion of IO curves based on insufficient number of conditions**. Each subplot contains an IO curve for one subject. Individual MEPs in grey dots, if the MEPs were marked as outliers, they are shown as blue crosses. Coloured markers represent mean MEP and the line represents line of best fit to the mean MEPs. 130
A.2 **IO curves were kept if spread of intensities covered the full curve**. Each subplot contains an IO curve for one subject. Individual MEPs in grey dots, if the MEPs were marked as outliers, they are shown as blue crosses. Coloured markers represent mean MEP and the line represents line of best fit to the mean MEPs. 131
A.3 **Exclusion of IO curves if the whole curve including the top plateau was not sampled**. Each subplot contains an IO curve for one subject. Individual MEPs in grey dots, if the MEPs were marked as outliers, they are shown as blue crosses. Coloured markers represent mean MEP and the line represents line of best fit to the mean MEPs. 132
A.4 **Exclusion of data in cases where IO curves could not be quantified**. Each subplot contains an IO curve for one subject. Individual MEPs in grey dots, if the MEPs were marked as outliers, they are shown as blue crosses. Coloured markers represent mean MEP and the line represents line of best fit to the mean MEPs. 132

Appendix A

Appendix

A.1 Exclusion of input-output curves in Chapter 3

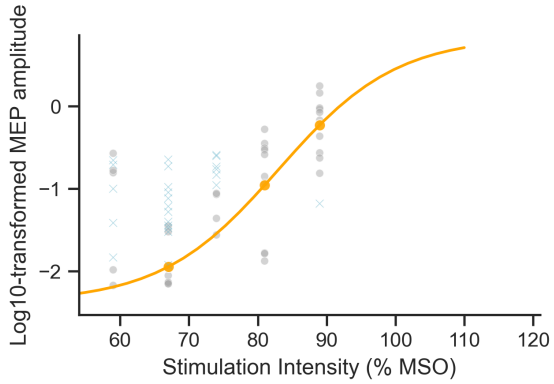
Here, I provide the individual input-output (IO) curve data referenced in section 3.2.4 of Chapter 3, where I excluded some IO curve data.

If excluding individual frames due to either a pre-contraction or outlier detection resulted in less than six frames per condition (intensity), all MEPs were then excluded for that condition. If this criterion resulted in 4 or less conditions per IO curve, that IO curve was excluded (Figure A.1).

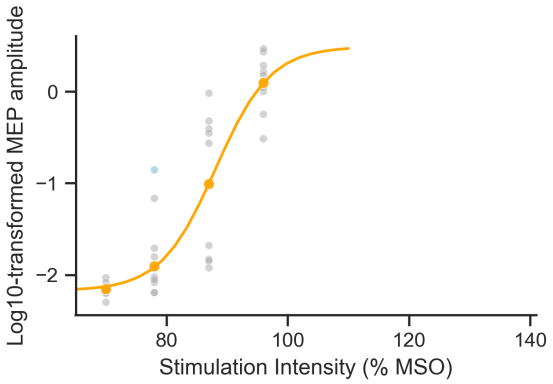
If five condition remained, the IO curves were manually inspected. If the five condition represented a good spread of intensities sampling the IO curve, where a plateau was visible, those IO curves were kept (Figure A.2).

If the five condition did not cover the full curve including the bottom and top plateaus, the curves were excluded (Figure A.3).

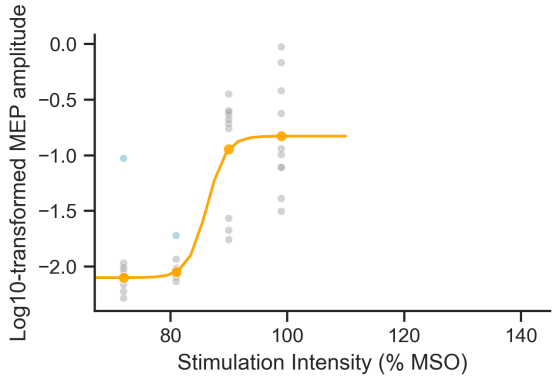
Data were also excluded for an IO curve if a sigmoid line of best fit could not be quantified (Figure A.4).



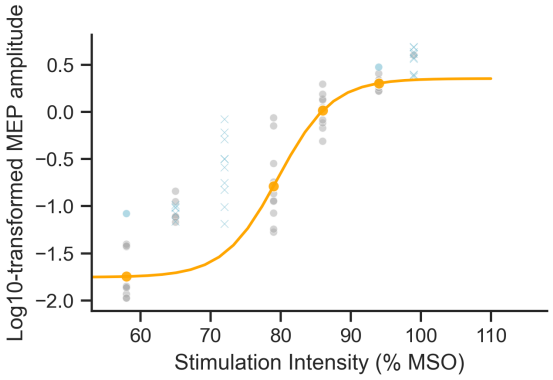
(a) 30 μs pulses



(b) 30 μs pulses

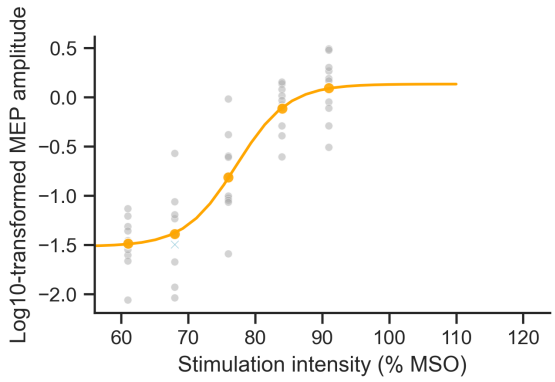


(c) 30 μs pulses

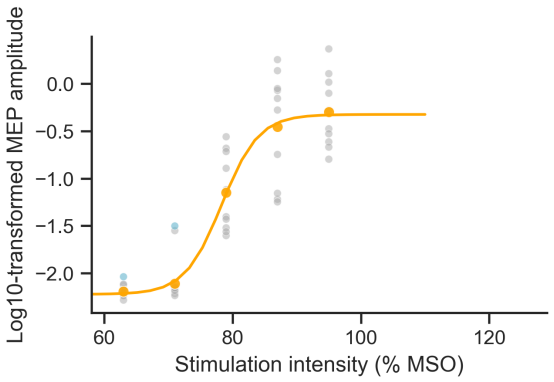


(d) 30 μs pulses

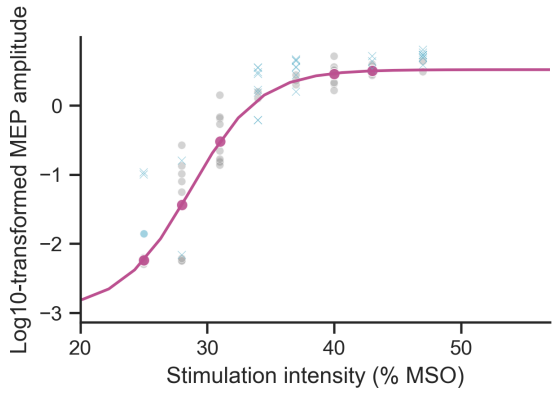
Figure A.1: Exclusion of IO curves based on insufficient number of conditions. Each subplot contains an IO curve for one subject. Individual MEPs in grey dots, if the MEPs were marked as outliers, they are shown as blue crosses. Coloured markers represent mean MEP and the line represents line of best fit to the mean MEPs.



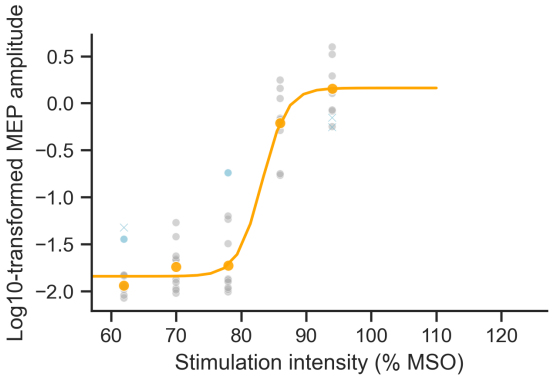
(a) 30 μs pulses



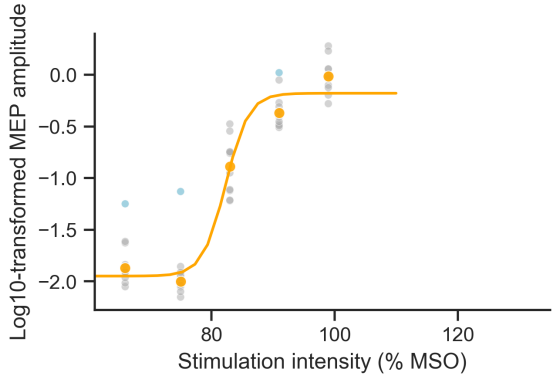
(b) 30 μs pulses



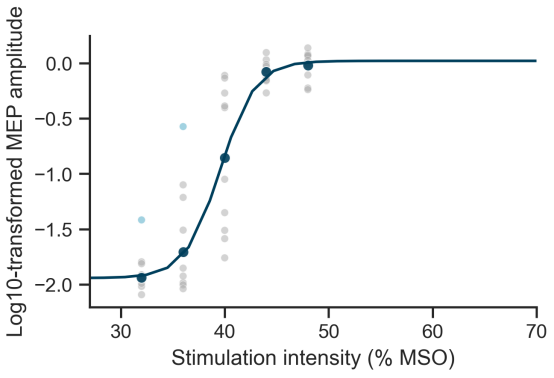
(c) 60 μs pulses



(d) 30 μs pulses

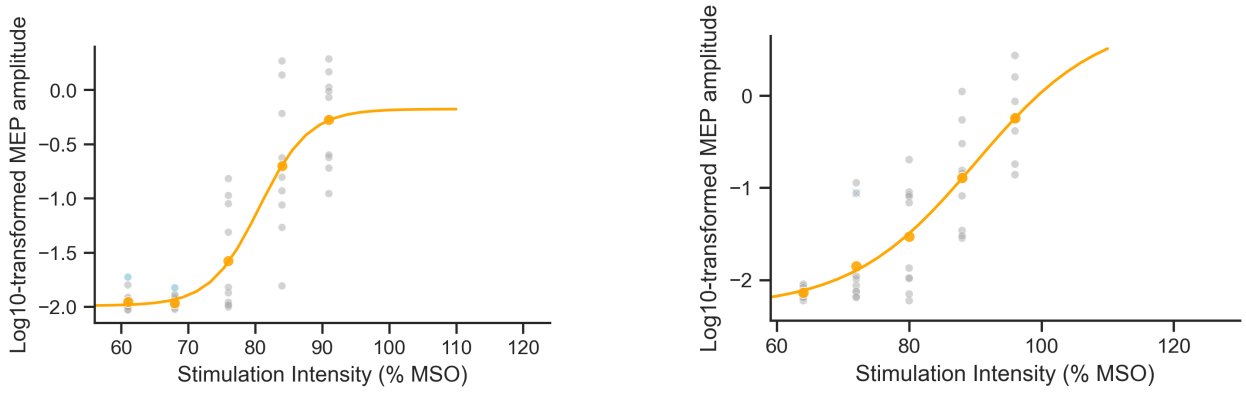


(e) 30 μs pulses



(f) 120 μs pulses

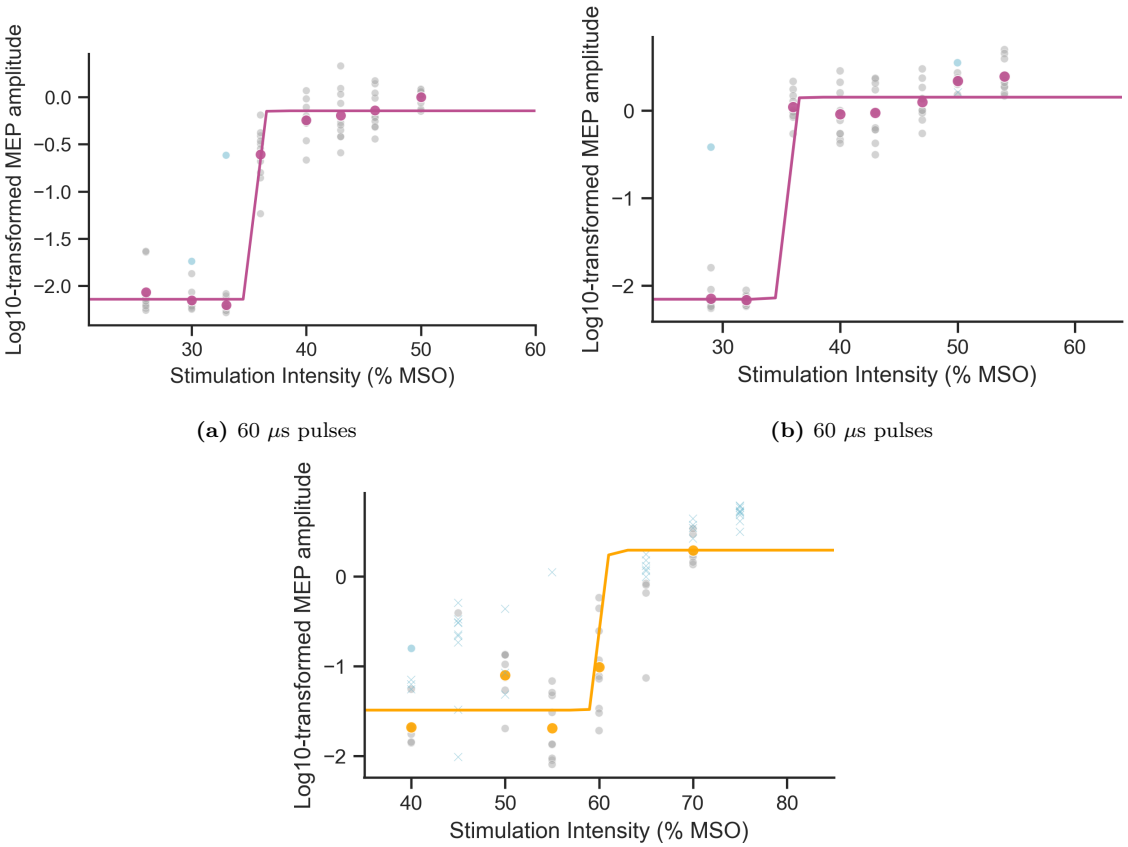
Figure A.2: IO curves were kept if spread of intensities covered the full curve. Each subplot contains an IO curve for one subject. Individual MEPs in grey dots, if the MEPs were marked as outliers, they are shown as blue crosses. Coloured markers represent mean MEP and the line represents line of best fit to the mean MEPs.



(a) 30 μs pulses

(b) 30 μs pulses

Figure A.3: Exclusion of IO curves if the whole curve including the top plateau was not sampled. Each subplot contains an IO curve for one subject. Individual MEPs in grey dots, if the MEPs were marked as outliers, they are shown as blue crosses. Coloured markers represent mean MEP and the line represents line of best fit to the mean MEPs.



(a) 60 μs pulses

(b) 60 μs pulses

(c) 30 μs pulses

Figure A.4: Exclusion of data in cases where IO curves could not be quantified. Each subplot contains an IO curve for one subject. Individual MEPs in grey dots, if the MEPs were marked as outliers, they are shown as blue crosses. Coloured markers represent mean MEP and the line represents line of best fit to the mean MEPs.

Bibliography

1 James Kolasinski, Emily L. Hinson, Amir P. Divanbeighi Zand, Assen Rizov, Uzay E. Emir, and Charlotte J. Stagg. The dynamics of cortical GABA in human motor learning. *The Journal of Physiology*, 597(1):271–282, January 2019. ISSN 0022-3751, 1469-7793. doi: 10.1113/JP276626. URL https://onlinelibrary.wiley.com/doi/10.1113/JP276626.

2 Peter McColgan, Julie Joubert, Sarah J. Tabrizi, and Geraint Rees. The human motor cortex microcircuit: insights for neurodegenerative disease. *Nature Reviews Neuroscience*, 21(8):401–415, August 2020. ISSN 1471-003X, 1471-0048. doi: 10.1038/s41583-020-0315-1. URL http://www.nature.com/articles/s41583-020-0315-1.

3 Naoki Yamawaki, Katharine Borges, Benjamin A Suter, Kenneth D Harris, and Gordon MG Shepherd. A genuine layer 4 in motor cortex with prototypical synaptic circuit connectivity. *Elife*, 3:e05422, 2014.

4 Farran Briggs. Organizing principles of cortical layer 6. *Frontiers in neural circuits*, 4: 750, 2010.

5 Kenneth D Harris and Gordon MG Shepherd. The neocortical circuit: themes and variations. *Nature neuroscience*, 18(2):170–181, 2015.

6 WA Grow. *Fundamental Neuroscience for Basic and Clinical Applications*, chapter 32, pages 468–479. Elsevier, 2018.

7 Robin Tremblay, Soohyun Lee, and Bernardo Rudy. GABAergic Interneurons in the Neocortex: From Cellular Properties to Circuits. *Neuron*, 91(2):260–292, July 2016. ISSN 08966273. doi: 10.1016/j.neuron.2016.06.033. URL https://linkinghub.elsevier.com/retrieve/pii/S0896627316303117.

8 Henry Markram, Maria Toledo-Rodriguez, Yun Wang, Anirudh Gupta, and Caizhi Wu. Interneurons of the neocortical inhibitory system. *Nature Reviews Neuroscience volume*, 5(10):793–807, June 2004.

9 Julie Duque, Ian Greenhouse, Ludovica Labruna, and Richard B. Ivry. Physiological Markers of Motor Inhibition during Human Behavior. *Trends in Neurosciences*, 40(4): 219–236, April 2017. ISSN 01662236. doi: 10.1016/j.tins.2017.02.006. URL https://linkinghub.elsevier.com/retrieve/pii/S0166223617300279.

10 V. Bachtiar and C.J. Stagg. The role of inhibition in human motor cortical plasticity. *Neuroscience*, 278:93–104, October 2014. ISSN 03064522. doi: 10.1016/j.neuroscience.2014.07.059. URL https://linkinghub.elsevier.com/retrieve/pii/S0306452214006320.

11 Andrew J. Peters, Haixin Liu, and Takaki Komiyama. Learning in the Rodent Motor Cortex. *Annual Review of Neuroscience*, 40(1):77–97, July 2017. ISSN 0147-006X, 1545-4126. doi: 10.1146/annurev-neuro-072116-031407. URL https://www.annualreviews.org/doi/10.1146/annurev-neuro-072116-031407.

12 J. Duque and R. B. Ivry. Role of Corticospinal Suppression during Motor Preparation. *Cerebral Cortex*, 19(9):2013–2024, September 2009. ISSN 1047-3211, 1460-2199. doi: 10.1093/cercor/bhn230. URL https://academic.oup.com/cercor/article-lookup/doi/10.1093/cercor/bhn230.

13 J. Duque, D. Lew, R. Mazzocchio, E. Olivier, and R. B. Ivry. Evidence for Two Concurrent Inhibitory Mechanisms during Response Preparation. *Journal of Neuroscience*, 30(10):3793–3802, March 2010. ISSN 0270-6474, 1529-2401. doi: 10.1523/JNEUROSCI.5722-09.2010. URL https://www.jneurosci.org/lookup/doi/10.1523/JNEUROSCI.5722-09.2010.

14 Florent Lebon, Célia Ruffino, Ian Greenhouse, Ludovica Labruna, Richard B Ivry, and Charalambos Papaxanthis. The Neural Specificity of Movement Preparation During Actual and Imagined Movements. *Cerebral Cortex*, 29(2):689–700, February 2019. ISSN 1047-3211, 1460-2199. doi: 10.1093/cercor/bhx350. URL https://academic.oup.com/cercor/article/29/2/689/4788773.

15 Letizia Leocani, Leonardo G. Cohen, Eric M. Wassermann, Katsunori Ikoma, and Mark Hallett. Human corticospinal excitability evaluated with transcranial magnetic stimulation during different reaction time paradigms. *Brain*, 123(6):1161–1173, June 2000. ISSN 1460-2156, 0006-8950. doi: 10.1093/brain/123.6.1161. URL https://academic.oup.com/brain/article-lookup/doi/10.1093/brain/123.6.1161.

16 J. Dupont-Hadwen, S. Bestmann, and C.J. Stagg. Motor training modulates intracortical inhibitory dynamics in motor cortex during movement preparation. *Brain Stimulation*, 12(2):300–308, March 2019. ISSN 1935861X. doi: 10.1016/j.brs.2018.11.002. URL https://linkinghub.elsevier.com/retrieve/pii/S1935861X18303681.

17 F. C. Hummel, B. Steven, J. Hoppe, K. Heise, G. Thomalla, L. G. Cohen, and C. Gerloff. Deficient intracortical inhibition (SICI) during movement preparation after chronic stroke. *Neurology*, 72(20):1766–1772, May 2009. ISSN 0028-3878, 1526-632X. doi: 10.1212/WNL.0b013e3181a609c5. URL https://www.neurology.org/lookup/doi/10.1212/WNL.0b013e3181a609c5.

18 Robert Chen, Zaneb Yaseen, Leonardo G Cohen, and Mark Hallett. Time course of corticospinal excitability in reaction time and self-paced movements. *Annals of neurology*, 44(3):317–325, 1998.

19 J Ibáñez, Ricci Hannah, L Rocchi, and JC Rothwell. Premovement suppression of corticospinal excitability may be a necessary part of movement preparation. *Cerebral Cortex*, 30(5):2910–2923, 2020.

20 K. Rosenkranz, A. Kacar, and J. C. Rothwell. Differential Modulation of Motor Cortical Plasticity and Excitability in Early and Late Phases of Human Motor Learning. *Journal of Neuroscience*, 27(44):12058–12066, October 2007. ISSN 0270-6474, 1529-2401. doi: 10.1523/JNEUROSCI.2663-07.2007. URL https://www.jneurosci.org/lookup/doi/10.1523/JNEUROSCI.2663-07.2007.

21 Simon X Chen, An Na Kim, Andrew J Peters, and Takaki Komiyama. Subtype-specific plasticity of inhibitory circuits in motor cortex during motor learning. *Nature Neuroscience*, 18(8):1109–1115, August 2015. ISSN 1097-6256, 1546-1726. doi: 10.1038/nn.4049. URL http://www.nature.com/articles/nn.4049.

22 Christopher Trepel and Ronald J Racine. Gabaergic modulation of neocortical long-term potentiation in the freely moving rat. *Synapse*, 35(2):120–128, 2000.

23 Anna Floyer-Lea, Marzena Wylezinska, Tamas Kincses, and Paul M. Matthews. Rapid Modulation of GABA Concentration in Human Sensorimotor Cortex During Motor Learning. *Journal of Neurophysiology*, 95(3):1639–1644, March 2006. ISSN 0022-3077, 1522-1598. doi: 10.1152/jn.00346.2005. URL https://www.physiology.org/doi/10.1152/jn.00346.2005.

24 Gyorgy Buzsaki. *Rhythms of the Brain*. Oxford university press, 2006.

25 Shingo Murakami and Yoshio Okada. Contributions of principal neocortical neurons to magnetoencephalography and electroencephalography signals. *The Journal of Physiology*, 575(3):925–936, September 2006. ISSN 0022-3751, 1469-7793. doi: 10.1113/jphysiol.2006.105379. URL https://physoc.onlinelibrary.wiley.com/doi/10.1113/jphysiol.2006.105379.

26 György Buzsáki and Andreas Draguhn. Neuronal Oscillations in Cortical Networks. *Science*, 304(5679):1926–1929, June 2004. ISSN 0036-8075, 1095-9203. doi: 10.1126/science.1099745. URL https://www.science.org/doi/10.1126/science.1099745.

27 Andreas K Engel and Pascal Fries. Beta-band oscillations — signalling the status quo? *Current Opinion in Neurobiology*, 20(2):156–165, April 2010. ISSN 09594388. doi: 10.1016/j.conb.2010.02.015. URL https://linkinghub.elsevier.com/retrieve/pii/S0959438810000395.

28 Magdalena Nowak, Catharina Zich, and Charlotte J. Stagg. Motor Cortical Gamma Oscillations: What Have We Learnt and Where Are We Headed? *Current Behavioral Neuroscience Reports*, 5(2):136–142, June 2018. ISSN 2196-2979. doi: 10.1007/s40473-018-0151-z. URL http://link.springer.com/10.1007/s40473-018-0151-z.

29 Benjamin Morillon, Luc H Arnal, Charles E Schroeder, and Anne Keitel. Prominence of delta oscillatory rhythms in the motor cortex and their relevance for auditory and speech perception. *Neuroscience & Biobehavioral Reviews*, 107:136–142, 2019.

30 György Buzsáki and Edvard I Moser. Memory, navigation and theta rhythm in the hippocampal-entorhinal system. *Nature neuroscience*, 16(2):130–138, 2013.

31 Ryan T Canolty, Erik Edwards, Sarang S Dalal, Maryam Soltani, Srikantan S Nagarajan, Heidi E Kirsch, Mitchel S Berger, Nicholas M Barbaro, and Robert T Knight. High gamma power is phase-locked to theta oscillations in human neocortex. *science*, 313 (5793):1626–1628, 2006.

32 Haya Akkad, Joshua Dupont-Hadwen, Edward Kane, Carys Evans, Liam Barrett, Amba Frese, Irena Tetkovic, Sven Bestmann, and Charlotte J Stagg. Increasing human motor skill acquisition by driving theta–gamma coupling. *eLife*, 10:e67355, November 2021. ISSN 2050-084X. doi: 10.7554/eLife.67355. URL https://elifesciences.org/articles/67355.

33 G Pfurtscheller, Ch Neuper, C Andrew, and G Edlinger. Foot and hand area mu rhythms. *International Journal of Psychophysiology*, 26(1-3):121–135, June 1997. ISSN 01678760. doi: 10.1016/S0167-8760(97)00760-5. URL https://linkinghub.elsevier.com/retrieve/pii/S0167876097007605.

34 Stéphanie Cochin, Catherine Barthelemy, Sylvie Roux, and Joëlle Martineau. Observation and execution of movement: similarities demonstrated by quantified electroencephalography. *European Journal of Neuroscience*, 11(5):1839–1842, May 1999. ISSN 0953-816X, 1460-9568. doi: 10.1046/j.1460-9568.1999.00598.x. URL https://onlinelibrary.wiley.com/doi/10.1046/j.1460-9568.1999.00598.x.

35 Giuseppe Di Pellegrino, Luciano Fadiga, Leonardo Fogassi, Vittorio Gallese, and Giacomo Rizzolatti. Understanding motor events: a neurophysiological study. *Experimental brain research*, 91:176–180, 1992.

36 P Zhuang, C Toro, J Grafman, Paolo Manganotti, L Leocani, and M Hallett. Event-related desynchronization (erd) in the alpha frequency during development of implicit and explicit learning. *Electroencephalography and clinical neurophysiology*, 102(4):374–381, 1997.

37 Ole Jensen, Pranay Goel, Nancy Kopell, Mikko Pohja, Riitta Hari, and Bard Ermentrout. On the human sensorimotor-cortex beta rhythm: sources and modeling. *Neuroimage*, 26(2):347–355, 2005.

38 MM McCarthy, C Moore-Kochlacs, X Gu, ES Boyden, X Han, and N Kopell. Striatal origin of the pathologic beta oscillations in parkinson's disease. *Proceedings of the national academy of sciences*, 108(28):11620–11625, 2011.

39 Jacopo Barone and Holly E. Rossiter. Understanding the Role of Sensorimotor Beta Oscillations. *Frontiers in Systems Neuroscience*, 15:655886, May 2021. ISSN 1662-5137. doi: 10.3389/fnsys.2021.655886. URL `https://www.frontiersin.org/articles/10.3389/fnsys.2021.655886/full`.

40 Maxwell A. Sherman, Shane Lee, Robert Law, Saskia Haegens, Catherine A. Thorn, Matti S. Hämäläinen, Christopher I. Moore, and Stephanie R. Jones. Neural mechanisms of transient neocortical beta rhythms: Converging evidence from humans, computational modeling, monkeys, and mice. *Proceedings of the National Academy of Sciences*, 113 (33), August 2016. ISSN 0027-8424, 1091-6490. doi: 10.1073/pnas.1604135113. URL `https://pnas.org/doi/full/10.1073/pnas.1604135113`.

41 A.D. Shaw, R.J. Moran, and S.D. Muthukumaraswamy. Neurophysiologically-informed markers of individual variability and pharmacological manipulation of human cortical gamma. *NeuroImage*, 161(August):19–31, 2017. doi: 10.1016/j.neuroimage.2017.08.034.

42 G. Pfurtscheller, A. Stancák, and C. Neuper. Post-movement beta synchronization. A correlate of an idling motor area? *Electroencephalography and Clinical Neurophysiology*, 98(4):281–293, April 1996. ISSN 00134694. doi: 10.1016/0013-4694(95)00258-8. URL `https://linkinghub.elsevier.com/retrieve/pii/0013469495002588`.

43 G. Pfurtscheller and F.H. Lopes da Silva. Event-related EEG/MEG synchronization and desynchronization: basic principles. *Clinical Neurophysiology*, 110(11):1842–1857, November 1999. ISSN 13882457. doi: 10.1016/S1388-2457(99)00141-8. URL `https://linkinghub.elsevier.com/retrieve/pii/S1388245799001418`.

44 Arjen Stolk, Loek Brinkman, Mariska J Vansteensel, Erik Aarnoutse, Frans Ss Leijten, Chris H Dijkerman, Robert T Knight, Floris P De Lange, and Ivan Toni. Electrocorticographic dissociation of alpha and beta rhythmic activity in the human sensorimotor system. *eLife*, 8:e48065, October 2019. ISSN 2050-084X. doi: 10.7554/eLife.48065. URL `https://elifesciences.org/articles/48065`.

45 S.D. Hall, I.M. Stanford, N. Yamawaki, C.J. McAllister, K.C. Rönnqvist, G.L. Woodhall, and P.L. Furlong. The role of GABAergic modulation in motor function related neuronal network activity. *NeuroImage*, 56(3):1506–1510, June 2011. ISSN 10538119. doi: 10.

1016/j.neuroimage.2011.02.025. URL https://linkinghub.elsevier.com/retrieve/pii/S1053811911001649.

46 Han Yuan, Christopher Perdoni, and Bin He. Relationship between speed and EEG activity during imagined and executed hand movements. *Journal of Neural Engineering*, 7 (2):026001, April 2010. ISSN 1741-2560, 1741-2552. doi: 10.1088/1741-2560/7/2/026001. URL https://iopscience.iop.org/article/10.1088/1741-2560/7/2/026001.

47 Huiling Tan, Ned Jenkinson, and Peter Brown. Dynamic Neural Correlates of Motor Error Monitoring and Adaptation during Trial-to-Trial Learning. *The Journal of Neuroscience*, 34(16):5678–5688, April 2014. ISSN 0270-6474, 1529-2401. doi: 10.1523/JNEUROSCI.4739-13.2014. URL https://www.jneurosci.org/lookup/doi/10.1523/JNEUROSCI.4739-13.2014.

48 Catharina Zich, Mark W Woolrich, Robert Becker, Diego Vidaurre, Jacqueline Scholl, Emily L Hinson, Laurie Josephs, Sven Braeutigam, Andrew J Quinn, and Charlotte J Stagg. Motor learning shapes temporal activity in human sensorimotor cortex. *BioRxiv*, page 345421, 2018.

49 Simon Little and Peter Brown. The functional role of beta oscillations in parkinson's disease. *Parkinsonism & related disorders*, 20:S44–S48, 2014.

50 Atefeh Asadi, Mojtaba Madadi Asl, Abdol-Hossein Vahabie, and Alireza Valizadeh. The origin of abnormal beta oscillations in the parkinsonian corticobasal ganglia circuits. *Parkinson's Disease*, 2022(1):7524066, 2022.

51 Varvara Mathiopoulou, Roxanne Lofredi, Lucia K Feldmann, Jeroen Habets, Natasha Darcy, Wolf-Julian Neumann, Katharina Faust, Gerd-Helge Schneider, and Andrea A Kühn. Modulation of subthalamic beta oscillations by movement, dopamine, and deep brain stimulation in parkinson's disease. *npj Parkinson's Disease*, 10(1):77, 2024.

52 Alek Pogosyan, Louise Doyle Gaynor, Alexandre Eusebio, and Peter Brown. Boosting cortical activity at beta-band frequencies slows movement in humans. *Current biology*, 19(19):1637–1641, 2009.

53 Adam Fry, Karen J. Mullinger, George C. O'Neill, Eleanor L. Barratt, Peter G. Morris, Markus Bauer, Jonathan P. Folland, and Matthew J. Brookes. Modulation of post-movement beta rebound by contraction force and rate of force development: Modulation of PMBR by force & RFD. *Human Brain Mapping*, 37(7):2493–2511, July 2016. ISSN 10659471. doi: 10.1002/hbm.23189. URL https://onlinelibrary.wiley.com/doi/10.1002/hbm.23189.

54 Flavie Torrecillos, Julie Alayrangues, Bjørg Elisabeth Kilavik, and Nicole Malfait. Distinct modulations in sensorimotor postmovement and foreperiod β-band activities re-

lated to error salience processing and sensorimotor adaptation. *Journal of Neuroscience*, 35(37):12753–12765, 2015.

55 Stuart N Baker. Oscillatory interactions between sensorimotor cortex and the periphery. *Current opinion in neurobiology*, 17(6):649–655, 2007.

56 N. Crone. Functional mapping of human sensorimotor cortex with electrocorticographic spectral analysis. II. Event-related synchronization in the gamma band. *Brain*, 121 (12):2301–2315, December 1998. ISSN 14602156. doi: 10.1093/brain/121.12.2301. URL https://academic.oup.com/brain/article-lookup/doi/10.1093/brain/121.12.2301.

57 Antonio Fernandez-Ruiz, Anton Sirota, Vítor Lopes-dos Santos, and David Dupret. Over and above frequency: Gamma oscillations as units of neural circuit operations. *Neuron*, 111(7):936–953, April 2023. ISSN 08966273. doi: 10.1016/j.neuron.2023.02.026. URL https://linkinghub.elsevier.com/retrieve/pii/S0896627323001307.

58 György Buzsáki and Xiao-Jing Wang. Mechanisms of Gamma Oscillations. *Annual Review of Neuroscience*, 35(1):203–225, July 2012. ISSN 0147-006X, 1545-4126. doi: 10.1146/annurev-neuro-062111-150444. URL https://www.annualreviews.org/doi/10.1146/annurev-neuro-062111-150444.

59 Douglas Cheyne, Sonya Bells, Paul Ferrari, William Gaetz, and Andreea C. Bostan. Self-paced movements induce high-frequency gamma oscillations in primary motor cortex. *NeuroImage*, 42(1):332–342, August 2008. ISSN 10538119. doi: 10.1016/j.neuroimage.2008.04.178. URL https://linkinghub.elsevier.com/retrieve/pii/S1053811908004965.

60 W. Gaetz, C. Liu, H. Zhu, L. Bloy, and T.P.L. Roberts. Evidence for a motor gamma-band network governing response interference. *NeuroImage*, 74:245–253, July 2013. ISSN 10538119. doi: 10.1016/j.neuroimage.2013.02.013. URL https://linkinghub.elsevier.com/retrieve/pii/S1053811913001407.

61 W. Gaetz, M. MacDonald, D. Cheyne, and O.C. Snead. Neuromagnetic imaging of movement-related cortical oscillations in children and adults: Age predicts post-movement beta rebound. *NeuroImage*, 51(2):792–807, June 2010. ISSN 10538119. doi: 10.1016/j.neuroimage.2010.01.077. URL https://linkinghub.elsevier.com/retrieve/pii/S1053811910000996.

62 Suresh D. Muthukumaraswamy. Functional Properties of Human Primary Motor Cortex Gamma Oscillations. *Journal of Neurophysiology*, 104(5):2873–2885, November 2010. ISSN 0022-3077, 1522-1598. doi: 10.1152/jn.00607.2010. URL https://www.physiology.org/doi/10.1152/jn.00607.2010.

63 G. Pfurtscheller, B. Graimann, J.E. Huggins, S.P. Levine, and L.A. Schuh. Spatiotemporal patterns of beta desynchronization and gamma synchronization in corticographic data during self-paced movement. *Clinical Neurophysiology*, 114(7):1226–1236, July 2003. ISSN 13882457. doi: 10.1016/S1388-2457(03)00067-1. URL https://linkinghub.elsevier.com/retrieve/pii/S1388245703000671.

64 Elisa Tatti, Alberto Cacciola, Federico Carrara, Adalgisa Luciani, Angelo Quartarone, and M.Felice Ghilardi. Movement-related ERS and connectivity in the gamma frequency decrease with practice. *NeuroImage*, 284:120444, December 2023. ISSN 10538119. doi: 10.1016/j.neuroimage.2023.120444. URL https://linkinghub.elsevier.com/retrieve/pii/S1053811923005955.

65 Magdalena Nowak, Emily Hinson, Freek van Ede, Alek Pogosyan, Andrea Guerra, Andrew Quinn, Peter Brown, and Charlotte J. Stagg. Driving Human Motor Cortical Oscillations Leads to Behaviorally Relevant Changes in Local GABA $_{a}$ Inhibition: A tACS-TMS Study. *The Journal of Neuroscience*, 37(17):4481–4492, April 2017. ISSN 0270-6474, 1529-2401. doi: 10.1523/JNEUROSCI.0098-17.2017. URL https://www.jneurosci.org/lookup/doi/10.1523/JNEUROSCI.0098-17.2017.

66 Benjamin Haverland, Lena S. Timmsen, Silke Wolf, Charlotte J. Stagg, Lukas Frontzkowski, Robert Oostenveld, Jan Feldheim, Focko L. Higgen, Christian Gerloff, Robert Schulz, Till R. Schneider, Bettina C. Schwab, and Fanny Quandt. Human cortical high-gamma power relates to movement speed and is disproportionately reduced after stroke, May 2024. URL http://biorxiv.org/lookup/doi/10.1101/2023.11.07.565934.

67 Vítor Lopes-dos Santos, Gido M van de Ven, Alexander Morley, Stéphanie Trouche, Natalia Campo-Urriza, and David Dupret. Parsing hippocampal theta oscillations by nested spectral components during spatial exploration and memory-guided behavior. *Neuron*, 100(4):940–952, 2018.

68 Laura Lee Colgin. Do slow and fast gamma rhythms correspond to distinct functional states in the hippocampal network? *Brain Research*, 1621:309–315, September 2015. ISSN 00068993. doi: 10.1016/j.brainres.2015.01.005. URL https://linkinghub.elsevier.com/retrieve/pii/S0006899315000086.

69 William Szurhaj, Etienne Labyt, Jean-Louis Bourriez, Philippe Kahane, Patrick Chauvel, François Mauguière, and Philippe Derambure. Relationship between intracerebral gamma oscillations and slow potentials in the human sensorimotor cortex. *European Journal of Neuroscience*, 24(3):947–954, August 2006. ISSN 0953-816X, 1460-9568. doi: 10.1111/j.1460-9568.2006.04876.x. URL https://onlinelibrary.wiley.com/doi/10.1111/j.1460-9568.2006.04876.x.

70 Catharina Zich, Magdalena Nowak, Emily L. Hinson, Camille Lasbareilles, Valentina Mancini, Alek Pogosyan, Oana Puicar, Ioana-Florentina Grigoras, Patricia Cambalova, Jacqueline Scholl, Laurie Josephs, Andrew J. Quinn, Mark W. Woolrich, and Charlotte J. Stagg. Human motor cortical gamma activity relates to GABAergic intracortical inhibition and motor learning. *Imaging Neuroscience*, 3:imag_a_00538, April 2025. ISSN 2837-6056. doi: 10.1162/imag_a_00538. URL https://direct.mit.edu/imag/article/doi/10.1162/imag_a_00538/128623/Human-motor-cortical-gamma-activity-relates-to.

71 Ling Kang, Jonas Ranft, and Vincent Hakim. Beta oscillations and waves in motor cortex can be accounted for by the interplay of spatially structured connectivity and fluctuating inputs. *eLife*, 12:e81446, March 2023. ISSN 2050-084X. doi: 10.7554/eLife.81446. URL https://elifesciences.org/articles/81446.

72 Stephen D. Hall, Gareth R. Barnes, Paul L. Furlong, Stefano Seri, and Arjan Hillebrand. Neuronal network pharmacodynamics of GABAergic modulation in the human cortex determined using pharmaco-magnetoencephalography. *Human Brain Mapping*, 31(4): 581–594, April 2010. ISSN 1065-9471, 1097-0193. doi: 10.1002/hbm.20889. URL https://onlinelibrary.wiley.com/doi/10.1002/hbm.20889.

73 Guang Chen, Yuan Zhang, Xiang Li, Xiaochen Zhao, Qian Ye, Yingxi Lin, Huizhong W. Tao, Malte J. Rasch, and Xiaohui Zhang. Distinct Inhibitory Circuits Orchestrate Cortical beta and gamma Band Oscillations. *Neuron*, 96(6):1403–1418.e6, December 2017. ISSN 08966273. doi: 10.1016/j.neuron.2017.11.033. URL https://linkinghub.elsevier.com/retrieve/pii/S0896627317310863.

74 G. Pfurtscheller and A. Berghold. Patterns of cortical activation during planning of voluntary movement. *Electroencephalography and Clinical Neurophysiology*, 72(3):250–258, March 1989. ISSN 00134694. doi: 10.1016/0013-4694(89)90250-2. URL https://linkinghub.elsevier.com/retrieve/pii/0013469489902502.

75 Michael T. Jurkiewicz, William C. Gaetz, Andreea C. Bostan, and Douglas Cheyne. Post-movement beta rebound is generated in motor cortex: Evidence from neuromagnetic recordings. *NeuroImage*, 32(3):1281–1289, September 2006. ISSN 10538119. doi: 10.1016/j.neuroimage.2006.06.005. URL https://linkinghub.elsevier.com/retrieve/pii/S1053811906006616.

76 James J Bonaiuto, Simon Little, Samuel A Neymotin, Stephanie R Jones, Gareth R Barnes, and Sven Bestmann. Laminar dynamics of high amplitude beta bursts in human motor cortex. *NeuroImage*, 242:118479, November 2021. ISSN 10538119. doi: 10.1016/j.neuroimage.2021.118479. URL https://linkinghub.elsevier.com/retrieve/pii/S1053811921007527.

77 Hyeyoung Shin, Robert Law, Shawn Tsutsui, Christopher I Moore, and Stephanie R Jones. The rate of transient beta frequency events predicts behavior across tasks and species. *eLife*, 6:e29086, November 2017. ISSN 2050-084X. doi: 10.7554/eLife.29086. URL https://elifesciences.org/articles/29086.

78 Simon Little, James Bonaiuto, Gareth Barnes, and Sven Bestmann. Human motor cortical beta bursts relate to movement planning and response errors. *PLOS Biology*, 17 (10):e3000479, October 2019. ISSN 1545-7885. doi: 10.1371/journal.pbio.3000479. URL https://dx.plos.org/10.1371/journal.pbio.3000479.

79 Kim C. Ronnqvist, Craig J. McAllister, Gavin L. Woodhall, Ian M. Stanford, and Stephen D. Hall. A Multimodal Perspective on the Composition of Cortical Oscillations. *Frontiers in Human Neuroscience*, 7, 2013. ISSN 1662-5161. doi: 10.3389/fnhum.2013.00132. URL http://journal.frontiersin.org/article/10.3389/fnhum.2013.00132/abstract.

80 S.D. Muthukumaraswamy, J.F.M. Myers, S.J. Wilson, D.J. Nutt, A. Lingford-Hughes, K.D. Singh, and K. Hamandi. The effects of elevated endogenous GABA levels on movement-related network oscillations. *NeuroImage*, 66:36–41, February 2013. ISSN 10538119. doi: 10.1016/j.neuroimage.2012.10.054. URL https://linkinghub.elsevier.com/retrieve/pii/S1053811912010579.

81 Naoki Yamawaki, Ian M Stanford, Stephen D Hall, and Gavin L Woodhall. Pharmacologically induced and stimulus evoked rhythmic neuronal oscillatory activity in the primary motor cortex in vitro. *Neuroscience*, 151(2):386–395, 2008.

82 C. J. Stagg, S. Bestmann, A. O. Constantinescu, L. Moreno Moreno, C. Allman, R. Mekle, M. Woolrich, J. Near, H. Johansen-Berg, and J. C. Rothwell. Relationship between physiological measures of excitability and levels of glutamate and GABA in the human motor cortex. *The Journal of Physiology*, 589(23):5845–5855, December 2011. ISSN 0022-3751, 1469-7793. doi: 10.1113/jphysiol.2011.216978. URL https://onlinelibrary.wiley.com/doi/10.1113/jphysiol.2011.216978.

83 Ilenia Paparella, Paolo Cardone, Benedetta Zanichelli, Laurent Lamalle, Fabienne Collette, Siya Sherif, Mikhail Zubkov, William T. Clarke, Charlotte J. Stagg, Pierre Maquet, and Gilles Vandewalle. 7 Tesla magnetic resonance spectroscopy estimates of GABA concentration relate to physiological measures of tonic inhibition in the human motor cortex. *The Journal of Physiology*, 603(9):2821–2838, May 2025. ISSN 0022-3751, 1469-7793. doi: 10.1113/JP287311. URL https://physoc.onlinelibrary.wiley.com/doi/10.1113/JP287311.

84 Thomas J. Baumgarten, Georg Oeltzschner, Nienke Hoogenboom, Hans-Jörg Wittsack, Alfons Schnitzler, and Joachim Lange. Beta Peak Frequencies at Rest Correlate with

Endogenous GABA+/Cr Concentrations in Sensorimotor Cortex Areas. *PLOS ONE*, 11(6):e0156829, June 2016. ISSN 1932-6203. doi: 10.1371/journal.pone.0156829. URL https://dx.plos.org/10.1371/journal.pone.0156829.

85 W. Gaetz, J.C. Edgar, D.J. Wang, and T.P.L. Roberts. Relating meg measured motor cortical oscillations to resting γ-aminobutyric acid (gaba) concentration. *NeuroImage*, 55(2):616–621, Mar 2011. ISSN 10538119. doi: 10.1016/j.neuroimage.2010.12.077.

86 Chia-Hsiung Cheng, Shang-Yueh Tsai, Chia-Yih Liu, and David M. Niddam. Automatic inhibitory function in the human somatosensory and motor cortices: An MEG-MRS study. *Scientific Reports*, 7(1):4234, June 2017. ISSN 2045-2322. doi: 10.1038/s41598-017-04564-1. URL https://www.nature.com/articles/s41598-017-04564-1.

87 Paul Tiesinga and Terrence J Sejnowski. Cortical enlightenment: are attentional gamma oscillations driven by ing or ping? *Neuron*, 63(6):727–732, 2009.

88 W. W. Lytton and T. J. Sejnowski. Simulations of cortical pyramidal neurons synchronized by inhibitory interneurons. *Journal of Neurophysiology*, 66(3):1059–1079, September 1991. ISSN 0022-3077, 1522-1598. doi: 10.1152/jn.1991.66.3.1059. URL https://www.physiology.org/doi/10.1152/jn.1991.66.3.1059.

89 Nicholas W. Johnson, Mazhar Özkan, Adrian P. Burgess, Emma J. Prokic, Keith A. Wafford, Michael J. O'Neill, Stuart D. Greenhill, Ian M. Stanford, and Gavin L. Woodhall. Phase-amplitude coupled persistent theta and gamma oscillations in rat primary motor cortex in vitro. *Neuropharmacology*, 119:141–156, June 2017. ISSN 00283908. doi: 10.1016/j.neuropharm.2017.04.009. URL https://linkinghub.elsevier.com/retrieve/pii/S0028390817301508.

90 Jessica A. Cardin, Marie Carlén, Konstantinos Meletis, Ulf Knoblich, Feng Zhang, Karl Deisseroth, Li-Huei Tsai, and Christopher I. Moore. Driving fast-spiking cells induces gamma rhythm and controls sensory responses. *Nature*, 459(7247):663–667, June 2009. ISSN 0028-0836, 1476-4687. doi: 10.1038/nature08002. URL http://www.nature.com/articles/nature08002.

91 Vikaas S. Sohal, Feng Zhang, Ofer Yizhar, and Karl Deisseroth. Parvalbumin neurons and gamma rhythms enhance cortical circuit performance. *Nature*, 459(7247):698–702, June 2009. ISSN 0028-0836, 1476-4687. doi: 10.1038/nature07991. URL http://www.nature.com/articles/nature07991.

92 Edward O Mann and Istvan Mody. Control of hippocampal gamma oscillation frequency by tonic inhibition and excitation of interneurons. *Nature Neuroscience*, 13(2):205–212, February 2010. ISSN 1097-6256, 1546-1726. doi: 10.1038/nn.2464. URL https://www.nature.com/articles/nn.2464.

93 S. K. Towers, T. Gloveli, R. D. Traub, J. E. Driver, D. Engel, R. Fradley, T. W. Rosahl, K. Maubach, E. H. Buhl, and M. A. Whittington. $\alpha 5$ subunit-containing gaba a receptors affect the dynamic range of mouse hippocampal kainate-induced gamma frequency oscillations in vitro. *The Journal of Physiology*, 559(3):721–728, Sep 2004. ISSN 0022-3751, 1469-7793. doi: 10.1113/jphysiol.2004.071191.

94 Markku Penttonen, Anita Kamondi, László Acsády, and György Buzsáki. Gamma frequency oscillation in the hippocampus of the rat: intracellular analysis *in vivo*. *European Journal of Neuroscience*, 10(2):718–728, February 1998. ISSN 0953-816X, 1460-9568. doi: 10.1046/j.1460-9568.1998.00096.x. URL `https://onlinelibrary.wiley.com/doi/10.1046/j.1460-9568.1998.00096.x`.

95 Johanna Balz, Julian Keil, Yadira Roa Romero, Ralf Mekle, Florian Schubert, Semiha Aydin, Bernd Ittermann, Jürgen Gallinat, and Daniel Senkowski. GABA concentration in superior temporal sulcus predicts gamma power and perception in the sound-induced flash illusion. *NeuroImage*, 125:724–730, January 2016. ISSN 10538119. doi: 10.1016/j.neuroimage.2015.10.087. URL `https://linkinghub.elsevier.com/retrieve/pii/S1053811915010204`.

96 Christine Wyss, Desmond H.Y. Tse, Michael Kometer, Jürgen Dammers, Rita Achermann, N. Jon Shah, Wolfram Kawohl, and Irene Neuner. GABA metabolism and its role in gamma-band oscillatory activity during auditory processing: An MRS and EEG study: GABA and Its Role in High-Frequency EEG Oscillations. *Human Brain Mapping*, 38(8):3975–3987, August 2017. ISSN 10659471. doi: 10.1002/hbm.23642. URL `https://onlinelibrary.wiley.com/doi/10.1002/hbm.23642`.

97 Suresh D. Muthukumaraswamy, Richard A.E. Edden, Derek K. Jones, Jennifer B. Swettenham, and Krish D. Singh. Resting GABA concentration predicts peak gamma frequency and fMRI amplitude in response to visual stimulation in humans. *Proceedings of the National Academy of Sciences*, 106(20):8356–8361, May 2009. ISSN 0027-8424, 1091-6490. doi: 10.1073/pnas.0900728106. URL `https://pnas.org/doi/full/10.1073/pnas.0900728106`.

98 Helena Cousijn, Saskia Haegens, George Wallis, Jamie Near, Mark G. Stokes, Paul J. Harrison, and Anna C. Nobre. Resting GABA and glutamate concentrations do not predict visual gamma frequency or amplitude. *Proceedings of the National Academy of Sciences*, 111(25):9301–9306, June 2014. ISSN 0027-8424, 1091-6490. doi: 10.1073/pnas.1321072111. URL `https://pnas.org/doi/full/10.1073/pnas.1321072111`.

99 Siân E. Robson, Suresh D. Muthukumarawswamy, C. John Evans, Alexander Shaw, Jennifer Brealy, Brittany Davis, Grainne McNamara, Gavin Perry, and Krish D. Singh. Structural and neurochemical correlates of individual differences in gamma frequency oscillations in human visual cortex. *Journal of Anatomy*, 227(4):409–417, October 2015.

ISSN 0021-8782, 1469-7580. doi: 10.1111/joa.12339. URL https://onlinelibrary.wiley.com/doi/10.1111/joa.12339.

100 Jan Kujala, Julien Jung, Sandrine Bouvard, Françoise Lecaignard, Amélie Lothe, Romain Bouet, Carolina Ciumas, Philippe Ryvlin, and Karim Jerbi. Gamma oscillations in V1 are correlated with GABAA receptor density: A multi-modal MEG and Flumazenil-PET study. *Scientific Reports*, 5(1):16347, November 2015. ISSN 2045-2322. doi: 10.1038/srep16347. URL https://www.nature.com/articles/srep16347.

101 David Nutt, Sue Wilson, Anne Lingford-Hughes, Jim Myers, Andreas Papadopoulos, and Suresh Muthukumaraswamy. Differences between magnetoencephalographic (MEG) spectral profiles of drugs acting on GABA at synaptic and extrasynaptic sites: A study in healthy volunteers. *Neuropharmacology*, 88:155–163, January 2015. ISSN 00283908. doi: 10.1016/j.neuropharm.2014.08.017. URL https://linkinghub.elsevier.com/retrieve/pii/S0028390814003001.

102 W. Gordon Frankle, Raymond Y. Cho, Konasale M. Prasad, N. Scott Mason, Jennifer Paris, Michael L. Himes, Christopher Walker, David A. Lewis, and Rajesh Narendran. In Vivo Measurement of GABA Transmission in Healthy Subjects and Schizophrenia Patients. *American Journal of Psychiatry*, 172(11):1148–1159, November 2015. ISSN 0002-953X, 1535-7228. doi: 10.1176/appi.ajp.2015.14081031. URL https://psychiatryonline.org/doi/10.1176/appi.ajp.2015.14081031.

103 Herbert Haug and Reinhard Eggers. Morphometry of the human cortex cerebri and corpus striatum during aging. *Neurobiology of Aging*, 12(4):336–338, July 1991. ISSN 01974580. doi: 10.1016/0197-4580(91)90013-A. URL https://linkinghub.elsevier.com/retrieve/pii/019745809190013A.

104 Katica Boric, Pablo Muñoz, Michela Gallagher, and Alfredo Kirkwood. Potential adaptive function for altered long-term potentiation mechanisms in aging hippocampus. *Journal of Neuroscience*, 28(32):8034–8039, 2008.

105 AM Davidson, H Mejía-Gómez, M Jacobowitz, and R Mostany. Dendritic spine density and dynamics of layer 5 pyramidal neurons of the primary motor cortex are elevated with aging. *Cerebral Cortex*, 30(2):767–777, 2020.

106 R. A. I. Bethlehem, J. Seidlitz, S. R. White, J. W. Vogel, K. M. Anderson, C. Adamson, S. Adler, G. S. Alexopoulos, E. Anagnostou, A. Areces-Gonzalez, D. E. Astle, B. Auyeung, M. Ayub, J. Bae, G. Ball, S. Baron-Cohen, R. Beare, S. A. Bedford, V. Benegal, F. Beyer, J. Blangero, M. Blesa Cábez, J. P. Boardman, M. Borzage, J. F. Bosch-Bayard, N. Bourke, V. D. Calhoun, M. M. Chakravarty, C. Chen, C. Chertavian, G. Chetelat, Y. S. Chong, J. H. Cole, A. Corvin, M. Costantino, E. Courchesne,

F. Crivello, V. L. Cropley, J. Crosbie, N. Crossley, M. Delarue, R. Delorme, S. Desrivieres, G. A. Devenyi, M. A. Di Biase, R. Dolan, K. A. Donald, G. Donohoe, K. Dunlop, A. D. Edwards, J. T. Elison, C. T. Ellis, J. A. Elman, L. Eyler, D. A. Fair, E. Feczko, P. C. Fletcher, P. Fonagy, C. E. Franz, L. Galan-Garcia, A. Gholipour, J. Giedd, J. H. Gilmore, D. C. Glahn, I. M. Goodyer, P. E. Grant, N. A. Groenewold, F. M. Gunning, R. E. Gur, R. C. Gur, C. F. Hammill, O. Hansson, T. Hedden, A. Heinz, R. N. Henson, K. Heuer, J. Hoare, B. Holla, A. J. Holmes, R. Holt, H. Huang, K. Im, J. Ipser, C. R. Jack, A. P. Jackowski, T. Jia, K. A. Johnson, P. B. Jones, D. T. Jones, R. S. Kahn, H. Karlsson, L. Karlsson, R. Kawashima, E. A. Kelley, S. Kern, K. W. Kim, M. G. Kitzbichler, W. S. Kremen, F. Lalonde, B. Landeau, S. Lee, J. Lerch, J. D. Lewis, J. Li, W. Liao, C. Liston, M. V. Lombardo, J. Lv, C. Lynch, T. T. Mallard, M. Marcelis, R. D. Markello, S. R. Mathias, B. Mazoyer, P. McGuire, M. J. Meaney, A. Mechelli, N. Medic, B. Misic, S. E. Morgan, D. Mothersill, J. Nigg, M. Q. W. Ong, C. Ortinau, R. Ossenkoppele, M. Ouyang, L. Palaniyappan, L. Paly, P. M. Pan, C. Pantelis, M. M. Park, T. Paus, Z. Pausova, D. Paz-Linares, A. Pichet Binette, K. Pierce, X. Qian, J. Qiu, A. Qiu, A. Raznahan, T. Rittman, A. Rodrigue, C. K. Rollins, R. Romero-Garcia, L. Ronan, M. D. Rosenberg, D. H. Rowitch, G. A. Salum, T. D. Satterthwaite, H. L. Schaare, R. J. Schachar, A. P. Schultz, G. Schumann, M. Schöll, D. Sharp, R. T. Shinohara, I. Skoog, C. D. Smyser, R. A. Sperling, D. J. Stein, A. Stolicyn, J. Suckling, G. Sullivan, Y. Taki, B. Thyreau, R. Toro, N. Traut, K. A. Tsvetanov, N. B. Turk-Browne, J. J. Tuulari, C. Tzourio, É. Vachon-Presseau, M. J. Valdes-Sosa, P. A. Valdes-Sosa, S. L. Valk, T. Van Amelsvoort, S. N. Vandekar, L. Vasung, L. W. Victoria, S. Villeneuve, A. Villringer, P. E. Vértes, K. Wagstyl, Y. S. Wang, S. K. Warfield, V. Warrier, E. Westman, M. L. Westwater, H. C. Whalley, A. V. Witte, N. Yang, B. Yeo, H. Yun, A. Zalesky, H. J. Zar, A. Zettergren, J. H. Zhou, H. Ziauddeen, A. Zugman, X. N. Zuo, 3R-BRAIN, AIBL, C. Rowe, Alzheimer's Disease Neuroimaging Initiative, Alzheimer's Disease Repository Without Borders Investigators, G. B. Frisoni, CALM Team, Cam-CAN, CCNP, COBRE, cVEDA, ENIGMA Developmental Brain Age Working Group, Developing Human Connectome Project, FinnBrain, Harvard Aging Brain Study, IMAGEN, KNE96, The Mayo Clinic Study of Aging, NSPN, POND, The PREVENT-AD Research Group, A. Pichet Binette, VETSA, E. T. Bullmore, and A. F. Alexander-Bloch. Brain charts for the human lifespan. *Nature*, 604(7906):525–533, April 2022. ISSN 0028-0836, 1476-4687. doi: 10.1038/s41586-022-04554-y. URL `https://www.nature.com/articles/s41586-022-04554-y`.

107 David H. Salat, Randy L. Buckner, Abraham Z. Snyder, Douglas N. Greve, Rahul S.R. Desikan, Evelina Busa, John C. Morris, Anders M. Dale, and Bruce Fischl. Thinning of the Cerebral Cortex in Aging. *Cerebral Cortex*, 14(7):721–730, March 2004. ISSN 1460-2199. doi: 10.1093/cercor/bhh032. URL `https://academic.oup.com/cercor/article-lookup/doi/10.1093/cercor/bhh032`.

108 Scott M. McGinnis, Michael Brickhouse, Belen Pascual, and Bradford C. Dickerson. Age-Related Changes in the Thickness of Cortical Zones in Humans. *Brain Topography*, 24(3-4):279–291, October 2011. ISSN 0896-0267, 1573-6792. doi: 10.1007/s10548-011-0198-6. URL http://link.springer.com/10.1007/s10548-011-0198-6.

109 Kaitlin Cassady, Holly Gagnon, Poortata Lalwani, Molly Simmonite, Bradley Foerster, Denise Park, Scott J. Peltier, Myria Petrou, Stephan F. Taylor, Daniel H. Weissman, Rachael D. Seidler, and Thad A. Polk. Sensorimotor network segregation declines with age and is linked to GABA and to sensorimotor performance. *NeuroImage*, 186:234–244, February 2019. ISSN 10538119. doi: 10.1016/j.neuroimage.2018.11.008. URL https://linkinghub.elsevier.com/retrieve/pii/S1053811918320780.

110 Elena Solesio-Jofre, Leen Serbruyns, Daniel G Woolley, Dante Mantini, Iseult AM Beets, and Stephan P Swinnen. Aging effects on the resting state motor network and interlimb coordination. *Human brain mapping*, 35(8):3945–3961, 2014.

111 Laura Zapparoli, Marika Mariano, and Eraldo Paulesu. How the motor system copes with aging: a quantitative meta-analysis of the effect of aging on motor function control. *Communications Biology*, 5(1):79, January 2022. ISSN 2399-3642. doi: 10.1038/s42003-022-03027-2. URL https://www.nature.com/articles/s42003-022-03027-2.

112 Rachel O Coats and John P Wann. The reliance on visual feedback control by older adults is highlighted in tasks requiring precise endpoint placement and precision grip. *Experimental brain research*, 214:139–150, 2011.

113 Ted K Turesky, Peter E Turkeltaub, and Guinevere F Eden. An activation likelihood estimation meta-analysis study of simple motor movements in older and young adults. *Frontiers in Aging Neuroscience*, 8:238, 2016.

114 S Hutchinson. Age-Related Differences in Movement Representation. *NeuroImage*, 17 (4):1720–1728, December 2002. ISSN 10538119. doi: 10.1006/nimg.2002.1309. URL https://linkinghub.elsevier.com/retrieve/pii/S1053811902913091.

115 V.S. Mattay, F. Fera, A. Tessitore, A.R. Hariri, S. Das, J.H. Callicott, and D.R. Weinberger. Neurophysiological correlates of age-related changes in human motor function. *Neurology*, 58(4):630–635, February 2002. ISSN 0028-3878, 1526-632X. doi: 10.1212/WNL.58.4.630. URL https://www.neurology.org/doi/10.1212/WNL.58.4.630.

116 James B. Rowe, Hartwig Siebner, Sasa R. Filipovic, Carla Cordivari, Willibald Gerschlager, John Rothwell, and Richard Frackowiak. Aging is associated with contrasting changes in local and distant cortical connectivity in the human motor system. *NeuroImage*, 32(2):747–760, August 2006. ISSN 10538119. doi: 10.1016/j.neuroimage.2006.03.061. URL https://linkinghub.elsevier.com/retrieve/pii/S1053811906002242.

117 Celine Maes, Jolien Gooijers, Jean-Jacques Orban de Xivry, Stephan P Swinnen, and Matthieu P Boisgontier. Two hands, one brain, and aging. *Neuroscience & Biobehavioral Reviews*, 75:234–256, 2017.

118 M. E. Galganski, A. J. Fuglevand, and R. M. Enoka. Reduced control of motor output in a human hand muscle of elderly subjects during submaximal contractions. *Journal of Neurophysiology*, 69(6):2108–2115, June 1993. ISSN 0022-3077, 1522-1598. doi: 10.1152/jn.1993.69.6.2108. URL https://www.physiology.org/doi/10.1152/jn.1993.69.6.2108.

119 Nick S. Ward, Orlando B.C. Swayne, and Jennifer M. Newton. Age-dependent changes in the neural correlates of force modulation: An fMRI study. *Neurobiology of Aging*, 29(9):1434–1446, September 2008. ISSN 01974580. doi: 10.1016/j.neurobiolaging.2007.04.017. URL https://linkinghub.elsevier.com/retrieve/pii/S0197458007001911.

120 Igor D. Grachev and A. Vania Apkarian. Aging alters regional multichemical profile of the human brain: an *in vivo* ^{1} H-MRS study of young versus middle-aged subjects. *Journal of Neurochemistry*, 76(2):582–593, January 2001. ISSN 00223042, 14714159. doi: 10.1046/j.1471-4159.2001.00026.x. URL http://doi.wiley.com/10.1046/j.1471-4159.2001.00026.x.

121 Madhavi Pandya, Thulani H. Palpagama, Clinton Turner, Henry J. Waldvogel, Richard L. Faull, and Andrea Kwakowsky. Sex- and age-related changes in GABA signaling components in the human cortex. *Biology of Sex Differences*, 10(1):5, December 2019. ISSN 2042-6410. doi: 10.1186/s13293-018-0214-6. URL https://bsd.biomedcentral.com/articles/10.1186/s13293-018-0214-6.

122 L.L. Ling, L.F. Hughes, and D.M. Caspary. Age-related loss of the GABA synthetic enzyme glutamic acid decarboxylase in rat primary auditory cortex. *Neuroscience*, 132(4):1103–1113, January 2005. ISSN 03064522. doi: 10.1016/j.neuroscience.2004.12.043. URL https://linkinghub.elsevier.com/retrieve/pii/S0306452205000643.

123 Donald M Caspary, Larry F Hughes, and Lynne L Ling. Age-related gabaa receptor changes in rat auditory cortex. *Neurobiology of aging*, 34(5):1486–1496, 2013.

124 D.M Caspary, T.M Holder, L.F Hughes, J.C Milbrandt, R.M McKernan, and D.K Naritoku. Age-related changes in GABAA receptor subunit composition and function in rat auditory system. *Neuroscience*, 93(1):307–312, June 1999. ISSN 03064522. doi: 10.1016/S0306-4522(99)00121-9. URL https://linkinghub.elsevier.com/retrieve/pii/S0306452299001219.

125 Emily M Stanley, Jim R Fadel, and David D Mott. Interneuron loss reduces dendritic inhibition and gaba release in hippocampus of aged rats. *Neurobiology of aging*, 33(2):431–e1, 2012.

126 Tianmiao Hua, Chuanchao Kao, Qingyan Sun, Xiangrui Li, and Yifeng Zhou. Decreased proportion of gaba neurons accompanies age-related degradation of neuronal function in cat striate cortex. *Brain research bulletin*, 75(1):119–125, 2008.

127 Xuanzi He, Bang-Bon Koo, and Ronald J Killiany. Edited magnetic resonance spectroscopy detects an age-related decline in nonhuman primate brain gaba levels. *BioMed research international*, 2016(1):6523909, 2016.

128 Celine Maes, Lize Hermans, Lisa Pauwels, Sima Chalavi, Inge Leunissen, Oron Levin, Koen Cuypers, Ronald Peeters, Stefan Sunaert, Dante Mantini, Nicolaas A. J. Puts, Richard A. E. Edden, and Stephan P. Swinnen. Age-related differences in GABA levels are driven by bulk tissue changes. *Human Brain Mapping*, 39(9):3652–3662, September 2018. ISSN 1065-9471, 1097-0193. doi: 10.1002/hbm.24201. URL `https://onlinelibrary.wiley.com/doi/10.1002/hbm.24201`.

129 Eric C Porges, Adam J Woods, Damon G Lamb, John B Williamson, Ronald A Cohen, Richard AE Edden, and Ashley D Harris. Impact of tissue correction strategy on gaba-edited mrs findings. *Neuroimage*, 162:249–256, 2017.

130 E Aufhaus, W Weber-Fahr, M Sack, N Tunc-Skarka, G Oberthuer, M Hoerst, A Meyer-Lindenberg, U Boettcher, and G Ende. Absence of changes in gaba concentrations with age and gender in the human anterior cingulate cortex: a mega-press study with symmetric editing pulse frequencies for macromolecule suppression. *Magnetic resonance in medicine*, 69(2):317–320, 2013.

131 Mark D. Zuppichini, Abbey M. Hamlin, Quan Zhou, Esther Kim, Shreya Rajagopal, Adriene M. Beltz, and Thad A. Polk. GABA levels decline with age: A longitudinal study. *Imaging Neuroscience*, 2:1–15, July 2024. ISSN 2837-6056. doi: 10.1162/imag_a_00224. URL `https://direct.mit.edu/imag/article/doi/10.1162/imag_a_00224/123270/GABA-levels-decline-with-age-A-longitudinal-study`.

132 Marisa McGinley, Richard L. Hoffman, David W. Russ, James S. Thomas, and Brian C. Clark. Older adults exhibit more intracortical inhibition and less intracortical facilitation than young adults. *Experimental Gerontology*, 45(9):671–678, September 2010. ISSN 05315565. doi: 10.1016/j.exger.2010.04.005. URL `https://linkinghub.elsevier.com/retrieve/pii/S0531556510001518`.

133 Martin V. Sale, Andrew P. Lavender, George M. Opie, Michael A. Nordstrom, and John G. Semmler. Increased intracortical inhibition in elderly adults with anterior–posterior current flow: A TMS study. *Clinical Neurophysiology*, 127(1):635–640, January 2016. ISSN 13882457. doi: 10.1016/j.clinph.2015.04.062. URL `https://linkinghub.elsevier.com/retrieve/pii/S1388245715003016`.

134 Apoorva Bhandari, Natasha Radhu, Faranak Farzan, Benoit H. Mulsant, Tarek K. Rajji, Zafiris J. Daskalakis, and Daniel M. Blumberger. A meta-analysis of the effects of aging on motor cortex neurophysiology assessed by transcranial magnetic stimulation. *Clinical Neurophysiology*, 127(8):2834–2845, August 2016. ISSN 13882457. doi: 10.1016/j.clinph.2016.05.363. URL https://linkinghub.elsevier.com/retrieve/pii/S1388245716304266.

135 Lize Hermans, Oron Levin, Celine Maes, Peter Van Ruitenbeek, Kirstin-Friederike Heise, Richard A.E. Edden, Nicolaas A.J. Puts, Ronald Peeters, Bradley R. King, Raf L.J. Meesen, Inge Leunissen, Stephan P. Swinnen, and Koen Cuypers. GABA levels and measures of intracortical and interhemispheric excitability in healthy young and older adults: an MRS-TMS study. *Neurobiology of Aging*, 65:168–177, May 2018. ISSN 01974580. doi: 10.1016/j.neurobiolaging.2018.01.023. URL https://linkinghub.elsevier.com/retrieve/pii/S0197458018300381.

136 Yves-Alain Kuhn, Sven Egger, Matteo Bugnon, Nico Lehmann, Marco Taubert, and Wolfgang Taube. Age-related decline in GABAergic intracortical inhibition can be counteracted by long-term learning of balance skills. *The Journal of Physiology*, 602(15):3737–3753, August 2024. ISSN 0022-3751, 1469-7793. doi: 10.1113/JP285706. URL https://physoc.onlinelibrary.wiley.com/doi/10.1113/JP285706.

137 Nicolas Coquelet, Vincent Wens, Alison Mary, Maxime Niesen, Delphine Puttaert, Mariagrazia Ranzini, Marc Vander Ghinst, Mathieu Bourguignon, Philippe Peigneux, Serge Goldman, et al. Changes in electrophysiological static and dynamic human brain functional architecture from childhood to late adulthood. *Scientific Reports*, 10(1):18986, 2020.

138 Carlos Gómez, Jose M Perez-Macias, Jesús Poza, Alberto Fernández, and Roberto Hornero. Spectral changes in spontaneous meg activity across the lifespan. *Journal of neural engineering*, 10(6):066006, 2013.

139 Maggie P Rempe, Lauren R Ott, Giorgia Picci, Samantha H Penhale, Nicholas J Christopher-Hayes, Brandon J Lew, Nathan M Petro, Christine M Embury, Mikki Schantell, Hallie J Johnson, et al. Spontaneous cortical dynamics from the first years to the golden years. *Proceedings of the National Academy of Sciences*, 120(4):e2212776120, 2023.

140 Elizabeth Heinrichs-Graham and Tony W. Wilson. Is an absolute level of cortical beta suppression required for proper movement? Magnetoencephalographic evidence from healthy aging. *NeuroImage*, 134:514–521, July 2016. ISSN 10538119. doi: 10.1016/j.neuroimage.2016.04.032. URL https://linkinghub.elsevier.com/retrieve/pii/S1053811916300726.

141 Christina Stier, Christoph Braun, and Niels K. Focke. Adult lifespan trajectories of neuromagnetic signals and interrelations with cortical thickness. *NeuroImage*, 278: 120275, September 2023. ISSN 10538119. doi: 10.1016/j.neuroimage.2023.120275. URL https://linkinghub.elsevier.com/retrieve/pii/S1053811923004263.

142 Holly E. Rossiter, Emma M. Davis, Ella V. Clark, Marie-Hélène Boudrias, and Nick S. Ward. Beta oscillations reflect changes in motor cortex inhibition in healthy ageing. *NeuroImage*, 91:360–365, May 2014. ISSN 10538119. doi: 10.1016/j.neuroimage.2014.01.012. URL https://linkinghub.elsevier.com/retrieve/pii/S1053811914000238.

143 Yang Hu, Steven J Petruzzello, and Manuel E Hernandez. Beta cortical oscillatory activities and their relationship to postural control in a standing balance demanding test: influence of aging. *Frontiers in aging neuroscience*, 15:1126002, 2023.

144 E Labyt, W Szurhaj, J.-L Bourriez, F Cassim, L Defebvre, A Destée, J.-D Guieu, and Ph Derambure. Changes in oscillatory cortical activity related to a visuomotor task in young and elderly healthy subjects. *Clinical Neurophysiology*, 114(6): 1153–1166, June 2003. ISSN 13882457. doi: 10.1016/S1388-2457(03)00058-0. URL https://linkinghub.elsevier.com/retrieve/pii/S1388245703000580.

145 Timothy Bardouille and Lyam Bailey. Evidence for age-related changes in sensorimotor neuromagnetic responses during cued button pressing in a large open-access dataset. *NeuroImage*, 193:25–34, June 2019. ISSN 10538119. doi: 10.1016/j.neuroimage.2019.02.065. URL https://linkinghub.elsevier.com/retrieve/pii/S1053811919301612.

146 Christina Schmiedt-Fehr, Birgit Mathes, Shwetha Kedilaya, Janna Krauss, and Canan Basar-Eroglu. Aging differentially affects alpha and beta sensorimotor rhythms in a go/nogo task. *Clinical Neurophysiology*, 127(10):3234–3242, 2016.

147 Etienne Sallard, Jessica Tallet, Gregor Thut, Marie-Pierre Deiber, and Jérôme Barral. Age-related changes in post-movement beta synchronization during a selective inhibition task. *Experimental brain research*, 234:3543–3553, 2016.

148 Svenja Espenhahn, Bernadette C.M. Van Wijk, Holly E. Rossiter, Archy O. De Berker, Nell D. Redman, Jane Rondina, Joern Diedrichsen, and Nick S. Ward. Cortical beta oscillations are associated with motor performance following visuomotor learning. *NeuroImage*, 195:340–353, July 2019. ISSN 10538119. doi: 10.1016/j.neuroimage.2019.03.079. URL https://linkinghub.elsevier.com/retrieve/pii/S1053811919302861.

149 Elizabeth Heinrichs-Graham, Timothy J. McDermott, Mackenzie S. Mills, Alex I. Wiesman, Yu-Ping Wang, Julia M. Stephen, Vince D. Calhoun, and Tony W. Wilson. The lifespan trajectory of neural oscillatory activity in the motor system. *Developmental Cognitive Neuroscience*, 30:159–168, April 2018. ISSN 18789293. doi: 10.1016/j.dcn.2018.02.013. URL https://linkinghub.elsevier.com/retrieve/pii/S1878929317302426.

150 Antonino Vallesi, Anthony R. McIntosh, Natasa Kovacevic, Sam C.C. Chan, and Donald T. Stuss. Age effects on the asymmetry of the motor system: Evidence from cortical oscillatory activity. *Biological Psychology*, 85(2):213–218, October 2010. ISSN 03010511. doi: 10.1016/j.biopsycho.2010.07.003. URL https://linkinghub.elsevier.com/retrieve/pii/S0301051110001845.

151 Brendan Brady, Lindsey Power, and Timothy Bardouille. Age-related trends in neuromagnetic transient beta burst characteristics during a sensorimotor task and rest in the Cam-CAN open-access dataset. *NeuroImage*, 222:117245, November 2020. ISSN 10538119. doi: 10.1016/j.neuroimage.2020.117245. URL https://linkinghub.elsevier.com/retrieve/pii/S105381192030731X.

152 Lindsey Power and Timothy Bardouille. Age-related trends in the cortical sources of transient beta bursts during a sensorimotor task and rest. *NeuroImage*, 245:118670, December 2021. ISSN 10538119. doi: 10.1016/j.neuroimage.2021.118670. URL https://linkinghub.elsevier.com/retrieve/pii/S1053811921009435.

153 William Gaetz, Timothy P.L. Roberts, Krish D. Singh, and Suresh D. Muthukumaraswamy. Functional and structural correlates of the aging brain: Relating visual cortex (V1) gamma band responses to age-related structural change. *Human Brain Mapping*, 33(9):2035–2046, September 2012. ISSN 1065-9471, 1097-0193. doi: 10.1002/hbm.21339. URL https://onlinelibrary.wiley.com/doi/10.1002/hbm.21339.

154 Suresh D. Muthukumaraswamy, Krish D. Singh, Jennifer B. Swettenham, and Derek K. Jones. Visual gamma oscillations and evoked responses: Variability, repeatability and structural MRI correlates. *NeuroImage*, 49(4):3349–3357, February 2010. ISSN 10538119. doi: 10.1016/j.neuroimage.2009.11.045. URL https://linkinghub.elsevier.com/retrieve/pii/S1053811909012300.

155 Stan Van Pelt, Elena Shumskaya, and Pascal Fries. Cortical volume and sex influence visual gamma. *NeuroImage*, 178:702–712, September 2018. ISSN 10538119. doi: 10.1016/j.neuroimage.2018.06.005. URL https://linkinghub.elsevier.com/retrieve/pii/S1053811918305123.

156 Dinavahi V.P.S. Murty, Keerthana Manikandan, Wupadrasta Santosh Kumar, Ranjini Garani Ramesh, Simran Purokayastha, Mahendra Javali, Naren Prahalada Rao, and Supratim Ray. Gamma oscillations weaken with age in healthy elderly in human EEG. *NeuroImage*, 215:116826, July 2020. ISSN 10538119. doi: 10.1016/j.neuroimage.2020.116826. URL https://linkinghub.elsevier.com/retrieve/pii/S105381192030313X.

157 A.T. Barker, R. Jalinous, and I.L. Freeston. NON-INVASIVE MAGNETIC STIMULATION OF HUMAN MOTOR CORTEX. *The Lancet*, 325(8437):1106–1107, 1985.

ISSN 0140-6736. doi: https://doi.org/10.1016/S0140-6736(85)92413-4. URL https://www.sciencedirect.com/science/article/pii/S0140673685924134.

158 Nigel C. Rogasch, Zafiris J. Daskalakis, and Paul B. Fitzgerald. Cortical Inhibition, Excitation, and Connectivity in Schizophrenia: A Review of Insights From Transcranial Magnetic Stimulation. *Schizophrenia Bulletin*, 40(3):685–696, May 2014. ISSN 1745-1701, 0586-7614. doi: 10.1093/schbul/sbt078. URL https://academic.oup.com/schizophreniabulletin/article-lookup/doi/10.1093/schbul/sbt078.

159 Ulf Ziemann. TMS and drugs. *Clinical Neurophysiology*, 115(8):1717–1729, August 2004. ISSN 13882457. doi: 10.1016/j.clinph.2004.03.006. URL https://linkinghub.elsevier.com/retrieve/pii/S1388245704001038.

160 Mark Hallett. Transcranial Magnetic Stimulation: A Primer. *Neuron*, 55(2):187–199, July 2007. ISSN 08966273. doi: 10.1016/j.neuron.2007.06.026. URL https://linkinghub.elsevier.com/retrieve/pii/S0896627307004606.

161 F Andrew Kozel, Ziad Nahas, Cart deBrux, Monica Molloy, Jeffrey P Lorberbaum, Daryl Bohning, S Craig Risch, and Mark S George. How coil–cortex distance relates to age, motor threshold, and antidepressant response to repetitive transcranial magnetic stimulation. *The Journal of neuropsychiatry and clinical neurosciences*, 12(3):376–384, 2000.

162 Kathleen A McConnell, Ziad Nahas, Ananda Shastri, Jeffrey P Lorberbaum, F Andrew Kozel, Daryl E Bohning, and Mark S George. The transcranial magnetic stimulation motor threshold depends on the distance from coil to underlying cortex: a replication in healthy adults comparing two methods of assessing the distance to cortex. *Biological psychiatry*, 49(5):454–459, 2001.

163 H. Devanne, B. A. Lavoie, and C. Capaday. Input-output properties and gain changes in the human corticospinal pathway:. *Experimental Brain Research*, 114(2):329–338, April 1997. ISSN 0014-4819. doi: 10.1007/PL00005641. URL http://link.springer.com/10.1007/PL00005641.

164 P.M. Rossini, D. Burke, R. Chen, L.G. Cohen, Z. Daskalakis, R. Di Iorio, V. Di Lazzaro, F. Ferreri, P.B. Fitzgerald, M.S. George, M. Hallett, J.P. Lefaucheur, B. Langguth, H. Matsumoto, C. Miniussi, M.A. Nitsche, A. Pascual-Leone, W. Paulus, S. Rossi, J.C. Rothwell, H.R. Siebner, Y. Ugawa, V. Walsh, and U. Ziemann. Non-invasive electrical and magnetic stimulation of the brain, spinal cord, roots and peripheral nerves: Basic principles and procedures for routine clinical and research application. An updated report from an I.F.C.N. Committee. *Clinical Neurophysiology*, 126(6):1071–1107, June 2015. ISSN 13882457. doi: 10.1016/j.clinph.2015.02.001. URL https://linkinghub.elsevier.com/retrieve/pii/S1388245715000711.

165 Katherine Dyke, Sophia E. Pépés, Chen Chen, Soyoung Kim, Hilmar P. Sigurdsson, Amelia Draper, Masud Husain, Parashkev Nachev, Penelope A. Gowland, Peter G. Morris, and Stephen R. Jackson. Comparing GABA-dependent physiological measures of inhibition with proton magnetic resonance spectroscopy measurement of GABA using ultra-high-field MRI. *NeuroImage*, 152:360–370, May 2017. ISSN 10538119. doi: 10.1016/j.neuroimage.2017.03.011. URL https://linkinghub.elsevier.com/retrieve/pii/S1053811917302197.

166 B Boroojerdi, F Battaglia, W Muellbacher, and L G Cohen. Mechanisms influencing stimulus-response properties of the human corticospinal system. *Clinical Neurophysiology*, 112:931–937, 2001.

167 James Mathew, Angelika Kübler, Robert Bauer, and Alireza Gharabaghi. Probing Corticospinal Recruitment Patterns and Functional Synergies with Transcranial Magnetic Stimulation. *Frontiers in Cellular Neuroscience*, 10, July 2016. ISSN 1662-5102. doi: 10.3389/fncel.2016.00175. URL http://journal.frontiersin.org/Article/10.3389/fncel.2016.00175/abstract.

168 Sahana N. Kukke, Rainer W. Paine, Chi-Chao Chao, Ana C. de Campos, and Mark Hallett. Efficient and Reliable Characterization of the Corticospinal System Using Transcranial Magnetic Stimulation. *Journal of Clinical Neurophysiology*, 31(3):246–252, June 2014. ISSN 0736-0258. doi: 10.1097/WNP.0000000000000057. URL https://journals.lww.com/00004691-201406000-00012.

169 Nezha Kouchtir-Devanne, Charles Capaday, François Cassim, Philippe Derambure, and Hervé Devanne. Task-dependent changes of motor cortical network excitability during precision grip compared to isolated finger contraction. *Journal of Neurophysiology*, 107(5):1522–1529, March 2012. ISSN 0022-3077, 1522-1598. doi: 10.1152/jn.00786.2011. URL https://www.physiology.org/doi/10.1152/jn.00786.2011.

170 Makoto Suzuki, Hikari Kirimoto, Hideaki Onishi, Sumio Yamada, Hiroyuki Tamaki, Atsuo Maruyama, and Jun-ichi Yamamoto. Reciprocal changes in input–output curves of motor evoked potentials while learning motor skills. *Brain Research*, 1473:114–123, September 2012. ISSN 00068993. doi: 10.1016/j.brainres.2012.07.043. URL https://linkinghub.elsevier.com/retrieve/pii/S0006899312012322.

171 E Houdayer, A Degardin, F Cassim, P Bocquillon, P Derambure, and H Devanne. The effects of low-and high-frequency repetitive tms on the input/output properties of the human corticospinal pathway. *Experimental brain research*, 187:207–217, 2008.

172 C. M. Buetefisch, K. P. Revill, M. W. Haut, G. M. Kowalski, M. Wischnewski, M. Pifer, S. R. Belagaje, F. Nahab, D. J. Cobia, X. Hu, D. Drake, and G. Hobbs. Abnormally reduced primary motor cortex output is related to impaired hand function in chronic

stroke. *Journal of Neurophysiology*, 120(4):1680–1694, October 2018. ISSN 0022-3077, 1522-1598. doi: 10.1152/jn.00715.2017. URL https://www.physiology.org/doi/10.1152/jn.00715.2017.

173 Påvel G. Lindberg, Pernille H. B. Skejø, Elisabeth Rounis, Zoltan Nagy, Christina Schmitz, Helena Wernegren, Annika Bring, Margareta Engardt, Hans Forssberg, and Jörgen Borg. Wallerian Degeneration of the Corticofugal Tracts in Chronic Stroke: A Pilot Study Relating Diffusion Tensor Imaging, Transcranial Magnetic Stimulation, and Hand Function. *Neurorehabilitation and Neural Repair*, 21(6):551–560, November 2007. ISSN 1545-9683, 1552-6844. doi: 10.1177/1545968307301886. URL http://journals.sagepub.com/doi/10.1177/1545968307301886.

174 Steve Vucic, Garth A. Nicholson, and Matthew C. Kiernan. Cortical hyperexcitability may precede the onset of familial amyotrophic lateral sclerosis. *Brain*, 131(6):1540–1550, June 2008. ISSN 1460-2156, 0006-8950. doi: 10.1093/brain/awn071. URL https://academic.oup.com/brain/article-lookup/doi/10.1093/brain/awn071.

175 Peter H. Gorman and J. Thomas Mortimer. The Effect of Stimulus Parameters on the Recruitment Characteristics of Direct Nerve Stimulation. *IEEE Transactions on Biomedical Engineering*, BME-30(7):407–414, July 1983. ISSN 0018-9294, 1558-2531. doi: 10.1109/TBME.1983.325041. URL http://ieeexplore.ieee.org/document/4121663/.

176 Angel V. Peterchev, Stefan M. Goetz, Gregory G. Westin, Bruce Luber, and Sarah H. Lisanby. Pulse width dependence of motor threshold and input–output curve characterized with controllable pulse parameter transcranial magnetic stimulation. *Clinical Neurophysiology*, 124(7):1364–1372, July 2013. ISSN 13882457. doi: 10.1016/j.clinph.2013.01.011. URL https://linkinghub.elsevier.com/retrieve/pii/S1388245713000527.

177 Crystal L. Massie and Matthew P. Malcolm. Considerations for Stimulus–Response Curves in Stroke: An Investigation Comparing Collection and Analysis Methods. *International Journal of Neuroscience*, 123(3):175–183, January 2013. ISSN 0020-7454, 1543-5245. doi: 10.3109/00207454.2012.738734. URL http://www.tandfonline.com/doi/full/10.3109/00207454.2012.738734.

178 Kevin D'Ostilio, Stefan M. Goetz, Ricci Hannah, Matteo Ciocca, Raffaella Chieffo, Jui-Cheng A. Chen, Angel V. Peterchev, and John C. Rothwell. Effect of coil orientation on strength–duration time constant and I-wave activation with controllable pulse parameter transcranial magnetic stimulation. *Clinical Neurophysiology*, 127(1):675–683, January 2016. ISSN 13882457. doi: 10.1016/j.clinph.2015.05.017. URL https://linkinghub.elsevier.com/retrieve/pii/S1388245715006124.

179 Jacinta O'Shea, Heidi Johansen-Berg, Danielle Trief, Silke Göbel, and Matthew F.S. Rushworth. Functionally Specific Reorganization in Human Premotor Cortex. *Neuron*,

54(3):479–490, May 2007. ISSN 08966273. doi: 10.1016/j.neuron.2007.04.021. URL https://linkinghub.elsevier.com/retrieve/pii/S0896627307003005.

180 S T Grafton, A H Fagg, and M A Arbib. Dorsal Premotor Cortex and Conditional Movement Selection: A PET Functional Mapping Study. *Journal of Neurophysiology*, 79(2):1092–1097, January 1998. doi: 10.1152/jn.1998.79.2.1092.

181 Matthew F.S. Rushworth, Philip D. Nixon, Derick T. Wade, Shelley Renowden, and Richard E. Passingham. The left hemisphere and the selection of learned actions. *Neuropsychologia*, 36(1):11–24, January 1998. ISSN 00283932. doi: 10.1016/S0028-3932(97)00101-2. URL https://linkinghub.elsevier.com/retrieve/pii/S0028393297001012.

182 N. Schluter. Temporary interference in human lateral premotor cortex suggests dominance for the selection of movements. A study using transcranial magnetic stimulation. *Brain*, 121(5):785–799, May 1998. ISSN 14602156. doi: 10.1093/brain/121.5.785. URL https://academic.oup.com/brain/article-lookup/doi/10.1093/brain/121.5.785.

183 Heidi Johansen-Berg, Matthew F. S. Rushworth, Marko D. Bogdanovic, Udo Kischka, Sunil Wimalaratna, and Paul M. Matthews. The role of ipsilateral premotor cortex in hand movement after stroke. *Proceedings of the National Academy of Sciences*, 99(22):14518–14523, October 2002. ISSN 0027-8424, 1091-6490. doi: 10.1073/pnas.222536799. URL https://pnas.org/doi/full/10.1073/pnas.222536799.

184 Ainslie Johnstone, Ioana Grigoras, Pierre Petitet, Liliana P. Capitão, and Charlotte J. Stagg. A single, clinically relevant dose of the GABA $_{\text{b}}$ agonist baclofen impairs visuomotor learning. *The Journal of Physiology*, 599(1):307–322, January 2021. ISSN 0022-3751, 1469-7793. doi: 10.1113/JP280378. URL https://onlinelibrary.wiley.com/doi/10.1113/JP280378.

185 Edwin M. Robertson, Alvaro Pascual-Leone, and Daniel Z. Press. Awareness Modifies the Skill-Learning Benefits of Sleep. *Current Biology*, 14(3):208–212, February 2004. ISSN 09609822. doi: 10.1016/j.cub.2004.01.027. URL https://linkinghub.elsevier.com/retrieve/pii/S0960982204000399.

186 Christian Gerloff, Brian Corwell, Robert Chen, Mark Hallett, and Leonardo G. Cohen. Stimulation over the human supplementary motor area interferes with the organization of future elements in complex motor sequences. *Brain*, 120(9):1587–1602, September 1997. ISSN 14602156. doi: 10.1093/brain/120.9.1587. URL https://academic.oup.com/brain/article-lookup/doi/10.1093/brain/120.9.1587.

187 Charlotte J. Stagg, Velicia Bachtiar, and Heidi Johansen-Berg. The Role of GABA in Human Motor Learning. *Current Biology*, 21(6):480–484, March 2011. ISSN 09609822.

doi: 10.1016/j.cub.2011.01.069. URL https://linkinghub.elsevier.com/retrieve/pii/S0960982211001254.

188 Sylvain Baillet. Magnetoencephalography for brain electrophysiology and imaging. *Nature Neuroscience*, 20(3):327–339, March 2017. ISSN 1097-6256, 1546-1726. doi: 10.1038/nn.4504. URL https://www.nature.com/articles/nn.4504.

189 Matti Hämäläinen, Riitta Hari, Risto J. Ilmoniemi, Jukka Knuutila, and Olli V. Lounasmaa. Magnetoencephalography—theory, instrumentation, and applications to noninvasive studies of the working human brain. *Reviews of Modern Physics*, 65(2):413–497, April 1993. ISSN 0034-6861, 1539-0756. doi: 10.1103/RevModPhys.65.413. URL https://link.aps.org/doi/10.1103/RevModPhys.65.413.

190 A. Hillebrand and G.R. Barnes. A Quantitative Assessment of the Sensitivity of Whole-Head MEG to Activity in the Adult Human Cortex. *NeuroImage*, 16(3):638–650, July 2002. ISSN 10538119. doi: 10.1006/nimg.2002.1102. URL https://linkinghub.elsevier.com/retrieve/pii/S105381190291102X.

191 Krish D. Singh, Gareth R. Barnes, Arjan Hillebrand, Emer M.E. Forde, and Adrian L. Williams. Task-Related Changes in Cortical Synchronization Are Spatially Coincident with the Hemodynamic Response. *NeuroImage*, 16(1):103–114, May 2002. ISSN 10538119. doi: 10.1006/nimg.2001.1050. URL https://linkinghub.elsevier.com/retrieve/pii/S105381190191050X.

192 Matthew J. Brookes, Andrew M. Gibson, Stephen D. Hall, Paul L. Furlong, Gareth R. Barnes, Arjan Hillebrand, Krish D. Singh, Ian E. Holliday, Sue T. Francis, and Peter G. Morris. GLM-beamformer method demonstrates stationary field, alpha ERD and gamma ERS co-localisation with fMRI BOLD response in visual cortex. *NeuroImage*, 26(1):302–308, May 2005. ISSN 10538119. doi: 10.1016/j.neuroimage.2005.01.050. URL https://linkinghub.elsevier.com/retrieve/pii/S1053811905000376.

193 David Cohen. Magnetoencephalography: evidence of magnetic fields produced by alpha-rhythm currents. *Science*, 161(3843):784–786, 1968.

194 Pilar Garcés, David López-Sanz, Fernando Maestú, and Ernesto Pereda. Choice of Magnetometers and Gradiometers after Signal Space Separation. *Sensors*, 17(12):2926, December 2017. ISSN 1424-8220. doi: 10.3390/s17122926. URL https://www.mdpi.com/1424-8220/17/12/2926.

195 Peter Hansen, Morten Kringelbach, and Riitta Salmelin. *MEG: An introduction to methods*. Oxford university press, 2010.

196 Marion Brickwedde, Paul Anders, Andrea A Kühn, Roxanne Lofredi, Martin Holtkamp, Angela M Kaindl, Tineke Grent-'t Jong, Peter Krüger, Tilmann Sander, and Peter J

Uhlhaas. Applications of opm-meg for translational neuroscience: a perspective. *Translational Psychiatry*, 14(1):341, 2024.

197 Joachim Gross, Sylvain Baillet, Gareth R. Barnes, Richard N. Henson, Arjan Hillebrand, Ole Jensen, Karim Jerbi, Vladimir Litvak, Burkhard Maess, Robert Oostenveld, Lauri Parkkonen, Jason R. Taylor, Virginie Van Wassenhove, Michael Wibral, and Jan-Mathijs Schoffelen. Good practice for conducting and reporting MEG research. *NeuroImage*, 65: 349–363, January 2013. ISSN 10538119. doi: 10.1016/j.neuroimage.2012.10.001. URL https://linkinghub.elsevier.com/retrieve/pii/S1053811912009895.

198 Natalie Schaworonkow and Vadim V Nikulin. Is sensor space analysis good enough? spatial patterns as a tool for assessing spatial mixing of eeg/meg rhythms. *NeuroImage*, 253:119093, 2022.

199 Jan-Mathijs Schoffelen and Joachim Gross. Source connectivity analysis with MEG and EEG. *Human Brain Mapping*, 30(6):1857–1865, June 2009. ISSN 1065-9471, 1097-0193. doi: 10.1002/hbm.20745. URL https://onlinelibrary.wiley.com/doi/10.1002/hbm.20745.

200 SanjayP Singh. Magnetoencephalography: Basic principles. *Annals of Indian Academy of Neurology*, 17(5):107, 2014. ISSN 0972-2327. doi: 10.4103/0972-2327.128676. URL https://journals.lww.com/10.4103/0972-2327.128676.

201 S. Baillet, J.C. Mosher, and R.M. Leahy. Electromagnetic brain mapping. *IEEE Signal Processing Magazine*, 18(6):14–30, November 2001. ISSN 10535888. doi: 10.1109/79.962275. URL http://ieeexplore.ieee.org/document/962275/.

202 Ana-Sofía Hincapié, Jan Kujala, Jérémie Mattout, Annalisa Pascarella, Sebastien Daligault, Claude Delpuech, Domingo Mery, Diego Cosmelli, and Karim Jerbi. The impact of MEG source reconstruction method on source-space connectivity estimation: A comparison between minimum-norm solution and beamforming. *NeuroImage*, 156: 29–42, August 2017. ISSN 10538119. doi: 10.1016/j.neuroimage.2017.04.038. URL https://linkinghub.elsevier.com/retrieve/pii/S1053811917303312.

203 Andrew J. Quinn, Diego Vidaurre, Romesh Abeysuriya, Robert Becker, Anna C. Nobre, and Mark W. Woolrich. Task-Evoked Dynamic Network Analysis Through Hidden Markov Modeling. *Frontiers in Neuroscience*, 12:603, August 2018. ISSN 1662-453X. doi: 10.3389/fnins.2018.00603. URL https://www.frontiersin.org/article/10.3389/fnins.2018.00603/full.

204 E Kucukaltun-Yildirim, Dimitrios Pantazis, and Richard M Leahy. Task-based comparison of inverse methods in magnetoencephalography. *IEEE Transactions on Biomedical Engineering*, 53(9):1783–1793, 2006.

205 André Mouraux and Gian Domenico Iannetti. Across-trial averaging of event-related eeg responses and beyond. *Magnetic resonance imaging*, 26(7):1041–1054, 2008.

206 Andreas Bruns. Fourier-, hilbert-and wavelet-based signal analysis: are they really different approaches? *Journal of neuroscience methods*, 137(2):321–332, 2004.

207 Partha P Mitra and Bijan Pesaran. Analysis of dynamic brain imaging data. *Biophysical journal*, 76(2):691–708, 1999.

208 Hugh L Fletcher and G Ivor Hickey. *Genetics*. Garland Science, 2013.

209 S Giampaoli, G Chillemi, F Valeriani, D Lazzaro, Marina Borro, Giovanna Gentile, Maurizio Simmaco, G Zanni, A Berti, and V Romano Spica. The snps in the human genetic blueprint era. *New biotechnology*, 30(5):475–484, 2013.

210 1000 Genomes Project Consortium et al. A global reference for human genetic variation. *Nature*, 526(7571):68, 2015.

211 Barkur S Shastry. Snps: impact on gene function and phenotype. *Single nucleotide polymorphisms: methods and protocols*, pages 3–22, 2009.

212 Robert B Jenkins, Yuanyuan Xiao, Hugues Sicotte, Paul A Decker, Thomas M Kollmeyer, Helen M Hansen, Matthew L Kosel, Shichun Zheng, Kyle M Walsh, Terri Rice, et al. A low-frequency variant at 8q24. 21 is strongly associated with risk of oligodendroglial tumors and astrocytomas with idh1 or idh2 mutation. *Nature genetics*, 44 (10):1122–1125, 2012.

213 Gilles Thomas, Kevin B Jacobs, Peter Kraft, Meredith Yeager, Sholom Wacholder, David G Cox, Susan E Hankinson, Amy Hutchinson, Zhaoming Wang, Kai Yu, et al. A multistage genome-wide association study in breast cancer identifies two new risk alleles at 1p11. 2 and 14q24. 1 (rad51l1). *Nature genetics*, 41(5):579–584, 2009.

214 Denise D Correa, Jaya Satagopan, Raymond E Baser, Kenneth Cheung, Elizabeth Richards, Michael Lin, Sasan Karimi, John Lyo, Lisa M DeAngelis, and Irene Orlow. Apoe polymorphisms and cognitive functions in patients with brain tumors. *Neurology*, 83(4):320–327, 2014.

215 Bernie Devlin, John R Kelsoe, Pamela Sklar, Mark J Daly, Michael C O'Donovan, Nicholas Craddock, Patrick F Sullivan, Jordan W Smoller, Kenneth S Kendler, et al. Genetic relationship between five psychiatric disorders estimated from genome-wide snps. *Nature genetics*, 45(9):984–994, 2013.

216 Stan van Pelt, Boomsma Dorret I, and Pascal Fries. Magnetoencephalography in twins reveals a strong genetic determination of the peak frequency of visually induced gamma-band synchronization. *Journal of Neuroscience*, 32(10):3388–3392, 2012. doi: 10.1523/JNEUROSCI.5592-11.2012.

217 John M Astle, Levi S Simpson, Yong Huang, M Muralidhar Reddy, Rosemary Wilson, Steven Connell, Johnnie Wilson, and Thomas Kodadek. Seamless bead to microarray screening: rapid identification of the highest affinity protein ligands from large combinatorial libraries. *Chemistry & biology*, 17(1):38–45, 2010.

218 Inc. Illumina. Illumina bead-based microarray technology, . URL `https://emea.illumina.com/science/technology/microarray.html`.

219 Inc. Illumina. Illumina microarray, . URL `https://www.illumina.com/documents/products/datasheets/datasheet-human-omni-express-exome.pdf`.

220 Hartwig R. Siebner, Gesa Hartwigsen, Tanja Kassuba, and John C. Rothwell. How does transcranial magnetic stimulation modify neuronal activity in the brain? Implications for studies of cognition. *Cortex*, 45(9):1035–1042, October 2009. ISSN 00109452. doi: 10.1016/j.cortex.2009.02.007. URL `https://linkinghub.elsevier.com/retrieve/pii/S001094520900063X`.

221 P. J. Basser and B. J. Roth. Stimulation of a myelinated nerve axon by electromagnetic induction. *Medical & Biological Engineering & Computing*, 29(3):261–268, May 1991. ISSN 0140-0118, 1741-0444. doi: 10.1007/BF02446708. URL `http://link.springer.com/10.1007/BF02446708`.

222 Ilona Mogyoros, Cindy Lin, Shareef Dowla, Julian Grosskreutz, and David Burke. Strength–duration properties and their voltage dependence at different sites along the median nerve. *Clinical Neurophysiology*, 110(9):1618–1624, September 1999. ISSN 13882457. doi: 10.1016/S1388-2457(99)00087-5. URL `https://linkinghub.elsevier.com/retrieve/pii/S1388245799000875`.

223 D. Boërio, J.-Y. Hogrel, J.-P. Lefaucheur, F.C. Wang, A. Verschueren, J. Pouget, E. Carrera, and T. Kuntzer. Stimulus–response curve of human motor nerves: Multicenter assessment of various indexes. *Neurophysiologie Clinique/Clinical Neurophysiology*, 38 (1):31–38, February 2008. ISSN 09877053. doi: 10.1016/j.neucli.2007.09.007. URL `https://linkinghub.elsevier.com/retrieve/pii/S0987705307001268`.

224 A.V. Peterchev, R. Jalinous, and S.H. Lisanby. A Transcranial Magnetic Stimulator Inducing Near-Rectangular Pulses With Controllable Pulse Width (cTMS). *IEEE Transactions on Biomedical Engineering*, 55(1):257–266, January 2008. ISSN 0018-9294, 1558-2531. doi: 10.1109/TBME.2007.900540. URL `http://ieeexplore.ieee.org/document/4360051/`.

225 Angel V Peterchev, Kevin D Ostilio, John C Rothwell, and David L Murphy. Controllable pulse parameter transcranial magnetic stimulator with enhanced circuit topology and

pulse shaping. *Journal of Neural Engineering*, 11(5):056023, October 2014. ISSN 1741-2560, 1741-2552. doi: 10.1088/1741-2560/11/5/056023. URL https://iopscience.iop.org/article/10.1088/1741-2560/11/5/056023.

226 Angel V Peterchev, David L Murphy, and Sarah H Lisanby. Repetitive transcranial magnetic stimulator with controllable pulse parameters. *Journal of Neural Engineering*, 8 (3):036016, June 2011. ISSN 1741-2560, 1741-2552. doi: 10.1088/1741-2560/8/3/036016. URL https://iopscience.iop.org/article/10.1088/1741-2560/8/3/036016.

227 Matthew C. Kiernan and Cindy Shin Yi Lin. *Chapter 15 - nerve excitability: A clinical translation*, page 345–365. W.B. Saunders, London, sixth edition edition, 2012. ISBN 978-1-4557-0308-1. doi: https://doi.org/10.1016/B978-1-4557-0308-1.00015-7. URL https://www.sciencedirect.com/science/article/pii/B9781455703081000157. Citation Key: KIERNAN2012345.

228 Marcela Panizza, Jan Nilsson, Bradley J. Roth, Peter J. Basser, and Mark Hallett. Relevance of stimulus duration for activation of motor and sensory fibers: implications for the study of H-reflexes and magnetic stimulation. *Electroencephalography and Clinical Neurophysiology/Evoked Potentials Section*, 85(1):22–29, February 1992. ISSN 01685597. doi: 10.1016/0168-5597(92)90097-U. URL https://linkinghub.elsevier.com/retrieve/pii/016855979290097U.

229 J Rapp, P Braun, W Hemmert, and B Gleich. Optimal pulse configuration for peripheral inductive nerve stimulation. *Biomedical Physics & Engineering Express*, 8 (2):025020, March 2022. ISSN 2057-1976. doi: 10.1088/2057-1976/ac52d8. URL https://iopscience.iop.org/article/10.1088/2057-1976/ac52d8.

230 S.S. Nagarajan, D.M. Durand, and E.N. Warman. Effects of induced electric fields on finite neuronal structures: a simulation study. *IEEE Transactions on Biomedical Engineering*, 40(11):1175–1188, November 1993. ISSN 00189294. doi: 10.1109/10.245636. URL http://ieeexplore.ieee.org/document/245636/.

231 Ilona Mogyoros, Matthew C. Kiernan, and David Burke. Strength-duration properties of human peripheral nerve. *Brain*, 119(2):439–447, 1996. ISSN 0006-8950, 1460-2156. doi: 10.1093/brain/119.2.439. URL https://academic.oup.com/brain/article-lookup/doi/10.1093/brain/119.2.439.

232 H Bostock and J C Rothwell. Latent addition in motor and sensory fibres of human peripheral nerve. *The Journal of Physiology*, 498(1):277–294, January 1997. ISSN 00223751. doi: 10.1113/jphysiol.1997.sp021857. URL https://onlinelibrary.wiley.com/doi/10.1113/jphysiol.1997.sp021857.

233 David Burke, Matthew C Kiernan, and Hugh Bostock. Excitability of human axons. *Clinical neurophysiology*, 112(9):1575–1585, 2001.

234 I Mogyoros, Matthew C Kiernan, and Hugh Bostock. Strength-duration properties of sensory and motor axons in amyotrophic lateral sclerosis. *Brain*, 121(5):851–859, May 1998. ISSN 14602156. doi: 10.1093/brain/121.5.851. URL https://academic.oup.com/brain/article-lookup/doi/10.1093/brain/121.5.851.

235 John H. Caldwell, Kristin L. Schaller, Robert S. Lasher, Elior Peles, and S. Rock Levinson. Sodium channel Na $_{v}$ 1.6 is localized at nodes of Ranvier, dendrites, and synapses. *Proceedings of the National Academy of Sciences*, 97(10):5616–5620, May 2000. ISSN 0027-8424, 1091-6490. doi: 10.1073/pnas.090034797. URL https://pnas.org/doi/full/10.1073/pnas.090034797.

236 Edward J. Tehovnik and Warren M. Slocum. Depth-dependent detection of microampere currents delivered to monkey V1. *European Journal of Neuroscience*, 29(7):1477–1489, April 2009. ISSN 0953816X, 14609568. doi: 10.1111/j.1460-9568.2009.06695.x. URL https://onlinelibrary.wiley.com/doi/10.1111/j.1460-9568.2009.06695.x.

237 Luana Saba, Maria Teresa Viscomi, Alessandro Martini, Silvia Caioli, Nicola Biagio Mercuri, Ezia Guatteo, and Cristina Zona. Modified age-dependent expression of NaV1.6 in an ALS model correlates with motor cortex excitability alterations. *Neurobiology of Disease*, 130:104532, October 2019. ISSN 09699961. doi: 10.1016/j.nbd.2019.104532. URL https://linkinghub.elsevier.com/retrieve/pii/S0969996119302001.

238 Aman S Aberra, Angel V Peterchev, and Warren M Grill. Biophysically realistic neuron models for simulation of cortical stimulation. *Journal of Neural Engineering*, 15(6): 066023, December 2018. ISSN 1741-2560, 1741-2552. doi: 10.1088/1741-2552/aadbb1. URL https://iopscience.iop.org/article/10.1088/1741-2552/aadbb1.

239 Hartwig R. Siebner, Klaus Funke, Aman S. Aberra, Andrea Antal, Sven Bestmann, Robert Chen, Joseph Classen, Marco Davare, Vincenzo Di Lazzaro, Peter T. Fox, Mark Hallett, Anke N. Karabanov, Janine Kesselheim, Mikkel M. Beck, Giacomo Koch, David Liebetanz, Sabine Meunier, Carlo Miniussi, Walter Paulus, Angel V. Peterchev, Traian Popa, Michael C. Ridding, Axel Thielscher, Ulf Ziemann, John C. Rothwell, and Yoshikazu Ugawa. Transcranial magnetic stimulation of the brain: What is stimulated? – A consensus and critical position paper. *Clinical Neurophysiology*, 140:59–97, August 2022. ISSN 13882457. doi: 10.1016/j.clinph.2022.04.022. URL https://linkinghub.elsevier.com/retrieve/pii/S1388245722002723.

240 R. Salvador, S. Silva, P.J. Basser, and P.C. Miranda. Determining which mechanisms lead to activation in the motor cortex: A modeling study of transcranial magnetic stimulation using realistic stimulus waveforms and sulcal geometry. *Clinical Neurophysiology*, 122(4): 748–758, April 2011. ISSN 13882457. doi: 10.1016/j.clinph.2010.09.022. URL https://linkinghub.elsevier.com/retrieve/pii/S1388245710007091.

241 Yasuo Kawaguchi and Yoshiyuki Kubota. GABAergic cell subtypes and their synaptic connections in rat frontal cortex. *Cerebral Cortex*, 7(6):476–486, September 1997. ISSN 14602199. doi: 10.1093/cercor/7.6.476. URL https://academic.oup.com/cercor/article-lookup/doi/10.1093/cercor/7.6.476.

242 Aman S. Aberra, Boshuo Wang, Warren M. Grill, and Angel V. Peterchev. Simulation of transcranial magnetic stimulation in head model with morphologically-realistic cortical neurons. *Brain Stimulation*, 13(1):175–189, January 2020. ISSN 1935861X. doi: 10.1016/j.brs.2019.10.002. URL https://linkinghub.elsevier.com/retrieve/pii/S1935861X19304097.

243 T Kujirai, M D Caramia, J C Rothwell, B L Day, P D Thompson, A Ferbert, S Wroe, P Asselman, and C D Marsden. Corticocortical inhibition in human motor cortex. *The Journal of Physiology*, 471(1):501–519, November 1993. ISSN 00223751. doi: 10.1113/jphysiol.1993.sp019912. URL https://onlinelibrary.wiley.com/doi/10.1113/jphysiol.1993.sp019912.

244 Kristina D Micheva, Dylan Wolman, Brett D Mensh, Elizabeth Pax, JoAnn Buchanan, Stephen J Smith, and Davi D Bock. A large fraction of neocortical myelin ensheathes axons of local inhibitory neurons. *eLife*, 5:e15784, July 2016. ISSN 2050-084X. doi: 10.7554/eLife.15784. URL https://elifesciences.org/articles/15784.

245 J. Stedehouder, J. J. Couey, D. Brizee, B. Hosseini, J. A. Slotman, C. M. F. Dirven, G. Shpak, A. B. Houtsmuller, and S. A. Kushner. Fast-spiking Parvalbumin Interneurons are Frequently Myelinated in the Cerebral Cortex of Mice and Humans. *Cerebral Cortex*, 27(10):5001–5013, October 2017. ISSN 1047-3211, 1460-2199. doi: 10.1093/cercor/bhx203. URL https://academic.oup.com/cercor/article/27/10/5001/4079814.

246 Yasuyo H. Tanaka, Yasuhiro R. Tanaka, Fumino Fujiyama, Takahiro Furuta, Yuchio Yanagawa, and Takeshi Kaneko. Local Connections of Layer 5 GABAergic Interneurons to Corticospinal Neurons. *Frontiers in Neural Circuits*, 5, 2011. ISSN 1662-5110. doi: 10.3389/fncir.2011.00012. URL http://journal.frontiersin.org/article/10.3389/fncir.2011.00012/abstract.

247 Amanda E. Casale, Amanda J. Foust, Thierry Bal, and David A. McCormick. Cortical Interneuron Subtypes Vary in Their Axonal Action Potential Properties. *The Journal of Neuroscience*, 35(47):15555–15567, November 2015. ISSN 0270-6474, 1529-2401. doi: 10.1523/JNEUROSCI.1467-13.2015. URL https://www.jneurosci.org/lookup/doi/10.1523/JNEUROSCI.1467-13.2015.

248 W.M. Grill and J.T. Mortimer. The effect of stimulus pulse duration on selectivity of neural stimulation. *IEEE Transactions on Biomedical Engineering*, 43(2):161–166, February 1996. ISSN 00189294. doi: 10.1109/10.481985. URL http://ieeexplore.ieee.org/document/481985/.

249 I. Halawa, Y. Shirota, A. Neef, M. Sommer, and W. Paulus. Neuronal tuning: Selective targeting of neuronal populations via manipulation of pulse width and directionality. *Brain Stimulation*, 12(5):1244–1252, September 2019. ISSN 1935861X. doi: 10.1016/j.brs.2019.04.012. URL https://linkinghub.elsevier.com/retrieve/pii/S1935861X19302049.

250 E.P. Casula, L. Rocchi, R. Hannah, and J.C. Rothwell. Effects of pulse width, waveform and current direction in the cortex: A combined cTMS-EEG study. *Brain Stimulation*, 11(5):1063–1070, September 2018. ISSN 1935861X. doi: 10.1016/j.brs.2018.04.015. URL https://linkinghub.elsevier.com/retrieve/pii/S1935861X18301372.

251 Ljubodrag Mihailovic and Jose M. R. Delgado. ELECTRICAL STIMULATION OF MONKEY BRAIN WITH VARIOUS FREQUENCIES AND PULSE DURATIONS. *Journal of Neurophysiology*, 19(1):21–36, January 1956. ISSN 0022-3077, 1522-1598. doi: 10.1152/jn.1956.19.1.21. URL https://www.physiology.org/doi/10.1152/jn.1956.19.1.21.

252 Martin M. Reich, Frank Steigerwald, Anna D. Sawalhe, Rene Reese, Kabilar Gunalan, Silvia Johannes, Robert Nickl, Cordula Matthies, Cameron C. McIntyre, and Jens Volkmann. Short pulse width widens the therapeutic window of subthalamic neurostimulation. *Annals of Clinical and Translational Neurology*, 2(4):427–432, April 2015. ISSN 23289503. doi: 10.1002/acn3.168. URL https://onlinelibrary.wiley.com/doi/10.1002/acn3.168.

253 N.V. Povysheva, G. Gonzalez-Burgos, A.V. Zaitsev, S. Kröner, G. Barrionuevo, D.A. Lewis, and L.S. Krimer. Properties of Excitatory Synaptic Responses in Fast-spiking Interneurons and Pyramidal Cells from Monkey and Rat Prefrontal Cortex. *Cerebral Cortex*, 16(4):541–552, April 2006. ISSN 1460-2199, 1047-3211. doi: 10.1093/cercor/bhj002. URL http://academic.oup.com/cercor/article/16/4/541/382271/Properties-of-Excitatory-Synaptic-Responses-in.

254 H. Rothkegel, M. Sommer, W. Paulus, and N. Lang. Impact of pulse duration in single pulse TMS. *Clinical Neurophysiology*, 121(11):1915–1921, November 2010. ISSN 13882457. doi: 10.1016/j.clinph.2010.04.006. URL https://linkinghub.elsevier.com/retrieve/pii/S1388245710003573.

255 DEYMED Diagnostic s.r.o. Duomag mp: Deymed diagnostic. URL https://deymed.com/duomag-mp.

256 Jong Seok Bae, Neil G. Simon, Parvathi Menon, Steve Vucic, and Matthew C. Kiernan. The Puzzling Case of Hyperexcitability in Amyotrophic Lateral Sclerosis. *Journal of Clinical Neurology*, 9(2):65, 2013. ISSN 1738-6586, 2005-5013. doi: 10.3988/jcn.2013.9.2.65. URL https://www.thejcn.com/DOIx.php?id=10.3988/jcn.2013.9.2.65.

257 Steve Vucic, Garth A Nicholson, and Matthew C Kiernan. Cortical hyperexcitability may precede the onset of familial amyotrophic lateral sclerosis. *Brain*, 131(6):1540–1550, 2008.

258 Louis-David Beaulieu, Véronique H. Flamand, Hugo Massé-Alarie, and Cyril Schneider. Reliability and minimal detectable change of transcranial magnetic stimulation outcomes in healthy adults: A systematic review. *Brain Stimulation*, 10(2):196–213, March 2017. ISSN 1935861X. doi: 10.1016/j.brs.2016.12.008. URL `https://linkinghub.elsevier.com/retrieve/pii/S1935861X16303904`.

259 RC Oldfield. Edinburgh handedness inventory. *Journal of Abnormal Psychology*, 1971.

260 Pauli Virtanen, Ralf Gommers, Travis E. Oliphant, Matt Haberland, Tyler Reddy, David Cournapeau, Evgeni Burovski, Pearu Peterson, Warren Weckesser, Jonathan Bright, Stéfan J. van der Walt, Matthew Brett, Joshua Wilson, K. Jarrod Millman, Nikolay Mayorov, Andrew R. J. Nelson, Eric Jones, Robert Kern, Eric Larson, C J Carey, İlhan Polat, Yu Feng, Eric W. Moore, Jake VanderPlas, Denis Laxalde, Josef Perktold, Robert Cimrman, Ian Henriksen, E. A. Quintero, Charles R. Harris, Anne M. Archibald, Antônio H. Ribeiro, Fabian Pedregosa, Paul van Mulbregt, and SciPy 1.0 Contributors. SciPy 1.0: Fundamental Algorithms for Scientific Computing in Python. *Nature Methods*, 17:261–272, 2020. doi: 10.1038/s41592-019-0686-2.

261 S. Groppa, A. Oliviero, A. Eisen, A. Quartarone, L.G. Cohen, V. Mall, A. Kaelin-Lang, T. Mima, S. Rossi, G.W. Thickbroom, P.M. Rossini, U. Ziemann, J. Valls-Solé, and H.R. Siebner. A practical guide to diagnostic transcranial magnetic stimulation: Report of an IFCN committee. *Clinical Neurophysiology*, 123(5):858–882, May 2012. ISSN 13882457. doi: 10.1016/j.clinph.2012.01.010. URL `https://linkinghub.elsevier.com/retrieve/pii/S1388245712000569`.

262 Raphael Vallat. Pingouin: statistics in python. *Journal of Open Source Software*, 3(31): 1026, 2018. doi: 10.21105/joss.01026. URL `https://doi.org/10.21105/joss.01026`.

263 Kenneth O McGraw and S.P. Wong. Forming Inferences About Some Intraclass Correlation Coefficients. *Psychological Methods*, 1(1):30–46, 1996.

264 Paula Davila-Pérez, Ali Jannati, Peter J. Fried, Javier Cudeiro Mazaira, and Alvaro Pascual-Leone. The Effects of Waveform and Current Direction on the Efficacy and Test–Retest Reliability of Transcranial Magnetic Stimulation. *Neuroscience*, 393:97–109, November 2018. ISSN 03064522. doi: 10.1016/j.neuroscience.2018.09.044. URL `https://linkinghub.elsevier.com/retrieve/pii/S0306452218306493`.

265 Henrica C.W. de Vet, Caroline B. Terwee, Dirk L. Knol, and Lex M. Bouter. When to use agreement versus reliability measures. *Journal of Clinical Epidemiology*, 59(10):

1033–1039, October 2006. ISSN 08954356. doi: 10.1016/j.jclinepi.2005.10.015. URL https://linkinghub.elsevier.com/retrieve/pii/S0895435606000291.

266 Heidi M. Schambra, R. Todd Ogden, Isis Martínez-Hernández, Xuejing Lin, Y. Brenda Chang, Asif Rahman, Dylan Edwards, and John W. Krakauer. The reliability of repeated TMS measures in older adults and in patients with subacute and chronic stroke. *Frontiers in Cellular Neuroscience*, 9, 2015. ISSN 1662-5102. doi: 10.3389/fncel.2015.00335. URL https://www.frontiersin.org/articles/10.3389/fncel.2015.00335/full. Publisher: Frontiers.

267 Ulla-Britt Flansbjer, Anna Maria Holmbäck, David Downham, Carolynn Patten, and Jan Lexell. Reliability of gait performance tests in men and women with hemiparesis after stroke. *Journal of Rehabilitation Medicine*, 37(2):75–82, Mar 2005. ISSN 1650-1977. doi: 10.1080/16501970410017215.

268 H Beckerman, M E Roebroeck, G J Lankhorst, J G Becher, P D Bezemer, and A L M Verbeek. Smallest real difference, a link between reproducibility and responsiveness. *Quality of life research*, 10:571–578, 2001.

269 Francis Houde, Sarah Laroche, Veronique Thivierge, Marylie Martel, Marie-Philippe Harvey, Frederique Daigle, Ailin Olivares-Marchant, Louis-David Beaulieu, and Guillaume Leonard. Transcranial Magnetic Stimulation Measures in the Elderly: Reliability, Smallest Detectable Change and the Potential Influence of Lifestyle Habits. *Frontiers in Aging Neuroscience*, 10:379, November 2018. ISSN 1663-4365. doi: 10.3389/fnagi.2018.00379. URL https://www.frontiersin.org/article/10.3389/fnagi.2018.00379/full.

270 Claire Kemlin, Eric Moulton, Sara Leder, Marion Houot, Sabine Meunier, Charlotte Rosso, and Jean-Charles Lamy. Redundancy Among Parameters Describing the Input-Output Relation of Motor Evoked Potentials in Healthy Subjects and Stroke Patients. *Frontiers in Neurology*, 10:535, May 2019. ISSN 1664-2295. doi: 10.3389/fneur.2019.00535. URL https://www.frontiersin.org/article/10.3389/fneur.2019.00535/full.

271 I. Premoli, N. Castellanos, D. Rivolta, P. Belardinelli, R. Bajo, C. Zipser, S. Espenhahn, T. Heidegger, F. Muller-Dahlhaus, and U. Ziemann. TMS-EEG Signatures of GABAergic Neurotransmission in the Human Cortex. *Journal of Neuroscience*, 34(16):5603–5612, April 2014. ISSN 0270-6474, 1529-2401. doi: 10.1523/JNEUROSCI.5089-13.2014. URL http://www.jneurosci.org/cgi/doi/10.1523/JNEUROSCI.5089-13.2014.

272 Ricci Hannah and John C. Rothwell. Pulse Duration as Well as Current Direction Determines the Specificity of Transcranial Magnetic Stimulation of Motor Cortex during Contraction. *Brain Stimulation*, 10(1):106–115, January 2017. ISSN 1935861X. doi:

10.1016/j.brs.2016.09.008. URL https://linkinghub.elsevier.com/retrieve/pii/S1935861X16302601.

273 Danny Spampinato. Dissecting two distinct interneuronal networks in M1 with transcranial magnetic stimulation. *Experimental Brain Research*, 238(7-8):1693–1700, August 2020. ISSN 0014-4819, 1432-1106. doi: 10.1007/s00221-020-05875-y. URL http://link.springer.com/10.1007/s00221-020-05875-y.

274 Ricci Hannah, Lorenzo Rocchi, Sara Tremblay, Eleanor Wilson, and John C. Rothwell. Pulse width biases the balance of excitation and inhibition recruited by transcranial magnetic stimulation. *Brain Stimulation*, 13(3):536–538, May 2020. ISSN 1935861X. doi: 10.1016/j.brs.2020.01.011. URL https://linkinghub.elsevier.com/retrieve/pii/S1935861X20300152.

275 Yuichiro Shirota, Martin Sommer, and Walter Paulus. Strength-Duration Relationship in Paired-pulse Transcranial Magnetic Stimulation (TMS) and Its Implications for Repetitive TMS. *Brain Stimulation*, 9(5):755–761, September 2016. ISSN 1935861X. doi: 10.1016/j.brs.2016.04.019. URL https://linkinghub.elsevier.com/retrieve/pii/S1935861X1630095X.

276 H Bostock. The strength-duration relationship for excitation of myelinated nerve: computed dependence on membrane parameters. *The Journal of Physiology*, 341(1): 59–74, August 1983. ISSN 00223751. doi: 10.1113/jphysiol.1983.sp014792. URL https://onlinelibrary.wiley.com/doi/10.1113/jphysiol.1983.sp014792.

277 Maria Drakaki, Claus Mathiesen, Hartwig R. Siebner, Kristoffer Madsen, and Axel Thielscher. Database of 25 validated coil models for electric field simulations for TMS. *Brain Stimulation*, 15(3):697–706, May 2022. ISSN 1935861X. doi: 10.1016/j.brs.2022.04.017. URL https://linkinghub.elsevier.com/retrieve/pii/S1935861X22000778.

278 Koen Cuypers and Anouk Marsman. Transcranial magnetic stimulation and magnetic resonance spectroscopy: Opportunities for a bimodal approach in human neuroscience. *NeuroImage*, 224:117394, January 2021. ISSN 10538119. doi: 10.1016/j.neuroimage.2020.117394. URL https://linkinghub.elsevier.com/retrieve/pii/S105381192030879X.

279 Ian Greenhouse, Maedbh King, Sean Noah, Richard J Maddock, and Richard B Ivry. Individual differences in resting corticospinal excitability are correlated with reaction time and gaba content in motor cortex. *Journal of Neuroscience*, 37(10):2686–2696, 2017.

280 Timothy J Carroll, Stephan Riek, and Richard G Carson. Reliability of the input–output properties of the cortico-spinal pathway obtained from transcranial mag-

netic and electrical stimulation. *Journal of Neuroscience Methods*, 112(2):193–202, December 2001. ISSN 01650270. doi: 10.1016/S0165-0270(01)00468-X. URL https://linkinghub.elsevier.com/retrieve/pii/S016502700100468X.

281 Hao Liu and Stephanie S.Y. Au-Yeung. Reliability of transcranial magnetic stimulation induced corticomotor excitability measurements for a hand muscle in healthy and chronic stroke subjects. *Journal of the Neurological Sciences*, page 5, 2014.

282 Angelo Cacchio, Nicola Cimini, Paolo Alosi, Valter Santilli, and Alfonso Marrelli. Reliability of transcranial magnetic stimulation-related measurements of tibialis anterior muscle in healthy subjects. *Clinical Neurophysiology*, 120(2):414–419, February 2009. ISSN 13882457. doi: 10.1016/j.clinph.2008.11.019. URL https://linkinghub.elsevier.com/retrieve/pii/S1388245708012649.

283 Rachel Malcolm, Simon Cooper, Jonathan Folland, Christopher Tyler, Ricci Hannah, and Caroline Sunderland. Reliability of transcranial magnetic stimulation measurements of maximum activation of the knee extensors in young adult males. *Human Movement Science*, 78:102828, August 2021. ISSN 01679457. doi: 10.1016/j.humov.2021.102828. URL https://linkinghub.elsevier.com/retrieve/pii/S0167945721000762.

284 Steven L Wolf, Andrew J Butler, Georgette I Campana, Trinity A Parris, Danielle M Struys, Sarah R Weinstein, and Paul Weiss. Intra-subject reliability of parameters contributing to maps generated by transcranial magnetic stimulation in able-bodied adults. *Clinical Neurophysiology*, 115(8):1740–1747, August 2004. ISSN 13882457. doi: 10.1016/j.clinph.2004.02.027. URL https://linkinghub.elsevier.com/retrieve/pii/S1388245704001737.

285 M Malcolm, W Triggs, K Light, O Shechtman, G Khandekar, and L Gonzalezrothi. Reliability of motor cortex transcranial magnetic stimulation in four muscle representations. *Clinical Neurophysiology*, 117(5):1037–1046, May 2006. ISSN 13882457. doi: 10.1016/j.clinph.2006.02.005. URL https://linkinghub.elsevier.com/retrieve/pii/S1388245706000575.

286 Stephanie A. H. Jones, Beverly C. Butler, Franziska Kintzel, Anne Johnson, Raymond M. Klein, and Gail A. Eskes. Measuring the Performance of Attention Networks with the Dalhousie Computerized Attention Battery (DalCAB): Methodology and Reliability in Healthy Adults. *Frontiers in Psychology*, 7, June 2016. ISSN 1664-1078. doi: 10.3389/fpsyg.2016.00823. URL http://journal.frontiersin.org/Article/10.3389/fpsyg.2016.00823/abstract.

287 Marina G. Falleti, Paul Maruff, Alexander Collie, and David G. Darby. Practice Effects Associated with the Repeated Assessment of Cognitive Function Using the CogState

Battery at 10-minute, One Week and One Month Test-retest Intervals. *Journal of Clinical and Experimental Neuropsychology*, 28(7):1095–1112, October 2006. ISSN 1380-3395, 1744-411X. doi: 10.1080/13803390500205718. URL https://www.tandfonline.com/doi/full/10.1080/13803390500205718.

288 Greg J. Elder, Sean J. Colloby, Michael J. Firbank, and John-Paul Taylor. Quantifying test-retest reliability of repeated objective attentional measures in Lewy body dementia. *Journal of Neurology*, 269(7):3605–3613, July 2022. ISSN 0340-5354, 1432-1459. doi: 10.1007/s00415-022-10977-4. URL https://link.springer.com/10.1007/s00415-022-10977-4.

289 Cátia M. Oliveira, Marianna E. Hayiou-Thomas, and Lisa M. Henderson. The reliability of the serial reaction time task: meta-analysis of test–retest correlations. *Royal Society Open Science*, 10(7):221542, July 2023. ISSN 2054-5703. doi: 10.1098/rsos.221542. URL https://royalsocietypublishing.org/doi/10.1098/rsos.221542.

290 Caroline Möller, Noritoshi Arai, Jörg Lücke, and Ulf Ziemann. Hysteresis effects on the input–output curve of motor evoked potentials. *Clinical Neurophysiology*, 120(5):1003–1008, May 2009. ISSN 13882457. doi: 10.1016/j.clinph.2009.03.001. URL https://linkinghub.elsevier.com/retrieve/pii/S1388245709002399.

291 Seyed Mohammad Mahdi Alavi, Stefan M. Goetz, and Angel V. Peterchev. Optimal Estimation of Neural Recruitment Curves Using Fisher Information: Application to Transcranial Magnetic Stimulation. *IEEE Transactions on Neural Systems and Rehabilitation Engineering*, 27(6):1320–1330, June 2019. ISSN 1534-4320, 1558-0210. doi: 10.1109/TNSRE.2019.2914475. URL https://ieeexplore.ieee.org/document/8705343/.

292 Julian Keil, Jana Timm, Iria SanMiguel, Hannah Schulz, Jonas Obleser, and Marc Schönwiesner. Cortical brain states and corticospinal synchronization influence tms-evoked motor potentials. *Journal of neurophysiology*, 111(3):513–519, 2014.

293 Lukas Schilberg, Sanne Ten Oever, Teresa Schuhmann, and Alexander T Sack. Phase and power modulations on the amplitude of tms-induced motor evoked potentials. *PloS one*, 16(9):e0255815, 2021.

294 Thomas G. Di Virgilio, Magdalena Ietswaart, Ragul Selvamoorthy, and Angus M. Hunter. The Reliability of Transcranial Magnetic Stimulation-Derived Corticomotor Inhibition as a Brain Health Evaluation Tool in Soccer Players. *Sports Medicine - Open*, 8(1):7, December 2022. ISSN 2199-1170, 2198-9761. doi: 10.1186/s40798-021-00399-3. URL https://sportsmedicine-open.springeropen.com/articles/10.1186/s40798-021-00399-3.

295 Joaquim P Brasil-Neto, Lisa M McShane, Peter Fuhr, Mark Hallett, and Leonardo G Cohen. Topographic mapping of the human motor cortex with m ic stimulation: factors

affecting accuracy and reproducibility. *Electroencephalography and clinical Neurophysiology*, 85:9–16, 1992.

296 MJ Smith, JC Keel, BD Greenberg, LF Adams, PJ Schmidt, DA Rubinow, and Eric M Wassermann. Menstrual cycle effects on cortical excitability. *Neurology*, 53(9):2069–2069, 1999.

297 Julien Q. M. Ly, Giulia Gaggioni, Sarah L. Chellappa, Soterios Papachilleos, Alexandre Brzozowski, Chloé Borsu, Mario Rosanova, Simone Sarasso, Benita Middleton, André Luxen, Simon N. Archer, Christophe Phillips, Derk-Jan Dijk, Pierre Maquet, Marcello Massimini, and Gilles Vandewalle. Circadian regulation of human cortical excitability. *Nature Communications*, 7(1):11828, September 2016. ISSN 2041-1723. doi: 10.1038/ncomms11828. URL http://www.nature.com/articles/ncomms11828.

298 Alexander S. Tamm, Olle Lagerquist, Alejandro L. Ley, and David F. Collins. Chronotype Influences Diurnal Variations in the Excitability of the Human Motor Cortex and the Ability to Generate Torque during a Maximum Voluntary Contraction. *Journal of Biological Rhythms*, 24(3):211–224, June 2009. ISSN 0748-7304, 1552-4531. doi: 10.1177/0748730409334135. URL http://journals.sagepub.com/doi/10.1177/0748730409334135.

299 Luigi De Gennaro, Cristina Marzano, Domenica Veniero, Fabio Moroni, Fabiana Fratello, Giuseppe Curcio, Michele Ferrara, Fabio Ferlazzo, Luana Novelli, Maria Concetta Pellicciari, Mario Bertini, and Paolo Maria Rossini. Neurophysiological correlates of sleepiness: A combined TMS and EEG study. *NeuroImage*, 36(4):1277–1287, July 2007. ISSN 10538119. doi: 10.1016/j.neuroimage.2007.04.013. URL https://linkinghub.elsevier.com/retrieve/pii/S1053811907003072.

300 Sebastian H. Doeltgen and Michael C. Ridding. Behavioural exposure and sleep do not modify corticospinal and intracortical excitability in the human motor system. *Clinical Neurophysiology*, 121(3):448–452, March 2010. ISSN 13882457. doi: 10.1016/j.clinph.2009.11.085. URL https://linkinghub.elsevier.com/retrieve/pii/S1388245709007494.

301 S. N. Baker, E. Olivier, and R. N. Lemon. Coherent oscillations in monkey motor cortex and hand muscle EMG show task-dependent modulation. *The Journal of Physiology*, 501 (1):225–241, May 1997. ISSN 00223751. doi: 10.1111/j.1469-7793.1997.225bo.x. URL http://doi.wiley.com/10.1111/j.1469-7793.1997.225bo.x.

302 V. N. Murthy and E. E. Fetz. Oscillatory activity in sensorimotor cortex of awake monkeys: synchronization of local field potentials and relation to behavior. *Journal of Neurophysiology*, 76(6):3949–3967, December 1996. ISSN 0022-3077, 1522-1598. doi: 10.1152/jn.1996.76.6.3949. URL https://www.physiology.org/doi/10.1152/jn.1996.76.6.3949.

303 Stephan Salenius, Karin Portin, Matti Kajola, Riitta Salmelin, and Riitta Hari. Cortical Control of Human Motoneuron Firing During Isometric Contraction. *Journal of Neurophysiology*, 77(6):3401–3405, June 1997. ISSN 0022-3077, 1522-1598. doi: 10.1152/jn.1997.77.6.3401. URL https://www.physiology.org/doi/10.1152/jn.1997.77.6.3401.

304 B A Conway, D M Halliday, S F Farmer, U Shahani, P Maas, A I Weir, and J R Rosenberg. Synchronization between motor cortex and spinal motoneuronal pool during the performance of a maintained motor task in man. *The Journal of Physiology*, 489(3): 917–924, December 1995. ISSN 00223751. doi: 10.1113/jphysiol.1995.sp021104. URL https://onlinelibrary.wiley.com/doi/10.1113/jphysiol.1995.sp021104.

305 Andrej Stancák and Gert Pfurtscheller. Event-related desynchronisation of central beta-rhythms during brisk and slow self-paced finger movements of dominant and nondominant hand. *Cognitive Brain Research*, 4(3):171–183, October 1996. ISSN 09266410. doi: 10.1016/S0926-6410(96)00031-6. URL https://linkinghub.elsevier.com/retrieve/pii/S0926641096000316.

306 James J Bonaiuto, Sofie S Meyer, Simon Little, Holly Rossiter, Martina F Callaghan, Frederic Dick, Gareth R Barnes, and Sven Bestmann. Lamina-specific cortical dynamics in human visual and sensorimotor cortices. *eLife*, 7:e33977, October 2018. ISSN 2050-084X. doi: 10.7554/eLife.33977. URL https://elifesciences.org/articles/33977.

307 Ryosuke Hosaka, Toshi Nakajima, Kazuyuki Aihara, Yoko Yamaguchi, and Hajime Mushiake. The Suppression of Beta Oscillations in the Primate Supplementary Motor Complex Reflects a Volatile State During the Updating of Action Sequences. *Cerebral Cortex*, 26(8):3442–3452, August 2016. ISSN 1047-3211, 1460-2199. doi: 10.1093/cercor/bhv163. URL https://academic.oup.com/cercor/article-lookup/doi/10.1093/cercor/bhv163.

308 Jason R. Taylor, Nitin Williams, Rhodri Cusack, Tibor Auer, Meredith A. Shafto, Marie Dixon, Lorraine K. Tyler, Cam-CAN, and Richard N. Henson. The Cambridge Centre for Ageing and Neuroscience (Cam-CAN) data repository: Structural and functional MRI, MEG, and cognitive data from a cross-sectional adult lifespan sample. *NeuroImage*, 144: 262–269, January 2017. ISSN 10538119. doi: 10.1016/j.neuroimage.2015.09.018. URL https://linkinghub.elsevier.com/retrieve/pii/S1053811915008150.

309 Meredith A Shafto, Lorraine K Tyler, Marie Dixon, Jason R Taylor, James B Rowe, Rhodri Cusack, Andrew J Calder, William D Marslen-Wilson, John Duncan, Tim Dalgleish, Richard N Henson, Carol Brayne, Fiona E Matthews, and Cam-CAN. The Cambridge Centre for Ageing and Neuroscience (Cam-CAN) study protocol: a cross-sectional, lifespan, multidisciplinary examination of healthy cognitive ageing. *BMC Neurology*,

14(1):204, December 2014. ISSN 1471-2377. doi: 10.1186/s12883-014-0204-1. URL https://bmcneurol.biomedcentral.com/articles/10.1186/s12883-014-0204-1.

310 Bernard Rosner. Percentage Points for a Generalized ESD Many-Outlier Procedure. *Technometrics*, 25(2):9, 1983.

311 Aapo Hyvarinen. Fast and robust fixed-point algorithms for independent component analysis. *IEEE transactions on Neural Networks*, 10(3):626–634, 1999.

312 Mark Woolrich, Laurence Hunt, Adrian Groves, and Gareth Barnes. MEG beamforming using Bayesian PCA for adaptive data covariance matrix regularization. *NeuroImage*, 57(4):1466–1479, August 2011. ISSN 10538119. doi: 10.1016/j.neuroimage.2011.04.041. URL https://linkinghub.elsevier.com/retrieve/pii/S105381191100440X.

313 B.D. Van Veen and K.M. Buckley. Beamforming: a versatile approach to spatial filtering. *IEEE ASSP Magazine*, 5(2):4–24, April 1988. ISSN 0740-7467. doi: 10.1109/53.665. URL http://ieeexplore.ieee.org/document/665/.

314 Chenguang Zheng, Kevin Wood Bieri, Yi-Tse Hsiao, and Laura Lee Colgin. Spatial Sequence Coding Differs during Slow and Fast Gamma Rhythms in the Hippocampus. *Neuron*, 89(2):398–408, January 2016. ISSN 08966273. doi: 10.1016/j.neuron.2015.12.005. URL https://linkinghub.elsevier.com/retrieve/pii/S0896627315010764.

315 David W. Purcell, Sasha M. John, Bruce A. Schneider, and Terence W. Picton. Human temporal auditory acuity as assessed by envelope following responses. *The Journal of the Acoustical Society of America*, 116(6):3581–3593, December 2004. ISSN 0001-4966, 1520-8524. doi: 10.1121/1.1798354. URL https://pubs.aip.org/jasa/article/116/6/3581/545252/Human-temporal-auditory-acuity-as-assessed-by.

316 Amy L. Proskovec, Rachel K. Spooner, Alex I. Wiesman, and Tony W. Wilson. Local cortical thickness predicts somatosensory gamma oscillations and sensory gating: A multimodal approach. *NeuroImage*, 214:116749, July 2020. ISSN 10538119. doi: 10.1016/j.neuroimage.2020.116749. URL https://linkinghub.elsevier.com/retrieve/pii/S1053811920302366.

317 Bálint Lasztóczi and Thomas Klausberger. Layer-Specific GABAergic Control of Distinct Gamma Oscillations in the CA1 Hippocampus. *Neuron*, 81(5):1126–1139, March 2014. ISSN 08966273. doi: 10.1016/j.neuron.2014.01.021. URL https://linkinghub.elsevier.com/retrieve/pii/S089662731400052X.

318 Hana Burianová, Lars Marstaller, Anina N Rich, Mark A Williams, Greg Savage, Margaret Ryan, and Paul F Sowman. Motor neuroplasticity: A meg-fmri study of motor imagery and execution in healthy ageing. *Neuropsychologia*, 146:107539, 2020.

319 Takashi Inamoto, Masaya Ueda, Keita Ueno, China Shiroma, Rin Morita, Yasuo Naito, and Ryouhei Ishii. Motor-Related Mu/Beta Rhythm in Older Adults: A Comprehensive Review. *Brain Sciences*, 13(5):751, April 2023. ISSN 2076-3425. doi: 10.3390/brainsci13050751. URL https://www.mdpi.com/2076-3425/13/5/751.

320 Constance Hammond, Hagai Bergman, and Peter Brown. Pathological synchronization in Parkinson's disease: networks, models and treatments. *Trends in Neurosciences*, 30 (7):357–364, July 2007. ISSN 01662236. doi: 10.1016/j.tins.2007.05.004. URL https://linkinghub.elsevier.com/retrieve/pii/S0166223607001233.

321 Peter Grummich, Christopher Nimsky, Elisabeth Pauli, Michael Buchfelder, and Oliver Ganslandt. Combining fmri and meg increases the reliability of presurgical language localization: a clinical study on the difference between and congruence of both modalities. *Neuroimage*, 32(4):1793–1803, 2006.

322 Jay N. Giedd, Jonathan Blumenthal, Neal O. Jeffries, F. X. Castellanos, Hong Liu, Alex Zijdenbos, Tomáš Paus, Alan C. Evans, and Judith L. Rapoport. Brain development during childhood and adolescence: a longitudinal MRI study. *Nature Neuroscience*, 2 (10):861–863, October 1999. ISSN 1097-6256, 1546-1726. doi: 10.1038/13158. URL https://www.nature.com/articles/nn1099_861.

323 Keith M McGregor, Zvinka Zlatar, Erin Kleim, Atchar Sudhyadhom, Andrew Bauer, Stephanie Phan, Lauren Seeds, Anastasia Ford, Todd M Manini, Keith D White, et al. Physical activity and neural correlates of aging: a combined tms/fmri study. *Behavioural Brain Research*, 222(1):158–168, 2011.

324 Stephanie R Jones. When brain rhythms aren't 'rhythmic': implication for their mechanisms and meaning. *Current Opinion in Neurobiology*, 40:72–80, October 2016. ISSN 09594388. doi: 10.1016/j.conb.2016.06.010. URL https://linkinghub.elsevier.com/retrieve/pii/S0959438816300769.

325 Scott R. Cole and Bradley Voytek. Brain Oscillations and the Importance of Waveform Shape. *Trends in Cognitive Sciences*, 21(2):137–149, February 2017. ISSN 13646613. doi: 10.1016/j.tics.2016.12.008. URL https://linkinghub.elsevier.com/retrieve/pii/S1364661316302182.

326 Freek Van Ede, Andrew J. Quinn, Mark W. Woolrich, and Anna C. Nobre. Neural Oscillations: Sustained Rhythms or Transient Burst-Events? *Trends in Neurosciences*, 41(7):415–417, July 2018. ISSN 01662236. doi: 10.1016/j.tins.2018.04.004. URL https://linkinghub.elsevier.com/retrieve/pii/S0166223618301036.

327 Catharina Zich, Andrew J. Quinn, Lydia C. Mardell, Nick S. Ward, and Sven Bestmann. Dissecting Transient Burst Events. *Trends in Cognitive Sciences*, 24(10):784–

788, October 2020. ISSN 13646613. doi: 10.1016/j.tics.2020.07.004. URL https://linkinghub.elsevier.com/retrieve/pii/S136466132030173X.

328 M. Bauer, R. Oostenveld, P. Maarten, and P. Fries. Tactile Spatial Attention Enhances Gamma-Band Activity in Somatosensory Cortex and Reduces Low-Frequency Activity in Parieto-Occipital Areas. *Journal of Neuroscience*, 26(2):490–501, 2006. doi: 10.1523/JNEUROSCI.5228-04.2006.

329 M. Brosch, E. Budinger, and H. Scheich. Stimulus-Related Gamma Oscillations in Primate Auditory Cortex. *Journal of Neurophysiology*, 87(6):2715–2725, 2002. doi: 10.1152/jn.2002.87.6.2715.

330 N. Hoogenboom, J.M. Schoffelen, R. Oostenveld, L.M. Parkes, and P. Fries. Localizing human visual gamma-band activity in frequency, time and space. *NeuroImage*, 29(3):764–773, 2006. doi: 10.1016/j.neuroimage.2005.08.043.

331 R.A. Joundi, N. Jenkinson, J.S. Brittain, T.Z. Aziz, and P. Brown. Driving Oscillatory Activity in the Human Cortex Enhances Motor Performance. *Current Biology*, 22(5):403–407, 2012. doi: 10.1016/j.cub.2012.01.024.

332 B. Pesaran, J.S. Pezaris, M. Sahani, P.P. Mitra, and R.A. Andersen. Temporal structure in neuronal activity during working memory in macaque parietal cortex. *Nature Neuroscience*, 5(8):805–811, 2002. doi: 10.1038/nn890.

333 J. Fell, P. Klaver, and K. Lehnertz. Human memory formation is accompanied by rhinal–hippocampal coupling and decoupling. *Nature Neuroscience*, 4(12):1259–1264, 2001. doi: 10.1038/nn759.

334 S.D. Muthukumaraswamy and K.D. Singh. Visual gamma oscillations: The effects of stimulus type, visual field coverage and stimulus motion on MEG and EEG recordings. *NeuroImage*, 69:223–230, 2013. doi: 10.1016/j.neuroimage.2012.12.038.

335 S. Ray and J.H.R. Maunsell. Differences in Gamma Frequencies across Visual Cortex Restrict Their Possible Use in Computation. *Neuron*, 67(5):885–896, 2010. doi: 10.1016/j.neuron.2010.08.004.

336 J.B. Swettenham, S.D. Muthukumaraswamy, and K.D. Singh. Spectral Properties of Induced and Evoked Gamma Oscillations in Human Early Visual Cortex to Moving and Stationary Stimuli. *Journal of Neurophysiology*, 102(2):1241–1253, 2009. doi: 10.1152/jn.91044.2008.

337 C. Börgers, S. Epstein, and N.J. Kopell. Background gamma rhythmicity and attention in cortical local circuits: A computational study. *Proceedings of the National Academy of Sciences of the United States of America*, 102(19):7002–7007, 2005. doi: 10.1073/pnas.0502366102.

338 P. Fries, D. Nikolić, and W. Singer. The gamma cycle. *Trends in Neurosciences*, 30(7): 309–316, 2007. doi: 10.1016/j.tins.2007.05.005.

339 Edward O. Mann and Ole Paulsen. Role of GABAergic inhibition in hippocampal network oscillations. *Trends in Neurosciences*, 30(7):343–349, July 2007. ISSN 01662236. doi: 10.1016/j.tins.2007.05.003. URL `https://linkinghub.elsevier.com/retrieve/pii/S0166223607001221`.

340 Michael Strüber, Jonas-Frederic Sauer, and Marlene Bartos. Parvalbumin expressing interneurons control spike-phase coupling of hippocampal cells to theta oscillations. *Scientific Reports*, 12(1):1362, December 2022. ISSN 2045-2322. doi: 10.1038/s41598-022-05004-5. URL `https://www.nature.com/articles/s41598-022-05004-5`.

341 P.J. Uhlhaas, F. Roux, E. Rodriguez, A. Rotarska-Jagiela, and W. Singer. Neural synchrony and the development of cortical networks. *Trends in Cognitive Sciences*, 14(2): 72–80, 2010. doi: 10.1016/j.tics.2009.12.002.

342 P.J. Uhlhaas and W. Singer. The development of neural synchrony and large-scale cortical networks during adolescence: Relevance for the pathophysiology of schizophrenia and neurodevelopmental hypothesis. *Schizophrenia Bulletin*, 37(3):514–523, 2011. doi: 10.1093/schbul/sbr034.

343 G.D. Hoftman and D.A. Lewis. Postnatal developmental trajectories of neural circuits in the primate prefrontal cortex: Identifying sensitive periods for vulnerability to schizophrenia. *Schizophrenia Bulletin*, 37(3):493–503, 2011. doi: 10.1093/schbul/sbr029.

344 H. Morishita, M. Kundakovic, L. Bicks, A. Mitchell, and S. Akbarian. Interneuron epigenomes during the critical period of cortical plasticity: Implications for schizophrenia. *Neurobiology of Learning and Memory*, 124:104–110, 2015. doi: 10.1016/j.nlm.2015.03.005.

345 D.E. Pafundo, C.A. Pretell Annan, N.M. Fulginiti, and J.E. Belforte. Early NMDA receptor ablation in interneurons causes an activity-dependent E/I imbalance in vivo in prefrontal cortex pyramidal neurons of a mouse model useful for the study of schizophrenia. *Schizophrenia Bulletin*, 47(5):1300–1309, 2021. doi: 10.1093/schbul/sbab030.

346 H.X. Wang and W.J. Gao. Cell-type Specific Development of NMDA Receptors in the Interneurons of Rat Prefrontal Cortex. *Neuropsychologia*, 34(8):2028–2040, 2009. doi: 10.1038/npp.2009.20.Cell-type.

347 A. Caballero, R. Granberg, and K.Y. Tseng. Mechanisms contributing to prefrontal cortex maturation during adolescence. *Neuroscience and Biobehavioral Reviews*, 70:4–12, 2016. doi: 10.1016/j.neubiorev.2016.05.013.

348 K.Y. Tseng and P. O'Donnell. Dopamine modulation of prefrontal cortical interneurons changes during adolescence. *Cerebral Cortex*, 17(5):1235–1240, 2007. doi: 10.1093/cercor/bhl034.

349 K.Y. Tseng, B.L. Lewis, B.K. Lipska, and P. O'Donnell. Post-Pubertal Disruption of Medial Prefrontal Cortical Dopamine-Glutamate Interactions in a Developmental Animal Model of Schizophrenia. *Biological Psychiatry*, 62(7):730–738, 2007. doi: 10.1016/j.biopsych.2006.10.012.

350 R. H. Andersson, A. Johnston, P. A. Herman, U. H. Winzer-Serhan, I. Karavanova, D. Vullhorst, A. Fisahn, and A. Buonanno. Neuregulin and dopamine modulation of hippocampal gamma oscillations is dependent on dopamine D4 receptors. *Proceedings of the National Academy of Sciences*, 109(32):13118–13123, August 2012. ISSN 0027-8424, 1091-6490. doi: 10.1073/pnas.1201011109. URL `http://www.pnas.org/cgi/doi/10.1073/pnas.1201011109`.

351 K.E. Furth, S. Mastwal, K.H. Wang, A. Buonanno, and D. Vullhorst. Dopamine, cognitive function, and gamma oscillations: role of D4 receptors. *Frontiers in Cellular Neuroscience*, 7, 2013. doi: 10.3389/fncel.2013.00102.

352 A. Mukherjee, F. Carvalho, and S. Eliez. Long-Lasting Rescue of Network and Cognitive Dysfunction in a Genetic Schizophrenia Model Article Long-Lasting Rescue of Network and Cognitive Dysfunction. *Cell. Published online*, 2019:1–16. doi: 10.1016/j.cell.2019.07.023.

353 E. Brazhnik, N. Novikov, A.J. McCoy, N.M. Ilieva, M.W. Ghraib, and JR Walters. Early decreases in cortical mid-gamma peaks coincide with the onset of motor deficits and precede exaggerated beta build-up in rat models for Parkinson's disease. *Neurobiology of Disease*, 155(105393), 2021. doi: 10.1016/j.nbd.2021.105393.

354 G. Foffani and M. Alegre. Brain oscillations and Parkinson disease. *Handbook of Clinical Neurology*, 184:259–271, 2022. doi: 10.1016/B978-0-12-819410-2.00014-X.

355 A. Guerra, D. Colella, and M. Giangrosso. Driving motor cortex oscillations modulates bradykinesia in Parkinson's disease. *Brain*, 145(1):224–236, 2022. doi: 10.1093/brain/awab257.

356 M. Muthuraman, M. Palotai, and B. Jávor-Duray. Frequency-specific network activity predicts bradykinesia severity in Parkinson's disease. *NeuroImage: Clinical*, 32(102857), 2021. doi: 10.1016/j.nicl.2021.102857.

357 S.L. Schmidt and W.M. Grill. <scp>Levodopa-Induced</scp> Dyskinesia Is Mediated by Cortical Gamma Oscillations in Experimental Parkinsonism. *Movement Disorders*, 36(4):1044–1045, 2021. doi: 10.1002/mds.28578.

358 C. Wiest, F. Torrecillos, and G. Tinkhauser. Finely-tuned gamma oscillations: Spectral characteristics and links to dyskinesia. *Experimental Neurology*, 351(113999), 2022. doi: 10.1016/j.expneurol.2022.113999.

359 X. Geng, J. Zhang, and Y. Jiang. Comparison of oscillatory activity in subthalamic nucleus in Parkinson's disease and dystonia. *Neurobiology of Disease*, 98:100–107, 2017. doi: 10.1016/j.nbd.2016.12.006.

360 S. Miocinovic, N.C. Swann, C. Hemptinne, A. Miller, J.L. Ostrem, and P.A. Starr. Cortical gamma oscillations in isolated dystonia. *Parkinsonism & Related Disorders*, 49: 104–105, 2018. doi: 10.1016/j.parkreldis.2018.01.017.

361 S. Dukic, R. McMackin, and T. Buxo. Patterned functional network disruption in amyotrophic lateral sclerosis. *Human Brain Mapping*, 40(16):4827–4842, 2019. doi: 10.1002/hbm.24740.

362 Richard W. Olsen and Werner Sieghart. International Union of Pharmacology. LXX. Subtypes of γ-Aminobutyric Acid $_{a}$ Receptors: Classification on the Basis of Subunit Composition, Pharmacology, and Function. Update. *Pharmacological Reviews*, 60(3): 243–260, September 2008. ISSN 0031-6997, 1521-0081. doi: 10.1124/pr.108.00505. URL `http://pharmrev.aspetjournals.org/lookup/doi/10.1124/pr.108.00505`.

363 Stephen G. Brickley and Istvan Mody. Extrasynaptic GABAA Receptors: Their Function in the CNS and Implications for Disease. *Neuron*, 73(1):23–34, January 2012. ISSN 08966273. doi: 10.1016/j.neuron.2011.12.012. URL `https://linkinghub.elsevier.com/retrieve/pii/S0896627311010932`.

364 Monica Beneyto, Andrew Abbott, Takanori Hashimoto, and David A. Lewis. Lamina-Specific Alterations in Cortical GABAA Receptor Subunit Expression in Schizophrenia. *Cerebral Cortex*, 21(5):999–1011, May 2011. ISSN 1460-2199, 1047-3211. doi: 10.1093/cercor/bhq169. URL `https://academic.oup.com/cercor/article-lookup/doi/10.1093/cercor/bhq169`.

365 L. Collado-Torres, E.E. Burke, and A. Peterson. Regional Heterogeneity in Gene Expression, Regulation, and Coherence in the Frontal Cortex and Hippocampus across Development and Schizophrenia. *Neuron*, 103(2):203–216, 2019. doi: 10.1016/j.neuron.2019.05.013.

366 C.R. Schubert, P. O'Donnell, and J. Quan. BrainSeq: Neurogenomics to Drive Novel Target Discovery for Neuropsychiatric Disorders. *Neuron*, 88(6):1078–1083, 2015. doi: 10.1016/j.neuron.2015.10.047.

367 J.J. Soghomonian and D.L. Martin. Two isoforms of glutamate decarboxylase: why? *Trends in Pharmacological Sciences*, 19(12):500–505, 1998. doi: 10.1016/S0165-6147(98)01270-X.

368 R.E. Straub, B.K. Lipska, and M.F. Egan. Allelic variation in GAD1 (GAD67) is associated with schizophrenia and influences cortical function and gene expression. *Molecular Psychiatry*, 12(9):854–869, 2007. doi: 10.1038/sj.mp.4001988.

369 Schahram Akbarian. Gene Expression for Glutamic Acid Decarboxylase Is Reduced Without Loss of Neurons in Prefrontal Cortex of Schizophrenics. *Archives of General Psychiatry*, 52(4):258, April 1995. ISSN 0003-990X. doi: 10.1001/archpsyc.1995.03950160008002. URL http://archpsyc.jamanetwork.com/article.aspx?doi=10.1001/archpsyc.1995.03950160008002.

370 Stephen J. Kaar, Ilinca Angelescu, Tiago Reis Marques, and Oliver D. Howes. Pre-frontal parvalbumin interneurons in schizophrenia: a meta-analysis of post-mortem studies. *Journal of Neural Transmission*, 126(12):1637–1651, December 2019. ISSN 0300-9564, 1435-1463. doi: 10.1007/s00702-019-02080-2. URL http://link.springer.com/10.1007/s00702-019-02080-2.

371 J A Brown, T S Ramikie, M J Schmidt, R Báldi, K Garbett, M G Everheart, L E Warren, L Gellért, S Horváth, S Patel, and Károly Mirnics. Inhibition of parvalbumin-expressing interneurons results in complex behavioral changes. *Molecular Psychiatry*, 20 (12):1499–1507, December 2015. ISSN 1359-4184, 1476-5578. doi: 10.1038/mp.2014.192. URL http://www.nature.com/articles/mp2014192.

372 Heike Weber, Claus Jürgen Scholz, Katharina Domschke, Christian Baumann, Benedikt Klauke, Christian P. Jacob, Wolfgang Maier, Jürgen Fritze, Borwin Bandelow, Peter Michael Zwanzger, Thomas Lang, Lydia Fehm, Andreas Ströhle, Alfons Hamm, Alexander L. Gerlach, Georg W. Alpers, Tilo Kircher, Hans-Ulrich Wittchen, Volker Arolt, Paul Pauli, Jürgen Deckert, and Andreas Reif. Gender Differences in Associations of Glutamate Decarboxylase 1 Gene (GAD1) Variants with Panic Disorder. *PLoS ONE*, 7(5):e37651, May 2012. ISSN 1932-6203. doi: 10.1371/journal.pone.0037651. URL https://dx.plos.org/10.1371/journal.pone.0037651.

373 A M Addington, M Gornick, J Duckworth, A Sporn, N Gogtay, A Bobb, D Greenstein, M Lenane, P Gochman, N Baker, R Balkissoon, R K Vakkalanka, D R Weinberger, J L Rapoport, and R E Straub. GAD1 (2q31.1), which encodes glutamic acid decarboxylase (GAD67), is associated with childhood-onset schizophrenia and cortical gray matter volume loss. *Molecular Psychiatry*, 10(6):581–588, June 2005. ISSN 1359-4184, 1476-5578. doi: 10.1038/sj.mp.4001599. URL http://www.nature.com/articles/4001599.

374 Masanobu Kogure, Nobuhisa Kanahara, Atsuhiro Miyazawa, Kengo Oishi, Yusuke Nakata, Yasunori Oda, and Masaomi Iyo. Interacting Roles of COMT and GAD1 Genes in Patients with Treatment-Resistant Schizophrenia: a Genetic Association Study of Schizophrenia Patients and Healthy Controls. *Journal of Molecular Neuroscience*, 71(12):2575–2582, December 2021. ISSN 0895-8696, 1559-1166.

doi: 10.1007/s12031-021-01866-y. URL https://link.springer.com/10.1007/s12031-021-01866-y.

375 Estela M. Bruxel, Glaucia C. Akutagava-Martins, Angélica Salatino-Oliveira, Julia P. Genro, Cristian P. Zeni, Guilherme V. Polanczyk, Rodrigo Chazan, Marcelo Schmitz, Luis A. Rohde, and Mara H. Hutz. *GAD1* gene polymorphisms are associated with hyperactivity in Attention-Deficit/Hyperactivity Disorder. *American Journal of Medical Genetics Part B: Neuropsychiatric Genetics*, 171(8):1099–1104, December 2016. ISSN 15524841. doi: 10.1002/ajmg.b.32489. URL https://onlinelibrary.wiley.com/doi/10.1002/ajmg.b.32489.

376 Toshinobu Kuki, Kazuyuki Fujihara, Hideki Miwa, Nobuaki Tamamaki, Yuchio Yanagawa, and Hajime Mushiake. Contribution of parvalbumin and somatostatin-expressing GABAergic neurons to slow oscillations and the balance in beta-gamma oscillations across cortical layers. *Frontiers in Neural Circuits*, 9, February 2015. ISSN 1662-5110. doi: 10.3389/fncir.2015.00006. URL http://journal.frontiersin.org/Article/10.3389/fncir.2015.00006/abstract.

377 A. Acheson, J.C. Conover, and J.P. Fandl. A BDNF autocrine loop in adult sensory neurons prevents cell death, March 1995.

378 P. Kowiański, G. Lietzau, E. Czuba, M. Waśkow, A. Steliga, and J. Moryś. BDNF: A Key Factor with Multipotent Impact on Brain Signaling and Synaptic Plasticity. *Cellular and Molecular Neurobiology*, 38(3):579–593, 2018. doi: 10.1007/s10571-017-0510-4.

379 M.F. Egan, M. Kojima, and J.H. Callicott. The BDNF val66met polymorphism affects activity-dependent secretion of BDNF and human memory and hippocampal function. *Cell*, 112(2):257–269, 2003. doi: 10.1016/S0092-8674(03)00035-7.

380 B. Lu, G. Nagappan, X. Guan, P.J. Nathan, and P. Wren. BDNF-based synaptic repair as a disease-modifying strategy for neurodegenerative diseases. *Nature Reviews Neuroscience*, 14(6):401–416, 2013. doi: 10.1038/nrn3505.

381 G. Ursini, T. Cavalleri, and L. Fazio. BDNF rs6265 methylation and genotype interact on risk for schizophrenia. *Epigenetics*, 11(1):11–23, 2016. doi: 10.1080/15592294.2015.1117736.

382 M.M. Youssef, M.D. Underwood, and Y.Y. Huang. Association of BDNF Val66MET polymorphism and brain BDNF levels with major depression and suicide. *International Journal of Neuropsychopharmacology*, 21(6):528–538, 2018. doi: 10.1093/ijnp/pyy008.

383 Ismail Abidin, Ulf T. Eysel, Volkmar Lessmann, and Thomas Mittmann. Impaired GABAergic inhibition in the visual cortex of brain-derived neurotrophic factor heterozygous knockout mice. *The Journal of Physiology*, 586(7):1885–1901, April 2008.

ISSN 0022-3751, 1469-7793. doi: 10.1113/jphysiol.2007.148627. URL https://physoc.onlinelibrary.wiley.com/doi/10.1113/jphysiol.2007.148627.

384 Kazuko Sakata, Newton H. Woo, Keri Martinowich, Joshua S. Greene, Robert J. Schloesser, Liya Shen, and Bai Lu. Critical role of promoter IV-driven BDNF transcription in GABAergic transmission and synaptic plasticity in the prefrontal cortex. *Proceedings of the National Academy of Sciences*, 106(14):5942–5947, April 2009. ISSN 0027-8424, 1091-6490. doi: 10.1073/pnas.0811431106. URL https://pnas.org/doi/full/10.1073/pnas.0811431106.

385 Rachel Anne Hill, Adrienne Mary Grech, Michael J. Notaras, Mauricio Sepulveda, and Maarten Van Den Buuse. Brain-Derived Neurotrophic Factor Val66Met polymorphism interacts with adolescent stress to alter hippocampal interneuron density and dendritic morphology in mice. *Neurobiology of Stress*, 13:100253, November 2020. ISSN 23522895. doi: 10.1016/j.ynstr.2020.100253. URL https://linkinghub.elsevier.com/retrieve/pii/S2352289520300436.

386 Sabrina Theresia Müller, Andreas Buchmann, Melanie Haynes, Carmen Ghisleni, Christopher Ritter, Ruth Tuura, and Gregor Hasler. Negative association between left prefrontal GABA concentration and BDNF serum concentration in young adults. *Heliyon*, 6(5):e04025, May 2020. ISSN 24058440. doi: 10.1016/j.heliyon.2020.e04025. URL https://linkinghub.elsevier.com/retrieve/pii/S2405844020308690.

387 T. Novkovic, T. Mittmann, and D. Manahan-Vaughan. BDNF contributes to the facilitation of hippocampal synaptic plasticity and learning enabled by environmental enrichment. *Hippocampus*, 25(1):1–15, 2015. doi: 10.1002/hipo.22342.

388 A.Y. Klintsova, E. Dickson, R. Yoshida, and W.T. Greenough. Altered expression of BDNF and its high-affinity receptor TrkB in response to complex motor learning and moderate exercise. *Brain Research*, 1028(1):92–104, 2004. doi: 10.1016/j.brainres.2004.09.003.

389 T. Andreska, S. Rauskolb, and N. Schukraft. Induction of BDNF Expression in Layer II/III and Layer V Neurons of the Motor Cortex Is Essential for Motor Learning. *The Journal of Neuroscience*, 40(33):6289–6308, 2020. doi: 10.1523/JNEUROSCI.0288-20.2020.

390 R. Sasaki, H. Watanabe, and S. Miyaguchi. Contribution of the brain-derived neurotrophic factor and neurometabolites to the motor performance. *Behavioural Brain Research*, 412(113433), 2021. doi: 10.1016/j.bbr.2021.113433.

391 R. Sasaki, S. Miyaguchi, and H. Onishi. Effect of brain-derived neurotrophic factor gene polymorphisms on motor performance and motor learning: A systematic review and

meta-analysis. *Behavioural Brain Research*, 420(113712), 2022. doi: 10.1016/j.bbr.2021.113712.

392 B. Fritsch, J. Reis, and K. Martinowich. Direct Current Stimulation Promotes BDNF-Dependent Synaptic Plasticity: Potential Implications for Motor Learning. *Neuron*, 66 (2):198–204, 2010. doi: 10.1016/j.neuron.2010.03.035.

393 A. Giordano, F. Clarelli, and M. Cannizzaro. BDNF Val66Met Polymorphism Is Associated With Motor Recovery After Rehabilitation in Progressive Multiple Sclerosis Patients. *Frontiers in Neurology*, 13, 2022. doi: 10.3389/fneur.2022.790360.

394 Vliet R, Ribbers GM, Vandermeeren Y, Frens MA, and Selles RW. BDNF Val66Met but not transcranial direct current stimulation affects motor learning after stroke. *Brain Stimulation*, 10(5):882–892, 2017. doi: 10.1016/j.brs.2017.07.004.

395 Y. Huang and A. Morozov. Hippocampal deletion of BDNF gene attenuates gamma oscillations in area CA1 by Up-regulating 5-HT3 receptor. *PLoS ONE*, 6(1):3–9, 2011. doi: 10.1371/journal.pone.0016480.

396 N.C. Jones, M. Hudson, and J. Foreman. Brain-derived neurotrophic factor haploinsufficiency impairs high-frequency cortical oscillations in mice. *European Journal of Neuroscience*, 48(8):2816–2825, 2018. doi: 10.1111/ejn.13722.

397 Inmaculada C. Rodríguez-Rojo, Pablo Cuesta, María Eugenia López, Jaisalmer de Frutos-Lucas, Ricardo Bruña, Ernesto Pereda, Ana Barabash, Pedro Montejo, Mercedes Montenegro-Peña, Alberto Marcos, Ramón López-Higes, Alberto Fernández, and Fernando Maestú. BDNF Val66Met Polymorphism and Gamma Band Disruption in Resting State Brain Functional Connectivity: A Magnetoencephalography Study in Cognitively Intact Older Females. *Frontiers in Neuroscience*, 12:684, October 2018. ISSN 1662-453X. doi: 10.3389/fnins.2018.00684. URL `https://www.frontiersin.org/article/10.3389/fnins.2018.00684/full`.

398 Jaana Simola, Felix Siebenhühner, Vladislav Myrov, Katri Kantojärvi, Tiina Paunio, J. Matias Palva, Elvira Brattico, and Satu Palva. Genetic polymorphisms in COMT and BDNF influence synchronization dynamics of human neuronal oscillations. *iScience*, 25(9):104985, September 2022. ISSN 25890042. doi: 10.1016/j.isci.2022.104985. URL `https://linkinghub.elsevier.com/retrieve/pii/S2589004222012573`.

399 R. Hiramoto, N. Kanayama, and T. Nakao. BDNF as a possible modulator of EEG oscillatory response at the parietal cortex during visuo-tactile integration processes using a rubber hand. *Neuroscience Research*, 124:16–24, 2017. doi: 10.1016/j.neures.2017.05.006.

400 R.F.H. Cash, K. Udupa, and C.A. Gunraj. Influence of BDNF Val66Met polymorphism on excitatory-inhibitory balance and plasticity in human motor cortex. *Clinical Neurophysiology*, 132(11):2827–2839, 2021. doi: 10.1016/j.clinph.2021.07.029.

401 Jingshan Chen, Barbara K. Lipska, Nader Halim, Quang D. Ma, Mitsuyuki Matsumoto, Samer Melhem, Bhaskar S. Kolachana, Thomas M. Hyde, Mary M. Herman, Jose Apud, Michael F. Egan, Joel E. Kleinman, and Daniel R. Weinberger. Functional Analysis of Genetic Variation in Catechol-O-Methyltransferase (COMT): Effects on mRNA, Protein, and Enzyme Activity in Postmortem Human Brain. *The American Journal of Human Genetics*, 75(5):807–821, November 2004. ISSN 00029297. doi: 10.1086/425589. URL `https://linkinghub.elsevier.com/retrieve/pii/S0002929707637860`.

402 Yasmin Potts and John M. Bekkers. Dopamine Increases the Intrinsic Excitability of Parvalbumin-Expressing Fast-Spiking Cells in the Piriform Cortex. *Frontiers in Cellular Neuroscience*, 16:919092, June 2022. ISSN 1662-5102. doi: 10.3389/fncel.2022.919092. URL `https://www.frontiersin.org/articles/10.3389/fncel.2022.919092/full`.

403 T.E. Goldberg, M.F. Egan, and T. Gscheidle. Executive Subprocesses in Working Memory. *Archives of General Psychiatry*, 60(9), 2003. doi: 10.1001/archpsyc.60.9.889.

404 E. Ira, M. Zanoni, M. Ruggeri, P. Dazzan, and S. Tosato. COMT, neuropsychological function and brain structure in schizophrenia: a systematic review and neurobiological interpretation. *Journal of Psychiatry & Neuroscience*, 38(6):366–380, 2013. doi: 10.1503/jpn.120178.

405 Y.H. Lee and G.G. Song. COMT Val158Met and PPARγ Pro12Ala polymorphisms and susceptibility to Alzheimer's disease: a meta-analysis. *Neurological Sciences*, 35(5):643–651, 2014. doi: 10.1007/s10072-014-1645-4.

406 P. Lopez-Garcia, L. Young Espinoza, P. Molero Santos, J. Marin, and F. Ortuño Sanchez-Pedreño. Impact of COMT genotype on cognition in schizophrenia spectrum patients and their relatives. *Psychiatry Research*, 208(2):118–124, 2013. doi: 10.1016/j.psychres.2012.09.043.

407 D.P. Prata, A. Mechelli, and C.H.Y. Fu. Opposite Effects of Catechol-O-Methyltransferase Val158Met on Cortical Function in Healthy Subjects and Patients with Schizophrenia. *Biological Psychiatry*, 65(6):473–480, 2009. doi: 10.1016/j.biopsych.2008.09.027.

408 A.S. Bassett and E.W.C. Chow. Schizophrenia and 22q11.2 deletion syndrome. *Current Psychiatry Reports*, 10(2):148–157, 2008. doi: 10.1007/s11920-008-0026-1.

409 O. Zarchi, M. Carmel, and C. Avni. Schizophrenia-like neurophysiological abnormalities in 22q11.2 deletion syndrome and their association to COMT and PRODH genotypes.

Journal of Psychiatric Research, 47(11):1623–1629, 2013. doi: 10.1016/j.jpsychires.2013.07.004.

410 S Kimoto, K Muraki, M Toritsuka, S Mugikura, K Kajiwara, T Kishimoto, E Illingworth, and K Tanigaki. Selective overexpression of Comt in prefrontal cortex rescues schizophrenia-like phenotypes in a mouse model of 22q11 deletion syndrome. *Translational Psychiatry*, 2(8):e146–e146, August 2012. ISSN 2158-3188. doi: 10.1038/tp.2012.70. URL `http://www.nature.com/articles/tp201270`.

411 Mario Altamura, Brita Elvevåg, Terry E. Goldberg, Frederick W. Carver, Daniel R. Weinberger, and Richard Coppola. The impact of Val108/158Met polymorphism of catechol-O-methyltransferase on brain oscillations during working memory. *Neuroscience Letters*, 610:86–91, January 2016. ISSN 03043940. doi: 10.1016/j.neulet.2015.10.018. URL `https://linkinghub.elsevier.com/retrieve/pii/S0304394015301816`.

412 Manuel Garcia-Garcia, Marc Via, Katarzyna Zarnowiec, Iria SanMiguel, Carles Escera, and Immaculada C. Clemente. COMT and DRD2/ANKK-1 gene-gene interaction account for resetting of gamma neural oscillations to auditory stimulus-driven attention. *PLOS ONE*, 12(2):e0172362, February 2017. ISSN 1932-6203. doi: 10.1371/journal.pone.0172362. URL `https://dx.plos.org/10.1371/journal.pone.0172362`.

413 A.A. Shukla, M. Jha, and T. Birchfield. COMT val158met polymorphism and molecular alterations in the human dorsolateral prefrontal cortex: Differences in controls and in schizophrenia. *Schizophrenia Research*, 173(1-2):94–100, 2016. doi: 10.1016/j.schres.2016.03.019.

414 Patricia Cambalova and Charlotte Stagg. Exploring the contribution of common single nucleotide polymorphisms to inter-individual variability in motor gamma-band activity, Mar 2025. URL `osf.io/86zxm`.

415 Richard N. Henson, Sana Suri, Ethan Knights, James B. Rowe, Rogier A. Kievit, Donald M. Lyall, Dennis Chan, Else Eising, and Simon E. Fisher. Effect of apolipoprotein E polymorphism on cognition and brain in the Cambridge Centre for Ageing and Neuroscience cohort. *Brain and Neuroscience Advances*, 4:239821282096170, January 2020. ISSN 2398-2128, 2398-2128. doi: 10.1177/2398212820961704. URL `http://journals.sagepub.com/doi/10.1177/2398212820961704`.

416 Jacob Cohen. *Statistical Power Analysis for the Behavioral Sciences*. Lawrence Erlbaum Associates, Hoboken, 2nd ed edition, 1988. ISBN 978-0-8058-0283-2.

417 Jennifer Anne Brealy. *The Relationship Between Variation in Genes, GABA, Structure and Gamma Oscillations in the Visual and Auditory System of Healthy Individuals and Psychiatric Disorder*. PhD thesis, Cardiff University, April 2015.

418 Richard A. E. Edden, Suresh D. Muthukumaraswamy, Tom C. A. Freeman, and Krish D. Singh. Orientation Discrimination Performance Is Predicted by GABA Concentration and Gamma Oscillation Frequency in Human Primary Visual Cortex. *The Journal of Neuroscience*, 29(50):15721–15726, December 2009. ISSN 0270-6474, 1529-2401. doi: 10.1523/JNEUROSCI.4426-09.2009. URL https://www.jneurosci.org/lookup/doi/10.1523/JNEUROSCI.4426-09.2009.

419 Farzin Tahvili and Alain Destexhe. A mean-field model of gamma-frequency oscillations in networks of excitatory and inhibitory neurons. *Journal of Computational Neuroscience*, 52(2):165–181, 2024.

420 Isabella Ferando and Istvan Mody. In vitro gamma oscillations following partial and complete ablation of δ subunit-containing gabaa receptors from parvalbumin interneurons. *Neuropharmacology*, 88:91–98, 2015.

421 Pantelis Antonoudiou, Yu Lin Tan, Georgina Kontou, A. Louise Upton, and Edward O. Mann. Parvalbumin and Somatostatin Interneurons Contribute to the Generation of Hippocampal Gamma Oscillations. *The Journal of Neuroscience*, 40(40):7668–7687, September 2020. ISSN 0270-6474, 1529-2401. doi: 10.1523/JNEUROSCI.0261-20.2020. URL https://www.jneurosci.org/lookup/doi/10.1523/JNEUROSCI.0261-20.2020.

422 Anne E Campbell, Petroc Sumner, Krish D Singh, and Suresh D Muthukumaraswamy. Acute effects of alcohol on stimulus-induced gamma oscillations in human primary visual and motor cortices. *Neuropsychopharmacology*, 39(9):2104–2113, 2014.

423 Diego Lozano-Soldevilla, Niels Ter Huurne, Roshan Cools, and Ole Jensen. Gabaergic modulation of visual gamma and alpha oscillations and its consequences for working memory performance. *Current Biology*, 24(24):2878–2887, 2014.

424 Howard J Edenberg, Danielle M Dick, Xiaoling Xuei, Huijun Tian, Laura Almasy, Lance O Bauer, Raymond R Crowe, Alison Goate, Victor Hesselbrock, Kevin Jones, Jennifer Kwon, Ting-Kai Li, John I Nurnberger, Sean J O'Connor, Theodore Reich, John Rice, Marc A Schuckit, Bernice Porjesz, Tatiana Foroud, and Henri Begleiter. Variations in GABRA2, Encoding the a2 Subunit of the GABAA Receptor, Are Associated with Alcohol Dependence and with Brain Oscillations. *Am. J. Hum. Genet.*, 2004.

425 Stefano Marenco, Antonina A Savostyanova, Jan Willem Van Der Veen, Matthew Geramita, Alexa Stern, Alan S Barnett, Bhaskar Kolachana, Eugenia Radulescu, Fengyu Zhang, Joseph H Callicott, Richard E Straub, Jun Shen, and Daniel R Weinberger. Genetic Modulation of GABA Levels in the Anterior Cingulate Cortex by GAD1 and COMT. *Neuropsychopharmacology*, 35(8):1708–1717, July 2010. ISSN 0893-133X, 1740-634X. doi: 10.1038/npp.2010.35. URL https://www.nature.com/articles/npp201035.

426 Patrick F Sullivan. The psychiatric gwas consortium: big science comes to psychiatry. *Neuron*, 68(2):182–186, 2010.

427 Paola Sebastiani, Nadia Timofeev, Daniel A Dworkis, Thomas T Perls, and Martin H Steinberg. Genome-wide association studies and the genetic dissection of complex traits. *American journal of hematology*, 84(8):504–515, 2009.

428 Guillaume Lettre, Christoph Lange, and Joel N Hirschhorn. Genetic model testing and statistical power in population-based association studies of quantitative traits. *Genetic Epidemiology: The Official Publication of the International Genetic Epidemiology Society*, 31(4):358–362, 2007.

429 Lucy Chipchase, Siobhan Schabrun, Leonardo Cohen, Paul Hodges, Michael Ridding, John Rothwell, Janet Taylor, and Ulf Ziemann. A checklist for assessing the methodological quality of studies using transcranial magnetic stimulation to study the motor system: An international consensus study. *Clinical Neurophysiology*, 123(9):1698–1704, September 2012. ISSN 13882457. doi: 10.1016/j.clinph.2012.05.003. URL `https://linkinghub.elsevier.com/retrieve/pii/S1388245712003355`.

430 Martin E. Héroux, Janet L. Taylor, and Simon C. Gandevia. The Use and Abuse of Transcranial Magnetic Stimulation to Modulate Corticospinal Excitability in Humans. *PLOS ONE*, 10(12):e0144151, December 2015. ISSN 1932-6203. doi: 10.1371/journal.pone.0144151. URL `https://dx.plos.org/10.1371/journal.pone.0144151`.

431 Zafer Iscan, Maria Nazarova, Tommaso Fedele, Evgeny Blagovechtchenski, and Vadim V. Nikulin. Pre-stimulus Alpha Oscillations and Inter-subject Variability of Motor Evoked Potentials in Single- and Paired-Pulse TMS Paradigms. *Frontiers in Human Neuroscience*, 10, October 2016. ISSN 1662-5161. doi: 10.3389/fnhum.2016.00504. URL `http://journal.frontiersin.org/article/10.3389/fnhum.2016.00504/full`.

432 Shanice EW Janssens and Alexander T Sack. Spontaneous fluctuations in oscillatory brain state cause differences in transcranial magnetic stimulation effects within and between individuals. *Frontiers in human neuroscience*, 15:802244, 2021.

433 Jean-Marc Therrien-Blanchet, Marie Chantal Ferland, Marie-Andrée Rousseau, Meriem Badri, Emelie Boucher, Amira Merabtine, Lydia Helena Hofmann, and Hugo Théoret. Stability and test–retest reliability of neuronavigated TMS measures of corticospinal and intracortical excitability. *Brain Research*, 1794:148057, November 2022. ISSN 00068993. doi: 10.1016/j.brainres.2022.148057. URL `https://linkinghub.elsevier.com/retrieve/pii/S0006899322002815`.

434 Nick J Davis. Variance in cortical depth across the brain surface: Implications for transcranial stimulation of the brain. *European Journal of Neuroscience*, 53(4):996–1007, 2021.

435 Lari M. Koponen, Miles Martinez, Eleanor Wood, David L. K. Murphy, Stefan M. Goetz, Lawrence G. Appelbaum, and Angel V. Peterchev. Transcranial magnetic stimulation input–output curve slope differences suggest variation in recruitment across muscle representations in primary motor cortex. *Frontiers in Human Neuroscience*, 18: 1310320, February 2024. ISSN 1662-5161. doi: 10.3389/fnhum.2024.1310320. URL https://www.frontiersin.org/articles/10.3389/fnhum.2024.1310320/full.

436 Joonas Iivanainen, Rasmus Zetter, and Lauri Parkkonen. Potential of on-scalp MEG: Robust detection of human visual gamma-band responses. *Human Brain Mapping*, 41 (1):150–161, January 2020. ISSN 1065-9471, 1097-0193. doi: 10.1002/hbm.24795. URL https://onlinelibrary.wiley.com/doi/10.1002/hbm.24795.

437 Mikael Lundqvist, Jonas Rose, Pawel Herman, Scott L. Brincat, Timothy J. Buschman, and Earl K. Miller. Gamma and Beta Bursts Underlie Working Memory. *Neuron*, 90(1):152–164, April 2016. ISSN 08966273. doi: 10.1016/j.neuron.2016.02.028. URL https://linkinghub.elsevier.com/retrieve/pii/S0896627316001458.

438 Rachel K Spooner and Tony W Wilson. Cortical theta–gamma coupling governs the adaptive control of motor commands. *Brain Communications*, 4(6):fcac249, November 2022. ISSN 2632-1297. doi: 10.1093/braincomms/fcac249. URL https://academic.oup.com/braincomms/article/doi/10.1093/braincomms/fcac249/6750028.

439 Spandan Sengupta, Afroditi Talidou, Jeremie Lefebvre, and Frances K. Skinner. Cell-type-specific contributions to theta-gamma coupled rhythms in the hippocampus. *Network Neuroscience*, 9(1):100–124, March 2025. ISSN 2472-1751. doi: 10.1162/netn_a_00427. URL https://direct.mit.edu/netn/article/9/1/100/125117/Cell-type-specific-contributions-to-theta-gamma.

440 Martin R Turner and Matthew C Kiernan. Does interneuronal dysfunction contribute to neurodegeneration in amyotrophic lateral sclerosis? *Amyotrophic Lateral Sclerosis*, 13(3):245–250, 2012.

441 Jeffrey D Rothstein, LIN Jin, Margaret Dykes-Hoberg, and Ralph W Kuncl. Chronic inhibition of glutamate uptake produces a model of slow neurotoxicity. *Proceedings of the National Academy of Sciences*, 90(14):6591–6595, 1993.

442 Davide Trotti, Andreas Rolfs, Niels C Danbolt, Robert H Brown, and Matthias A Hediger. Sod1 mutants linked to amyotrophic lateral sclerosis selectively inactivate a glial glutamate transporter. *Nature neuroscience*, 2(5):427–433, 1999.

443 Susanne Petri, Klaus Krampfl, Fariba Hashemi, Claudia Grothe, Akira Hori, Reinhard Dengler, and Johannes Bufler. Distribution of gabaa receptor mrna in the motor cortex of als patients. *Journal of Neuropathology & Experimental Neurology*, 62(10):1041–1051, 2003.

444 CM Lloyd, MP Richardson, DJ Brooks, A Al-Chalabi, and PN Leigh. Extramotor involvement in als: Pet studies with the gabaa ligand [11c] flumazenil. *Brain*, 123(11): 2289–2296, 2000.

445 Lucette Lacomblez, Gilbert Bensimon, P Nigel Leigh, Philippe Guillet, and Vincent Meininger. Dose-ranging study of riluzole in amyotrophic lateral sclerosis. amyotrophic lateral sclerosis/riluzole study group ii. *Lancet (London, England)*, 347(9013):1425–1431, 1996.

446 Robert G Miller, Dan H Moore, et al. Riluzole for amyotrophic lateral sclerosis (als)/motor neuron disease (mnd). *Cochrane database of systematic reviews*, (3), 2012.

447 Nimeshan Geevasinga, Parvathi Menon, Garth A Nicholson, Karl Ng, James Howells, Jillian J Kril, Con Yiannikas, Matthew C Kiernan, and Steve Vucic. Cortical function in asymptomatic carriers and patients with c9orf72 amyotrophic lateral sclerosis. *JAMA neurology*, 72(11):1268–1274, 2015.

448 Steve Vucic, Benjamin C Cheah, Con Yiannikas, and Matthew C Kiernan. Cortical excitability distinguishes als from mimic disorders. *Clinical neurophysiology*, 122(9): 1860–1866, 2011.

449 Takanori Yokota, Akiko Yoshino, Akira Inaba, and Yukinobu Saito. Double cortical stimulation in amyotrophic lateral sclerosis. *Journal of Neurology, Neurosurgery & Psychiatry*, 61(6):596–600, 1996.

450 Ulf Ziemann, Martin Winter, Carl D Reimers, Karin Reimers, Frithjof Tergau, and Walter Paulus. Impaired motor cortex inhibition in patients with amyotrophic lateral sclerosis: evidence from paired transcranial magnetic stimulation. *Neurology*, 49(5): 1292–1298, 1997.

451 Steve Vucic and Matthew C Kiernan. Novel threshold tracking techniques suggest that cortical hyperexcitability is an early feature of motor neuron disease. *Brain*, 129(9): 2436–2446, 2006.

452 Parvathi Menon, Mana Higashihara, Mehdi van den Bos, Nimeshan Geevasinga, Matthew C Kiernan, and Steve Vucic. Cortical hyperexcitability evolves with disease progression in als. *Annals of Clinical and Translational Neurology*, 7(5):733–741, 2020.

453 Kazumoto Shibuya, Neil G Simon, Nimeshan Geevasinga, Parvathi Menon, James Howells, Susanna B Park, William Huynh, Yu-ichi Noto, Steve Vucic, and Matthew C Kiernan. The evolution of motor cortical dysfunction in amyotrophic lateral sclerosis. *Clinical Neurophysiology*, 128(6):1075–1082, 2017.

454 Katja Stefan, Erwin Kunesch, Reiner Benecke, and Joseph Classen. Effects of riluzole on cortical excitability in patients with amyotrophic lateral sclerosis. *Annals of neurology*, 49(4):536–539, 2001.

455 Steve Vucic, Cindy Shin-Yi Lin, Benjamin C Cheah, Jenna Murray, Parvathi Menon, Arun V Krishnan, and Matthew C Kiernan. Riluzole exerts central and peripheral modulating effects in amyotrophic lateral sclerosis. *Brain*, 136(5):1361–1370, 2013.

456 Susanna B. Park, Matthew C. Kiernan, and Steve Vucic. Axonal Excitability in Amyotrophic Lateral Sclerosis. *Neurotherapeutics*, 14(1):78–90, January 2017. ISSN 18787479. doi: 10.1007/s13311-016-0492-9. URL https://linkinghub.elsevier.com/retrieve/pii/S1878747923015155.

457 Michael Trubshaw, Chetan Gohil, Katie Yoganathan, Oliver Kohl, Evan Edmond, Malcolm Proudfoot, Alexander G Thompson, Kevin Talbot, Charlotte J Stagg, Anna C Nobre, Mark Woolrich, and Martin R Turner. The cortical neurophysiological signature of amyotrophic lateral sclerosis. *Brain Communications*, 6(3):fcae164, May 2024. ISSN 2632-1297. doi: 10.1093/braincomms/fcae164. URL https://academic.oup.com/braincomms/article/doi/10.1093/braincomms/fcae164/7670820.

458 N. Riva, A. Falini, A. Inuggi, J.J. Gonzalez-Rosa, S. Amadio, F. Cerri, R. Fazio, U. Del Carro, M. Comola, G. Comi, and L. Leocani. Cortical activation to voluntary movement in amyotrophic lateral sclerosis is related to corticospinal damage: Electrophysiological evidence. *Clinical Neurophysiology*, 123(8):1586–1592, August 2012. ISSN 13882457. doi: 10.1016/j.clinph.2011.12.013. URL https://linkinghub.elsevier.com/retrieve/pii/S1388245711011382.

459 Malcolm Proudfoot, Gustavo Rohenkohl, Andrew Quinn, Giles L. Colclough, Joanne Wuu, Kevin Talbot, Mark W. Woolrich, Michael Benatar, Anna C. Nobre, and Martin R. Turner. Altered cortical beta-band oscillations reflect motor system degeneration in amyotrophic lateral sclerosis. *Human Brain Mapping*, 38(1):237–254, January 2017. ISSN 1065-9471, 1097-0193. doi: 10.1002/hbm.23357. URL https://onlinelibrary.wiley.com/doi/10.1002/hbm.23357.